DURBAN UNIVERSITY OF TECHNOLOGY

IMPROVEMENT OF SCRATCH AND ABRASION RESISTANCE PROPERTIES OF AUTOMOBILE PAINT

DEBASMITA MOHANTY

IMPROVEMENT OF SCRATCH AND ABRASION RESISTANCE PROPERTIES OF AUTOMOBILE PAINT

A THESIS SUBMITTED TO THE

DURBAN UNIVERSITY OF TECHNOLOGY

FOR THE DOCTOR OF ENGINEERING DEGREE

(IN MECHANICAL ENGINEERING)

BY

DEBASMITA MOHANTY

DEPARTMENT OF MECHANICAL ENGINEERING

FACULTY OF ENGINEERING AND BUILT ENVIRONMENT

DURBAN 4000, SOUTH AFRICA

2022

FINAL APPROVED SUBMISSION

PROFESSOR KRISHNAN KANNY

(SUPERVISOR)

DR. SMITA MOHANTY

(CO-SUPERVISOR)

DECLARATION

The thesis is being submitted to the Durban University of Technology for the degree of Doctor of Engineering (Mechanical Engineering) award. I declare that the thesis entitled "**Improvement of Scratch and Abrasion resistance properties of Automobile paint**" is a record of my research work. This thesis, in full or in parts, has not been submitted to any other institute or university for the award of any degree or diploma. I further declare that the only part of this work that has been published is in the form of peer-reviewed manuscripts with details provided in "Publications and Conference Presentations"

Signature of Student **30th November 2022**

(Debasmita Mohanty)

Signature of Supervisor **30th November 2022**

(Professor Krishnan Kanny)

Signature of Co-supervisor **30th November 2022**

(Dr. Smita Mohanty)

TO EVERYONE WHO HELPED

ACKNOWLEDGEMENTS

I would express my sincere thanks to Dr. Smita Mohanty, Director and Head (Principal Scientist), SARP: LARPM-CIPET, Bhubaneswar, India to give me the opportunity to join the Ph.D. program under the collaboration of CIPET, India, and Durban University of Technology, South Africa, without her kind support it would have never been possible for me to pursue a candidature at Durban University of Technology with Professor Krishnan Kanny. I sincerely thank my research supervisor Professor Krishnan Kanny for providing me with timely help in form of technical advice on research work and financial support during my stay in the Durban University of Technology. Many thanks to my co-supervisor Dr. Smita Mohanty for helping me from all possible perspectives. I will be always thankful to Dr. Smita Mohanty for her kind effort to go through my every paper and thesis before submission and showing me the proper direction about how to represent my work. I will always cherish the time and guidance I have got from her during Ph.D. I would also like to thank the head of the department, Dr. Festus Maina Mwangi for his support during the submission of this thesis and the overseas registration procedure. I would also like to thank Dr. T. P. Mohan for his support, guidance, and immediate response in every official work during my study period. I would also like to thank good and kind offices of, High Commission of South Africa (New Delhi) and South African Consulate General (Mumbai) for providing study permit. I would like to place a sincere thanks to staff of department of mechanical engineering, faculty of engineering and built environment, finance department, housing department and faculty research committee (Specially Mrs. Denisha Govender) for their timely support for academic activities. I would like to thank all the authors whose work have been used and well cited in this study. I would like to thank all my lab mates in Durban University of Technology and CIPET, Bhubaneswar for providing me with all the support needed during initial stages of laboratory experiment. I would specially thank my colleagues Dr. Sudheer Kumar, Mr. Smruti ranjan Mohanty, Ms. Rikarani Roychowdhury, Ms. Rosalin Rath, and Ms. Rookmoney Thakur for helping me in my work.

I would like to thank my Husband Mr. Debasis Mohanty for his support and help

during my study period. His moral support as well as his enthusiasm in providing study materials to getting chemicals, that are not easily available are the greatest strength for me. I would also like to thank my parents and my younger sister (Mr. Debendra Ku. Mohanty, Mrs. Debahuti Mohanty, and Mrs. Subhasmita Mohanty) for taking care of my daughter during my Ph.D. work and to be always there for me as my back in every possible manner. During my stay in Durban they are the ones that took care of my daughter in my absence. I would also like to thank my daughter Annwika for being a sensible child and making my journey a very smooth one. Despite her young age she understood me and despite her tender age, she stayed with her grandparents without showing any weakness. I wiil be thankful to god for her. Lastly I would like to thank my family members for their support and the almighty god for his blessings.

Debasmita Mohanty

TABLE OF CONTENTS

Abbreviations

Castor oil	CO
Isophorone diisocyanate	IPDI
Di butylene tin dilaurate	DBTDL
Epoxy	Ep
Nano-silica	NS
Polyurethane	PU
Epoxidized castor oil	ECO
Transesterified epoxidized castor oil	TECO
Acrylated transesterified epoxidized castor oil	ATECO
Aminopropyl triethoxysilane	APTES
p-Trisulfonyl isocyanate	TSI
Triallyl isocyanurate	TI
Fourier Transform Infrared	FTIR
Hydrogen nuclear magnetic resonance	^{1}HNMR
Scanning electron microscopy	SEM
Transmission electron microscopy	TEM
X-ray diffraction	XRD

Ultraviolet	UV
Dynamic mechanical analysis	DMA
Differential scanning calorimetry	DSC
Thermogravimetric analysis	TGA
Hydrogen peroxide	H_2O_2
Formic acid	HCOOH
Ammonia solution	NH_4OH
Sodium bicarbonate	$NaHCO_3$
Titanium-based pigment	TP
Commercial basecoat	BC
Commercial clearcoat	CP
Sodium methoxide	CH_3ONa
Glass transition Temperature	T_g
Glass transition temperature of soft segment	T_{gs}
Glass transition temperature of hard segment	T_{gh}
Melting temperature	T_m
Degree of Crystallinity	X
Cross-linking density	ϑ_c

Water contact angle	WCA
Epoxy/PU/NS composite	EPNS
Critical stress intensity factor	K_{IC}
Strain energy rate	G_{IC}
Volatile oxidizing compound	VOC
APTES modified NS	APTES-NS
TI modified NS	TI-NS
PU/NS composite	PUNS
PU/NS/TP composite	PUNSTP

List of Figures

Figure Name Page no.

List of Tables

Name of the Table — Page No.

List of Schemes

Publications and Conferences Attended

Publications

1. “Characteristic properties of Base-coat of Automobile paint: Enhancement in Scratch and Abrasion Resistance by Nanoscale reinforcement- A Review”: Accepted and Published in the journal of “ Polymer Bulletin” (I: F- 2.87). Accepted on 4th January 2022. DOI: 10.1007/s00289-022-04081-w

2. “Highly Transparent Castor Oil-Derived Polyurethane/Silica Nanocomposite coating synthesized by In-situ polymerization.” Journal Details- Journal of “Polymer For Advanced Technology” (I: F- 3.66). Accepted on 17 th July 2022. DOI: 10.1002/pat.5814 Internal Article ID: 17475106 Article ID: PAT5814

3. “Eco-friendly Automobile Base Coats derived from Castor oil: Evaluation of nanoscale reinforcements on the performance characteristics of coatings”: Accepted and published on 1st June 2022 in the journal of “ Pigment and Resin Technology” (I: F-1.51). DOI: http://doi.org/10.1108/PRT-01-2022-0013.

4. “Synthesis of Castor oil-based Polyols applicable in Acrylated Polyurethane Coating with Higher Mechanical Properties” Journal of “Polymer International” (I: F-3.44): Accepted on 22.9.2022

5. “Bio-based polyurethane coating synthesized from modified castor oil - applicable in base-coat of automobile paint”: Accepted and published on 25th October 2021 in the Conference of the South African Advanced materials Initiative, Vol 40 NO 1

6. “Bio-based epoxy-PU/Silica nanocomposite based Automobile sealer synthesized by ultrasonication method with higher mechanical and Thermal properties” Communicated in Progress in Organic Coating (I: F -5.16)

7. “Modification of Nano Silica by Silane coupling agent and Isocyanate to be Applicable in property enhancement of Automobile Coating”: Accepted in the “AIP Conference Proceedings” (I: F-0.4)

Conferences Attended

1. **Debasmita Mohanty, Krishnan Kanny, Smita Mohanty.** To improve the scratch and abrasion resistance of Automobile paint, 4th Interdisciplinary Research and Innovation conference 2019, 17 -20 September, 2019.
2. **Debasmita Mohanty, Krishnan Kanny, Smita Mohanty.** Bio-based Automobile paint: A new era of research, International Conference on Frontiers in manufacturing Technology (FMT-2020), 13-14 October, 2020
3. **Debasmita Mohanty, Krishnan Kanny, Smita Mohanty.** Basecoat of Automobile paintderived from Castor oil: Enhancement in properties by Nanoscale reinforcement, Advanced Polymeric Material conference (APM-2021), 9-13 March, 2021.
4. **Debasmita Mohanty, Krishnan Kanny, Smita Mohanty.** Bio-based coating synthesized from Modified Castor oil- Applicable in Basecoat of Automobile paint, Conference of South African Advanced Materials Initiative (COSAAMI-2021), 18-22 October, 2021.
5. **Debasmita Mohanty, Krishnan Kanny, Smita Mohanty.** Modification of Nano-silica by silane coupling agent and Isocyanate to be applicable in property enhancement in Automobile coating, NANOICON-2022, 11-15 January, 2022.
6. **Debasmita Mohanty, Krishnan Kanny, Smita Mohanty.** Influence of surface modified Nano-silicaby Triallyl isocyanurate on Thermal and Mechanical properties of Acrylated Polyurethane, International e-conference on Nanomaterisls & Nanoengineering. APA NANOFORUM-2022. 22-26 February,2022. **(Got the Best Poster Award)**

Abstract

The automobile paint industry normally consumes petro-based feedstock as the raw material, which is non-renewable and emits a higher amount of volatile organic compound (VOC), that pollutes the environment. This study focuses on the use of eco-friendly castor oil (CO) as a substitute for petro-based feedstocks; while synthesizing polyurethane (PU)-based automobile coats. The novelty and objective of this work is paints derived from bio-based CO as a substitute for petro-based feedstocks.CO is a nonedible oil, hence it does not affect the food chain. Paints derived are with fewer VOCs, thus having a less detrimental effect on the environment and is cost-effective.

Modified castor oil (CO) based polyurethane (PU)/nano-silica (NS)/titanium pigment (TP) hybrid coating with an organic-inorganic covalent bond was synthesized by the in-situ polymerization method. Aminopropyl tri-ethoxy silane (APTES) modified NS particles along with TP were added to the PU matrix at various wt. %. Thermal, mechanical, and chemical resistance properties of the coating samples were significantly enhanced with the addition of NS and TP. Char residue, Glass transition temperature, pencil hardness, Young's modulus, water contact angle (WCA), cross-sectional density, cross-cut tape adhesion %, abrasion % increased from 0.29%, -24.5ºC, 2H, 251MPa, 77.61º, 0.16mol/m^3, 65±5%, 0.040% to 1.26%, 1.94ºC, 3H, 1199MPa, 88.89º, 2.4mol/m^3, 93±2% and 0.016% with addition of modified NS particles along with TP particles. Paint formulation with 0.5 wt% NS and 0.2 wt% TP was optimized to be applicable as an automobile base coat and its characteristic properties can be comparable with a commercial base coat (BC).

An acrylate-PU/NS hybrid coating was developed, which was derived from CO-based polyol. CO was modified by employing a process that includes epoxidation, followed by transesterification, and acrylation to synthesize the required polyols, which is used for acrylate-PU paint synthesis via the in-situ polymerization process. Triallyl isocyanurate (TI) modified NS particles were incorporated with the paint matrix by the ultrasonication method to enhance the paint properties. Experimental findings revealed that with the incorporation of NS particles, char residue, Young's modulus, abrasion resistance, and cross-cut adhesion % increased by 71.31%, 42%, 0.28%, and 5% respectively. Also, glass transition temperature, pencil hardness,

nanoindentation depth, water contact angle (WCA), and cross-linking density were increased from -12.16 ºC, 2H, 3300 nm, 81.71 º, and 0.90 mol/m^3 to 1.65 ºC, 3H, 2000 nm, 92.26 º, and 1.78 mol/m^3 respectively. The UV-visibility spectra, haze, transmittance, and gloss parameter showed the enhanced optical properties of the paint samples. PU/NS composite coating developed showed equivalent properties as that of the commercial clear coat.

Epoxy/PU composite applicable as automobile sealer was synthesized by the ultrasonication mixing process. TI-modified NS particles were incorporated into the blend to enhance the characteristic properties. Structural properties of the composite were studied using FTIR spectra. Char residue %, glass transition temperature, cross-linking density, and WCA were observed to increase from 3.10%, 50.60 °C, 0.98 mol/m^3, and 85.63 ° to 4.55%, 73.76 °C, 3.75 mol/m^3, and 91.45 ° respectively after incorporation of NS. The impact strength, tensile strength, and fracture toughness of the blend were studied to increase after NS reinforcement. The epoxy-PU/NS nanocomposite developed fulfilled the parameters of automobile sealer.

CHAPTER 1

Introduction and Overview

Chapter 1

1.1 Introduction

The automotive paint industry has 100 years of history. In the early stage of the automobile paint industry, varnish-type products were used to paint the automobile body with the help of paint brushes. Those varnish-based paints were applied in two layers. The first layer was sanded and smoothed, and after that the second layer was applied and polished to make the substrate body shine[1]. Between 1920 to 1940, the use of spray technology was developed in the automotive paint industry. That development in technology decreased the drying time and resulted in a more even surface finish, which led to less sanding requirement[2]. In 1923 DuPont et al. developed a lacquer, which gave the concept of colour. But those lacquer paint had certain drawbacks such as; the requirement of 3 to 4 layers of the coating and less chemical and acidic environment resistance properties. In the early 1930, there was a tremendous development in the paint industry with the introduction of alkyd enamel paints in some car models which had significant surface properties[3]. In the early stage of the paint industry, coating steps were executed manually which needed weeks to complete. T. Sagar et al. stated that to overcome these disadvantages there were several types of research on the development of automotive paint having specific properties like reduced drying time, more corrosion resistance, the longevity of colour, and better environmental compatibility[4, 5]. In general, there are 3 basic layers in the coating system i.e., primer, base coat, and clear coat. Primer is the first coat, which responsible for the adhesion and base leveling of the automobile paint followed by the base coat, which gives the automobile body colour and topmost layer is clear coat, which is a transparent protective coat, that gives gloss to the paint[6]. Automobile paint gives a significant colour to the automobile body, as well as acts as a protective layer. It has an approximant thickness 100 µm. Fig.1.1.a shows different layers of automobile paints.

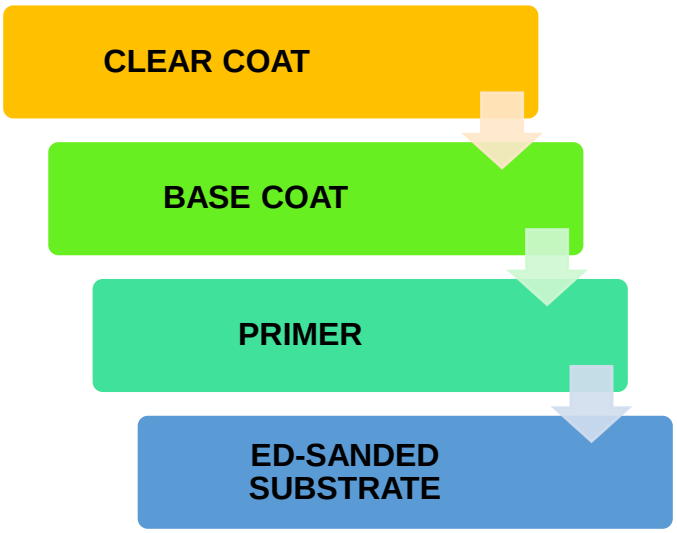

Fig 1.1.a: Different layers of Automobile Paint

D. Lopes et al. stated that in the early stages of paint industry lead, chromium, and other heavy metals were used in paint preparation. But in a later stage, the environmental law prohibited the use of these materials, as around 85% of these paints evaporated into the environment, which makes severe environmental pollutions. This problem led the researcher for the development of water-based and solvent-based paints[7]. Y. G. June et al. stated that the automobile paint acts as a protective coating that increases the durability of the automobile body and it also protects the automobile body from harsh weather exposure, UV degradation, and mechanical damage that can result in scratches and abrasion. The scratches and abrasion are also formed by many external impacts like sun, rain, UV exposure, snow, dirt as well as road salt, etc. Another reason for the formation of tiny scratches is an improper car wash, which is caused by brushes and multiplies over time and decreases the paint properties[8]. According to N. Coinvestigator et al. automobile paint has a very large role in the protection of the automobile body from mechanical wear and climatic impacts[9]. C. Seubert et al. stated that most of the automobile paints are made up of organic polymers[10]. With the incorporation of a small number of inorganic nanoparticles into the organic polymer matrix, makes the paint flexible, elastic, and weather-resistive. M. A. Ala et al. stated that these inorganic nanomaterials normally have excellent mechanical, chemical, thermal, and optical properties, which disperse in the matrix homogeneously. The organic and inorganic components are covalent, which helps them to bond very well with each other[11].

Alkyds, acrylics, epoxy and polyurethane (PU) are in general used as paint matrix in automobile paint industry. M. A. Alaa et al. stated that PU is the most commonly used organic paint matrix, due to its specific properties like; high tensile strength, tear and abrasion resistance, solvent resistance, and highly versatile chemical structure[11]. PU is synthesized by polymerizing polyols with isocyanates, which creates a urethane linkage. In General, petro-based feedstocks like; polypropylene glycol is used as polyol during PU synthesis. But it has a high cost and affects the non-renewable source of materials. To overcome this, in recent research works polyols derived from different vegetable oils like, castor oil (CO), soybean oil, linseed oils, etc. are used in PU synthesis. S. Das et al. stated that CO is the most abundantly available vegetable oil in India. It has a high hydroxyl value for which it is used in several chemical industries, especially in the production of PU[12]. G. Acik et al. stated that bio-based materials have a great requirement to achieve environmental sustainability. The bio-based materials normally used are starch, cellulose, vegetable oils, sugar, and wood. Among them, the vegetable oils, consisting of triglycerides and ricinoleic acid are most suitable for several polymer synthesis like; alkyds, polyamides, and PU[13]. To synthesize polymers of high molecular weight the vegetable oils need to be modified to increase the reactivity. The modification process normally followed is epoxidation, transesterification, acrylation, etc.[13].

Gradual depletion of petro-based resources and sharp fluctuations in oil prices has led to increased environmental awareness in finding renewable resources based feed-stock[14]. R. Shen et al. stated that, currently, most of the raw materials i.e., polyols and isocyanates are extracted from petroleum-based feedstocks, which are non-renewable. Replacing them with renewable alternatives like lignin, cellulose, and vegetable oils that have a low environmental impact has become the new research trend[15]. J. Zhang et al. have reported that among all the renewable resources vegetable oils are most frequently employed to prepare polymeric materials for their structural advantages as well as their ease of availability, low price, and potential degradability. Additionally, due to the hydrophobicity of plant oils, the resultant polymeric materials becomes hydrophobic[16]. Hence, vegetable oil based Polyols can be implemented to reduce the use of petroleum-based feedstock thereby protecting the environment[17]. These are primarily composed of triglycerides having

90% unsaturated fatty acids, resulting in higher functionality and polymerization, which leads to its application in chemical industries as polyols[18]. The inherent biodegradability of these oils also provides a significant characteristics in the growing environmental concerns[19]. Depending on the application, the renewable content of commercially available bio-based polyols varies between 30-100%[20]. Metallic corrosion on automobile body occurs due to harsh and substandard environment leads to crack on material surfaces, which creates safety hazards[21]. A number of methods have been reported to prevent the extent of corrosion such as, electro deposition, electroless plating, gas phase deposition and organic coatings etc. Among the aforementioned methods, organic polymer based anti-corrosion coating derived from vegetable oil is an effective and economical way to prevent corrosion[22].

CO is one of the most preferred vegetable oil in the chemical industry because of its low toxicity and presence of hydroxyl-containing fatty acids which creates many feasible reactions[23]. Polyurethane (PU)-based organic coating has been the most abundantly used due to its wide range of applications ranging from coatings, footwear materials, and sealants as well as its chemical stability, mechanical strength and good wear resistance[15]. R. Liu et al. stated that in recent decades, CO has been widely used in the synthesis of PU elastomers and waterborne PU (WPU) dispersions. Generally, the characteristics of PU depends on the structure and ratio of the soft segment and the hard segment. Due to the unique triglyceride structure, the PU network with CO as the soft segment usually has a higher crosslink density, excellent mechanical properties, and chemical resistance. The hard segment is a rigid structure cross-linked by PU. Tightly packed hard segment produce better mechanical properties but poor chain mobility for PU network, while loosely packed hard segment produce the opposite effect[14]. Bio-based PU coatings possess low VOC emission, high curing efficiency, low energy consumption, etc[16].

A. Das, P. Mahanwar et al. stated that PU is used in most industries for its simple production process and excellent properties[24]. In a recent study, it is found that PU has a maximum market share in the polymer industry and is mostly applicable in coatings, adhesives, sealants, and elastomers. Fig. 1.1.b attributes various applications of PU. The main advantage of PU has been its durability, toughness, and

excellent chemical resistance, which led it to be the replacement for many metals, plastics, and rubber-based engineering as well as commodity application[24].

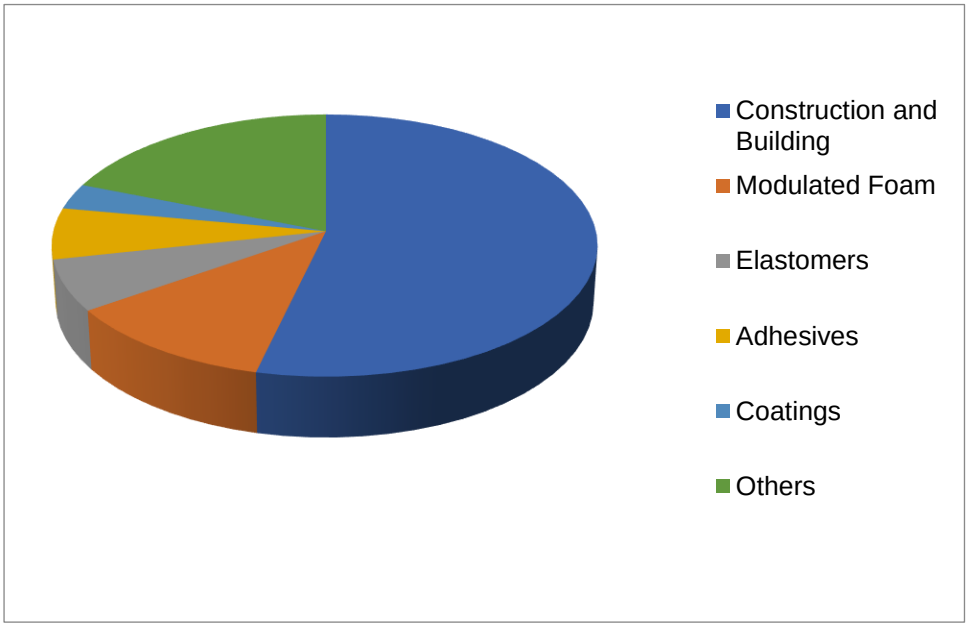

Fig 1.1.b: Different Applications of Polyurethane

According to G. Acik et al. PU has been receiving increasing attention recently in diverse applications including automotive paint, building insulation, furniture and bedding, refrigerators and freezers, footwear, coatings, adhesives, and so on[25]. PU is the sixth most used commercial polymer and is synthesized by the polymerization of polyols containing –OH groups with diisocyanate containing –NCO group, which polymerize to synthesize urethane (-NHCOO) linkage. H. F. Karabutul et al.. stated that reinforcement of nanoparticles into PU matrix increases its mechanical durability which helps to improve the scratch and mar resistance properties[26]. Ching et al. stated that due to the very high length to diameter ratio of the nanoparticles, these are used to increase the mechanical properties of coating, which helps both the coating film and substrate to become resistant to marring, cracking, wear, scratch and mild abrasions[27]. Ching et al.. have reported that among the nanoparticle additives the reinforcement of nano-silica and nano-alumina especially enhances the hardness, abrasion resistance, scratch resistance, and the tensile strength of the polymer

coating. Blees et al., stated that reinforcement of nano-silica into the PU coating increases the water resistance capability as well as thermal stability of the coating. From the Fourier Transformation spectroscopy, it is found that there is no chemical reaction between nano-silica and PU.

S. Gaur et al. stated that recently the paint industries are increasing the use of nanoparticle additives such as; nano-silver, photo-catalytically active nano titanium dioxide, functionalized nano-silica, or functionalized nano alumina, which enhances the properties of the paint, such as water resistance, scratch resistance, and antimicrobial properties. For PU coating, in most of the cases, nano-silica or nano-alumina are used as additives to achieve scratch, and abrasion resistance properties. Nano-silica and nano-alumina particles generally enhance the mechanical properties of coatings. G. Fettis et al.. stated that on the Mohs scale of hardness, silica and alumina have hardness 9 and 7 respectively, for which these are mostly used in scratch and abrasion resistance improvement of paint and coatings. In the paint industry, nano-silica particles are normally preferred over nano alumina, because nano-silica particles never affect the transparency of the coating, as these particles possess low refractive index, high modulus, and hardness[19][14]

1.2 Statement of the problem

Most paints are manufactured contain a large number of VOCs i.e., lead, mercury, and chromium. These elements are very hazardous and can pose a threat to both human health and the environment. Under the current policies of environment protection, the paint industries are trying to come up with new techniques of paint production to minimize the amount of VOC. Also, the content of lead, chromium, and mercury should be very less thereby making the paint eco-safe[29].

The prices of paints largely depend on the cost of raw materials. There are around 300 odd raw materials required for the manufacturing of paints, which consumes around 50% of the total cost of the paint. Most of the paint companies use petro-based feedstock as the main raw material. Hence, any change in the price of crude oil in the global market greatly affects the price of paint. The pressure further increased due to the recession and thereafter a decreased consumption. Even under the best of

circumstances, raw materials represent a near-constant headache for paint and coating producers. With the world simmering with tensions and a global trade war growing more intense, volatile raw material prices have posed severe challenges for the paint and coating industry. The countries like India, which are entirely dependent on the imports of crude oil are mostly affected on the account of rising prices and uncertainty due to political reasons and recession[30].

1.3 Aim

The study aims to synthesize a bio-based automobile base coat and clear coat from modified CO incorporated with NS particles, with better scratch and abrasion resistance properties. It also aims to synthesize epoxy-PU/silica nano composite applicable as automobile sealer.

1.4 Objectives

- Single-step modification of Castor oil by epoxidation process
- Surface modification of nano-silica particles by using Aminopropyl-triethoxysilane
- Synthesis of polyurethane-based automobile base coat using epoxidized castor oil incorporated with nano-silica and titanium-based colour pigments.
- Three-step modification of castor oil by epoxidation, transesterification followed by acrylation process
- Surface modification of nano-silica particles by triallyl isocyanurate
- Property comparison of acrylate-polyurethane-based clear coat incorporated with both aminopropyl-triethoxysilane modified nano-silica and triallyl isocyanurate modified nano-silica.
- Synthesis of bio-based acrylate-PU automobile clear coat using epoxidized transesterified acrylate castor oil incorporated with isocyanate modified nano-silica.
- Synthesis of epoxy-PU blend incorporated with nano-silica, which can be used as automobile sealer.

1.5 Significance of the study

The primary raw material used to synthesize automobile paint is derived from petro-based feedstock, which is non-renewable. During the drying process, the paint synthesized from petro-based feedstock emits a lot of VOCs, that are toxic, which greatly affects the environment. The cost of production is also very high.

This study is important as the implementation of CO can replace the application of petroleum-based products in the automotive paint industry. With the incorporation of inorganic NS, paint parameters studied are equivalent to commercial-grade paint.

The study will be beneficial to relevant automobile paint industries, as it would provide information on the synthesis of paint from CO and study various parameters of the paint across the globe and its applicability to the global market.

The study is also significant to academia as it will provide an understanding of the differences and doubts in existing literature regarding bio-based automobile paint and its effect on the environment and human health.

1.6 Justification of the study

Depletion of petro-based feedstocks and its effect on environment and human race is one of the most concerned topics in research industries. With development of technology, the automobile industry has become a large driving force in current economy. The vast expansion of automotive industry requires a large scale of paint industry, which leads to gradual depletion of non-renewable petro-based feedstocks. To overcome this crisis, researchers are opting to the use of bio-based raw materials in the paint industry.

Vegetable oils like CO, soybean oil, canoballa oil etc. are the most preferred bio-based raw materials used in chemical industries. These oils have unsaturated fatty acids and around 90% triglycerides, and higher functionality, which make them significantly reactive during chemical reactions. CO is the most preferred vegetable oil, because it is cheaper in price, most abundantly available and it do not affect the environment. Also, it does not affect the food chain, as it is a non-edible oil. Hence, it can be used

in paint industry as the main raw material in place of petro-based raw materials. Further addition of nano-scale fillers can enhance the characteristic properties of the paint.

The current study implies the use of CO in paint industry to synthesize bio-based automobile paint with incorporated NS particles. This leads to prevention of decrease in non-renewable petro-based feedstocks and also there is less number of VOCs during paint process, which lesser affect the environment.

1.7 Limitations

The current study takes a long period of time to synthesize the bio-based automobile paint. The small-scale synthesis process is only limited to laboratory due to lack of advanced equipments long time consuming process, which lead to facing difficulty in replacing the petro-based commercial automobile paint.

1.8 Delimitations

The current study depicted the synthesis of bio-based automobile basecoat, clearcoat, and sealer synthesized from castor oil, which can help in prevention of gradual depletion of petro-based feedstock. Castor oil is a non-edible bio oil, hence the paint synthesized have less VOCs and also it does not affect the food chain.

1.9 Structure of Dissertation

The study comprises five chapters:

Chapter 1 - Introduction and Background

This chapter presented an overview of the study covering aspects such as background, statement of problem, aim of the study, objectives of the study, justification of the study, Limitations and Delimitations of the study, and the structure of the study.

Chapter 2 – Review of Literature

This chapter reviews related literature from journals, periodicals, books, and conference proceedings. It highlights the application of naoparticles in paint industry, and provides an overview about the scratch and abrasion resistance improvement properies of automobile paints by incorporation of various nanoparticles and their effect on the characteristic properties of the paint. It also gives a brief idea about the various paint components like different colour pigments, different resins, and additives as well as it also describes the factors affecting automobile paint.

Chapter 3 – Research Design and Methodology

This chapter covers the manufacturer or supplier and all the general characteristics along the structure of the materials used. This also covers the methods used for the synthesis and characterization of bio-based automobile basecoat, clearcoat, and sealer.

Chapter 4 – Results and Discussion- 1

Deals with the results and discussions of bio-base automobile basecoat synthesized from ECO incorporated with both APTES-NS and TP. CO was modified by epoxidation process, which is used as the polyol to synthesize bio-based automobile basecoat. NS filler was modified by using APTES and was incorporated into the paint matrix along with TP particles at optimized wt. % to obtain the desired bio-based basecoat.

Chapter 5 – Results and Discussion- 2

Deals with results and discussions of bio-based automobile clearcoat synthesized from ATECO incorporated with TI-NS. ECO was further modified by transesterification followed by acrylation process, which is used as the polyol to synthesize bio-based automobile clearcoat. NS particles were modified by using TI and were incorporated at optimized wt.% into the paint matrix to enhance the characteristic properties.

Chapter 6 – Results and Discussion- 3

Deals with results and discussions of bio-based automobile sealers synthesized from epoxy resin blended with acrylic-PU. ATECO and epoxy were blended at optimized

wt.% ratios to synthesize bio-based automobile sealer. Optimized wt.% of TI-NS was incorporated into the sealer matrix to enhance the characteristic properties of the nanocomposite.

Chapter 7 – Conclusions and Future study

This chapter covers the general conclusion derived from this study, future aspects that can be drawn from this study, and the prototype of this study.

CHAPTER 2

Literature Review

Chapter 2

2. Literature Review

2.1 Different Types of Coatings

Various types of coatings are described in Fig. 2.1.a.

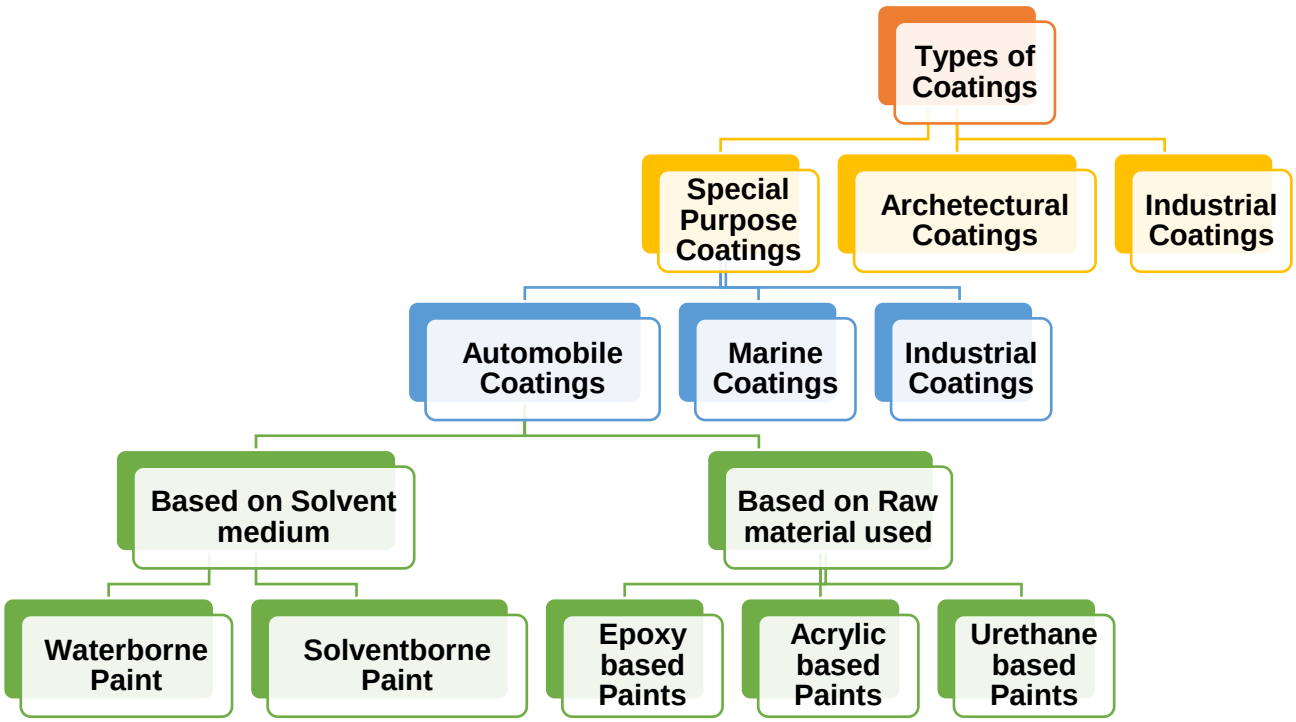

Fig. 2.1.a: Types of Coatings

Coatings are mainly divided into three types i.e., industrial coating, architectural coating, and special purpose coating.

2.1.1 Industrial Coating:

Industrial coatings have primary purpose of protection, while their secondary purpose is looks and gloss. This coating has a wide range of application such as, aircraft coating, cane coating, coil coating, general industrial coating, high performance coating, instrumental coating etc[31].

2.1.2 Architectural Coating:

This type of coating is used to paint the exterior and interior of buildings. It has significant properties like, gloss, durability and protection[32].

2.1.3 Special Purpose Coating:

Special purpose coatings are normally synthesized for specific applications. This type of coating has some special properties, which satisfies all the characteristics required for the field of application. This coating is in general divided into three types i.e., special industrial coatings, marine coatings, and automobile paints[33].

2.1.3.1 Special Industrial Coatings:

Special industrial coatings are applied in industrial parts like tanks, bridges etc. The substrate used in this type of coating is normally steel and one of the most important functions of this coating is to control corrosion. Aircraft coating also comes under special industrial coating which is coated mainly with epoxy or amine primers followed by urethane top coats[33].

2.1.3.2 Marine Coating:

Marine coatings are the protective coating used mostly in marine environment to protect ships, vessels, tankers, and other material from saline atmosphere. Marine coatings have specific functional properties, which provides superior long-term protection to the substrate. These coatings protect submerged surfaces as well as above sea water surfaces. Marine coatings protect materials from corrosion, abrasion as well as it prevents fouling[34].

2.1.3.3 Automobile Paint:

Automobile paint are normally used to coat the automobile body parts for both protection and gloss purpose. According to T. Sagar et al. automotive spray painting is considered as one of the most sophisticated industrial coatings, which is performed under controlled atmosphere[5]. The automobile paints have significant properties, which can withstand extreme weather conditions. These are divided into five basic categories based on the raw materials used and the solvent used such as, (a) Water-

borne paint (b) Solvent-borne paint (c) Epoxy-based paint (d) Acrylic-based paint (e) Urethane-based paint

2.1.3.3(a) Water-borne paint: In case of waterborne paints, water with other co-solvents is used, where water is the primary solvent and the co solvent is up to 30 wt.% of the total solvent, which makes it 80% eco-friendly. F. Sbardella et al. stated that, waterborne resins include acrylics, epoxies, alkyds, and polyurethane. Water-borne paints have specific properties like, low toxicity, low VOCs emission, and no flammability. In some cases, the quality of waterborne paints is comparable with solvent borne paints[35]. C. Sanchez et al. stated that nowadays there is a demand of paint spraying with less VOC. In waterborne paints as water is used to dissolve the resin, it leads to an environment friendly paint[36]. Due to the reduced VOC emissions, water-borne paint is less prone to risk of fires, easy to clean up. But it has the disadvantage of lower mechanical properties and less weather resistance. Waterborne paints are divided into the following types[37].

Water soluble paint- It gives Complete solubility in water. Resins used are normally synthesized by polycondensation or polymerization reactions in organic medium using alcohols or ethers as co-solvents and in general are polyalkyds, epoxies or epoxy ester based[38].

Water dispersible paint- After dispersion in water some small clusters of the paint remain insoluble which can be dissolved using both organic co-solvents and mechanical force. The resins used in these types of dispersion paints include vinyl propionate copolymers, vinyl acetate copolymers, acrylate methacrylate copolymers, and styrene-butadiene copolymers and polymers. Colloidal dispersions are normally used for the coating purpose of porous materials[39].

Emulsion Paint- This type of paint is similar to the water dispersible paint however, the size of cluster formed is larger in case of emulsion paint and emulsifier is used to make it suspended in water. In general resins used in this paint are styrene-butadiene copolymers, acrylics, alkyds, polyvinyl acetates and polystyrene. It has higher permeability, which leads to less peeling and blistering of the paint[40].

Water based alkyds- These coatings have longer curing time in comparison to solvent-borne coatings but have similar properties. The viscosity range of this paint is very large and can be applied by spray or dip coating method[41].

Water-borne paints have the following advantages:

- Have good resistance to heat and abrasion
- Excellent adhesion
- Low toxicity and flammability due to low VOC emission
- Cost effective
- Less amount of coating material is required in comparison to other coatings
- Higher pot life
- The paint guns can be cleaned easily with water or water-based solutions and do not require paint thinner, acetone, or methyl acetate

Despite all these advantages, water-borne paints have also some shortcomings like,

- Higher curing time
- Low coating thickness range
- Corrosion resistance equipment required
- Lower thermal stability

2.1.3.3(b) Solvent-borne Paint: Solvent-borne paints are normal known as oil paints. These paints contain solid constituents dispersed in the solvent and the solvent medium used is hydrocarbon-based organic compounds. These organic compounds provide a durable and hard finish to the paint. The most significant advantage of this paint over water-based paint is, it is less susceptible to environmental conditions like temperature and humidity during curing process[42]. Solvent-borne paints contain high level of volatile organic compounds (VOC), which is hazardous to the environment. The solid dispersion content in this paint is up to the range of 80%. The solvents used are normally consists of hydrogen and carbon[43]. There is a wide range of solvents used in paint industry like,

- Aliphatic (white spirit)
- Aromatic (xylene, toluene)
- Ketones (methyl ethyl ketone)
- Esters
- Alcohols
- Glycol ethers
- Glycol ether esters

Solvent-borne paints have the following advantages;

- Less amount of paint is required for coating purpose
- Wide range of coating thickness can be obtained
- Few numbers of spraying operation are required to get the desired coating thick ness.
- Helps self-orientation of metallic flakes in automotive coating application.
- Better scratch resistance and hardness properties are observed in comparison to water-based paint.

Despite all the advantages this coating also has some demerits. Such as;

- Toxicity content due to presence of VOCs.
- Higher viscosity
- More expensive
- Shorter pot life
- Requirement of modified equipment for painting application

2.1.3.3(c) Epoxy based paint: Epoxy is an excellent two component coating material i.e., epoxy resin and curing agent or hardener. Epoxy coating becomes rigid after curing with improved mechanical properties. Epoxy coatings are anti corrosive in nature; thus, these are mostly used for protection purpose. But it is very prone to defects due to its brittleness. Hence, during application the brittleness should be controlled. R. Jain et al. stated that epoxy-based paints normally have a high range of tolerance when applied on a surface. For this

particular property these paints are used as protective coating for marine application[44].

Epoxy coating has the following advantages;

- Very high strength and stiffness
- Excellent insulation capacity
- Good adhesive and cohesive strength
- Higher chemical resistance
- Resistance to corrosion and fouling

Nagshah et al. stated that epoxy has high cross-linking capacity, which makes it tough with significantly resistance to mechanical forces, chemicals and also to heat and electricity. Hence, it is used in structural crack repair and under water adhesives and coatings[45]. Epoxy coatings have a vast range of application from aerospace, automotive to industrial field. By addition of field emission particles epoxy coatings can protect the substrate from electromagnetic waves. Substrates used for epoxy coating can be metals, concrete or polymeric. Epoxy coatings are resistant to strain and are highly durable. These coatings do not form any cross-linking bond with water, chemicals or ultraviolet radiation. Epoxy to hardener ratio is always predetermined by the industry experts. Epoxy is derived from the latex acrylic paints and is thermosetting in nature. It has excellent adhesion properties due the presence of polar bonding in between the resin and the hardener. Epichlorohydrin reacts with acidic hydroxy group to produce epoxy. The hydroxyl groups are in general derived from aliphatic diols, polyols, phenolic compounds or dicarboxylic acid. Among all the hydroxyl groups bisphenol A is mostly used to produce epoxy. The epoxy produced is also known as diglyceride ethers. The epoxy bond is observed in ring like structure, which is known as oxirane ring. Fig. 2.1.b shows the epoxy ring.

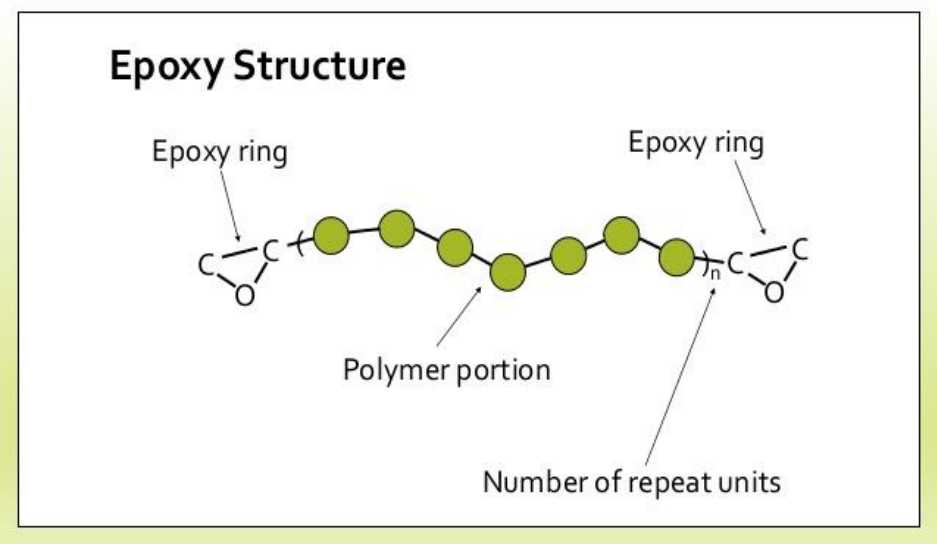

Fig. 2.1.b: Epoxy structure

The epoxy ring in epoxy resin consists of one oxygen atom bounded with two carbon atoms. This epoxy resin can be cured by various curing agents to achieve the required properties. The oxirane rings reacts with suitable hydroxyl group to form a rigid thermosetting epoxy[46].

Despite all the advantages of epoxy paints these also have the following short comings;

- These paints cannot withstand UV exposure
- After some time, these paints tend to become yellow in color
- Brittleness is very high
- High viscosity
- Lower thermal properties

2.1.3.3(d) Acrylic based paint: Henry Levison first discovered Liquitex, which was later recognized as acrylic paint. Acrylic emulsions are composed of particles of amorphous polymer suspended in water. The two-phased system is held in suspension by using surfactants and other surface stabilizers. During its curing process, water evaporates to draw the spherical polymer particles closer, which then molded together to form a ‘honeycomb’ network. A coalescing-solvent additive

confirms malleability of the polymer particles of the paint, to get complete compaction, even after the water has evaporated. Eventually, the boundaries between particles become un-detectable and the film is considered continuous. However, it has been shown that pores or micro-voids are often left within the film, which can be seen with light microscopy and. Yamuchi et al. stated that acrylic paints are fast drying paints having pigments suspended in acrylic emulsion. It is water soluble in prior curing but becomes rigid to water after curing. The coating obtained from aqueous acrylate polymer emulsion drying either at room temperature or at heated condition gives a good quality of durability. For this property acrylic paint is used as a resin for water soluble paints. But the disadvantage of this paint is, when it is exposed to UV radiation, its luster and gloss becomes dull gradually[47]. To overcome this problem some additives can be reinforced into the paint to improve the properties. The most commonly used additive for acrylic paint used is silicon, which protects it from environmental exposure. Clarket al. stated that acrylic paints can enhance the appearance, hardness, flexibility, texture of the paint by using the acrylic medium. The chemicals used in acrylic paints are more flexible, which makes the paint very much suitable for application purpose as they can expand and contract properly with fluctuation of temperature[48]. Fig. 2.1.c below reveals the application of acrylic based coating.

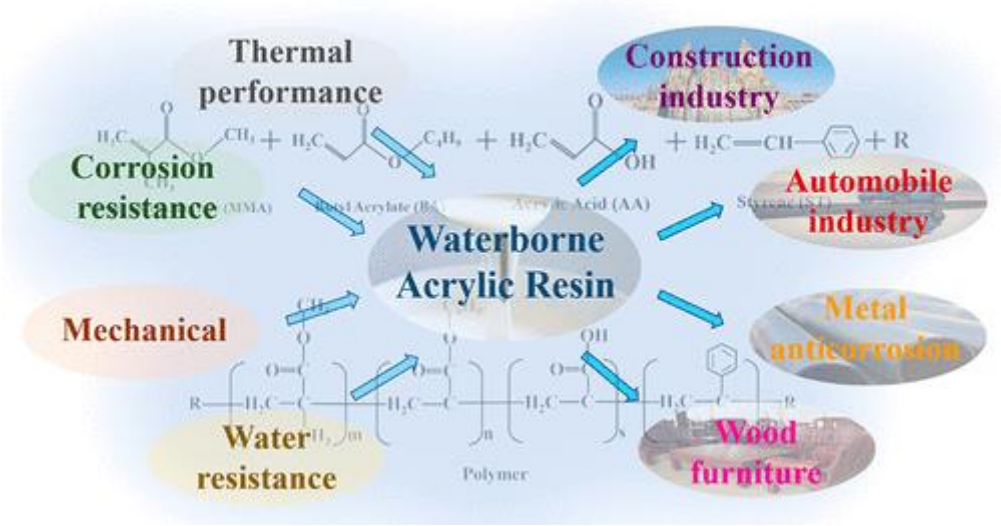

Fig. 2.1.c: Application of Acrylic resins

Acrylic paints have the following advantages;

- Good weatherability
- Higher chemical resistance
- Good mechanical properties
- Faster drying
- Retain original color
- Wide range of flexibility
- Can be cleaned easily
- They can adhere to any substrate smoothly
- Vast range of applicability
- Low odour, less fumes and non-flammable
- Characteristics of the paint can be changed with change in mediums

Waterborne acrylic resins are usually copolymerized by acrylic acid, methacrylic acid, and their esters or other derivatives, whose properties can be tailored by regulating the compositions. There are many ways to synthesize waterborne acrylic resins (including emulsion, solution polymerization, bulk polymerization, and suspension polymerization), of which emulsion polymerization is the most widely used. It is synthesized by monomers, emulsifiers, water, and initiators. The synthetic macromolecular chain is mainly composed of a carbon chain, which is divided into a soft segment and a hard segment. The hard segment is mainly composed of hard monomers (methacrylate, styrene, etc.), which can improve the hardness of the resin, and the soft segment mainly contains soft monomers such as acrylate, which can provide flexibility for the resin. The structure and composition of the resin framework affect the product performance[49].

The acrylic paint is mainly divided into two types depending on the grades i.e., aristocratic grade or professional grade and student grade. The wide variety of acrylic paints used is as follows

- ***Heavy body acrylics:*** These are highly viscous paints best suitable for heavier paint applications.
- ***Medium viscosity acrylics:*** These paints have a lower viscosity but same pigment quality as the heavy body acrylics. This type of paint is

most desired for smooth coverage for water color application. This can be modified to heavy body acrylics by addition of acrylics.

- ***Open acrylics:*** The open acrylic paints have a viscosity that can be managed to be applicable in wide range of viscosity level.

Despite of all these advantages, acrylic paints have following disadvantages;

- More prone to scratches
- Non heat resistant
- Difficult to remove
- Very less variety of colors

2.1.3.3(e) Urethane based paint: These paints protect the substrates from various types of defects such as corrosion, weathering, abrasion and other deteriorating processes. PU itself is a type of polymer that is connected to a chemical compound group known as carbamides[50]. This polymer material is also thermosetting in nature. These paints can be formulated to be glossy, opaque or transparent. From the past two decades urethane paints are considered as the best for industrial use, and is considered as the best in automobile paint industries. It two parts i.e., one soft segment the polyol and another hard segment the isocyanate part. In this paint the isocyanate acts as the curing agent, which is toxic in nature causing harm to lungs and skin. Hence, precaution should be taken during application process. PU coating can be divided into two-component type and one-component type. The two-component PU paint is composed of one hard segment i.e., isocyanate and one soft segment i.e., polyol having hydroxyl groups. The –OH group of polyol reacts with the –NCO group of isocyanates to produce urethane linkage, and the property of the paint depends on OH: NCO ratio of the urethane linkage[51].

Urethane based paints have the following advantages over other paints;

- Can achieve very high gloss and finish, which enhances the looks of the automobile body
- Higher durability

- Can resist the adverse environmental effects
- Work very well with modern high volume, low-pressure spray guns
- Gives highest level of protection to the automobile body
- Wide range of versatility
- Can save energy

For the above-mentioned outstanding properties, urethane-based paints are now considered as the best paint material in automotive painting industry.

Types of PU-based paint: Ismail et al. stated that PU-based paint is categorized according to the type of polyol used i.e., petroleum based or bio-based. Majority of the polyols are synthesized from polyether, which are derived from ethylene and propylene oxides[52] M.C.C. Ferrar et al. stated that now-a-days a large scale of vegetable oils are used as polyols in PU synthesis. The most used vegetable oils are castor oil and soybean oil[53].The chemical composition of vegetable oils is triglycerides of long chain fatty acids. In these fatty acids, the most common chain length are 18 or 20 carbon atoms which can be either saturated or unsaturated, where the unsaturated double bonds are present at the 9, 12 and 15 carbon. Fig. 2.1.d shows the chemical structure of PU.

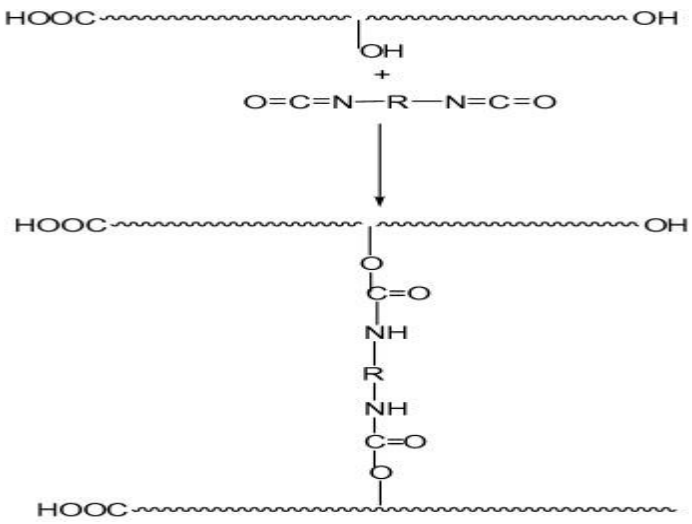

Fig. 2.1.d: Chemical Structure of PU

PU used in paint industry is generally divided into two types i.e., reactive and non-reactive[54]. According to number of components used PU is again of two types i.e.,

two components or 2k system and one component or 1k system. In 2k system there is a chemical reaction between polyisocyanate and polyol or polyamine to prepare the PU paint. In 1k system there is a single component which hardens when exposed to heat, light or atmosphere.

1K paint dries very fast, but has less hardness in comparison to 2k paints. Thus, these are used for substrates that are less prone to scratch and abrasion resistance. But the 2k paints have more hardness and scratch resistance ability, thus used in most of the paint industries[55]. The types of PU-paints are described in Table 2.a

Table 2.a: Reactive and Non-reactive PU paints.

PU Type	Curing Type	Product Description
Reactive	Oven cured	These are 2k system paints. This includes powder coating and most other PU based coatings
	Moisture cured	These are 1k paints having higher molecular weight and low free isocyanate which cures by reaction with moisture and forms urea linkage
Nonreactive	Non-isocyanate	In this type of paint isocyanate is non-reactive during the reaction

2.2 Automotive paint:

The introduction of automobile paint in early 1900 brought a tremendous revolution in the paint industry. A. Gimpieria et al. stated that in the beginning of paint industry both primer and the upper coat were prepared from oleo resinous material i.e., a mixture of resin and oil. Multiple numbers of coats were required for the painting purpose and the time of drying was very long i.e., around 2-3 weeks[28]. Larger covered areas were required for the painting purpose and the resultant paint was dull in appearance and was not resistant to environmental effects[3]. Also, the colour selection was limited to some particular colours. These problems in the paint industry led the researchers to

development of an advanced revised form of paints. Table 2.b depicts different types of oleo resinous binders.

Table 2.b: Different types of oleoresinouss binders

Resin	Oil	Pigment	Filler	Solvent
Amber	Linseed oil	White lead	Chalk	Oil of turpentine
Copal	Wood oil	Zinc oxide	Caolin	Pine oil
Rosins	Perilla oil	Bone black		Alcohol
Shellac	Castor oil	Cobalt blue		

Significant research is going on the automotive paint industry to reduce the consumption of high energy and water and also volatile hazardous compounds (VOC) emissions. The improvement of the automotive paint industry has been started since 1940s, with the development of electro-deposition. It was further improved in 1960s by producing low VOC. W.A. Frye et al. stated that in 1990s there was development of waste minimization and in 2000s the environment legislation brought significant changes in paint industry[20]. Fig. 2.2 shows the revolution in automotive paint industry.

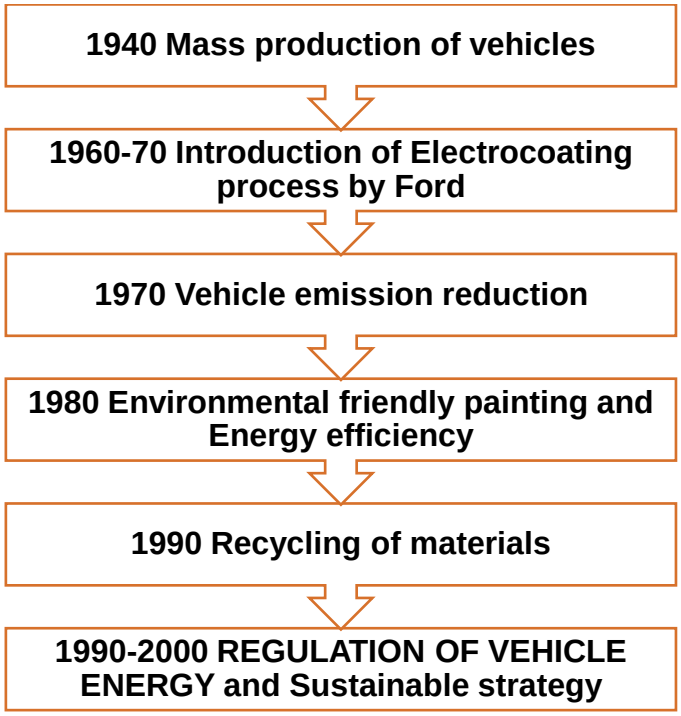

Fig. 2.2: Automotive paint revolution

According to S. Papasavva et al. the automobile paint generally consists of 3 layers i.e., primer which is used for adhesion and levelling of the substrate, base coat i.e., responsible for the colour of the paint and applied on the primer coat and clear coat is the upper most transparent coat of paint i.e., responsible for the gloss and scratch resistance of the paint. The paint helps in both appearance of automobile as well as weather, scratch and environmental effects[57]. R. Gray et al. stated that the liquid coats are either waterborne or solvent borne. The resins used in these coats as base polymer are normally epoxies, urethanes, acrylics or polyesters[58].

According S. Kara et al. the painting unit is the most environmental effective among all other units of an automobile industry[59]. Up to 90% of VOCs emission occurs during painting and curing process. Around 60% of energy is consumed in the Painting unit in an automotive industry[60]. Fernades et al. stated that emissions during painting process are in the form of air, water, and soil as paint sludge. Air emissions include PM, VOCs, Sox, NOx, CO, and CO_2[61]. The most dangerous one is VOC, which converts into smog on exposure to sunlight due to photochemical reaction. A.B. Rahim et al. stated that main source of volatile oxide emissions are solvents that are used in paints/coats formulations. Solvent cannot be avoided because it is required to

give proper adhesion and fluidity of the material and also it maintains the paint viscosity[62]. Kahikaet al. stated that there are no clear studies in changing the type of paint can lower the paint emission.

2.3. Painting Process:

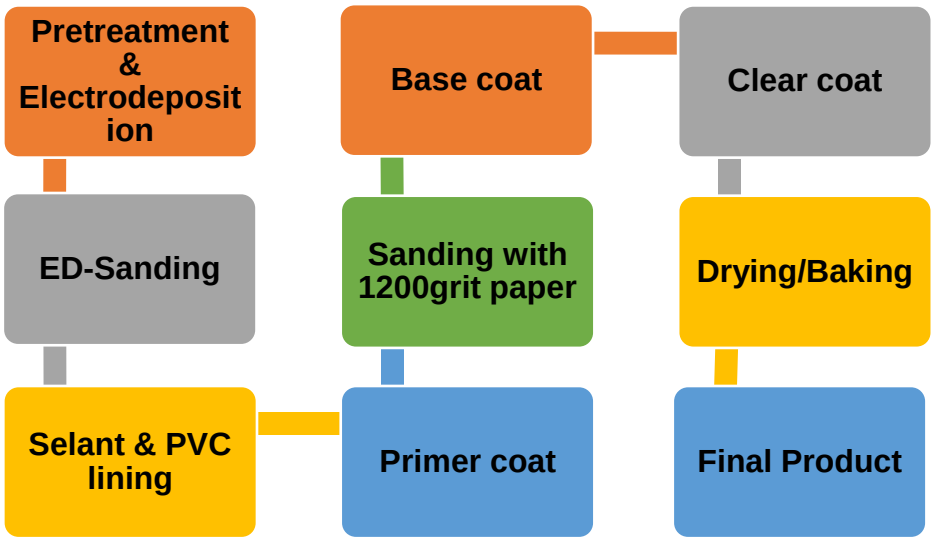

Fig. 2.3.a: Painting process

Fig. 2.3.a shows the steps followed in the painting process. According to S. Mishra et al. in case of liquid paint and powder coating, resins, pigments, solvent and additives are added and then baked during the curing process of the paint. In case of liquid paint, the volume shrinkage occurs, because there are more than 40% VOC in a liquid paint, which evaporates while drying. There are different steps of painting, which are followed step by step in the automobile paint industry[63]. These steps are described below;

- Pretreatment
- Electrode deposition
- ED sanding
- Sealant & PVC lining
- Primer coat
- Base coat
- Clear coat

2.3.1 Pre-treatment:

Pre-treatment is a very important process in paint industry, which is applied to the automobile body by spray baths or immersion baths. This process has following advantages like[64];

- Excellent corrosion resistance
- Higher cleanliness of metal
- Very good adhesion of the paint

Zinc phosphate is the most used pre-treatment agent in paint industry. This process involves a number of cleaning stages, which is followed by titinated activated rinse with deionized water. This process helps to prevent metal oxidation and creates uniformity in the appearance.

The materials required for pre-treatment process are;

- Activating agents
- Phosphate
- Sealant
- Plastic

2.3.2 Electrode deposition:

This process is followed by pre-treatment; in which paint dispersed in water is electrically deposited on the automobile body the process followed is electrolysis. Z. Hemedon et al. stated that it forms a uniform coating which is resistive to corrosion. This process starts with pre-treatment process which includes pre-cleaning, pre-degreasing, degreasing, water rinse, surface conditioning, phosphating, final water rinse and deionized water rinse. After the pre-treatment process, electro-deposition process is done which include electro-deposition, ultra-filtration and final deionized water rinse. After the electro-deposition process, the automobile body goes for baking[62]. The fundamental process in electrode deposition is similar to electroplating. The automobile body is given strong negative charge and then dipped in positively charged paint tank having a DC power supply. This process is called cathodic deposition. Fig. 2.3.b shows the function of an electro-deposition tank.

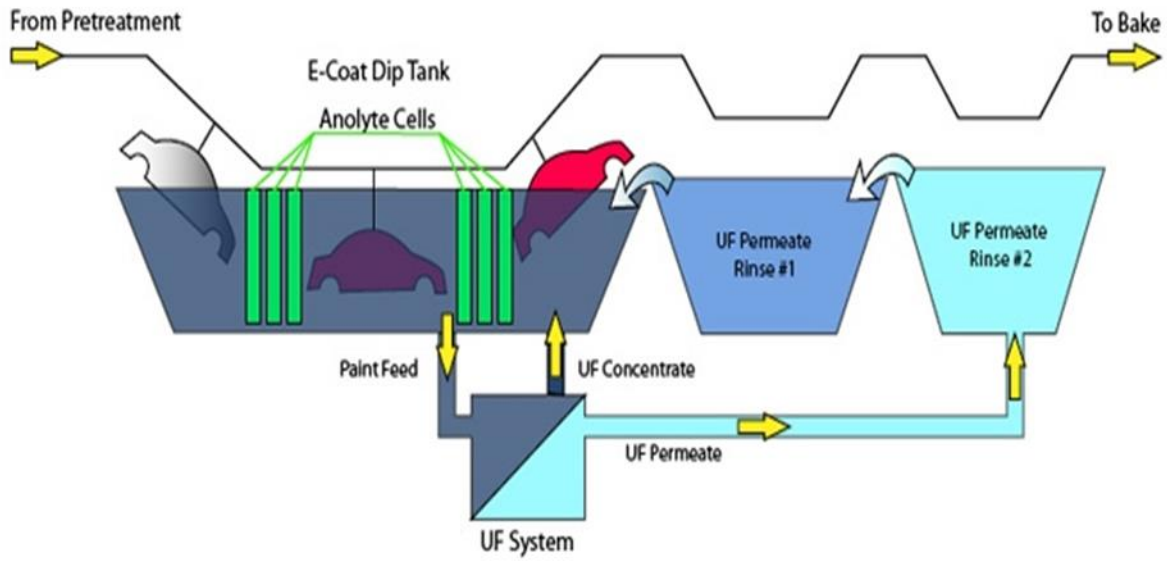

Fig. 2.3.b: Electrode deposition tank

The process has following advantages;

- Very good corrosion resistance
- Thin film thickness
- Less requirement of electric current
- Access to all the areas of automobile body

After coming out from the electro-deposition dip tank, the automobile body is rinsed several times before going to the baking oven. This baking process is done in a number of steps with different instruments like,

ELPO Oven*:* This oven helps in curing the paint after coming from the paint dip tank. It increases the cross-linking density and creates a single uniform coating.

Sealing: Sealing compounds are applied to improve corrosion of particular parts of an automobile body. This process is handled by robots having number of cameras to get the visionary system.

Anti-Chip: Anti-chip is a urethane layer coated on the front, underside and lower body panel, which acts as a protective layer for the metal body. The anti-chip booth uses an electrostatic bell-shaped applicator, attached with an automatic trigger. This coating is

highly negative and the metal body is grounded to give positive charge, which makes the spray-coated on the metal substrate.

Anti-chip Oven: Anti-chip oven is used to cure the sealant and anti-chip. During the curing process, the sealant flows to the cracks and crevices of automobile body to form a water-resistive barrier.

Preparation: After baking the automobile body is cooled down and then enters the to paint shop area. After coming to the paint area, it is dusted with the help of four rolls of ostrich features, air suction and air jet.

Clean room: It contains robotic electrostatic modular paint booths, switching system controller, fire suspension system. This helps to get contamination free paint on the vehicle body.

2.3.3 ED-Sanding:

ED-sanding is required to remove the defects of the automobile paint before applying the paint. S. M. Mahajan et al. stated that the most common defect in electro-deposition process is presence of water spots (beats) on the metal substrate. These beats are generally removed by sanding the metal body. In some cases, surfactants or ultra filtrates can be added[65].

2.3.4 Sealants & PVC Lining:

The automobile industry uses sealants to seal the vehicles interior and exterior parts like chassis, under the hood, lower panel etc. to bond them perfectly. Loeschen et al. stated that it also helps to make the metal body lighter, which increases the fuel efficiency of the automobile. Normally PVC lining is used as the sealant in automobile industry.

2.3.5 Primer:

In automobile paint industry, primer is generally applied after ED- sanding and before applying the top coat. The main purpose of applying primer is adhesion and proper levelling of paint. Before applying primer, the following steps are followed[66].

- Complete rust removal by sanding
- Filling the dents, scratches etc. on the vehicle body
- Substrate should be completely dry.

There are various types of primer used in automobile industry like,

- Epoxy primer
- Urethane primer
- Polyester primer
- Urethane sealer
- Acid Etch primer
- Enamel primer
- Lacquer primer
- Moisture cure urethane primer

2.3.6 Base Coat:

This is one of the most important layers of automobile paint. It has colour pigments, which is responsible for the colour of the paint. It is applied above the primer and below the top coat. It mainly attracts the buyer's decision during the purchase. It is normally urethane based and its properties mostly affect the paint. As in recent research there are tremendous works going on colour pigments and researchers are trying to develop the properties of paint by improving the pigment properties and then reinforcing it with the paint. Approximately 1000 different colours are developed every year in paint industry. There are three different types of basecoats that are used in automobile paint industry, i.e., solvent borne medium solids (MS), solvent borne high solids (HS) and water-borne[67].

2.3.7 Clear coat:

This is the top most layer of automobile paint. This is a transparent glossy layer, which give both gloss and protection to the paint. It protects the paint from fading by sun, dirt and environmental effects. It also makes the repair of scratches easier[67].

2.4. Different Components of Automotive paint

Normally paint contains some important components like pigment, additive, binder, thinner and hardener. These are the main components of paint and the paint property normally depends on the components and their chemical properties. Fig. 2.4.a shows thew different components of automobile paint.

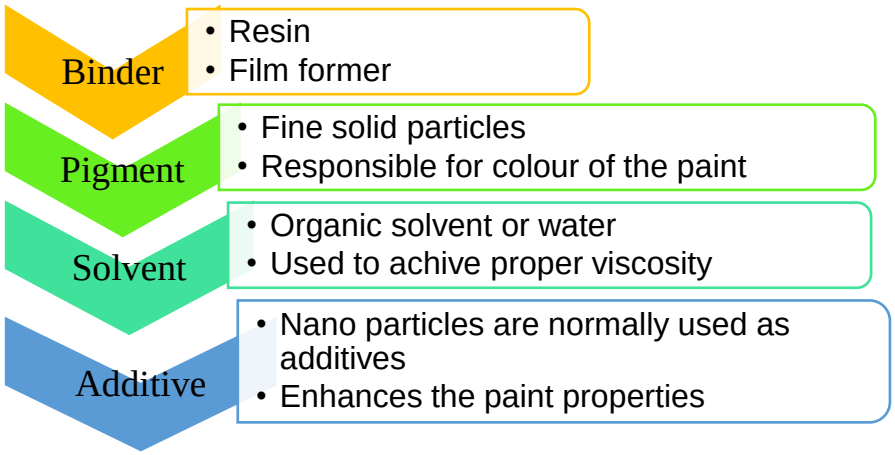

Fig 2.4.a: Different components of automotive paint

2.4.1 Pigment:

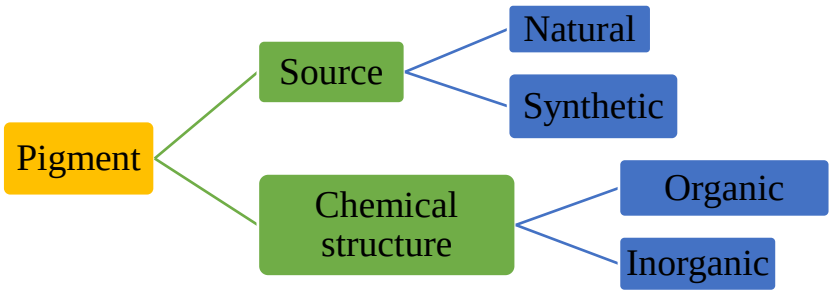

Fig 2.4.b: Types of pigment

According to Chakraborty et al. pigment is the component of paint which is responsible for colour of the paint. According to source of production, pigment is divided into two types i.e., natural pigment and synthetic pigment. According to chemical structure it is divided into organic and inorganic pigment. The classification of pigment is described in Fig. 2.4.b. Pigments are responsible for the colours in each and every thing in the world and plants and plant products are measure provider of pigment. Fruits, vegetables, flowers and other living beings have particular colour, these colours are due to some natural pigments i.e., the green chlorophylls, the yellow-orange-red carotenoids, the red-blue-purple anthocyanins and the red betanin[68].

Synthetic pigment is the pigment which is derived from various chemical reactions. The discovery of man-made synthetic pigment was in the mid-19th century, gradually replaced the natural pigment, as it produced in bulk amounts and is capable of fulfilling the needs of market.

According to chemical structure the pigments can be organic or inorganic. Organic pigments are defined as the pigments, that are derived from organic compounds. The examples of organic pigment are azo pigments, lake pigments, pthalocyanine pigments and quinacridone pigments. These pigments are composed of carbon rings and carbon chains. The pigments derived from inorganic compounds are known as inorganic pigments.

Comstock et al. stated that organic pigments are normally of three types i.e., carbon pigments, polyacrylic pigment, and azo pigments[69].

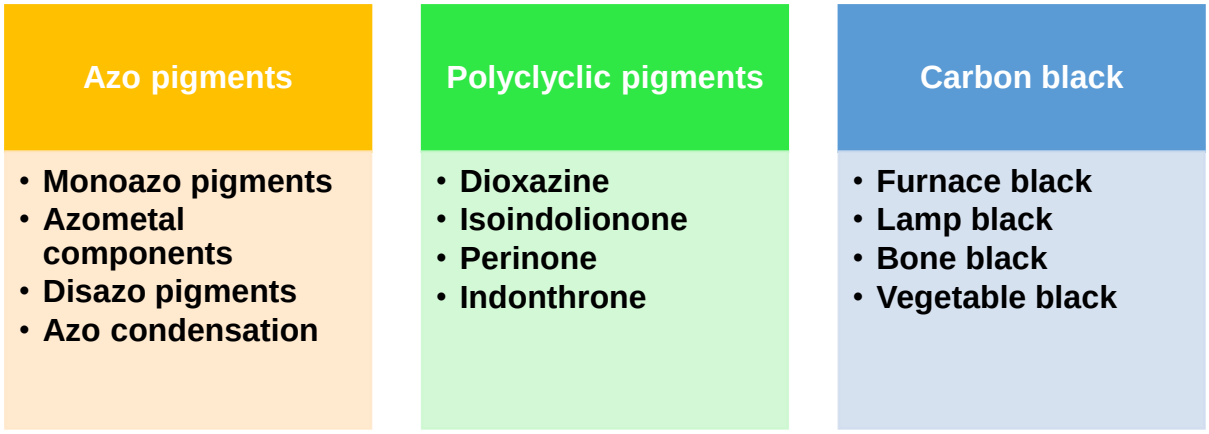

Fig. 2.4.c: Different types of Organic Pigment

Fig. 2.4.c shows the different types of organic pigments and its origin. Carbon black comes from furnace black, lamp black, bone black, vegetable black etc. Polycyclic pigments come from perylene, perinone etc. The source of azo pigment is mono azo pigments, azo metal complexes etc. Edriss et al. stated that dyes are soluble in a polymeric system, but pigments are the particular colorants, which do not dissolve in the resin, but remain essentially unchanged during the processing. Pigments reside as a separate phase, and there are interfacial boundaries to consider, which play a role in the physics of coloration[70]. Naturally occurring inorganic-coloured pigments, prepared from minerals or their combustion products, have been used since prehistoric times. The weathering of minerals and rocks containing iron oxides produces yellow, orange, red, brown, and black pigments. Lead, mercury, arsenic, and copper oxides, sulphides and carbonates produce red, blue, and green colours. Inorganic coloured Pigments (CICPs) were developed in large part for colouring ceramic bodies and glazes and used in glass matrices and porcelain enamels. Different types of synthetic inorganic pigments are described in Fig. 2.4.d. Today they are used extensively in the coloration of plastics and paints, especially when heat and weather resistance are required[70].

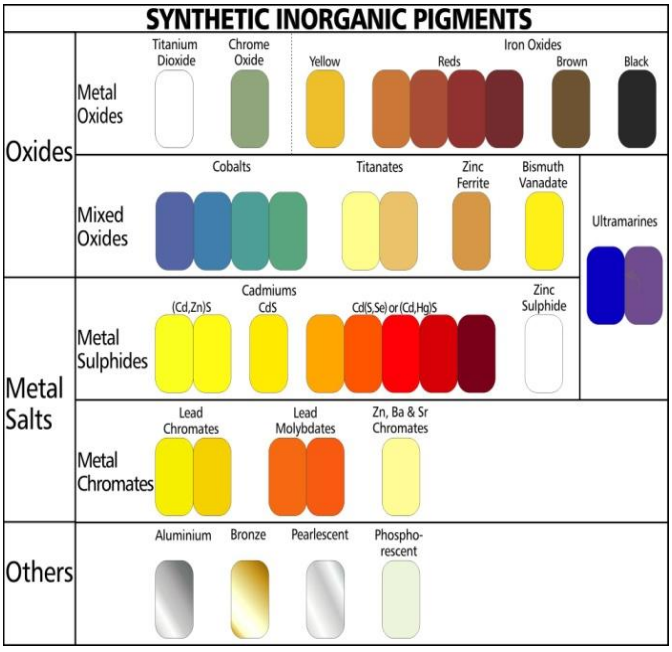

Fig. 2.4.d: Synthetic Inorganic pigments

Pigments not only give the paint its colour and finish, but also protects the substrate from corrosion and weathering as well as helps to hold the paint. Both inorganic Special pigments can be used to give metallic finishes e.g., pearl colours used in cars for higher gloss[71].

2.4.2 Binder/Resin:

Binder/resin is the main ingredient of paints. Binders are polymer resins, which form a continuous film on the substrate surface and give proper adhesion. The binder holds the pigment particles distributed throughout the paint. The binder is dispersed in a carrier i.e., water or organic solvent before using in the paints or coatings. Normally binders used are of four types based on their origin i.e., alkyd resins, epoxy resins, urethane resins and vinyl and acrylic resins i.e., shown in Fig. 2.4.e[52–54].

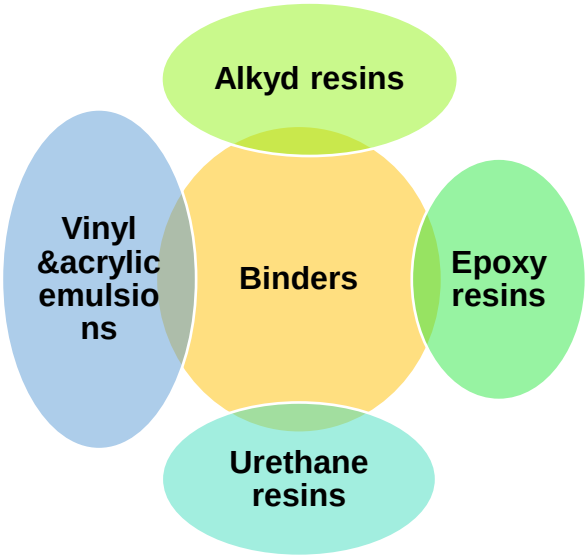

Fig. 2.4.e: Types of binders used in paint

2.4.3 Additive:

Normally most of the paint properties depend on the polymeric resin used and the pigment [74]. In some studies, it is proved that by increasing cross-linking density using higher functionality oligomers and larger amounts of cross-linking agents, paint properties can be improved. In recent studies it is proved that incorporation of nanoparticles in paint matrix can make a huge enhancement in mechanical properties.

The commercial availability of nanoparticles allows researchers to obtain new properties which were unachievable in past[55, 56].

These nanoparticles, which are incorporated into the paint matrix to improve the properties of the paint are called additives. Nano-silica, nano-alumina, nano-silver, nano-clay etc. are the most abundantly used additives in automobile paint industry.

2.5. Important Factors affecting Automobile paint

Factors affecting automobile paint is described in Table 2.c.

Table 2.c: Factors affecting automobile paint

Variable	Parameter
Spray variable	Distance between spray gun and substrate Air spray, Bell Voltage, Spray pressure
Paint variable	Viscosity, Temperature, Paint type, Solid and Nonvolatile materials present
Booth variable	Temperature, Humidity, Air current speed
Movement variable	Conveyer speed, Automobile length
Vehicle variable	Thickness of substrate, Panel temperature

2.5.1 Paint Temperature*:*

Paint temperature is a very important factor in the painting technology. Simon et al. stated that it must be within a particular range while spray painting. Below this value it could not crosslink properly and above this value it becomes brittle. So, it is very important to maintain a proper paint temperature[77].

2.5.2 Paint Viscosity*:*

In automobile paint industry viscosity is a very important property, because it should be perfect. If it is very low the paint cannot flow on the automobile body properly and if it is very high the paint becomes hard and brittle. Proper viscosity could be maintained by adding some thinners in the paint. For thinner materials normally acetone, alcohol and commercial thinners are used[77]. Viscosity can be calculated from shear stress and shear strain following the Equation (2.5)

(ή) Viscosity = (T) shear stress/ (D) shear rate----------(2.5)

Viscosity is expressed in poise or centipoises

2.6. Reasons of Scratch in Automobile paint

Normally the automobile body is made up of steel with some parts made of plastics like rear view. When the automobile body is exposed to dirt, road chips, outer collisions etc., there occur some scratches on the body part. N.R. Whitehouse et al. stated that the most common cause of scratch and abrasion is road salt and dirt. The paint is more prone to scratch when exposed to humidity than the dry environment, as the moisture in environment causes more scratch by binding with the dirt[78]. Another main reason for scratch is accident and cleaning the automobile body with brush.

There are normally five reasons to create scratch in an automobile body

- There is a chance of scratch and abrasion, if there is improper washing of automobile body. If the washing material is improper like rug, it can cause scratch and if the drying is not done perfectly, it also can lead to scratch formation
- If we go for automatic wash, it can also create scratches, the brushes used in automatic wash can easily collect dirt and its sharp end can deteriorate the paint.
- Dirt and road salt is another reason for scratch in automobile body.
- Rubbing the automobile body with sharp objects can also create scratches in the paint

- Accidents are reason, which is mostly responsible for scratch in automobile body.

Fig. 2.6.a describes the various types of scratch and it's the reasons for scratch propagation.

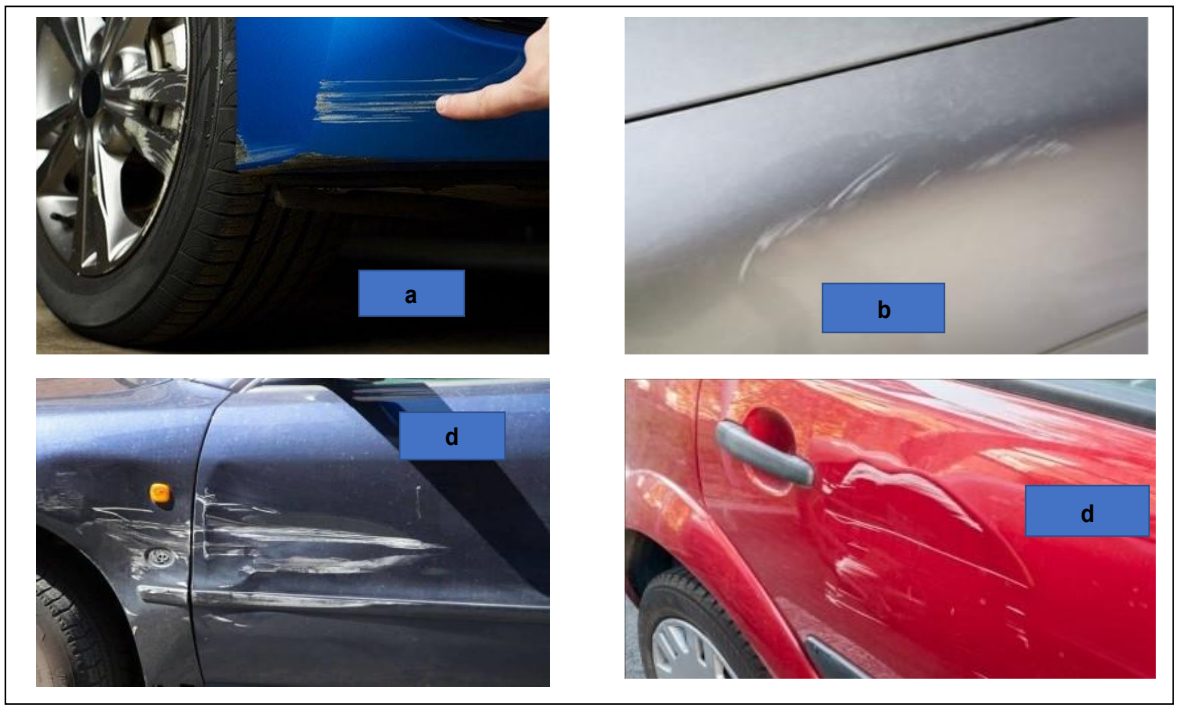

Fig 2.6.a: Automobile scratches occur due to (a) dirt and road salts (b) automatic wash (c) accident (d) rubbing with sharp objects.

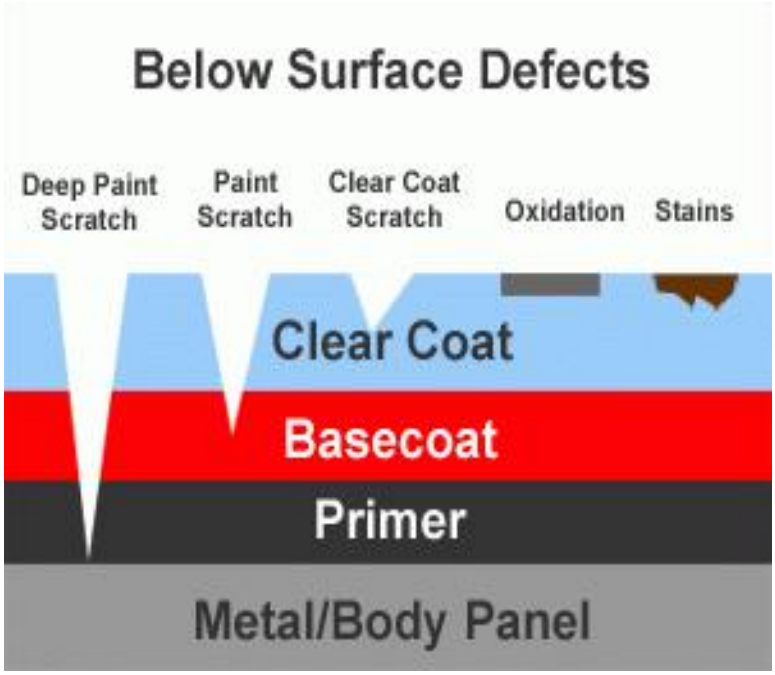

Fig 2.6.b: Types of scratches

According to Fig. 2.6.b, there are five types of scratches i.e.,

2.6.1 Stains:

Stains are known as mars, as these are slight scratches caused by dirt and road salts.

2.6.2 Oxidation:

Oxidation is the type of scratch that occurs due to humidity in the environment. When the moisture content the in environment is very high, it tries to make oxide of the outer body part, which leads to scratches.

2.6.3 Clear coat scratch:

If the scratch is only on the upper most transparent layer of the paint it is known as a clear coat scratch and it is very easy to remove by treatment.

2.6.4 Paint scratch:

If the scratch is on both the clear coat and paint coat, it is known as paint scratch. It is not considered as minor scratch.

2.6.5 Deep paint scratch:

When the scratch is very severe and the steel part of the body is visible, it is known as a deep scratch. Here the scratch is on all three layers of paint i.e., primer, basecoat and clear coat.

2.7. Scratch and Abrasion resistance improvement of Automobile paint

Roger et al. stated that, the advancement of nanotechnology developed a wide range of applications resulting in improved mechanical properties, thermal stability, UV resistance, chemical and solvent resistance, and better optical properties in coating industries[79]. The nanoparticles in general are incorporated as additives in the paint matrix. Nanoparticles like nano-silica, nano-alumina, nano-zirconia and nano-titania are used in property enhancement of paints. Nanoparticles are incorporated into the paint matrix by using the following processes.

- High-speed stirring
- Dispersion
- In-situ polymerization
- Sol-gel process

High speed stirring: In this process the polymer matrix was stirred at very high speed and during the stirring process, the nanoparticles are added gradually to it along with some solvents. In another process the nanoparticles are added to solvent in a high-speed stirrer and then the solution was added to the polymer matrix[80].

Dispersion: In this process the nanoparticles are added to the polymer matrix by ultrasonication dispersion method, which results in proper homogenization of nanoparticles into the polymer matrix[80].

In-situ polymerization: In this process nanoparticles are first dispersed in the liquid monomer and form a homogeneous mixture. Then the polymerization reaction was initiated by addition of suitable initiator. After complete polymerization, nanocomposite is synthesized having nanoparticles attached to the polymer matrix[81].

Sol-gel process: This process is a wet chemical process which is also known as chemical solution deposition. This process follows a number of steps like hydrolysis, polycondensation, gelation, aging, drying, densification and crystallization. This process forms an inorganic colloidal suspension i.e., sol and gelation of the sol in a continuous liquid phase i.e., gel to form a three-dimensional network structure[82].

2.7.1 Scratch resistance improvement of Paint by using Polydimethylsiloxane (PDMS):

PDMS has silicon particles, which increases corrosion, scratch and water resistance properties of the paint. It has a unique chemical structure i.e., siloxane having Si-O-Si group. Eduok et al. stated that, it has low glass transition temperature and also has siloxane group, which makes it more preferable over simple silanes[83]. It is mostly used in coating for anti-fouling and anti-microbial properties and has weak intermolecular forces between the particles.

Simple flame treatment methods are used to prepare micro/nano size of PDMS. For flame source wipe papers soaked with ethanol are taken and the reaction temperature range is within 700±20 °C. After 30 sec of flame treatment a flower petal nanoparticle is formed, which is divided into three patterns according to their structure i.e., flat PDMS, square pillar pattern PDMS and rectangular ridge PDMS pattern[84]. X. Xue et al. stated that these different patterns of PDMS matrix increases its roughness, attributing to the hydrophobicity and scratch resistance properties of the paint substrate[85].

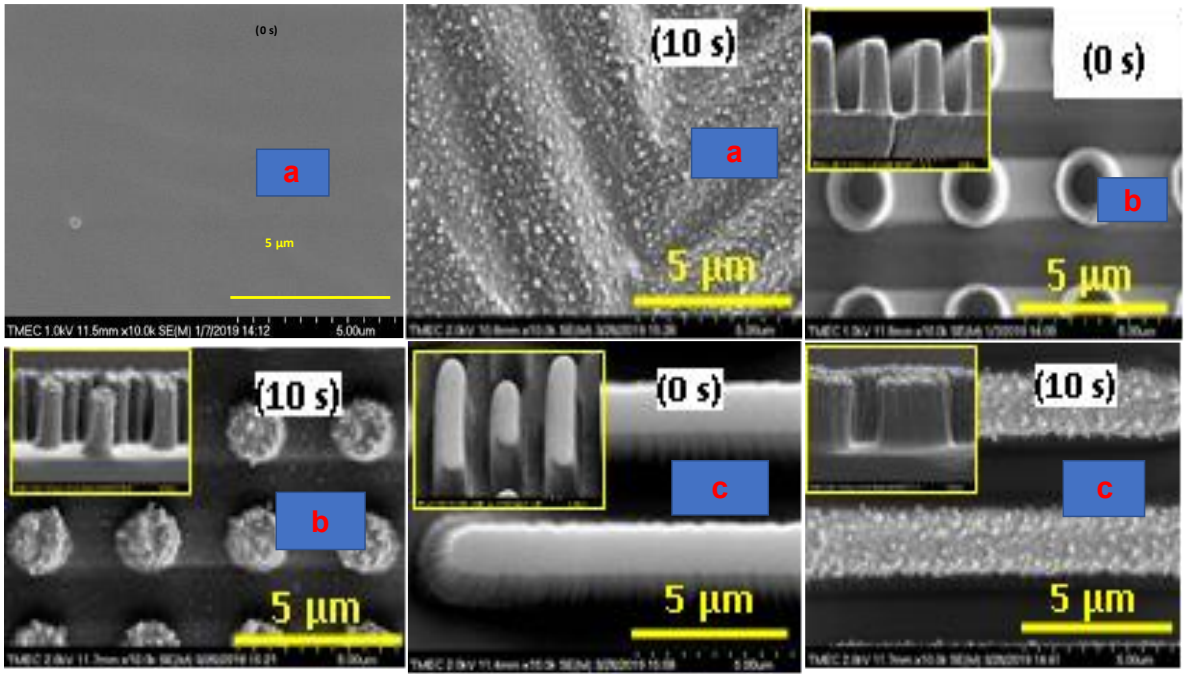

Fig 2.7.a: SEM image after flame treatment for 0s, 10s a) Flat- PDMS, b) Square pillar pattern PDMS, c) Rectangular ridge PDMS. Copyrights reserved from ELSEVIER[84]

From the Fig. 2.7.a, it was found that the surface roughness of the PDMS increases with increasing the flame treatment time. According to Hossenzadeh et al. this increase in roughness of the surface increases the hardness and water repellency capacity of the surface. It was also found that there is more surface roughness in square pillar pattern and rectangular pattern than the flat PDMS structure. Most of the super hydrophobic paint are water repellant but are not resistant to some oils or other organic components, so now the researchers are trying to develop super oleophobic paint[86]. PDMS is mainly used for the hydrophobicity properties, to enhance it to oleophilicity[87].

D.Lv.et al. stated that PDMS can also be used in the modification of PU/Ag composite coating, which results in super hydrophobic and low infrared emissive paint. In this experiment PU considered as resin, Ag powder as modifier and PDMS as pigment[88].From the experiment it is concluded that, the ratio of Ag powder and silica particle of PDMS determines the hydrophobicity of the coating. At ratio 6:4, optimum hydrophobicity and self-cleaning properties are achieved. At this particular ratio the water contact angle of the coating is 151 ° and the sliding angle is 9 °[89].

W. Zhang et al. stated that PDMS can be used in modification of PU and aluminium composite coating to achieve super hydrophobicity and low infrared emissivity[90]. From the result it is found that when the curing temperature is 80 °C, the coating has lowest infrared emissivity and gloss and with addition of aluminium particle increased the water contact angle of the coating up to 117 °. The ratio of aluminium to silica particles of PDMS normally determines the hydrophobicity and self-cleaning capability of a coating.

Super hydrophobic paint

Super hydrophobic means the material which is highly water repellent. Xue et al. stated that super hydrophobic surface is normally prepared by roughening the surface with low surface energy or by chemical modification. In most of the cases silicon or PDMS are used for hydrophobicity purpose.

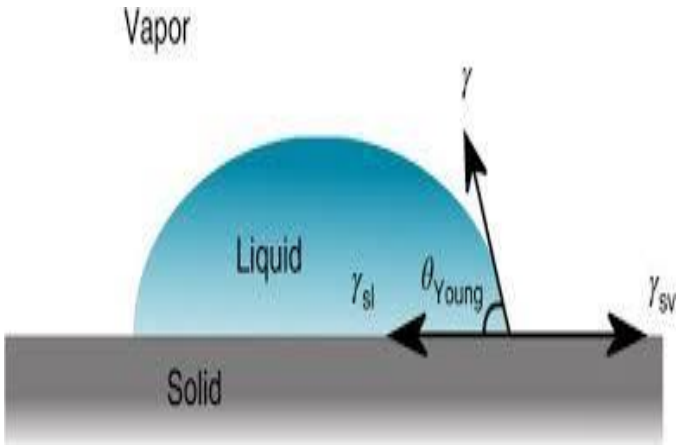

Fig 2.7.b: Image of contact angle of a substrate

The hydrophobicity is measured from the contact angle that water forms with the coating surface. It is measured from the angle the water droplet creates when it touches the surface. Fig. 2.7.b shows the contact angle forms at the solid and liquid-vapor interface. The formula of contact angle is derived from Equation (2.7.a)

$$\frac{\gamma SV-\gamma SL}{\gamma LV} = cos\theta \text{----------(2.7.a)}$$

Where θ is the contact angle

γSV is solid surface tension

γLV is liquid surface tension

γSL is solid and liquid boundary tension.

Contact angle is measured by the instrument, goneometer. If it is between 0-90 ° the surface is considered to be hydrophilic, but for hydrophobic surface the WCA must be greater than 90 ° and its limit is up to180 degree. For super hydrophobic surface it should be more than 120 °.

J. Riberio et al. stated that the roughness of the surface helps in formation of super hydrophobic layer of coating[91]. M. A. Alam et al. stated that in case of automobile body surface is a very important part. The scratches that occur on the body very much depend on the type of substrate used for painting[91]. If the surface is hydrophobic there is less chance of scratch formation. The hydrophobicity is measured from the contact angle, water forms with the surface. The characteristics of surface like wetting, de-wetting and adhesion also can be determined from the contact angle.

2.7.2 Scratch resistance improvement by nano-silica (NS)

F. L. King et al. stated the most used polymer for automobile paint is PU. It has unique properties like excellent transparency, very good mechanical strength, and chemical resistance[92]. To further improve the properties of paint some inorganic nanoparticles are incorporated into it. The nanoparticle additives help to prevent micro cracks, cavities, and scratch and abrasion[92]. The most common failure mechanism occurs in paint is scratch, abrasion, and improper adhesion. To overcome these problems nano-additives are added to it. Among the nano additives, NS is one of the mostly used materials. F. Fallah et al. stated that NS particles can significantly enhance the performance of paint by increasing its mechanical strength and durability. It was observed that addition of NS particles into the paint matrix improved its mechanical, thermal, chemical and optical properties[93]. F. Velasco et al. stated that NS particles are non-toxic, optically transparent and chemically inert[94]. Silica has anti reflective

properties which help in energy conservation. The polymer matrix normally used in paint industry for NS incorporation are PU, epoxy, acrylic and alkyds.

Epoxy polymer matrix: Epoxy is considered as a high-performance coating material in the chemical industries. Epoxy matrix with low viscosity is mostly preferred to achieve excellent adhesion to the surface. Incorporating NS particles into the epoxy matrix, increased its mechanical properties significantly. Rasha et al. stated that the properties of nanocomposite depend on the particle size, particle shape and degree of dispersion of nanoparticles. Nanoparticle can be incorporated into the paint matrix by employing the following processes, i.e., high speed stirring, high energy processing, ultrasonication, in-situ polymerization etc. The NS particles reinforced in epoxy matrix is normally ranges from 5-75 nm in size. NS additives are used to improve the abrasion resistance, wetting properties, corrosion resistance, thermal properties and mechanical properties of the epoxy matrix[95].

PU-based polymer matrix: PU is the most common polymer matrix used in paint industries due to its excellent transparency, weathering stability, higher mechanical strength and chemical resistance. Some different microstructures are developed due to reinforcement of nanoparticles in the matrix, which prevents the propagation of cracks resulting in improved mechanical properties. According to Mallaki et al. normally precipitated silica of size 8-15 nm and fumed silica of size 7-12 nm are preferred to be used as nano additives. The dispersibility and mechanical properties enhance significantly by addition of NS additives. By incorporating NS particles erosion resistance, hardness, mar resistance and the transparency of the PU paint improve significantly[96]. The NS particles are reinforced in different processes like blending, high-speed stirring or in-situ polymerization.

Acrylic based Polymer matrix: Acrylic paints are modified by NS particles to achieve transparent, non-yellowing and chemically stable paint. Incorporation of NS particles in acrylic paint enhances the corrosion resistance and scratch resistance properties. Rahimi et al. stated that the NS particles are developed by sol-gel process from methyl-ethoxy-silane. The NS reinforced acrylic paint is achieved by emulsion polymerization process. The particle size of NS ranges from 5-100 nm[97].

Alkyd based Polymer matrix: Alkyds are normally used in exterior coating industry. These are known as thermosetting polyesters and are synthesized by condensation reaction of polyhydroxy alcohols and acid anhydrides. These are then modified with triglycerides. Anand et al. stated that the unsaturated triglycerides help them in cross-linking and curing through auto-oxidation. Addition of NS particles makes the auto oxidation process faster. Additionally, they also increase the stiffness, hardness and abrasion resistance properties of the paint. Normally colloidal NS particles with high concentration are preferred for alkyd paint. The NS particles increase the cross-linking density of the paint[98]. Particle size of NS used in alkyd matrix ranges from 30-500 nm. Incorporation of NS particles into alkyd matrix is done by reflux condensation process.

I. Rehman et al. stated silica nanoparticles can be synthesized by two main processes i.e. top-down and bottom-up. Top-down is the method by which the size of NS can be reduced in dimension by physical approach. In bottom-up or chemical approach process a common route is used to synthesize NS particles from atomic or molecular scale. Rahman et al. stated that the methods mostly used in bottom-up process are sol-gel process, reverse micro-emulsion, and flame synthesis process. Sol-gel process is the most widely used method to produce pure silica particles due to its ability to control the particle size, size distribution and morphology through systematic monitoring of reaction parameters[99]. In reverse micro-emulsion, the surfactants molecules dissolved in organic solvents forms spherical micelles. The polar head groups which are known as reverse micelles make themselves micro-cavities to contain water in the presence of water particles. The NS particles are grown inside the micro-cavities. The major drawbacks of the reverse micro-emulsion approach are high cost and difficulties in removal of surfactants in the final products. NS particles can also be produced through high temperature flame decomposition of metal-organic precursors. This process is also referred to as chemical vapor condensation (CVC). In a typical CVC process, NS particles are produced by reacting silicon tetrachloride with hydrogen and oxygen. The drawbacks of this process are difficulty in controlling the particle size, morphology, and phase composition. Sol-gel process is widely used to produce NS particles due to its ability to form pure and homogenous products at mild conditions. The process involves hydrolysis and condensation of metal alkoxides (Si

$(OR)_4$) such as tetraethyl orthosilicate (TEOS, Si $(OC2H_5)_4$) or inorganic salts such as sodium silicate (Na_2SiO_3) in the presence of mineral acid e.g., HCl or base e.g., NH_3 as catalyst. The hydrolysis of TEOS molecules forms silanol groups. The condensation/polymerization between the silanol groups and ethoxy groups creates siloxane bridges (Si–O–Si) that form entire silica structure. The formation of silica particles can be divided into two stages: nucleation and growth. M. Alghdeir et al. stated that among all the wt.% of NS i.e., 0.5, 1, 2.5, 5 and 7.5, the coating with 1 wt.% of NS was optimized. From the Stress-strain curves, it was observed that the stress at break gradually increases with the increase of NS wt.% up to 1 wt.%. This result reveals that, NS particles would reinforce stress and cause the increase of the tensile strength of the nanocomposite. Beyond 1 wt.%, it was observed that the values of both the tensile strength and elongation at break of the nano composite decrease with the increase in the NS particle[100].

NS is amorphous in nature and is available in 3 forms i.e., precipitated form, fumed form and colloidal form. Scratch resistance is a very important property of automobile paint, as it affects the optical stability, mechanical properties and corrosion resistance of the paint. Malaki and co-workers have worked on the scratch resistance properties of NS-PU nanocomposite. In their work they had taken 2, 4 and 6 wt.% of both fumed and precipitated NS incorporated PU paint matrix for study. Fig. 2.7.c and 2.7.d shows the SEM images of PU paints with both fumed and precipitated silica.

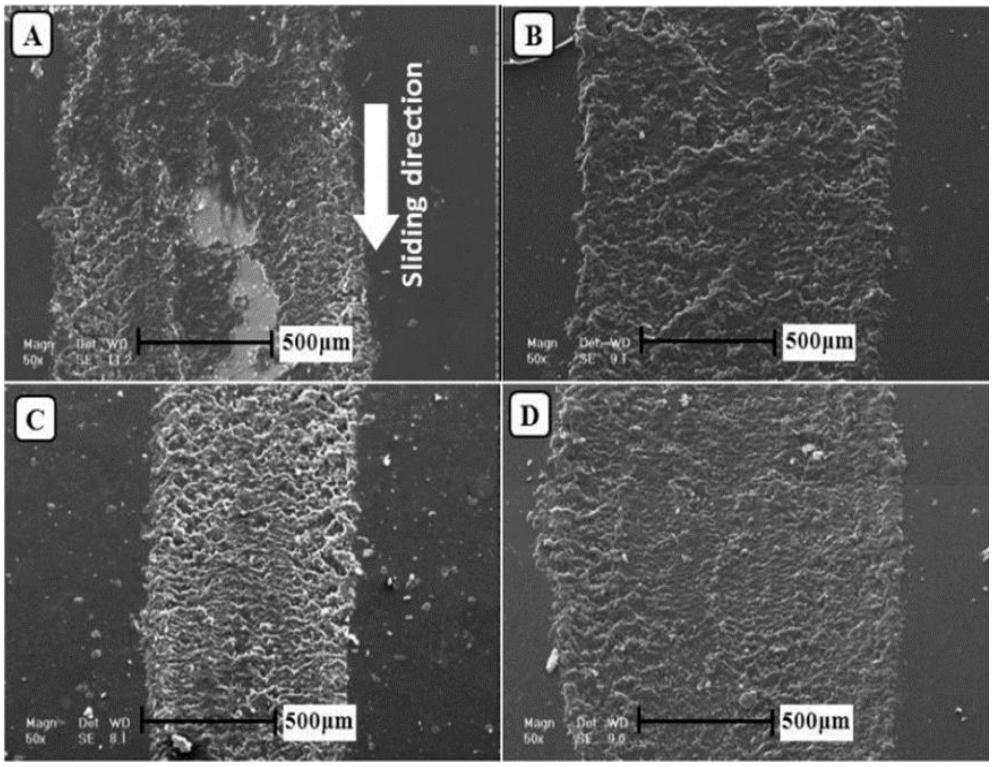

Fig 2.7.c: SEM images of abraded fumed nano-silica clear coats; (a) PU, (b) FS2, (c) FS4 (d) FS6. Applied force is 2.5 N. Copy rights reserved from ELSVIER[96]

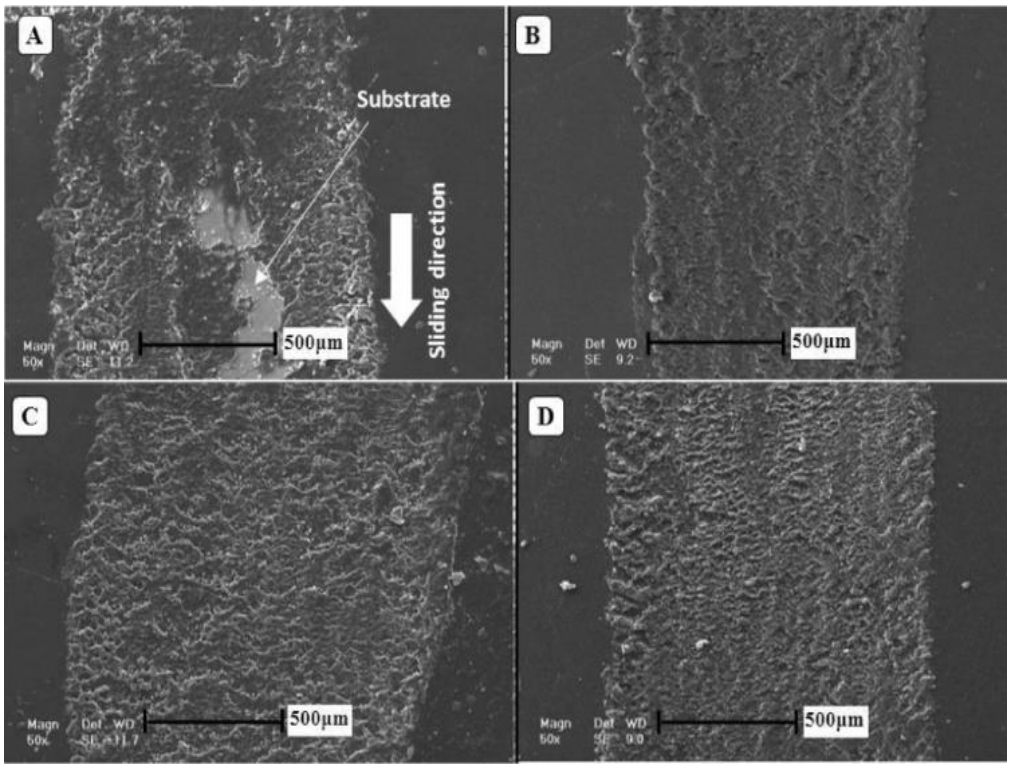

Fig 2.7.d: SEM image of abraded nano silica clear coats a) PU (b) PU2S (c) PU4S (d) PU6S. Copyrights reserved from ELSEVIER[96].

X. Shi et al. stated that NS has high value of toughness, which makes it highly scratch resistive[101]. It increases the interfacial adhesion, which leads to increase in toughness of the paint. Due to increment in toughness property of the paint, naturally the scratch resistance characteristic increases significantly. From the above figures, the SEM images of substrate without NS and with different wt.% of NS, it was studied that the scratch resistance of the paint increases with remarkable percentage with addition of NS in both fumed form and precipitate form. Here FS is for fumed NS and PS is for precipitated NS.

S. Das et al. stated that by reinforcing NS in neat PU paint, its scratch resistance increased from 65% to 88% and abrasion resistance increased by 25%[102]. According to Z. Ling and L. Chungzhong et al. the scratch resistance of paint improved to 73.3% from 49% by inducing NS particles in to it. Moreover, the nanoparticle reinforced paint exhibited an excellent transmittance of 91%, pencil hardness of 3H and a superior hardness of nano-indentation test (HIT), which is 58.3% higher than pure coating[103]. Y. Wang et al. stated that the indentation depth in nano-indentation test decreased from 1167 nm to 1069 nm by inducing NS in the paint[104]. The NS particle has Si-O-Si linkage, which increases the cross-linking density of the matrix when reinforced into the paint matrix. This increased cross-linking density leads to scratch and abrasion resistance properties of the paint.

Functionalization of NS

Aminopropyl-triethoxy-silane (APTES) is normally used as a functionalizing agent for its two dimensional character, where the ethoxy groups of APTES react with hydroxyl groups of silica forming siloxane (Si-O-Si) linkages, and the amino group extending from the surface, which acts as a link of attachment with other chemicals by nucleophilic substitution reaction. Hence, this can be used as a substitute of aromatic ring. This property of APTES makes it the best reagent for NS functionalization as it increases the functionality of the base chemical and also increases the bonding or linkage capacity of nano silica[105].

M. Mohammadi et al. stated that in this process the NS particles are added with APTES and dissolved in toluene or any suitable solvent and then after proper mixing, it is centrifuged and then dried. After drying the final product is known as the modified

nano-silica[106]. It can be determined from FTIR, XRD or TEM. Functionalization of NS can also be carried out by using bis[3- (triethoxy-silyl) propyl] tetra sulphide (Si_{69}). K. Yu et al. stated that the functionalization process is governed by mixing of water and subsequent rapid drying with a hot gas[107]. In this process the Si_{69} hydrolysate was formed. Then it is collected in low concentration and thoroughly mixed with NS with the help of microinjection. Thus, resulting in increased hydrolysate grafting density on the surface of NS particles and dispersibilities characteristic of this functionalized NS increases significantly. Unmodified NS normally exhibits a strong polarity, as it has higher amount of silanol particle, which can easily cause agglomeration and inhomogeneous dispersion. Surface modification of NS particle is an efficient technique to increase the dispersibility and other physical and chemical properties[108]. Si_{69} is the most commonly used silane coupling agents. The functionalized NS formed with the help of Si69 is normally in three forms 1) particle silica, 2) fumed silica, 3) colloidal silica[109].

2.7.3 Scratch and Abrasion resistance improvement by Nano Alumina

P. Nguyen et al. stated that alumina nanoparticles are considered as one of the best nano-additives used to enhance significant properties like scratch and abrasion resistance of the paint surface[110]. S. T. Aruna stated that nano-alumina has special properties like high mechanical and high thermal resistance; it is low cost and can help in developing super hydrophobic surfaces[111]. L. Chen et al. stated that nano-alumina is easily available and is cost effective. Alumina nanoparticles can improve hardness without affecting the transparency and brightness of a composite coating[112]. The increase in hardness leads to increase in erosion, corrosion and wear resistance of the paint. S. K. Dhoke et al. stated that incorporation of nano-alumina can improve the corrosion resistance, UV resistance, and mechanical properties without affecting optical clarity of the paint[113]. Incorporation of nano-alumina particles into the polymer matrix enhances the anti-scratch and mar property. Alumina and silica nanoparticles were found to enhance the glass transition temperature of paints by hindering the mobility of macromolecular chains at the interface around the nanoparticles. S. K. Dhoke et al. have taken three different wt.% of nano-alumina additives i.e., 0.1, 0.2 and 0.3 wt.%. From the results it was observed that, the mechanical properties increased gradually with increase in additive wt.%. O.

M. Yusori et al. has taken four different wt.% of nano-alumina i.e., 0.25%, 0.5%, 0.75% and 1%. The flexural properties were found to increase by 7% by addition of 0.25% nano-alumina. But further increase in additive decreased the flexural property due to agglomeration and the same results were observed in hardness property[114].

The polymer matrixes used in paint industry to reinforce nano-alumina are PU, epoxy, acrylic and alkyds.

Epoxy based polymer matrix: Epoxy is a thermosetting polymer applicable in various fields due to its significant properties like excellent chemical and solvent resistance properties, toughness, low shrinkage, resistance to corrosion, and improved mechanical properties. But this resin also has some drawbacks like polar properties and having high surface energy, which makes its application limited and also unsuitable for anti-fouling, self-cleaning and water proof coatings. To develop the super hydrophobic epoxy paint, nano-alumina was applied to the epoxy coating by bi-layer method, where the nano-alumina particle suspension was deposited or sprayed on the neat epoxy paint. The nano-alumina particle used has size range from 5-15 nm[114].

PU-based polymer matrix: PU-based polymer paint has significant characteristics like toughness and flexibility, excellent chemical and solvent resistance, good adhesion and good thermal properties. S. K. Dhoke et al. stated that nano-alumina is a harder material and by adding it into the PU matrix, the hardness and mar resistance of the coating surface increases significantly. Nano-alumina particles are incorporated into the PU matrix either by ultrasonic probe dispersion process or high-speed stirring process. The particle size ranges from 20-60 nm[113].

Acrylic based polymer matrix: Acrylic based polymer is normally used as water proof paints. This paint has special characteristics like, excellent hydrophobicity, good thermal properties and mechanical properties. R. Zhang et al. stated that by adding nano-alumina particles of 4-60 nm size, the microstructure and macrostructure changes, which leads to excellent scratch resistance properties. The method used for nano-alumina insertion is high speed stirring, in-situ polymerization and ultrasonic dispersion[115].

Alkyd based polymer matrix: Alkyd is a polyester resin derived from polyols and organic acids. These are used for paints varnishes and moulds for casting. By adding nano-alumina of size 30-300 nm range the corrosion resistance, UV resistance and mechanical properties are found to be improved. The nanoparticles are added to the polymer matrix by sol-gel method, in-situ polymerization or ultrasonication process.

Nanoparticles normally give their best properties, when functionalized properly. In most of the studies the alumina nanoparticles are functionalized with the help of silane coupling agents. W. Shatty et. al. stated that nano-alumina particles can be functionalized with the help of stearic acid, and the coating layer obtained by using this functionalized nano-alumina becomes super hydrophobic having contact angle around 130 °[116]. The use of highly branched carboxylic acids in functionalization of alumina nanoparticles, leads to the increase in water contact angle of the paint surface up to 155 °[113].

According to F. Ahmad et al. hardness of alumina on the Mohs scale is 9, so it is a relatively harder material and mostly used to maximize the hardness properties of paints[117]. S. Said et al.. have stated that the fire resistance of paint could increase tremendously by incorporating nano-alumina particles in the paint matrix[118]. From this study it was found that, the nano-alumina reinforced paint can withstand temperature up to 800 °C for 2 hrs. in the furnace and the fire resistance increase is about 45%.

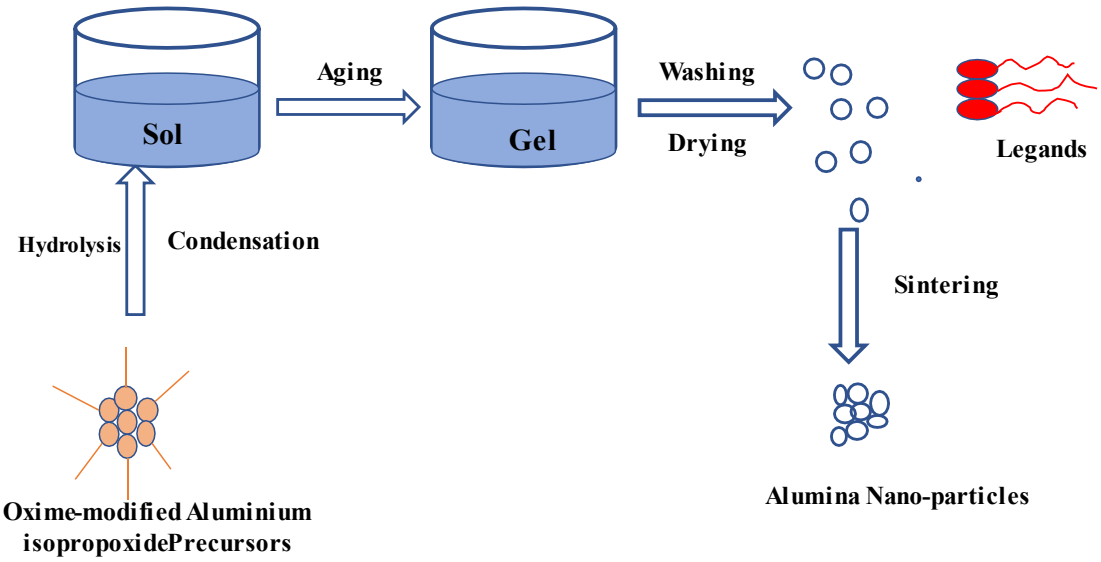

Fig 2.7.e: Synthesis of Nano-alumina through sol-gel method.

Alumina nanoparticles can be synthesized by many techniques like ball milling, sol-gel process, pyrolysis, sputtering, hydrothermal, and laser ablation. Among them, the laser ablation and sol-gel process are widely used technique for the synthesis of nanoparticles. From the Fig. 2.7.e it was found that, the oxime modified aluminium isopropoxide precursors are undergone through hydrolysis and condensation process to form sol. Then, it is aged to form the gel and then washed and dried to form ligands. These ligands undergo sintering process to produce aluminium nanoparticles[119]. Alumina nanoparticles are functionalized by using either toluene or 2-propanol. S. Swain et al.. Stated that nano-alumina can be functionalized by the carboxylation process, in which nano-alumina particles are added with stearic acid and then refluxed with either toluene or 2-propanol, then centrifuged, washed and dried to get the functionalized nano-alumina particles[120]. The extent of functionalization can be obtained by the Thermogravimetric analysis (TGA) curves.

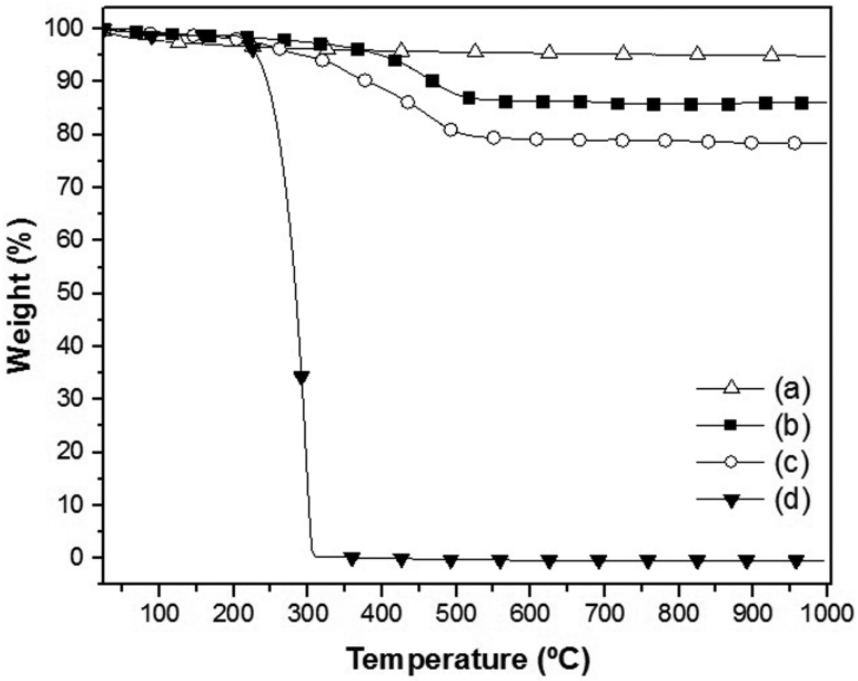

Fig 2.7.f: TGA analysis of (a) Non functionalized alumina; functionalized alumina particles: (b) Al-T_I (c) Al-P and (d) Pure stearic acid. Copy rights reserved from ELSVIER[120].

From the Fig. 2.7.f it was found that, the temperature range taken was 1000 °C. The toluene and propanol functionalized alumina nanoparticles started to lose weight at around 400 °C and 300 °C, respectively. This starting temperature range of weight loss temperature is very high in comparison to pure stearic acid. From the TGA curve it was found that, stearic acid incorporation in alumina is 14% for Al-T and 22% for Al-P. Thus, it was found that 2-propanol is the better option to get nano-alumina to be functionalized. From the study it was found that, by infusion of nano-additive like alumina or silica, there is significant increase of thermal as well mechanical properties of paint. From the study it was found that the tensile strength of PU matrix is increased around 50% and 41% by infusing 1wt.% of nano-alumina and NS respectively. But the nanoparticles addition more than 3 wt.% causes agglomeration[121].

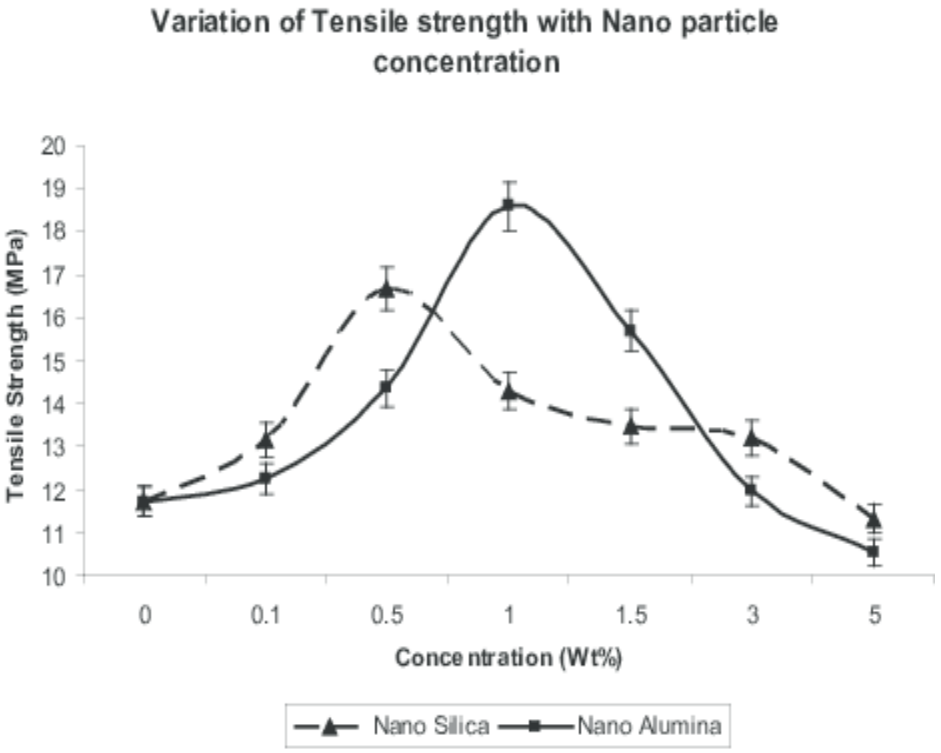

Fig 2.7.g: Variation of tensile strength with nano particle concentration. Copy rights taken from Research gate[120].

From the Fig. 2.7.g it was found that the tensile strength of the matrix increases continuously with increase in concentration of nanoparticles up to a yield point. But after that with addition of nanoparticles the tensile strength decreases. In this study it was found that the NS particles have a better tensile strength at lower concentration (from 0.1 wt.% to 0.5 wt.%), in comparison to nano-alumina at the same concentration, but above 1 wt.% of nanoparticle addition nano-alumina has higher tensile strength than NS. There is no agglomeration at this concentration for nano-alumina, due to its lower surface area in comparison to NS. With further increase in the concentration, there is decrease in the tensile strength value for both the composites, due to agglomeration of the nanoparticles in the polymer matrix.

W. Su et al. stated that by reinforcing 0.5 wt.% of nano-alumina in to the matrix, the hardness increased from 1620 HV_{30} to 1760 HV_{30}, the rupture strength increased from 2135 MPa to 2728 MPa and fracture toughness increased from 11.8 to 12.95 $MPa.m^{1/2}$[122]. Alumina nanoparticles have hardness 9 in Moh 's scale. When these particles are reinforced into the polymer matrix, they automatically increase the cross-

linking density by creating a strong bond between the polymer matrix and alumina particles, which results in enhancement of strength and mechanical properties. This leads to improvement in scratch and abrasion resistance. Aluminium naturally generates a protective thin oxide coating which keeps the metal from making further contact with the environment. It is particularly useful for applications where it is exposed to corroding agents.

2.7.4 Scratch and Abrasion Resistance improvement by incorporation of Zinc nanoparticles (Zirconia)

Zirconia is considered as a very good choice for UV-protection of paint and coating. L. F. Sturd et al. stated that zirconia nanoparticles have unique properties like corrosion resistant, fungus resistant, photochemical, catalytic, and bacteria resistant, UV resistant etc.[123]. N. Wint et al.. stated that zirconia is used as a filler material as well as a pigment to get the white colour in the paint[124]. Zirconia is considered as the stiffest material among the fillers used in paint. So, the paint containing zirconia has very high value of hardness compared to paints containing other nano-fillers. But the problem is that sometimes very high hardness causes brittleness in paint. J. Abenojar et al. stated that zirconia nanoparticles can develop excellent properties like strength, fracture toughness, wear resistance, chemical resistance, and hardness of a paint. In recent researches zirconia nanoparticles are found to be corrosion inhibitor, so used in metal substrates to prevent corrosion. In some researches it was found that zirconia is both corrosion and thermal resistive[125]. Nano-scale zirconia shows improved mechanical characteristics and superior biocompatibility. A. Adreans et al. stated that Zinc is widely used as a protective coating to prevent corrosion of steel. Zinc is more electronegative than iron, and hence offers anodic sacrifice protection to steel in corrosive media[126]. It is a material of great technological importance, having good natural colour, high strength, transformation toughness, high chemical stability, excellent corrosion resisting material, and chemical and microbial resistance. Magnesium has very good corrosion resistive properties, so in recent studies they are used as protective coatings for steel. When this magnesium makes an alloy with the zirconia, it creates a protective paint against corrosion. Zinc-based paints are rich in zinc metal pigments i.e., around 90%, which creates a metallic zinc film to act as a barrier for outer forces and impurities and it acts as a cathodic protection layer for the

substrate. This type of paint is considered as the best anti corrosive paint. The main application of zinc-based paint is the protection of industrial units like, steel infrastructure, pipe lines, wind mills etc. These are also used in marine industry for antifouling and anti-corrosive paint in ships.

The polymer matrixes used for zirconia nano particles reinforcement in paint industry are epoxy, PU, acrylic and alkyds.

Epoxy based polymer matrix: Epoxy polymer matrix are used to prepare corrosion resistive coating due to its good adhesion properties. According to M. A. Atta et al. this has high brittleness and less crack resistance properties, which results in formation of micro cracks and affects the adhesion properties. The zirconia nanoparticles reinforced in the epoxy matrix increases the adhesion properties of the coating. It also increases the toughness, mechanical properties and thermal properties of the epoxy coating. Size of nanoparticle used in epoxy coating ranges from 10-40 nm. Sol-gel method is used to disperse zirconia nanoparticle into epoxy matrix[127].

PU based polymer matrix: PU is considered as most versatile coating material. By adding zirconia nanoparticles into the PU matrix, the absorption and emissivity coefficient of the paint increases significantly. Zirconia was added to the matrix by either high-speed stirring or ultrasonication process. The particle size is up to 100 nm[128].

Acrylic based polymer matrix: Acrylic based matrix is normally used in protection coating and applied on the top layer of the paint. Zirconia nanoparticles reinforced to the matrix increases its transverse strength and mechanical properties. The reinforcement of nanoparticles in the matrix can be obtained by following methods like high-speed mixing and ultrasonication process. The size of the nano particle is up to 100 nm[129].

Alkyd based polymer matrix: Alkyds have broad range of commercial application. L. Hammad et al. stated that when nanoparticles are incorporated into the alkyd resin, they enhance the paint characteristics. If zirconia nanoparticles are added into the alkyd resin, they significantly increase the catalyst and corrosion resistance of the

matrix. The particle size is around 1-2 µm and is added to the polymer matrix by high-speed dispersion process[130].

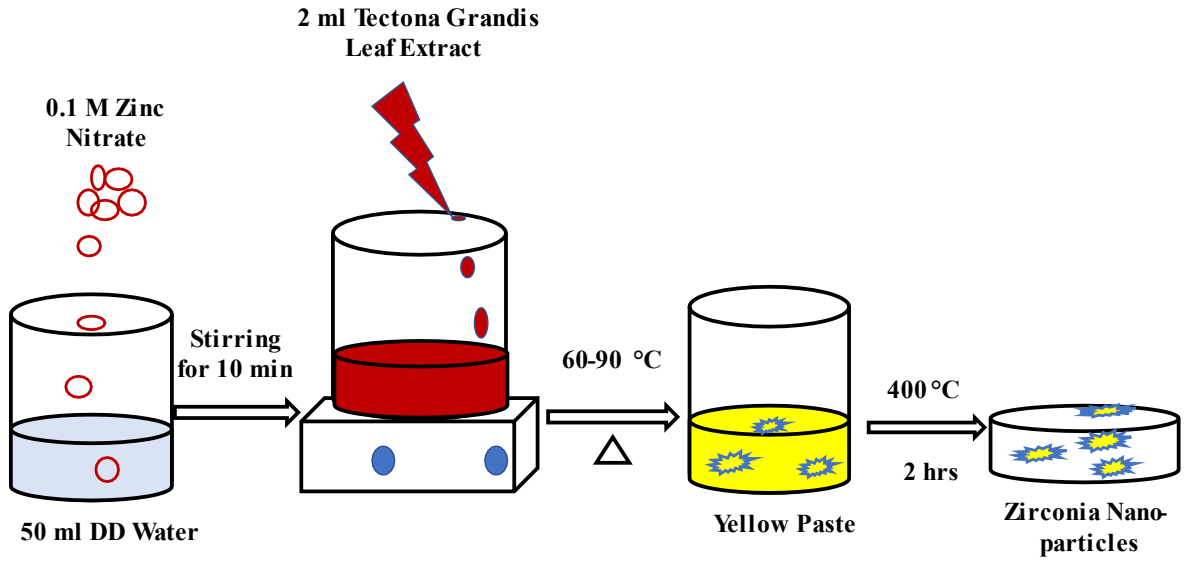

Fig 2.7.h: Synthesis of zinc oxide nano particles.

Fig. 2.7.h shows the synthesis of zirconia nanoparticles. There is a number of synthesis processes to produce zirconia nanoparticles such as sol-gel method, vapor phase method, pyrolysis, spray pyrolysis, hydrolysis, hydrothermal, and microwave plasma. However, these methods have many drawbacks like complicated procedures, high reaction temperature, extended reaction time, toxic reagents and by-products and high cost of production. Senthilkumar and co-workers have studied about the synthesis of zirconia nanoparticles in a new process[131]. In their work 0.1 M zinc nitrate is taken as the precursor, which is dissolved in distilled water and stirred for 10 mins. Then extract of a particular leaf i.e., Tectona grandis (L) is added to the precursor, which acts as reducing agent and the stirring continues at 60-90 ºC. When a yellow colour paste is obtained, it is dried at 400 ºC for 2 hrs. to get the zirconia nanoparticles[131].

R. Suriano et al. stated that by reinforcing zirconia nanoparticles in hybrid coatings synthesized from sol-gel method, the pencil hardness increased from F to 4H for glass substrate and 6B to HB for polycarbonate substrate. Maximum indentation decreased

from 155 nm to 31 nm[132]. P. F. He et al. stated that the scratch resistance of zirconia reinforced paint was increased by 38.6% in comparison to the non-reinforced paint, which proves that zirconia nanoparticles play a great role in enhancing the scratch and abrasion resistance of a paint124]. When zirconia nanoparticles are reinforced in a polymer matrix, they create a bond with the polymer matrix which acts as protective layer against the mechanical damages. This results in improvement in scratch and abrasion resistance. At room temperature zirconium exhibits a hexagonally close-packed crystal structure, α-Zr, which changes to β-Zr, a body-centered cubic crystal structure, at 863 °C. Zirconium exists in the β-phase until the melting point. It has an exceptional fracture toughness and chemical resistance, especially in its cubic form. These properties make it useful as a thermal barrier in paints. B. S. Hadavand et al. have taken three different wt.% of zirconia nanoparticles in paint application i.e., 0.1%, 0.3% and 0.5%. From the all the analysis it was observed that the optimum result was found at 0.5 wt.%. When the nanoparticle amount was increased above 0.5% agglomeration and reduction in properties of the paint was observed[134].

2.7.5 Titanium dioxide particles reinforced paint

S. B. Torun et al.. stated that antimony trioxide along with titanium dioxide acts as a fire retardant in paint[135]. N. S. Allen et al. have studied about photochemical characteristics of titanium dioxide known as titania in common[136]. One study is about the use of photo-catalytic property of titania to convert hazardous organic waste products into environment friendly materials. Another study is about enhancing the durability of paint or coating by controlling the photo catalytic activity of titania. D. Kocaefe et al. stated that the water contact angle and degree of penetration of acrylic PU paint increases with reinforcement of titania nanoparticles as it increases the degree of orientation of the paint[137]. Photocatalytic titania nanoparticles are used in the development of self-cleaning paints and microbiological surfaces. Its photocatalytic process in water is effective against a wide range of organisms, such as algae, viruses, fungi and bacteria. Titania nanoparticles have high refractive index, exceptional chemical resistance and strong UV absorption capacity, so this is used in mostly photocatalytic applications[136].

The polymer matrixes normally used in paint industry are epoxy, PU, acrylic and alkyds.

Epoxy based polymer matrix: Epoxy is considered as one of the most versatile coating materials for its specific properties like chemical resistance, low cost and mechanical properties. But due to its faster curing process, a number of micro-pores and cracks are observed in the coating. L. Ying et al. stated that when titania nanoparticles of size 17-50 nm are added into the matrix enhancement of mechanical properties and corrosion resistance properties are observed. Titania nanoparticles are added in sol-gel method into the polymer matrix[138].

PU-based polymer matrix: Titania nanoparticles when added to PU matrix mechanical properties, thermal properties, weather resistance and antimicrobial properties increase significantly. T. V. Nguyen et al. stated that the titania nanoparticles used as additives are of size 40-50 nm and added by ultrasonication process[139].

Acrylic based polymer matrix: Waterborne acrylic resin is widely used in paint industry for its excellent comprehensive properties. But it has poor UV resistance and water resistance properties. To overcome these shortcomings, acrylic paint is modified with nanoparticles. Bin. Du et al. stated that among the nanoparticles, nano-titania are used for their significant properties like, UV absorbance and photocatalytic activity, self-cleaning properties and non-toxicity. These are added to the acrylic resin by dispersion method. Size of the nano particleused is 20-50 nm[140].

Alkyd based polymer matrix: Alkyd resins are oil-based polyesters mostly used in expensive exterior paints. According to A. Grozdanov et al. by adding titania nanoparticles of around 21 nm size by high-speed dispersion method the water resistance and corrosion resistance of the paint increases significantly[141].

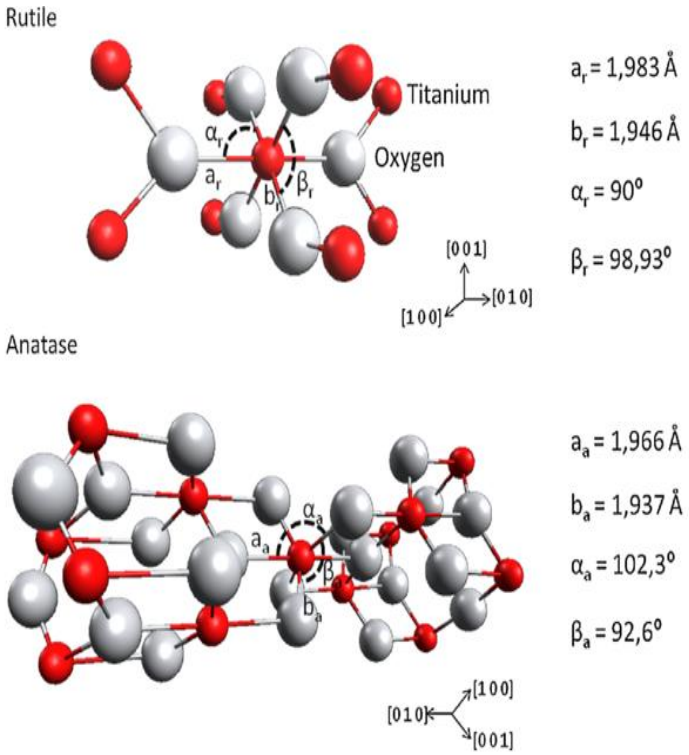

Fig 2.7.i: Atomic structure of Rutile and Anatase titania

Normally the titania particles are divided into two categories i.e., rutile and anatase according to their chemical structure, which is shown in Fig. 2.7.i. T. Luttrell et al. studied those organic pollutants are effectively decomposed by photo catalysis process and titania is the best suitable material used as photo catalyst[142]. There are number of methods to synthesize titania nanoparticles i.e., co-precipitation, flame hydrolysis, impregnation, chemical vapour deposition, etc. L. Uon et al. stated that among all methods sol-gel process is the most widely used one for its high potential to control the bulk and surface properties. Since this method is carried out in solution, homogeneity, grain size, particle morphology and porosity could be maintained uniformly. The sol-gel route is considered as very promising one for the synthesis of ultra-fine metallic oxide[143]. M. C. F. Karlsson et al.. Studied that titania is used as the pigment for white colour. Most of the white pigments used are now days are developed from rutile. But the production of titania pigment needs large amount of carbon. So, he developed some method to recover it from the waste paint, which is described in Fig. 2.7.j[144].

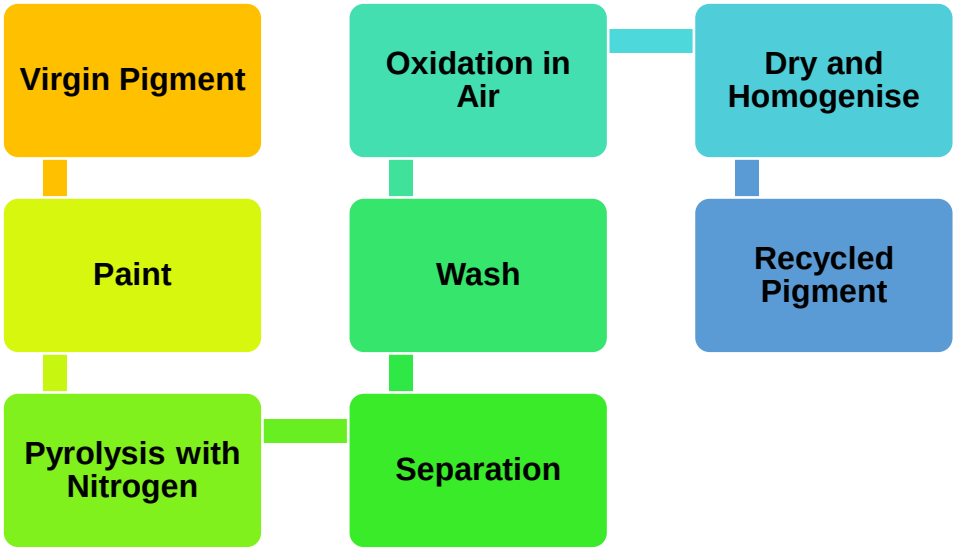

Fig 2.7.j: Process to recycle the titania pigment from waste paint

Haider et al. stated that, titania has very unique properties like photo catalytic, anti-bacterial, self-cleaning etc. for which it is used in paints as a pigment. Normally titania is doped with other suitable materials and then used in the paints. Most of the characteristics of titania depends on the crystal structure, size and shape of the particle. The band gap of titania particles determines the photo catalytic property of the particle[145].

Samsudin et al. stated that organic pollutants including reactive dyes can be effectively decomposed by photo catalysis process and titanium dioxide is one of the best photocatalytic agent[146]. B. Ohtani et al.. stated that titania is less toxic, greater oxidizing ability, and gives longer photo stability in comparison to other photocatalysts[147]. J. Byrne et al.. stated that titania occurs naturally as rutile, anatase and brookite. Among these phases, anatase has been proven to be the best one for photo catalytic activity[148].

P. F. He et al. stated that by incorporating titania nanoparticles into the paint matrix, scratch depth decreased from 1500 nm to 550 nm. P. K. Jaseela et al. stated that by reinforcing titania into a paint, the corrosion resistance is increased by 98%[149]. Titania is photochemical in nature, which helps to destroy the organic contaminants with sun light. This leads to extremely wear resistive polymer coating and increases

the mechanical properties of the paint. Titania particles reinforced polymers are characterized by very high tensile strength at high temperatures, light weight, high corrosion resistance, and ability to withstand extreme temperatures. Titanium is as strong as steel but 45% lighter. This metal forms a passive but protective oxide coating when exposed to elevated temperatures in air but at room temperatures it resists tarnishing. These properties make titania an excellent additive for scratch and abrasion resistance improvement. The transmittance of the titania reinforced paints increases with increasing titania content from 0.5 wt.% to 4.5 wt.%. This may be caused by the aggregation degree of composite particles in system due to the addition of titania nanoparticles. However, when 6.5 wt.% nano-titania is incorporated into the paints, the transmittance decreases sharply to less than that of bare glass[150].

Effect of Different Nano particle additives and their influence

Table 2.d: Influence of different nanoparticles[150]

Nanoparticle	Effect	Application
Nano-Silica	Improved scratch resistance and optical properties, stabilizes the paint, increase in wettability	Construction, Paint, Coating
Nano-Alumina	Improved scratch resistance and optical properties, stabilizes the paint, increase in wettability	Automotive, information and communication, parquet flooring, consumer goods (furniture), optics
Nano-Zirconia	Automotive, information and communication, parquet flooring, consumer goods (furniture), optics	Construction, wood preservation, glass, plastics, paints
Nano-Titania	Removal of grease, dirt, algae, bacteria, fungi, odorants and pollutants, transformation of NOx and ozone from the atmosphere into harmless compounds	Construction, road surface, vehicles, wood preservation, glass, paints

2.8. Paint Spraying Technology

Automobile body is made of different materials like metals, plastics, composites etc. e.g the car body and door are made of steel but the rear part is made up of plastics. When we apply the same paint on different parts of automobile body the colour slightly differs after drying, because the plastic parts have less heat absorption capacity than others. To overcome these problem two different types of spraying technologies are used. For metal part normally electrostatic spraying technology and for plastic part conventional spraying technology are used[151].

In recent studies there used a wide variety of paint spraying technology, which depends on several factors like; desired finish quality, transfer efficiency, speed of spray gun, paint quality and shape of the substrate, which is shown in Fig. 2.8.a[151].

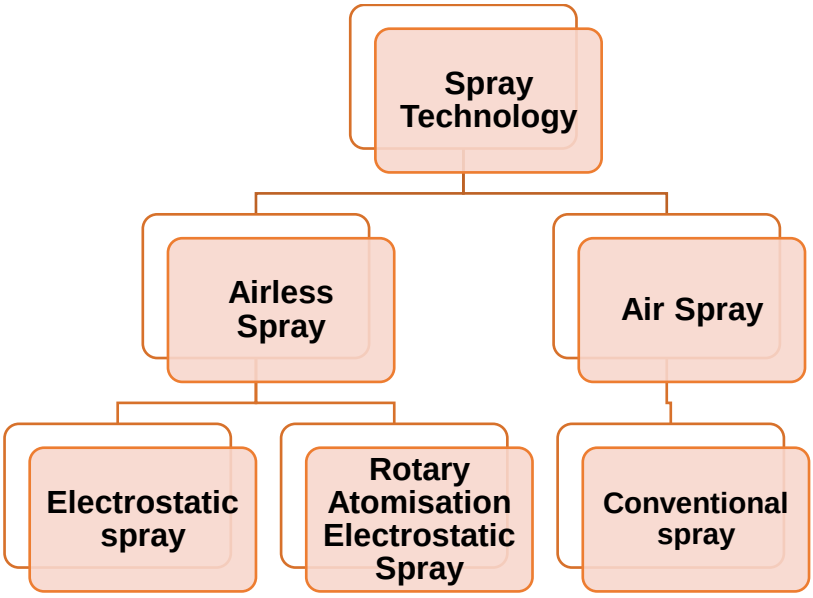

Fig 2.8.a: Types of spray technology

2.8.1 Conventional spraying Technology/ Air spray Technology

A conventional spray gun is the oldest system of paint spraying discovered in 1920s[152]. In the air spray process a low-pressure stream of fluid mixes with compressed air and atomize the paint particles at the air cap in a controlled manner. It is normally used for the low viscosity materials. The major components required for

conventional spray are, fluid nozzle, fluid needle, air cap and retaining ring, trigger, adjustment knob, fluid inlet, air inlet, gun body, compressed air supply etc.[153].

Advantages: Conventional spray has two basic advantages over the other spraying processes.

1. This is one of the most controlled spray processes. A properly trained operator can create a spray pattern from very small dot like pattern to very large-scale paint application. In this type of spraying the degree of atomization can be controlled there is no need of changing the air gun for every paint spraying.

2. It is also one of the most versatile processes, as it covers a very wide range of coating material.

Disadvantages: Conventional air spray has also some disadvantages like, lower transfer efficiency, more wastage of paint material and higher consumption of energy.

How the System Works

In the conventional spraying process as described in Fig. 2.8.b first the air spray gun was connected to the air compressor. Then the paint material is poured inside the air gun. Then the fluid paint material then mixes with the air pressure and when the air gun is triggered, the paint comes through the fluid nozzle of the gun in the form of liquid streams. This liquid stream of paint gets deposited on the substrate and makes a coating on it[152].

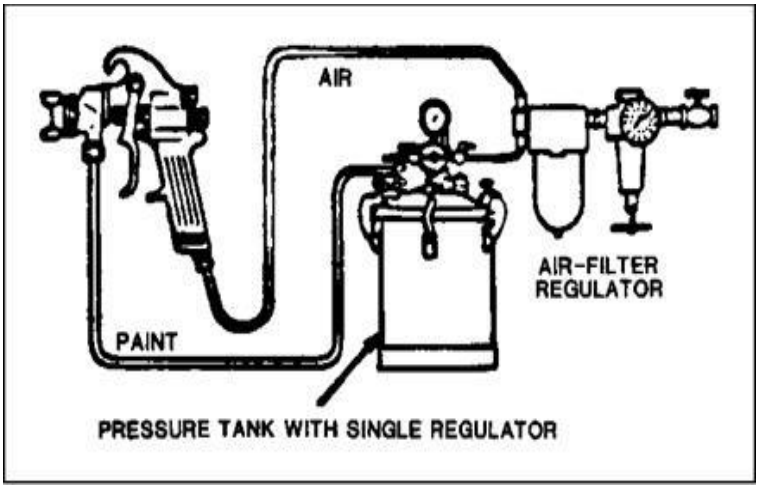

Fig 2.8.b: Schematic Diagram of Conventional Sprayer

2.8.2 Rotary Bell Electrostatic Spraying Technology/Airless Spray Technology

Airless spray is the method of paint spraying where atomization of paint occurs without using compressed air. In this process the paint is discharged forcefully in very high pressure through a small opening called orifice. While coming from the orifice the paint breaks down to form a particular pattern, this process are called atomization[154].

Advantages of Airless Spray: Airless spray has the following advantages[155]

1. Less overspray means less wastage of paint
2. More transfer efficiency i.e., around 60-90%.
3. We can get a thicker coat in single.
4. As the pressure is very high in this process, we can atomize highly viscous materials without costly solvent reduction.
5. Faster in production
6. Good penetration can be achieved

Two adjustments are also very much required in airless spray painting i.e., material viscosity and the system pressure. Normally the paint with lower viscosity is preferred, as it gives very fine atomization and the pressure is adjusted to a lower value to get the best type of paint.

In Electrostatic spraying process an electric charge is given to the paint to make it activate and coat properly all over the substrate in a very clean and efficient way[156]. Electrostatic paint was first discovered in early 1950s. According to Joel et al.. it significantly increases the transfer efficiency of the paint[157]. As shown in Fig. 2.8.c, the concept of airless spray is that the fast-moving high-pressure liquid stream provides the energy required to overcome the paint's viscosity and surface tension and creates a very fine spray. Then this fluid comes through the orifice and emerges as solid stream at very high speed. When the solid stream comes in contact with air, it breaks into fragments and, then ultimately becomes very small droplets, which forms the spray pattern[157].

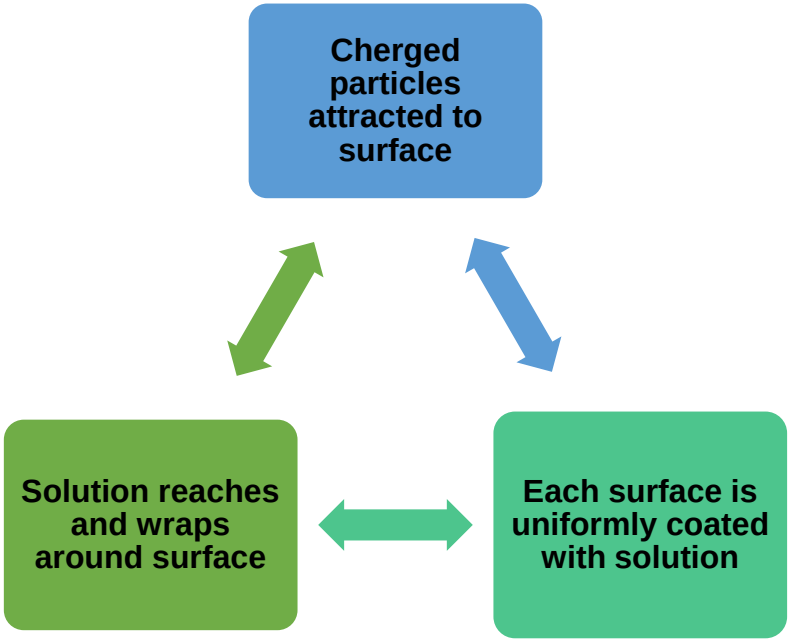

Fig 2.8.c: Electrostatic spraying technology.

In electrostatic spraying technology, a charging electrode is present at the tip of the orifice. This electrode receives an electrical charge from a power supply. When the paint passes through the orifice, it comes in contact with the electrode, which makes it ionized. Thus, an electrostatic field is created between the electrode and the grounded substrate, which is neutral. The negatively charged paint particles are attracted to the neutral ground substrate. After the paint has been deposited on the substrate, the charge returns back to power supply through ground by completing an

electrical circuit. Due to presence of electric field the paint coats homogeneously throughout the substrate[156].

High-speed rotary bell atomizers are normally used to spray the paint on the metal body to get very high quality of product. This process is a very effective process giving a highly uniform film thickness and very less transfer efficiency, because it has additional electrostatic field which helps the droplet go towards the target. The functionality of rotary-bell atomization is shown in Fig. 2.8.d.

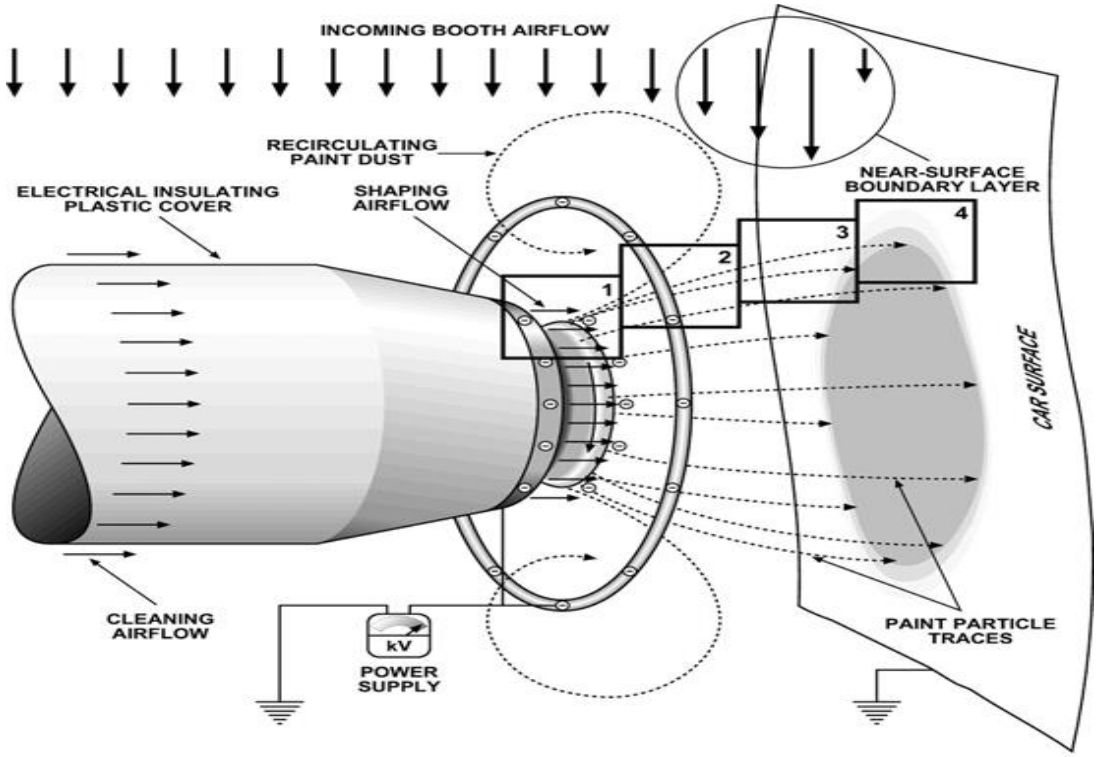

Fig 2.8.d: Schematic diagram of rotary bell sprayer

CHAPTER 3

Research Methodology

Chapter 3

3.1 Materials

3.1.1 Castor Oil:

Castor Oil (CO) is one of the most abundantly available vegetable oil, which is applicable in various fields. The chemical structure of CO is represented in Fig. 3.1.a It has triglycerides around 85-90% and unsaturated fatty acids, which forms a number of reactive sites for chemical modification. In the experiment, CO was procured from M/s Merck Chemicals Pvt. Ltd, Kochi, India. Table 3.1.a depicts the chemical and physical properties of CO whereas the major compositions of CO are summarized in Table 3.1.b

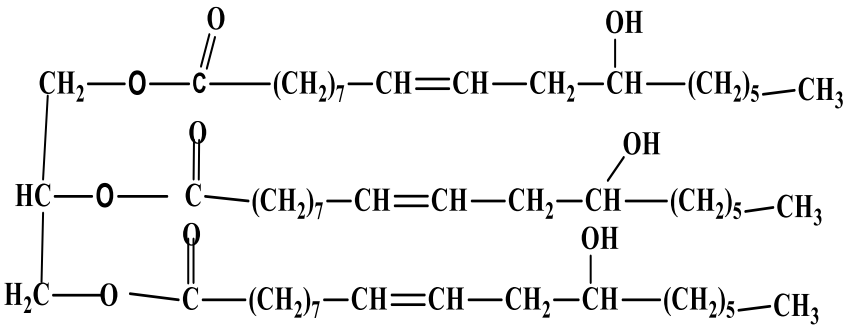

Fig. 3.1.a: Chemical structure of Castor oil

Table 3.1.a: Properties of CO

Characteristics	Specifications
Chemical Formula	$C_{57}H_{104}O_9$
Molar mass	930 g/mol
Hydroxyl value	170
Acid value	2

Colour	Pale yellow
Refractive Index	1.47-1.14
Density	0.9 g/cm^3
Oxidative stability	25 min

Table 3.1.b: Composition of CO

Compositions	Average %
Ricinoleic acid	90
Linoleic acid	4.1
Oleic acid	2.8
Stearic acid	1.2
Palmitic acid	1.3
Others	0.7

3.1.2: Nano-silica (NS):

Silica, is an oxide of silicon with the chemical formula SiO_2, most commonly found in nature as quartz, sand, and in various living organisms. Silica is one of the most complex and most abundant families of materials, existing as a compound of several minerals and as a synthetic product. Notable examples include fused quartz, fumed silica, silica gel, opal and aerogels. Silica in nano-scale is known as NS, which has significant mechanical, thermal and optical properties. It is also used as a filler material and incorporated in the matrix, to obtain enhanced characteristic properties. It is used

in structural materials, microelectronics (as an electrical insulator), and as components in the food and pharmaceutical industries. NS used in the current study was procured from M/s Sigma Aldrich Pvt. Ltd., Bengaluru. Chemical structure and physical properties of NS are described in Fig. 3.1.b and Table 3.1.c respectively. It was incorporated as a filler material in the paint and sealer matrix.

Fig. 3.1.b: Chemical structure of NS

Table 3.1.c: Properties of NS

Characteristics	Specification
Particle size	75 nm
Chemical formula	SiO_2
Molar mass	59.96 g/mol
Density	2.4 g/cm^3
Melting point	1600 ºC
Boiling point	2230 ºC

3.1.3 Isophorone Diisocyanate (IPDI):

Isophorone diisocyanate is an aliphatic isocyanate which are used in special applications, such as coatings, that are resistant to abrasion and degradation. These properties are particularly desirable for the exterior painting. IPDI exists in two stereoisomers, cis and trans having similar reactivity properties. IPDI in the current study was used as curing agent and was procured from M/s Sigma Aldrich Pvt. Ltd., Bengaluru. The chemical structure and physical properties of IPDI are depicted in Fig. 3.1.c and Table 3.1.d respectively.

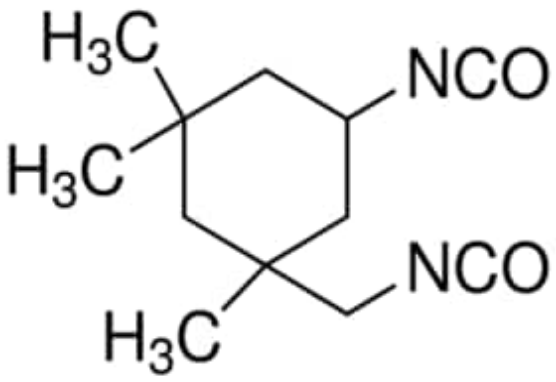

Fig. 3.1.c: Chemical structure of IPDI

Table 3.1.d: Properties of IPDI

Characteristics	Specification
Chemical formula	$C_{12}H_{18}N_2O_2$
Molar mass	222 g/mol
Density	1.06 g/cm^3
Melting point	-60 ºC
Boiling point	158 ºC

3.1.4 Hydrogen peroxide (H_2O_2):

H_2O_2 is the simplest kind of peroxide available having an oxygen-oxygen single bond. It is a colourless liquid and is used in aqueous solution for safety reasons. It acts as a bleaching agent and is also used as a disinfectant. Concentrated H_2O_2 is a very reactive oxygen species and is used as a propellant in rocketry. In the current study H_2O_2 was used as a catalyst during epoxidation of CO and was procured from M/s NICE Pvt. Ltd., Kochi. Fig. 3.1.d shows the chemical structure and Table 3.1.e reveals the physical properties of it.

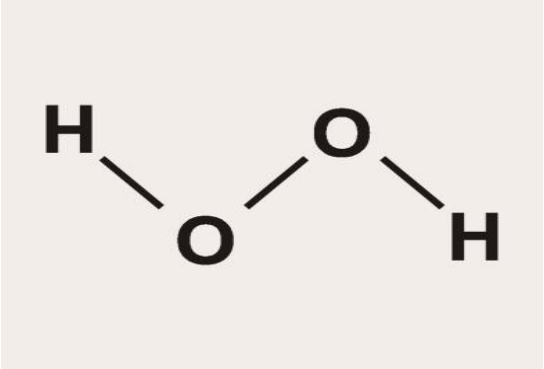

Fig. 3.1.d: Chemical structure of H_2O_2

Table 3.1.e: Properties of H_2O_2

Characteristics	Specification
Chemical formula	H_2O_2
Molecular weight	34 g/mol
Density	1.45 g/cm^3
Boiling point	152 ºC
Melting point	-0.43 ºC

3.1.5 Formic acid (HCOOH):

Formic acid, also known as methanoic acid, is the simplest carboxylic acid, and has the chemical formula HCOOH. It is an important intermediate in chemical synthesis and occurs naturally, most notably in some ants. In the current study, HCOOH acts as an oxidizing agent in the epoxidation process. It was procured from M/s Merck chemicals Pvt. Ltd., Mumbai. Chemical structure and physical properties of HCOOH are depicted in Fig. 3.1.e and Table 3.1.f respectively.

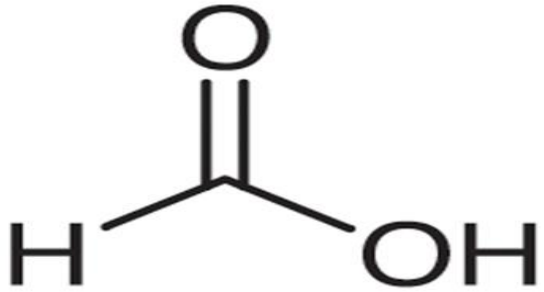

Fig. 3.1.e: Chemical structure of HCOOH

Table 3.1.f: Properties of HCOOH

Characteristics	Specification
Chemical formula	HCOOH
Molecular weight	46 g/mol
Density	1.22 g/cm^3
Boiling point	100 ºC
Viscosity	1.57cP

3.1.6 Sodium bicarbonate ($NaHCO_3$):

$NaHCO_3$, commonly known as baking soda or bicarbonate of soda, is a salt composed of a sodium cation and a bicarbonate anion. $NaHCO_3$ is a white solid that is crystalline, but often appears as a fine powder. It is used to neutralize the acidity of reaction mixture during epoxidation process. In the current investigation $NaHCO_3$ was procured from M/s CDH Pvt. Ltd., New Delhi. Fig. 3.1.f and Table 3.1.g shows the chemical structure and physical properties of $NaHCO_3$.

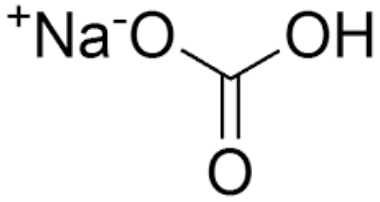

Fig. 3.1.f: Chemical structure of $NaHCO_3$

Table 3.1.g: Properties of $NaHCO_3$

Characteristics	Specification
Chemical formula	$NaHCO_3$
Molecular mass	84 g/mol
Density	2.2 g/cm^3

3.1.7 Ammonia solution (NH_4OH):

Ammonia solution, also known as ammonia water, ammonium hydroxide, aqua ammonia, aqueous ammonia, or ammonia. It is a solution of ammonia in water. NH_4OH can be used as a precursor to some alkyl amines. It was added to neutralize the acidity of the solution mixture during epoxidation process. For the current study NH_4OH was purchased from M/s Research-Lab Fine Chem Industries

Pvt. Ltd., Mumbai. Fig. 3.1.g shows the chemical structure and Table 3.1.h describes the physical properties of NH_4OH.

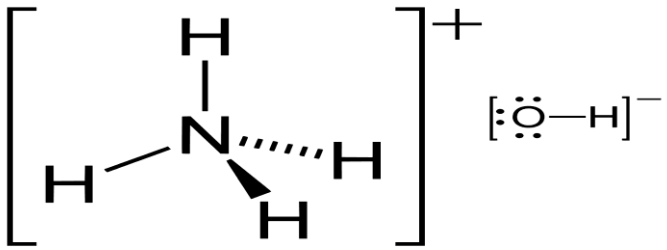

Fig.3.1.g Chemical structure of NH_4OH

Table 3.1.h: Properties of NH_4OH

Characteristics	Specification
Chemical formula	NH_4OH
Molecular weight	35 g/mol
Density	0.88 g/cm^3
Melting point	-91 ºC
Boiling point	37 ºC

3.1.8 Sodium Methoxide:

Sodium methoxide is a chemical compound with the formula CH_3ONa. This white solid, which is formed by the deprotonation of methanol, is a widely used reagent in industry and the laboratory. It is also a dangerously caustic base. For the current work CH_3ONa was procured from M/s Avra Synthesis Pvt. Ltd., Hyderabad. The chemical structure and physical properties are shown in Fig. 3.1.h and Table 3.1.i respectively.

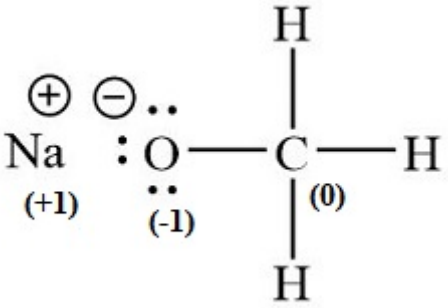

Fig.3.1.h: Chemical structure of Sodium methoxide

Table 3.1.i: Properties of Sodium methoxide

Characteristic	Specification
Chemical formula	CH_3NaO
Molecular weight	54 g/mol
Melting point	127 ºC
Boiling point	350 ºC

3.1.9 Methanol:

Methanol, also known as methyl alcohol, amongst other names, is considered as the simplest form of alcohol, with the formula CH_3OH. It is a light, volatile, colourless, flammable liquid with a distinctive alcoholic odour and was procured from M/s NICE Chemicals Pvt. Ltd., Kochi. Fig. 3.1.i and Table 3.1.j shows the chemical structure and physical properties of CH_3OH.

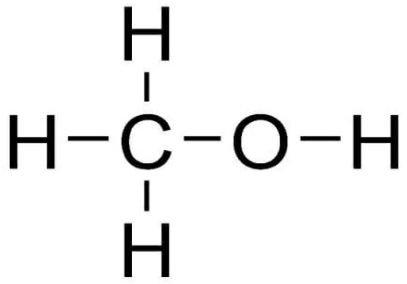

Fig.3.1.i: Chemical structure of Methanol

Table 3.1.j: Properties of Methanol

Characteristic	Specification
Chemical formula	CH_3OH
Molecular weight	32 g/mol
Density	0.79 g/cm^3
Melting point	-97 ºC

3.1.10 Hydroquinone:

Hydroquinone, also known as benzene-1,4-diol or quinol, is an aromatic organic compound that comes under phenol group. It is a derivative of benzene, having the chemical formula $C_6H_4(OH)_2$. It has two hydroxyl groups bonded to a benzene ring in a para position. It acts as polymerization inhibitor to control the chemical reaction during acrylation of CO. It is a white granular solid and in case of the current study, it was purchased from M/s NICE chemicals Pvt. Ltd., Kochi. The chemical structure and physical properties of hydroquinone are described in Fig. 3.1.j and Table 3.1.k.

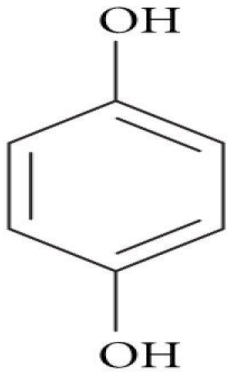

Fig. 3.1.j: Chemical structure of Hydroquinone

Table 3.1.k: Properties of hydroquinone

Characteristics	Specification
Chemical formula	$C_6H_6O_2$
Molar mass	110.11 g/mol
Boiling point	286 ºC

3.1.11 Acrylic acid:

Acrylic acid (IUPAC: propenoic acid) is an organic compound with the formula CH_2=CHCOOH. It is the simplest unsaturated carboxylic acid, consisting of a vinyl group connected directly to a carboxylic acid terminus. This colourless liquid has a characteristic acrid or tart smell. It is used to produce acrylic-ester based resins, which can be used in adhesive and coating industries. In this current study acrylic acid was procured from M/s Sigma Aldrich Pvt. Ltd., Bengaluru. Fig. 3.1.k and Table 3.1.l show the chemical structure and physical properties of CH_2=CHCOOH.

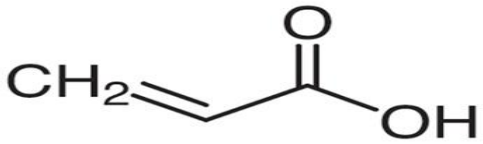

Fig. 3.1.k: Chemical structure of acrylic acid

Table 3.1.l: Properties of Acrylic acid

Characteristics	Specifications
Chemical formula	$C_3H_4O_2$
Molar mass	72 g/mol
Density	1.05 g/cm^3
Boiling point	141 ºC

3.1.12 Tryphenyl phosphine:

Triphenylphosphine is a common organophosphorus compound with the formula $P(C_6H_5)_3$. It is abbreviated as PPh_3 or Ph_3P and is widely used in the synthesis of organic and organometallic compounds. It is a colourless crystal which is relatively stable in air. It was purchased from M/s Research-Lab Fine-Chem Industries, Mumbai. In this study it was used as a reducing agent during acrylation process. The chemical structure and physical properties of PPh_3 are depicted in Fig. 3.1.l and Table 3.1.m respectively.

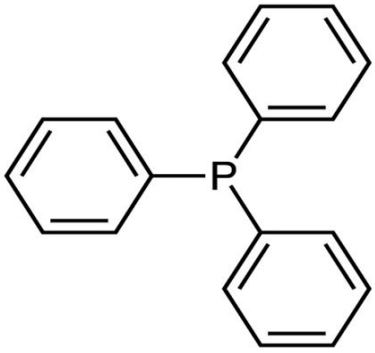

Fig.3.1.l: Chemical structure of Triphenyl phosphene

Table 3.1.m: Properties of Triphenyl phosphene

Characteristic	Specification
Chemical formula	$C_{18}H_{15}P$
Molar mass	262.29 g/mol
Density	1.1 g/cm^3
Boiling point	377 ºC

3.1.13 p-Toluene sulphonyl isocyanate (TSI):

TSI undergoes palladium-catalyzed bis-allylation reaction with allylstannanes and allyl chlorides. TSI has been used to determine the hydroxyl value of polyols using Fourier transform infrared (FTIR) spectroscopy method. It was procured from M/s Sigma Aldrich, Pvt. Ltd., Bengaluru for its use in the current study. Fig. 3.1.m and Table 3.1.n show the chemical structure and physical properties of TSI.

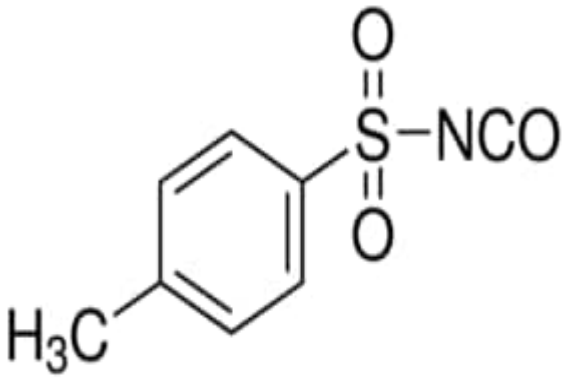

Fig.3.1.m: Chemical structure of TSI

Table 3.1.n: Properties of TSI

Characteristic	Specification
Chemical formula	$CH_3C_6H_4SO_2NCO$
Molar mass	197.21 g/mol
Density	1.29 g/cm^3
Refractive index	1.54
Boiling point	144 ºC

3.1.14 1-Nonanol:

1-Nonanol is a straight chain fatty alcohol with nine carbon atoms with molecular formula is $CH_3(CH_2)_8OH$. It is a colourless oily liquid with a citrus odour similar to citronella oil. The primary use of 1-nonanol is in the manufacture of artificial lemon oil. Nonan-1-ol is a fatty alcohol consisting of a hydroxy function at C-1 of an unbranched saturated chain of nine carbon atoms. In this study it is used to synthesize the reaction mixture for polyol to determine the hydroxyl value through FTIR spectra. Fig. 3.1.n and Table 3.1.o show the chemical structure and physical properties of 1-nonanol. It was procured from M/s Research Lab Fine Chem. Pvt. Ltd., Mumbai.

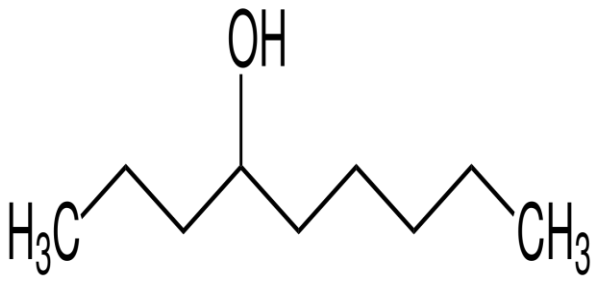

Fig. 3.1.n: Chemical structure of 1-nonanol

Table 3.1.o: Properties of 1-nonanol

Characteristics	Specification
Chemical formula	$C_9H_{20}O$
Molar mass	144 g/mol
Density	0.827 g/cm^3
Boiling point	214 ºC
Solubility in water	0.13 g/L

3.1.15 Aminopropyl triethoxy silane (APTES):

APTES is an amino-based silane coupling agent, frequently used in the process of silanization, and the functionalization of surfaces with alkoxysilane molecules. It can also be used for covalent attaching of organic films to metal oxides such as silica and titania. In this current study, it was procured from M/s TCI Chemicals Pvt. Ltd., Tokyo. The chemical structure and physical properties of APTES are depicted in Fig. 3.1.o and Table 3.1.p.

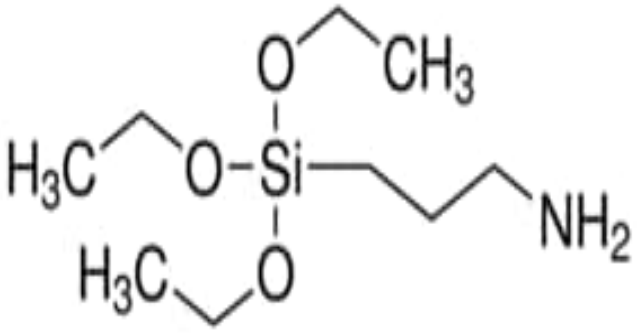

Fig. 3.1.o: Chemical structure of APTES

Table 3.1.p: Properties of APTES

Characteristic	Specification
Chemical formula	$C_9H_{23}NO_3Si$
Molar mass	221g/mol
Density	0.94g/cm^3
Boiling point	217ºC

3.1.16 Triallyl isocyanurate (TI):

TI has an unique feature having an acrylic group attached with the isocyanate, which helps in single-step surface modification of nanoparticles. It was procured from M/s TCI Chemicals, Pvt. Ltd., Tokyo for its use in the current work. Fig. 3.1.p and Table 3.1.q describe the chemical structure and physical properties of TI.

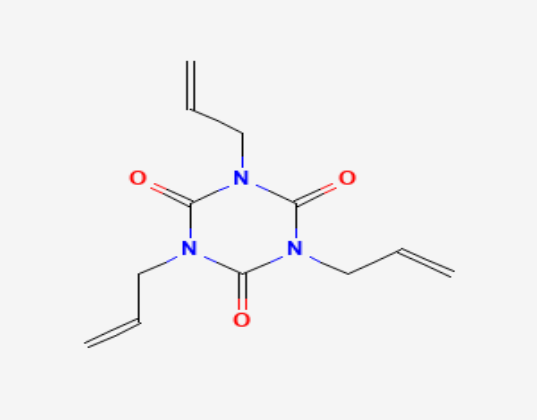

Fig. 3.1.p: Chemical structure of TI

Table 3.1.q: Properties of TI

Characteristics	Specification
Chemical formula	$C_{12}H_{15}N_3O_3$
Molar mass	249 g/mol
Density	1.15 g/cm^3
Boiling point	312 ºC

3.1.17 EPOFINE 1556:

EPOFINE 1556 is an epoxy, that comes under Bisphenol-A group. It is a reactive prepolymer containing epoxide group. It has significant properties like resistance to heat, chemicals, and corrosion, higher tensile, compression, and bend strength and can be applicable as an adhesive to most of the materials. It is applicable in various fields like coatings, adhesives, electronics, electrical insulators etc. This product is recommended for room temperature curing or low temperature baking. It is a clear and colourless liquid, which is stored at room temperature. It was procured from FINE

FINISH ORGANICS Pvt. Ltd., Mumbai. The chemical structure and physical properties of EPOFINE 1556 are shown in Fig. 3.1.q and Table 3.1.r respectively.

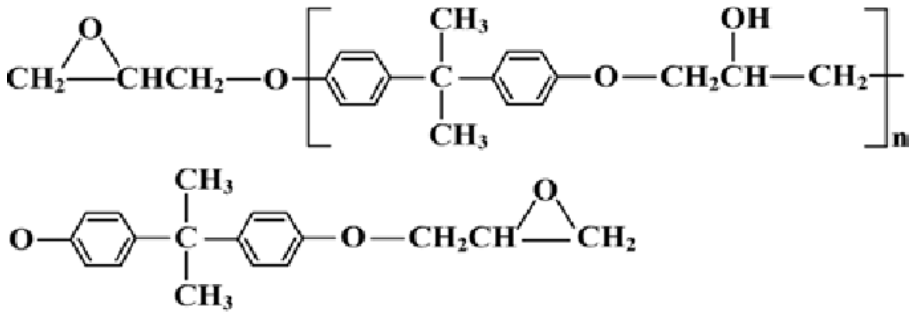

Fig. 3.1.q: Chemical structure of EPOFINE 1556

Table 3.1.r: Physical properties of EPOFINE 1556

Characteristics	Specification
Viscosity at 25 °C	9000-11000 mPa-s
Epoxy content	185-192 g/eq
Density at 25 °C	1.15-2.0 g/cc
Flash point	>200 °C
Storage life	3 years

3.1.18 FINEHARD 3486:

FINEHARD 3486 is an amine group epoxy hardener. Epoxy resin in general comes in two parts i.e., one epoxy resin part and another epoxy curing agent part, which is known as hardener. It reacts with epoxy group of the resin, resulting in a thermoset hard material. Epoxy hardeners are normally amine based. In this study FINEHARD 3486 was procured from FINE FINISH ORGANICS Pvt. Ltd., Mumbai. Its chemical structure and physical properties are shown in Fig. 3.1.r and Table 3.1.s respectively. Mixing ratio i.e., resin: hardener employed in the study was 100:34

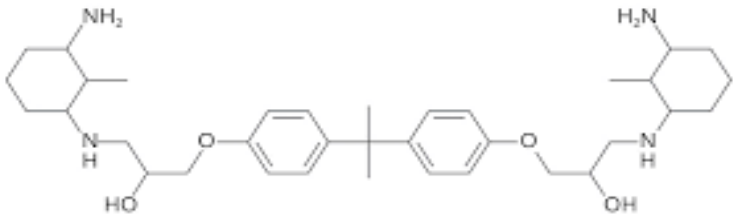

Fig. 3.1.r: Chemical structure of FINEHARD 3486

Table 3.1.s: Physical properties of FINEHARD 3486

Characteristics	Specification
Visual	Colourless to pale yellow liquid
Viscosity at 25 °C	<50 mPa-s
Flash point	>123 °C
Density at 25 °C	0.94-0.95 g/cc
Storage life	1 year

3.1.19 Solvent and additional materials used

Table 3.1.t: Solvents and Additional materials

Material name	Chemical formula	Procured from
AR-grade Ethanol	C_2H_5OH	M/s NICE Pvt. Ltd., Kochi
AR-grade Xylene	C_8H_{10}	M/s Merck Chemicals Pvt. Ltd., Mumbai
AR-grade Toluene	C_7H_8	M/s NICE Pvt. Ltd., Kochi
AR-grade Dimethylformamide (DMF)	C_3H_7NO	M/s NICE Pvt. Ltd. Kochi
AR-grade Acetone	C_3H_6O	M/s NICE Pvt. Ltd. Kochi
Automobile primer		M/s Soniac Co. Pvt. Ltd., Gujarat
80, 400, 600, 1200, 2000 grit sand paper		Phulwari paints Pvt. Ltd., Bhubaneswar, India
Polyurethane based commercial Automobile base coat (BC)		Phulwari paints Pvt. Ltd., Bhubaneswar, India
Polyurethane based commercial Automobile Clear coat (CP)		Phulwari paints Pvt. Ltd., Bhubaneswar, India
HOSTASPARM GREEN (Titanium based colour pigment) (TP)		Clariant Pvt. Ltd., Australia

3.2 Experimental Methods

3.2.1 Synthesis of bio-based Automobile base coat derived from CO, incorporated with NS and TP

(a) Epoxidation of CO

As reported by A. Sardari et al.[158], 100 g of CO was taken in a three-necked round-bottom flask immersed in oil bath attached to both nitrogen atmosphere and condenser. At 45 ºC, the solution was stirred with a magnetic stirrer to which H_2O_2 was added drop-wise in a molar ratio of H_2O_2 and CO of 1.8: 1. HCOOH was added afterwards at a molar ratio of 1:1 with H_2O_2. The reaction was continued for 5 hrs. and then, NH_4OH and $NaHCO_3$ were added to the solution to neutralize the acidity. The reaction mixture was then washed twice with ethanol and purified in a rotary evaporator. The resultant solution was derived as epoxidized CO (ECO). The reaction mechanism is described in scheme 3.2.1.a

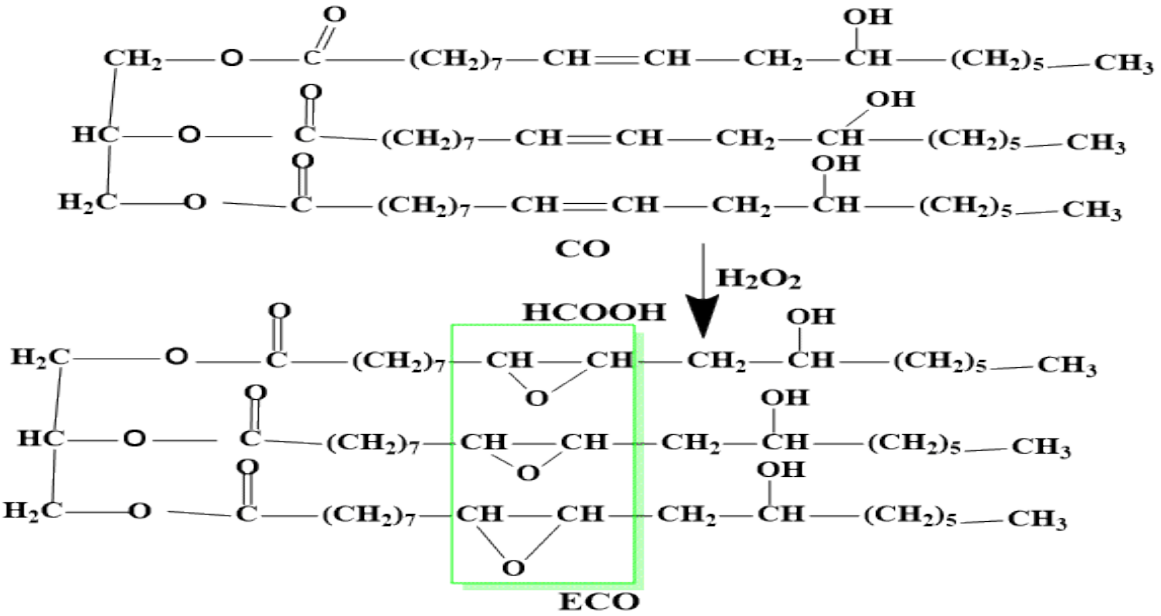

Scheme 3.2.1.a: Synthesis of Epoxidised Castor oil

(b) Functionalization of NS with APTES:

NS was functionalized with APTES using the following procedure. First 1:1 ratio of NS and APTES were dissolved in toluene. The solution was then stirred at room temperature for 12 hrs, centrifuged at 3000 rpm for 10 mins. Finally, APTES functionalized NS was washed with ethanol twice and dried in vacuum oven at 70 °C for 8 hrs.

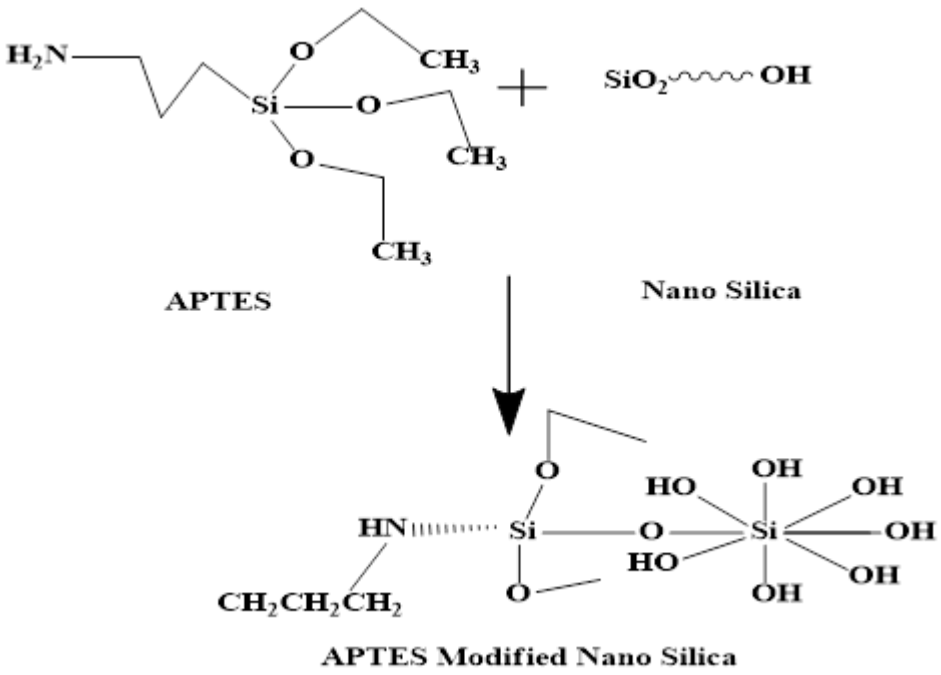

Scheme 3.2.1.b: APTES Modification of NS

(c) Synthesis of PU-based basecoat.

ECO was dissolved in xylene at a ratio of ECO: xylene of 1:0.5. After that IPDI was added to it at variable OH: NCO ratios of 1:1, 1:1.1, 1:1.2 and 1:1.3 respectively. The reaction temperature was maintained at 45 °C and the synthesis was carried out for 2 hrs. The whole process was undertaken in nitrogen atmosphere, connected with a condenser. Among the PU synthesized, the OH: NCO ratio of 1:1.2 was optimized based on the cross-cut adhesion properties. This ratio was taken for further study with NS as reinforcement.

(d) Synthesis of PU-based basecoat reinforced with NS

APTES functionalized NS was incorporated into the paint at different weight % ranging from 0.5 wt.% to 1.5 wt.% and was examined for its performance characteristics. The PU matrix with 0.5 wt.% NS was optimized based on scratch resistance and adhesion properties. TP was added in different wt.% i.e., 0.1 wt.%, 0.2 wt.%, and 0.3 wt.%. Paint formulation with 0.5 wt.% NS and 0.2 wt.% TP was the final optimized composition. The NS particles and pigment particles were dispersed in xylene solvent and stirred for 12 hours, then was immersed in the polyol, which results in proper homogenization. The chemical reactions that occur during the synthesis process are shown in scheme 3.2.1.c and the paint compositions are depicted in Table 3.2.a.

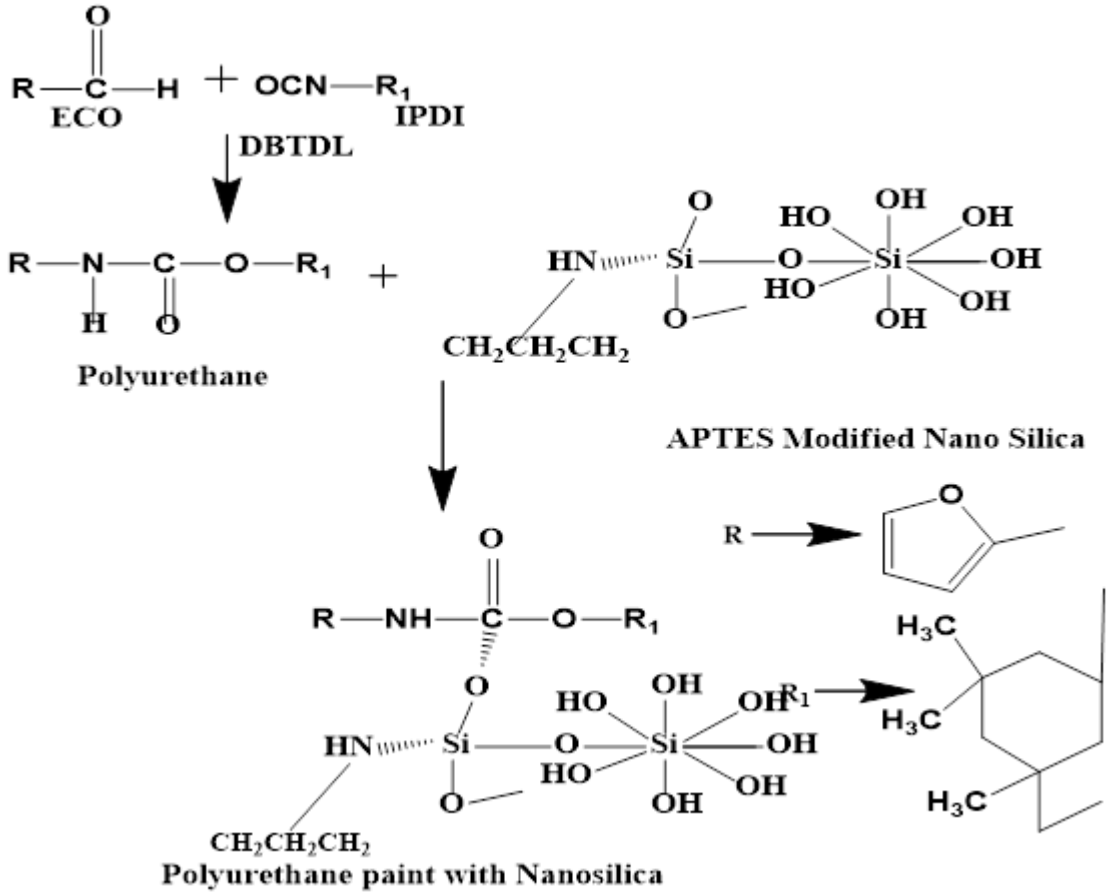

Scheme 3.2.1.c: Synthesis of PU-based base coat incorporated with NS.

Table 3.2.a: Paint composition

Paint sample	Polyol (g)	OH:NCO	NS (wt%)	DBTDL 0.02wt % (g)	Pigment (wt%)	Dry to touch time (min)	Complete dry time (min)
PU_1	20	1:1	0	0.004	0	90±10	3900±8
PU_2	20	1:1.1	0	0.004	0	65±7	3120±5
PU_3	20	1:1.2	0	0.004	0	50±2	2800±5
PU_4	20	1:1.3	0	0.004	0	45±3	2500±4
PU_3NS_1	20	1;1.2	0.5	0.004	0	40±2	2300±6
PU_3NS_2	20	1:1.2	1	0.004	0	38±2	2150±5
PU_3NS_3	20	1:1.2	1.5	0.004	0	33±4	1900±6
$PU_3NS_1TP_1$	20	1:1.2	0.5	0.004	0	37±3	2050±5
$PU_3NS_1TP_2$	20	1:1.2	0.5	0.004	0	32±2	1800±3
$PU_3NS_1TP_3$	20	1:1.2	0.5	0.004	0	30±5	1720±4
BC	20	-	-	-	-	60±2	2880±5

3.2.2 Synthesis of Bio-based Automobile Clear coat derived from Acrylated Transesterified Epoxidized CO, incorporated with NS.

(a) Transesterification of ECO:

50 g of ECO was placed in a round-bottomed, three-necked flask under nitrogen atmosphere connected to a condenser and a magnetic stirrer at 50 ºC. 1 wt.% of CH_3ONa was dissolved in 15 ml of CH_3OH. The solution mixture was added to the ECO and stirred for 40 mins. Which was subsequently washed twice with ethanol and the impurities and unused methanol were removed from the sample by a rotary evaporator to obtain transesterified ECO (TECO) [12]. The reaction mechanism is described in scheme 3.2.2.a

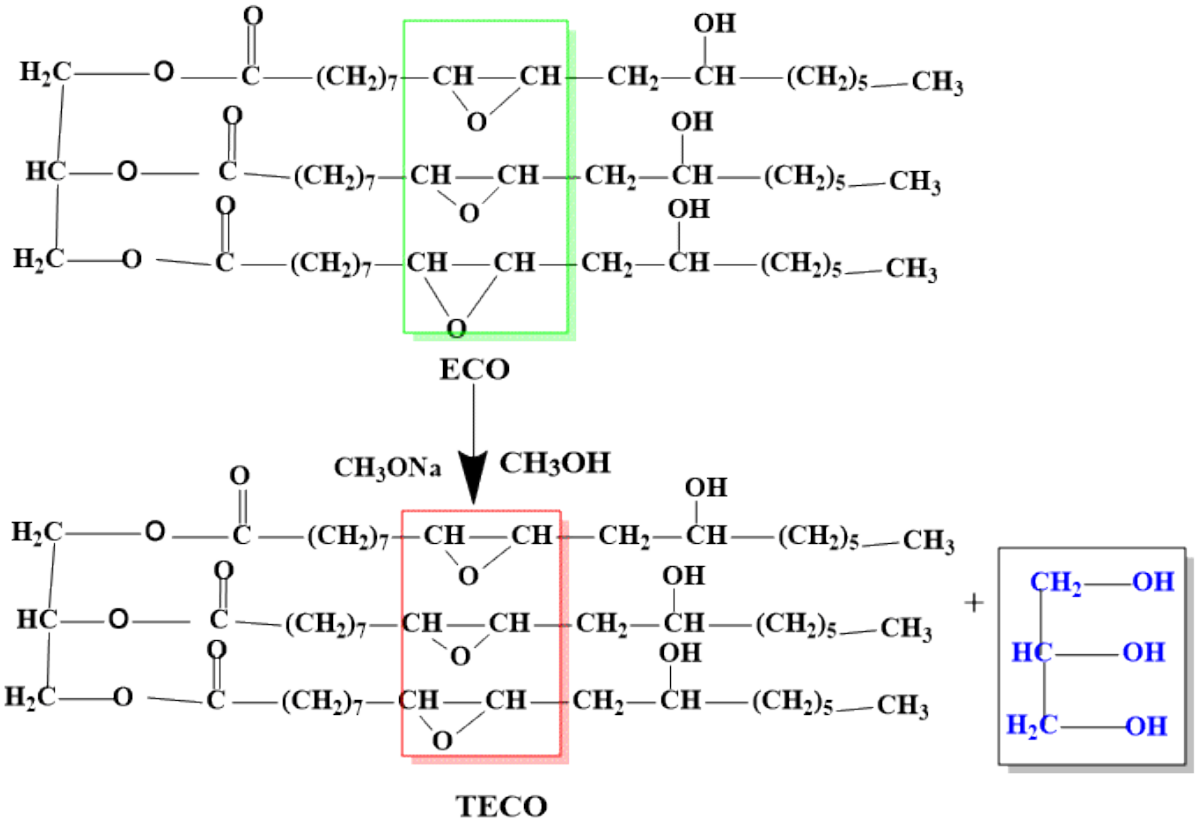

Scheme 3.2.2.a: Synthesis of TECO

(b) Acrylation of Transesterified Epoxidised CO:

At 60 ºC, 50 g of TECO was placed in a round-bottomed, three-necked flask equipped with a nitrogen atmosphere, condenser, and magnetic stirrer.10 g of acrylic acid was added to the solution. Then, at 75 ºC, 0.5 wt.% of hydroquinone was added and stirred for 20 mins. Subsequently, at 60 ºC, 4 g of triphenylphosphene was added and stirred for 1 hr. After that, an additional 8 g of acrylic acid was added to the solution mixture and stirred for another 1 hr at 60 ºC. The solution was dissolved in diethyl ether and washed. The product was extracted by removing the solvent and other impurities with a rotary evaporator to obtain acrylated TECO (ATECO) [12]. The reaction scheme is shown in 3.2.2.b.

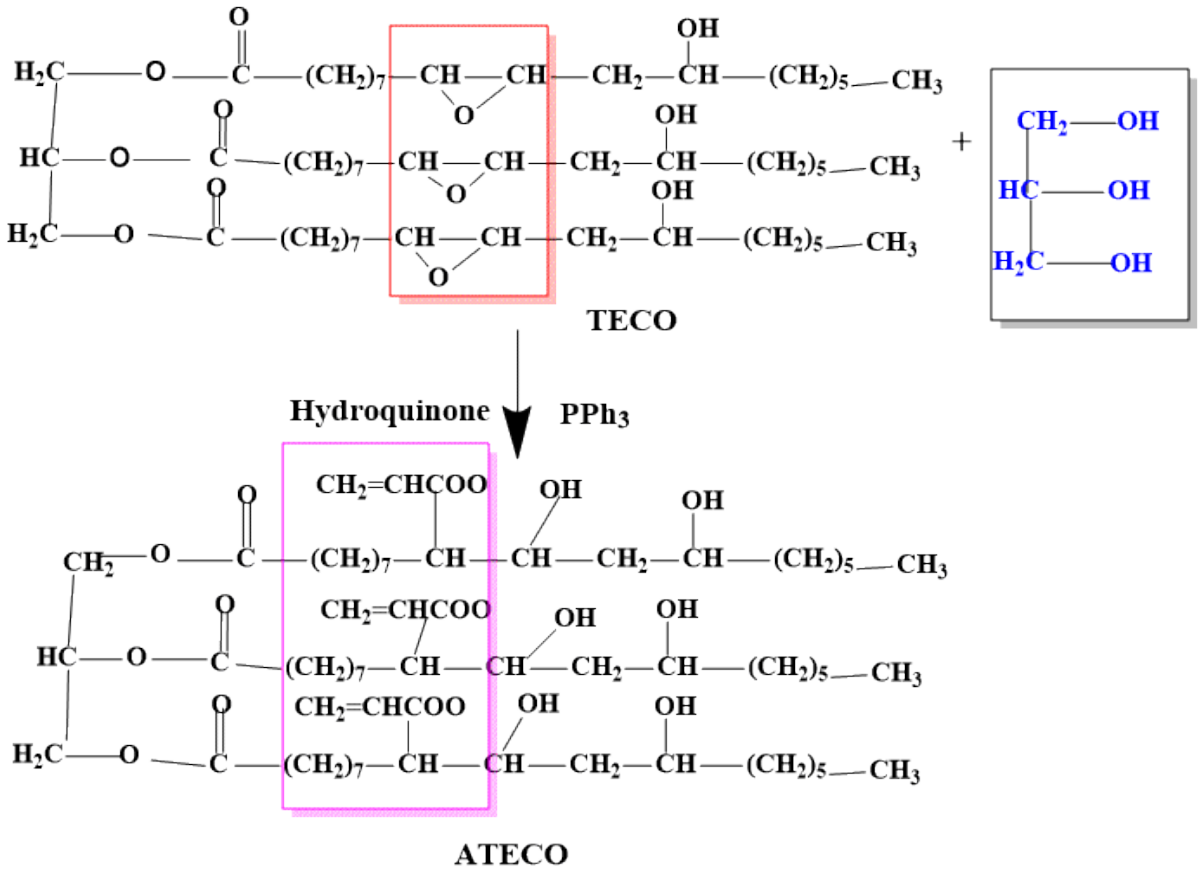

Scheme 3.2.2.b: Synthesis of Acrylated transesterified epoxidized castor oil

(c) TI Modification of NS:

NS was initially pre-dried in a vacuum oven at 110 °C for 24 hrs. Then it was sonicated in toluene by ultrasonicator (M/s ANTECH, USA). The solution was then taken in a round bottom flask attached to condenser and nitrogen atmosphere and was stirred in a magnetic stirrer. TI was added to the solution mixture at NS: TI ratio 1: 0.8 and DBTDL was added as catalyst. The resultant solution was then centrifuged and washed for purification. The solution mixture was subsequently dried in a vacuum oven for 8 hrs. at 70 °C to get the modified NS particles[159]. The reaction scheme is described in 3.2.2.c.

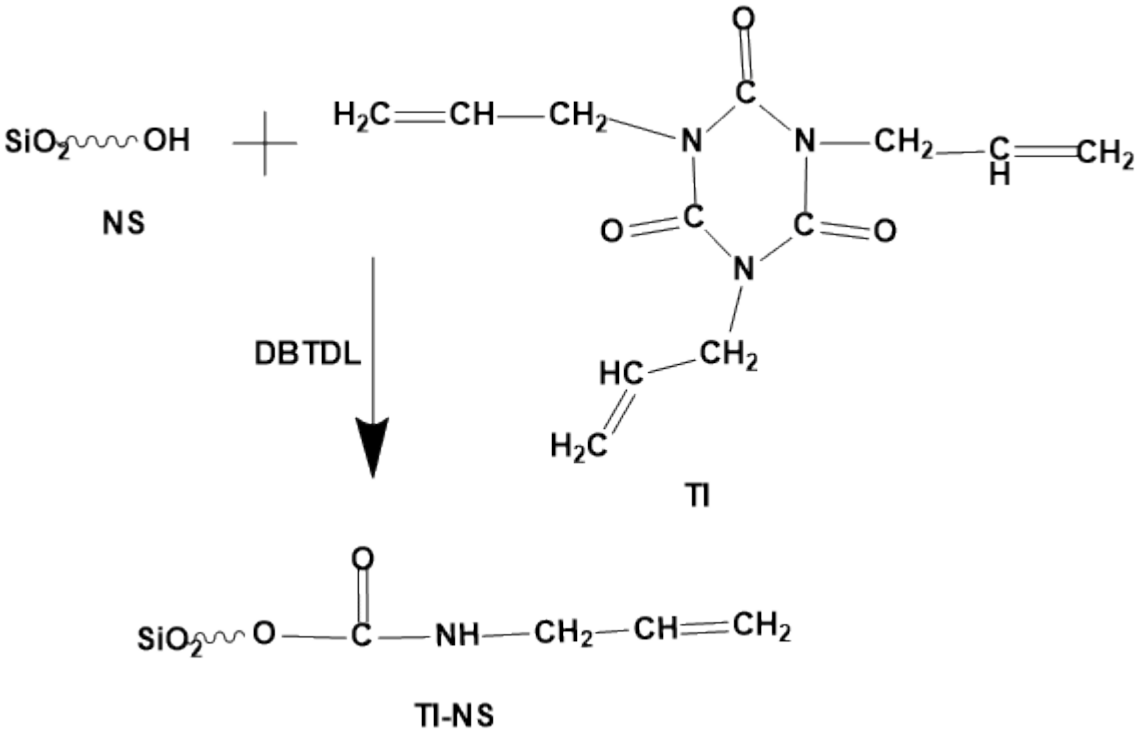

Scheme 3.2.2.c: TI Modification of NS

(d) Synthesis of clear coat formulations:

Acrylic-PU-based clear coat was synthesized by using both TECO and ATECO as polyols and IPDI as a curing agent with a resin to xylene solvent ratio of 1:0.4. DBTDL was taken as the catalyst. Three different compositions of paint formulations were synthesized with OH: NCO ratio of 1: 0.9, 1: 1, and 1: 1.1 for both the polyols, and the paint formulation with an OH: NCO ratio of 1:1 using ATECO was optimized by the

adhesion tape test. TI-NS was added to the optimized paint formulations at different wt.% of 0.5 wt.%, 1 wt.%, and 1.5 wt.%, respectively. The paint formulation with ATECO, OH: NCO ratio of 1:1 and NS wt.% of 0.5 wt.% was optimized by the adhesion tape test.

The compositions of various formulations developed in the current study and the curing times of paint formulations are enumerated in Table 3.2.b.

Synthesis of acrylic polyurethane based clear coat has been described in scheme 3.2.2.d.

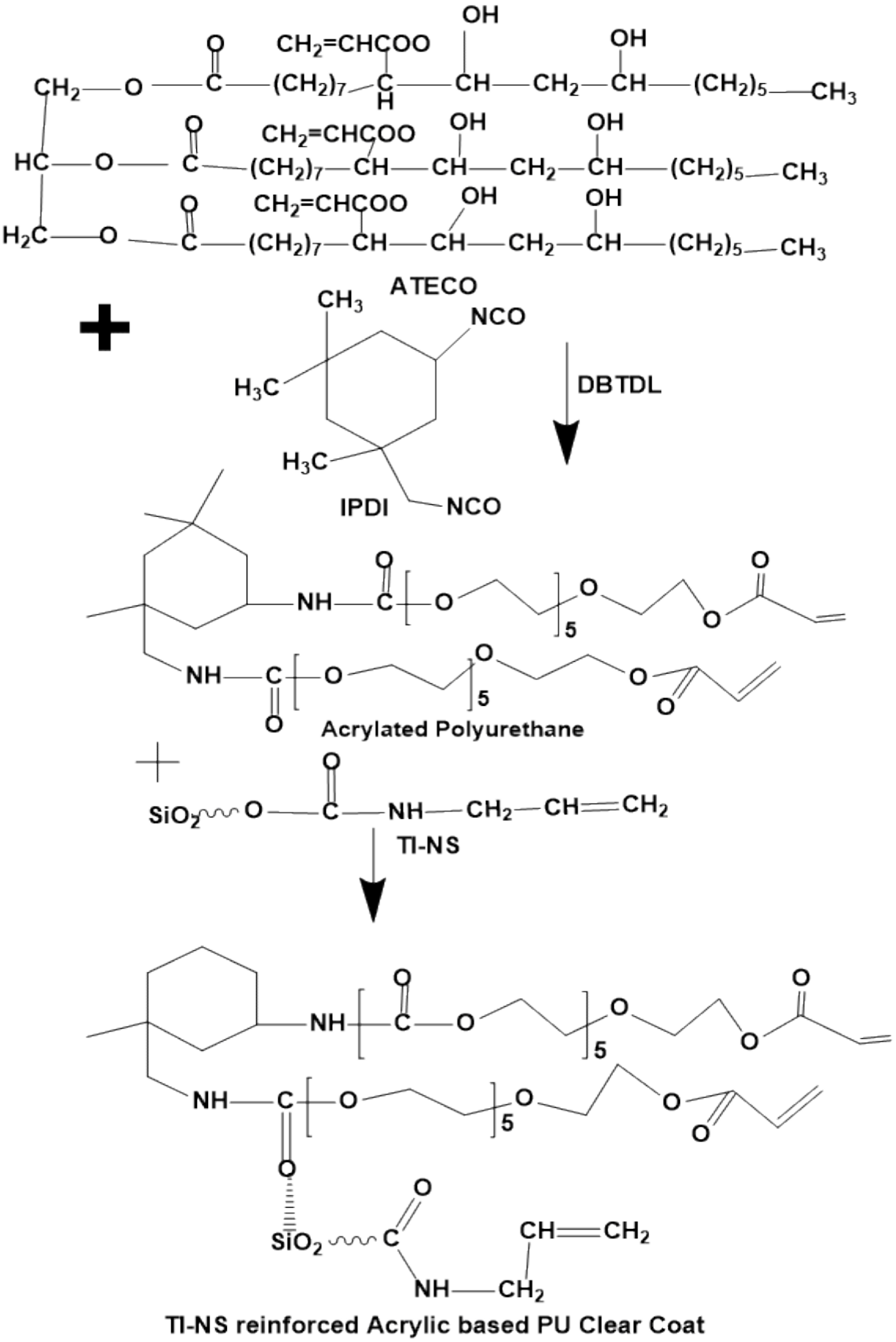

Scheme 3.2.2.d: Synthesis of TI-NS reinforced acrylic-PU-based Clear coat

Table 3.2.b: Composition of various formulations developed

Sl. No.	Paint sample	Polyol Name	Polyol taken (g)	OH:NCO	DBTDL (0.02%)g	NS (%)	Dry to touch (min)	Complete dry(min)
1	CP	-	-	-	-	-	35±2	1800±3
2	PU_i	TECO	20.3	1:0.9	0.004	0	68±3	2900±5
	PU_{ii}	TECO	20.7	1:1	0.004	0	52±2	2460±3
	PU_{iii}	TECO	20.4	1:1.1	0.004	0	45±4	2130±5
3	$PU_{ii}NS_1$	TECO	20.7	1:1	0.004	0.5	39±5	1910±3
	$PU_{ii}NS_2$	TECO	20.7	1:1	0.004	1	35±6	1800±6
	$PU_{ii}NS_3$	TECO	20.7	1:1	0.004	1.5	32±2	1675±5
4	PU_1	ATECO	20.2	1:0.9	0.004	0	60±3	2880±5
	PU_2	ATECO	20.8	1:1	0.004	0	48±2	2400±4
	PU_3	ATECO	20	1:1.1	0.004	0	40±3	2100±6
5	PU_2NS_1	ATECO	20.8	1:1	0.004	0.5	36±3	1860±4
	PU_2NS_2	ATECO	20.8	1:1	0.004	1	33±5	1740±7
	PU_2NS_3	ATECO	20.8	1:1	0.004	1.5	31±4	1620±5

3.2. Synthesis of Epoxy-PU blend incorporated with NS: Applicable as Automobile Sealer

(a) Synthesis of Epoxy-PU blend:

EPOFINE 1556 was blended with ATECO with various EPOFINE: ATECO ratios such as; 100:0, 80:20, and 60:40 and the blend were referred as EP_1, EP_2, and EP_3 respectively. Amine based epoxy hardener FINEHARD 3684 was added to the solution mixture at epoxy: hardener ratio of 100:34. The blended mixture was then poured into a mould of 180x180x3 mm size and cured at room temperature. The blends were optimized by using impact test and the Epoxy-PU blend of composition epoxy: PU ratio of 80: 20 (EP_2) was optimized.

(b) Synthesis of Epoxy-PU/ Silica nanocomposite.

In the previous work TI-NS at 0.5 wt.% was optimized based on its characteristic properties. Hence, during sealer synthesis this composition of TI-NS was incorporated into the optimized Epoxy-PU, referred as EP_2NS to enhance the characteristic properties of the sealer. The reaction mechanism is shown in scheme 3.2.3 and the sealer compositions are described in Table 3.2.c

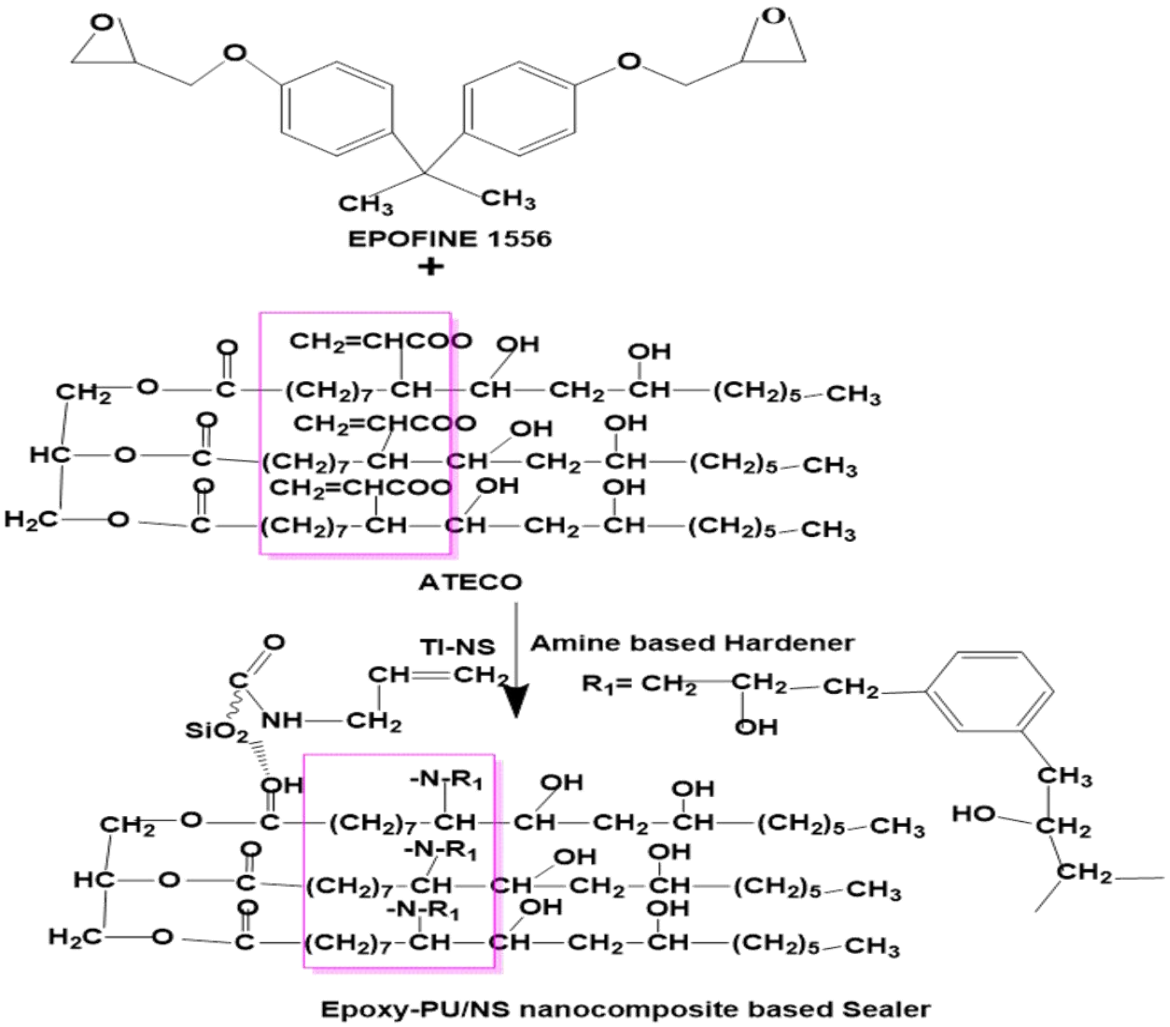

Scheme 3.2.3: Synthesis of Epoxy-PU/NS nano composite-based Sealer

Table 3.2.2: Sealer compositions

Sealer compositions	Epoxy: PU ratio	NS wt.%	Curing time (mins)
EP_1	100: 0	0	1440±5
EP_2	80: 20	0	1520±4
EP_3	60: 40	0	1590±5
EP_2NS	80: 20	0.5 wt.%	1380±3

3.3 Characterization

3.3.1 Physical properties

3.3.1.1 Hydroxyl value calculation:

Hydroxyl value is defined as the number of milligrams of potassium hydroxide (KOH) required to neutralise one gram equivalent of polymer material. It also measures the number of free hydroxyl groups present in a chemical structure. Hydroxyl value helps to determine stoichiometry of a chemical structure, as well as it can determine the equivalent weight and molecular weight of a chemical structure. Hydroxyl value can be calculated by following ASTM D 6342-12 method.

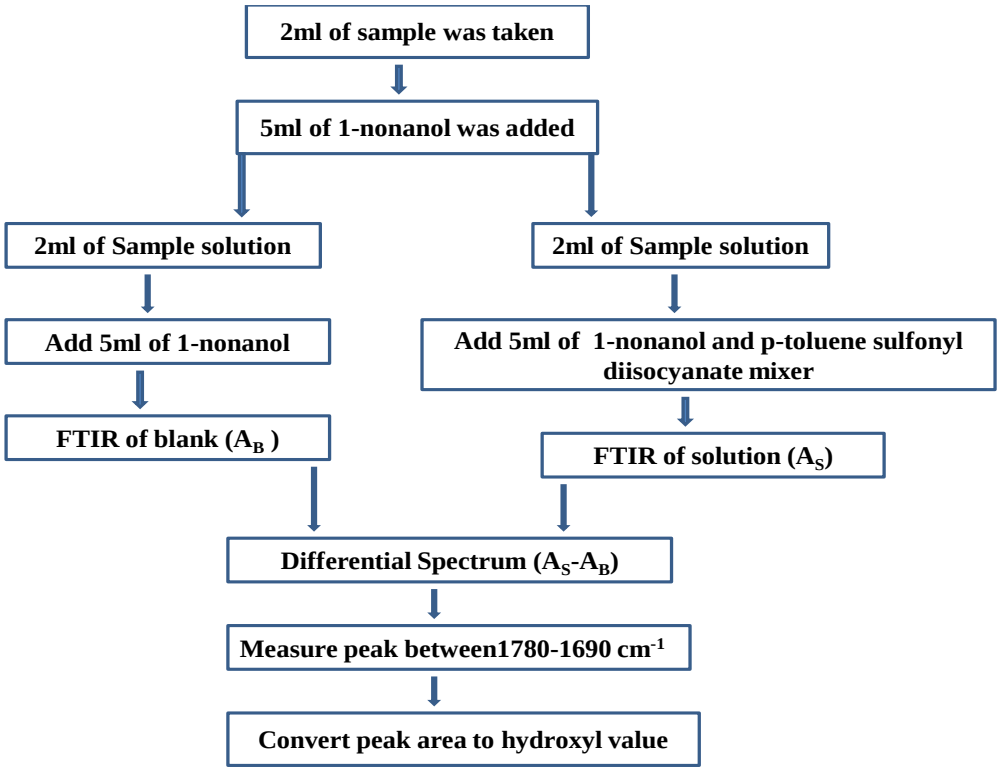

The hydroxyl value was calculated using the following Equation (3.3.1.a)

OH value = $(S \times A - B) \times (V2 + V3) \times (\frac{V1}{V2}) \times (\frac{1}{W}) \times (\frac{388.9}{1000})$----------(3.3.1.a)

Where S = Slope of the calibration curve

B = Intercept of calibration curve

A = Integrated intensity between 1780-1690 cm^{-1}

V_1 = Initial volume of the sample taken

V_2 = Volume taken first from the initial solution

V_3 = Volume of nonanol/TSI solution added

W = Weight of the sample

388.9 = OH value of 1-nonanol

3.3.1.2 Acid value:

Acid value is the mass of KOH in mg to neutralise the free fatty acids of one gram of chemical substance. Acid value is an important indicator in oxidation of oil. Higher acid value results in more oxidising value, which is hazardous to health. Hence, a lower acid value is expected in an ideal oil. It was calculated following DIN EN ISO 2114:2002-06 standards. In this standard first a solvent was prepared by adding two parts of toluene with one part of ethanol. Following the standard for acid value between 0-5, the sample taken was 16 g. and solvent was 150 ml. Titration of blank and sample mixed with solvent was carried out. From the titration results, acid value can be calculated following the given Equation (3.3.1.b);

Acid value = $\left[56.1 \times N \times \left(V_b - V_{eq}\right)\right]/W$----------(3.3.1.b)

Where, N = Normality

V_b = Volume equivalent in blank

V_{eq}= Volume equivalent of solution

W = Weight of the sample

3.3.1.3 Amine value:

Amine value is the number of milligrams of KOH equivalent to the fatty amine basicity in 1 g of sample. Amine value of the polyols can be calculated by volumetric titration process. 2 g of polyol sample was dissolved in isopropanol. This solution was then titrated by using 0.5 N HCl. Amine value was calculated by following the Equation (3.3.1.c)

$$Amine\ value = \frac{56.1 \times Volume\ of\ HCl \times N\ of\ HCl}{Weight\ of\ Sample}$$ ----------(3.3.1.c)

3.3.1.4 Non-volatile content:

The synthesized polyols were first weighed and then put in a vacuum oven for 48 hrs. and the weight of the polyols was measured again. The non-volatile content of the polyols can be derived from the Equation (3.3.1.d);

Non-volatile content (%) = $\frac{W_i - W_f}{W_i} \times 100$----------(3.3.1.d)

Where, W_i = Initial weight

W_f = Final weight

3.3.1.5 Viscosity:

Viscosity (η) is defined as the measure of resistance of a liquid or gas sample to change in movement or shape. It is inversely proportional to fluidity of a sample. Dynamic viscosity is the constant that is derived by dividing shear stress to shear strain at constant temperature. It can be measured by following the Equation (3.3.1.e). Unit for viscosity is Pascal-second (Pa-s).

$$\eta = [ForceXtime]/Area$$ ----------(3.3.1.e)

Viscosity of the polyols ECO, TECO, and ATECO was measured using Parallel-plate viscometer from M/s Thermofisher Scientific, Germany under shear rate of 500 Pa/s. The test was conducted at room temperature at constant shear rate.

3.3.1.6 Equivalent weight:

Equivalent weight is defined as the amount of substance required to react with other fixed amount of substance in a particular chemical reaction.

Equivalent weight can be derived by using the Equations (3.3.1.f) and (3.3.1.g);

$$Equivalent\ Weight\ of\ Polyol = \frac{56100}{OH\ value} \text{----------(3.3.1.f)}$$

$$Equivalent\ weight\ of\ Isocyanate = \frac{4200}{NCO\ content} \text{----------(3.3.1.g)}$$

3.3.1.7 Flash point:

Flash point is the minimum temperature at which a liquid gives off vapor within a test vessel in a sufficient concentration to form an ignitable mixture with the air near the surface of the liquid. The lower the flash point, the easier it is to ignite a liquid solvent. The flashpoint of each polyol sample was determined in accordance with ASTM D92-12b, by the Cleveland open cup COC method. 70 ml of each oil sample was poured into an open test cup, which was placed on a hotplate. A thermometer was immersed gently into each of the polyol samples while gradually regulating the heat from the hotplate. A test flame was passed across the open cup containing the samples at regular interval. A blue flame ignition with the vapour of the oil sample indicated the flashpoint of that sample under test. The flashpoint of each of the oil samples was read and recorded.

3.3.1.8 Water contact angle (WCA):

The water contact angle test can give an idea regarding the wettability of a surface. The contact angle is the angle where a liquid–vapor interface meets a solid surface. It depends on the hydrophobicity and surface energy of the surface.

The contact angle of commercial automobile base coat, synthesized base coat samples, commercial automobile clear coat, synthesized acrylic-PU-based clear coats, epoxy, blends and nanocomposites were measured at room temperature using sessile drop method using Apex Instruments, Germany. In sessile drop method, a small drop of water was placed on the substrate. A CCD camera with inbuilt zoom lens

makes a close inspection and measures the angle of contact between the water droplet and surface of the substrate. Deionized water was taken as the testing liquid.

3.3.1.9 Grafting %:

The grafting percentage is used to observe the effect of modification on NS. The weight of NS before and after modification is measured (W_1 is the weight of NS modified, and W_2 is the weight of NS before modification). The percentage grafting of the reaction is calculated by using Equation (3.3.1.h):

Grafting % = $([W_1 - W_2]/W_1)$ x 100 ----------(3.3.1.h)

3.3.1.10 Ethanol and water solubility:

NS before and after modification were weighed and placed in different beakers. After that deionized water and ethanol were added to different beakers which was dispersed for 30 mins in an ultrasonicator to observe the precipitation of NS in water.

3.3.2 Structural properties

3.3.2.1 Fourier Transform infrared (FTIR) Spectroscopy:

FTIR Spectroscopy provides specific information about reactions. When IR radiation is passed through a sample, some radiation is absorbed by the sample while some are transmitted. FTIR spectroscopy is an analytical methodology used to understand the structure of individual molecules and the composition of molecular mixtures. FTIR spectroscopy uses modulated, mid-infrared energy to interrogate a sample. The infrared light is absorbed at specific frequencies directly related to the atom-to-atom vibrational bond energies in the molecule. When the bond energy of the vibration and the energy of mid-infrared light are equivalent, the bond can absorb that energy. Different bonds in a molecule vibrate at different energies, and therefore absorb different wavelengths of the IR radiation. The position (frequency) and intensity of these individual absorption bands contribute to the overall spectrum, creating a characteristic fingerprint of the molecule.

FTIR analysis of polyols, synthesized and commercial base coat samples, synthesized and commercial clear coat samples, epoxy-PU blends and epoxy-PU nanocomposite was studied in a range of 4000-400 cm^{-1} using Nicolet 6700 spectrometer (M/s Thermoscientific, USA). The spectra obtained at 4 cm^{-1} resolution having 64 number of scans with standard wave range of 4000-400 cm^{-1}.

3.3.2.2 Hydrogen Nuclear Magnetic Resonance (^{1}HNMR) Spectroscopy:

It is a process in which selective absorption of very high frequency radio waves are observed, which is subjected to a strong constant magnetic field. The process occurs near resonance when the oscillation and intrinsic frequency of the nuclei matches with each other. The most commonly used nuclei are ^{1}H, ^{13}C, and ^{19}F.

Proton nuclear magnetic resonance (^{1}H NMR) spectra of polyols and paint samples were recorded employing deuterated chloroform ($CDCl_3$) as solvent using JEOL DELTA2 500 MHz FX-1000 Spectrometer (M/s INSTRON, USA). The samples when subjected to magnetic field, transfers of energy occur at a radio frequency wavelength.

3.3.3 Mechanical properties

3.3.3.1 Cross-cut Tape test:

Cross-cut tape test was used to measure the resistance of a paint/coating to separate from the substrate by using a cutting tool, that creates a right-angle lattice pattern penetrating all the way to the substrate.

The adhesion and scratch resistance properties of a paint formulations were evaluated using cross-cut Tape test in accordance with ASTM D 3359-97 using sample size of 50x50x3 mm mild steel plate. A cross cutter was used to draw 11 lines of 30 mm length within 10 mm width at equal distance on the coating surface applied on mild steel substrate. The same cross cutter was used to draw another 11 lines in similar manner in cross sectional way.

Then an adhesion tape of 25 mm width, semi-transparent and pressure sensitive tape (3M scotch tape) was pressed on the cutting surface for 1 min and then peeled forcefully at 180 ° angle to observe the scratch resistance and adhesion properties of paint. The adhesion value was calculated using the Equation (3.3.3.a);

$$Adhesion=\left(\frac{Number\ of\ squares\ attached\ to\ the\ adhesion\ tape}{Total\ number\ of\ squres\ on\ the\ coated\ substrate}\times 100\right)\%\text{----------}\quad(3.3.3.a)$$

3.3.3.2 Lap-shear test:

Lap-shear test can determine the ability of a material to withstand stress, where a shear force is moving the two joint substrates in opposite direction. It is also known as the failure strength of material, which can be calculated by dividing the failure load to bond area. A shear force is a force i.e., applied on a surface in opposite directions. The SI unit of shear force is N/mm^2 or MPa. The shear stress is a significant characteristic in a material to determine its structural integrity.

In the current study, BC, bio-based base coats, CP, bio-based clear coats, EP-PU blend, and EP-PU blend nanocomposites were subjected to Lap shear test in accordance with ASTM D 1002 using a Universal Testing Machine (M/s Instron, UK). The paints applied on a steel bar of 12.7 mm length and another bar was overlapped through this length to join the two bars after which it was kept for complete drying. Subsequently, Lap shear test was carried out at a load of 10 mm/min. The stress-strain curve obtained from the test was evaluated for the ability of the material to withstand the stress. The test was carried out at a standard laboratory condition of temperature of 23±2 °C and 55% RH.

3.3.3.3 Abrasion resistance test:

Abrasion resistance test determines the ability to withstand external impact forces of a material as well as it also can gives an idea about the quality, toughness, and durability of a material. In other words, the objective of this test is to observe the ability of the material to withstand the wear and tear friction caused by continuous rubbing or scratching at same place.

The abrasion resistance test for the coated samples of 110x110x3 mm size were

carried out at a load of 500 g using abrading wheels CS10 for 500 cycles in a Taber Abrasion Resistance Tester (M/s Taber Model 530 Abrader, USA) in accordance with ASTM D 1044-08. The results were evaluated from the weight loss of test disc induced by the abrading wheels. Three consecutive tests were carried out for each sample to determine the abrasion resistance.

3.3.3.4 Pencil Hardness test:

It is the simplest form of hardness test and is also known as wolf-wilborn test. In this method the 14 ° of graphite pencil ranging from 6B to 6H are used to determine the hardness of a coating sample.

The pencil hardness of the paint formulations was determined at room temperature following ASTM D 3363-05 method. Wood was removed up to 5-6mm from the pencil tip and sharpened with 400 grit sand paper. The pencils used are stroked at 45 º angles up to 3mm in length with a grade ranging from 6H to 6B.

3.3.3.5 Nano-indentation test:

Nanoindentation test is used to measure various mechanical properties like, hardness, viscoelasticity, and elastic modulus of a material. The parameters required in this test are loading force and indentation depth. It is used to characterize microhardness and viscoelasticity of packaging thin films, cutting tool alloys, and coatings. In this test the surface of the sample taken is plain, thus the surface roughness plays in measure role in determining the contact depth.

A UMIS Nanoindentation system using a UMIS Nanoindentation system (M/s Frsher-cripps, Australia) with a Berkovich indenter of tip radius 150 nm and face angle of 63.5 ° was used to determine the hardness (H) and elastic modulus (E′) and displacement of PU_2, PU_2NS_1 and commercial coatings. Maximum load applied was 10 mN and at least 10 indentations were carried out for each specimen at different position and the average value was reported. Oliver and Pharr method was used to determine the H and E′ values using Equations. (3.3.3.b) and (3.3.3.c)

$$H = F_{max}/A \text{----------(3.3.3.b)}$$

$$\frac{1}{E_r} = \left[1 - \frac{V^2}{E}\right] + \left[1 - \frac{V_i^2}{E_i}\right] \text{----------(3.3.3.c)}$$

Where, H= Hardness

F_{max}= Maximum load applied

A= Projected contact area between the indentor tip and substrate

E= Elastic modulus of substrate

V_2= Poisson's ratio of substrate

V_{i2}= Poisson's ratio of indentor tip

E_i= Elastic modulus of indentor tip

E_r= Residual or effective elastic modulus

3.3.3.6 Tensile test:

This test can be used to measure the tensile strength, yield strength, and ductility of a material. In this test the sample material is gripped in both the ends in a tensile tester and is slowly pulled until it fractures.

Tensile strength, tensile modulus, and elongation at break of neat epoxy, biobased epoxy blends and its composites having specimen dimension of 165x25x3 mm were analysed at a crosshead speed of 1 mm/min and a gauge length of 50 mm using Universal Testing Machine (M/s Instron, USA) in accordance with ASTM D 3039.

3.3.3.7 Impact test:

Impact test is used to determine the toughness, impact strength, and notch sensitivity of a material. The impact strength is calculated by dividing impact energy in joule (J) to the notch area. Higher impact strength leads to higher toughness of a material. This test helps to study the brittleness of a material as well as its resistance to sudden load.

Both un-notched and notched Izod impact samples of EP-PU blends and EP-PU nanocomposites having dimensions of 63.5 × 12.7 × 3 mm were used for impact testing using IT 504 Plastic Impactometer (M/s Tinius Olesan, UK) in accordance to ASTM D 256 employing a Notch cutter. The notch depth was kept 2.54 mm and the notch angle was 45 °.

3.3.3.8 Fracture Toughness:

Fracture toughness is defined as the resistance of a material to crack propagation under load. Factors affecting fracture toughness are temperature, strain rate, stress and ductility relationship and notch. It is also known as the critical stress intensity factor of a sharp crack, where the propagation of crack becomes rapid.

In the current study, blend samples of size 30x6x3 mm were taken for single notch test, with initial notch length 2.54 mm using Universal Testing Machine (M/s Instron, USA) as per ASTM D 5045. The span length was set at 24 mm and load applied with a speed of 1mm/min. The critical stress intensity (K_{IC}) can be measured by following Equation (3.3.3.d) and (3.3.3.e).

$$K_{IC} = 6YP/BW^{1/2} \text{----------(3.3.3.d)}$$

$$y = 1.93(\frac{a}{W})^{1/2} - 3.07\left(\frac{a}{W}\right)^{\frac{3}{2}} + 14.53\left(\frac{a}{W}\right)^{\frac{5}{2}} - 25.11\left(\frac{a}{W}\right)^{\frac{7}{2}} + 25.80(\frac{a}{W})^{9/2} \text{--------(3.3.3.e)}$$

Where, a = Pre-crack length

P = Maximum load

B = Specimen Thickness

W = Specimen width

The specimen strain energy release rate (G_{IC}) can be calculated by following Equation (3.3.3.f)

$$G_{IC} = (K_{IC})\frac{2}{E} - - - - - - - (3.3.3.f)$$

Where, E = Young's Modulus

All the mechanical characterizations were carried out at 23±2 °C temperature with relative humidity 55±5 %

3.3.4 Thermal Properties

3.3.4.1 Dynamic Mechanical Analysis (DMA):

DMA is used to determine the characteristic properties of a material as a function of time, temperature, stress, and frequency. In this test a small deformation is applied on the sample in cyclic manner to study the storage modulus, loss modulus, and damping. Storage modulus shows the elastic behavior of the sample, while the ratio of storage modulus to loss modulus is known as tan delta (tan δ) or damping.

DMA and cross-linking density of paint samples and sealer samples were carried out in a dynamic mechanical analyser (DMA Q 800, M/s TA Instruments, USA) as per ASTM E 5418. The samples were scanned from -50 ºC to 100 ºC for paint samples and -50 °C to 140 °C for sealer samples respectively at a heating rate of 10 ºC/min. The storage modulus and tan delta were recorded. The cross-linking density (ϑ_c) can be calculated by using the rubber elasticity concept provided by the DMA graph. The following Equation (3.3.4) is used to determine the ϑ_c value.

$$E' = 3RT\vartheta_c \quad \text{----------(3.3.4)}$$

Where, E'= Storage modulus

R= Universal gas constant

T= Absolute temperature

3.3.4.2 Differential scanning calorimetry (DSC):

DSC is a thermal analysis process in which heat flow of a sample is measured as function of temperature and time under a controlled temperature atmosphere. It is used to determine the glass transition temperature (T_g), melting point (T_m), degree of

crystallization (T_c), specific heat capacity, curing behaviour, and thermal stability of a material.

DSC analysis of polyols, paint samples and sealer samples were carried out using DSC Q 20 equipment (M/s TA Instruments, USA) at temperature range of -50 ºC to 80 ºC for polyols and paint samples and -50 °C to 160 °C for sealer samples respectively at a heating rate of 10 ºC/min.

3.3.4.3 Thermogravimetric analysis (TGA):

TGA is a thermal analysis process in which, the thermal stability and the volatile fraction present in a material is studied. The parameters, that affect the TGA study are weight loss at constant rise in temperature and derivative weight loss. It can be used to determine moisture loss, pyrolysis, solvent loss, plasticizer loss, oxidation as well as phase changes occur during decomposition of a material.

Thermogravimetric analysis (TGA) analysis of polyols, paint samples and sealer samples were studied at temperature range of 30–600 ºC for polyols and paints and 30-750 °C for sealer samples respectively at a heating rate of 10 ºC/min using TGA Q 50 equipment (M/s TA Instruments, USA) as per ASTM E 1868. The corresponding initial and final degradation temperatures and char percent were recorded.

3.3.5 Optical properties

3.3.5.1 UV-visible spectra:

UV-visible spectroscopy is based on the absorption of electromagnetic radiation in UV-visible region, where the wavelength ranging from 200-400 nm is called UV region and the wavelength ranging from 400-800 nm is known as visible region. It is used to study the quantitation to quality control of a material. The basic principle of UV-visible spectra defines that, a sample is subjected to a beam of electromagnetic radiation, then the absorbance and transmittance of the beam was observed and studied as a function of radiation wavelength.

UV-visibility spectra of PU_2 and PU_2NS_1 were carried out at wavelength range of 200-800 nm using a Cary-60 UV visible spectrometer (M/s Agilent Technologies, Pvt. Ltd., USA) to study the absorbance and transmittance properties of the synthesized clear coat samples.

3.3.5.2 Haze and Transmittance:

Haze is defined as the degree of opaqueness of a transparent or semi-transparent thin film material, when a light beam passes through it. Transmittance measures the amount of light passes though the film material and is inversely proportional to haze. Haze is expressed in %, and lower haze value better transparency of a film.

Transmittance and haze test of clear coat films of dimensions 50×50×1.5 mm was carried out at room temperature using a Spherical Haze meter (M/s RDM Test Equipment Co. Ltd., England) as per ASTM D 1003. The % of haze and transmittance was observed by studying three samples from each paint formulation.

3.3.5.3 Gloss and weather resistance:

Gloss test can be used to determine the reflective properties a material at particular angle based on its refractive index. A Gloss meter is used to measure the gloss of a surface by projecting a beam of light at fixed angle and intensity on the surface, where the amount of reflected light at equal but opposite direction. Weather resistance test determines the capability of a material to withstand harsh change in weather. A weatherometer enhances the property changes of a material influenced by a combining effect of sunlight, moisture and heat, and ultraviolet environment.

Gloss study of paint formulations were carried out using Digital Gloss meter, SFM-115 (M/s S. C. Dey & Co., Kolkata) at 45 $^{\circ}$ angle. Weather resistance test for paint formulations with dimensions 150x60x3 mm was carried out using QUV/SE equipment (M/s in presence of UV environment for 1200 hrs. and gloss was taken as the parameter to study the change in properties.

3.3.6 Morphological properties

3.3.6.1 X-ray diffraction (XRD):

XRD is a non-destructive test, which is used to determine the crystalline structure, lattice parameter as well as chemical composition of a material. It helps to observe the geometry of the molecules of a material by using X-ray beams. When an x-ray beam is subjected to a powder sample, the scatter intensity is measured. After the beam is separated, the scatter which is known as diffraction pattern, shows the crystalline structure of the sample. The principle followed in XRD test follows the Bragg's law which is defined in the Equation (3.3.6)

$$\lambda = 2dsin\theta \text{----------(3.3.6)}$$

Where, λ = Wave length of x-ray beam

d = Spacing of the diffracting planes

θ = Angle between incident ray and diffracting plane

XRD of ATES-NS, TI-NS, and NS were carried out using 2-θ range from 5-80 ° using XRD- 7000 L equipment (M/s Schimadzu, Japan) as per ASTM E 1426. The specifications during testing were voltage 40 kV, current 30 mA, scanning speed was 10 °/min and accuracy was 0.0002 °.

3.3.6.2 Scanning Electron Microscopy (SEM):

SEM uses a focused beam of electrons to scan the surface of a sample to create a high-resolution image, which helps to study the surface composition and topography of the material. This test gives high-resolution images to study surface fracture, contamination, corrosion, and flaws of the sample.

SEM analysis of the paint formulations and sealer formulations mounted on a carbon sticker were conducted with acceleration voltage of 0.2-30 kV and magnification 5-1,000 KX using EVO MA 15 Microscope (M/s Carl Zeiss SMT, Germany). Prior to analysis, the samples were sputter coated with Au/Pd mixture.

3.3.6.3 Transmission Electron Microscopy (TEM):

In TEM a very high energy electron beam was subjected to the sample i.e., partially electron transparent and the shadow of electron was digitally recorded and viewed. It is used to study the morphology of very small samples in nm range.

TEM was carried out with Accelerating voltage 200 KV, Resolution: Point: 0.194 nm, Lattice 0.14 nm, 5-axis eucentric goniometer stage, and Specimen tilt ±60 ° using JEM 2100 Plus High-Resolution Transmission Electron Microscope (M/s JOEL, Japan). NS and TI-NS particles were first dispersed in ethanol and 2 ml of solution was taken and dried on a carbon-coated copper grid, subsequent to which the images were taken using the dried samples. The PU/NS composite film was cut into thin cross-sections of 100 nm range using ultramicrotomy. The thin sections were taken for TEM micrography.

3.3.7 Chemical and Oil Resistance properties

3.3.7.1 Petrol resistance:

Paint samples along with commercial paint samples coated on mild steel sheet are immersed in petrol for 8 hrs. at room temperature. After that the paint sheets were washed thoroughly with water and dried. The change in paint surface was observed from optical microscopy.

3.3.7.2 Diesel resistance:

Paint samples along with commercial paint samples coated on mild steel substrate were immersed in diesel for 8 hrs. Optical microscopy was carried out to study the changes in paint surface.

3.3.7.3 Engine oil resistance:

Paint samples coated on mild steel plate was immersed in engine oil at 100 °C for 8 hrs. After that the paint samples were thoroughly washed and dried. Optical microscopy was used to study the changes in paint surface after its immersion in engine oil.

3.3.7.4 Acid resistance:

Paint samples coated on mild steel plate were taken for acid resistance test. Three polyethylene washers were placed on the paint surface and 2 ml of sulfuric acid (H_2SO_4) was dropped within the washer area. After 24 hrs. the paint samples were washed and changes in paint surface was studied.

3.3.7.5 Alkali resistance:

Paint formulation subjected to alkali resistance test follows the similar steps of acid resistance test, on the contrary in pace of H_2SO_4, NAOH solution is used to study the alkali resistance properties of paint samples.

3.3.7.6 Solvent resistance:

Solvent resistance test of the paint formulations was studied as per ASTM D 543-67. Samples of dimensions 10×10 mm size with thickness 1-3 mm. then the samples were immersed in four different solvents i.e., acetone, DMF, xylene and toluene for 7days. The weight of each sample was measured in every 24 hrs. The process was continued till the weight of the sample become constant in the solvent. The change in weight in the sample was calculated in wt.% from the following formula.

$$\text{Wt. loss \%} = \frac{W1-W}{W} \times 100$$

Where, W=Initial weight of sample

W1=Final weight of sample

CHAPTER 4

Chapter 4

Synthesis of bio-based Automobile base coat derived from CO, incorporated with NS and TP

Introduction

Polymers are the foundation of coating industries and have applicability in many fields [160]. Among all the polymers used in coating industry, PU is considered as one of the most versatile coating material due to its specific properties such as high resistance to scratch and abrasion, chemical resistivity and ability to withstand the environmental effects [161]. In the recent trend most of the automobile paint is predominantly PU or acrylic based. The automobile body is first pre-treated, and then dipped in electro-deposition tanker for e-coating. Then it is e-sanded and sealer is applied to the substrate. Subsequently, primer layer, base coat and clear coat are applied [53]. Base coat applied to the automobile body primarily constitutes of PU which are predominantly petro-based polyols and diisocyanates. However, with the rising global concerns for the use of eco-friendly materials in coating applications, there have been considerable research interests in moving towards alternative resources, while reducing the dependency on petro-based feed-stock.

In the recent years, vegetable oil-based polymers have generated considerable research interests due to its unique chemical structure consisting of unsaturated fatty acids. These oils are renewable, cost effective and environment friendly [19]. The molecular structure of vegetable oils contains triglycerides and unsaturated carbon–carbon double bonds, which can be functionalized into polyols. Functionalization techniques include epoxidation, hydro formylation, transesterification, amidation, thioene coupling etc. [162]. Oils like castor oil (CO), soybean oil, sunflower oil, linseed oil etc. have been extensively used as polyol for synthesis of PU [163]. Among all the vegetable oils, castor oil (CO) has been widely used in the synthesis of bio-based coatings due to its abundance and low cost. CO has around 85-90% of recinoleic acid, which is highly reactive [164]. The reactive hydroxyl groups can be suitably used as a polyol for synthesis of polymers like PU, polyamide, polyester, epoxy etc. CO also has

the specific properties for its use in coating application like, high viscosity and lubrication properties, high flash point value, and nonvolatile due to presence of triglycerides. However, several impediments like low thermal properties and low oxidative properties of CO due to presence of higher number of unsaturated fatty acids restrict its extensive application in different sectors. Hence, chemical modification of CO such as transforming the carbon double bonds of the unsaturated fatty acids to oxirane rings through epoxidation process increases its reactivity significantly [165]. Further, in order to enhance the applicability of PU coating, an in-depth analysis in terms of improvement of properties has been studied by addition of various nano fillers like TiO_2, ZnO, SiO_2, Al_2O_3 etc. [2, 9]. Nano fillers reinforced within polymeric matrix results in enhancement in mechanical, thermal and chemical resistance properties of the coatings [167].

In the current study, bio-based PU base coat was synthesized by employing epoxidized castor oil (ECO) as polyol and Isophorone diisocynate (IPDI) as the isocyanate. To improve the applicability of the synthesized base coat, NS particles were added within the PU matrix. Further, NS was surface modified with the APTES to achieve proper interfacial adhesion between PU and filler. TP was also added to the prepared paint for colouring purpose. For better assessment regarding the effect of NS and TP, a comparative study of properties of neat PU, PUNS and PUNSTP has been studied. An in-depth analysis employing, FTIR spectroscopy, SEM and XRD analysis in addition to mechanical, thermal and chemical resistance test have been reported.

4.1 Properties of ECO

4.1.1 FTIR

FTIR spectra of CO and ECO are displayed in Fig. 4.1.a

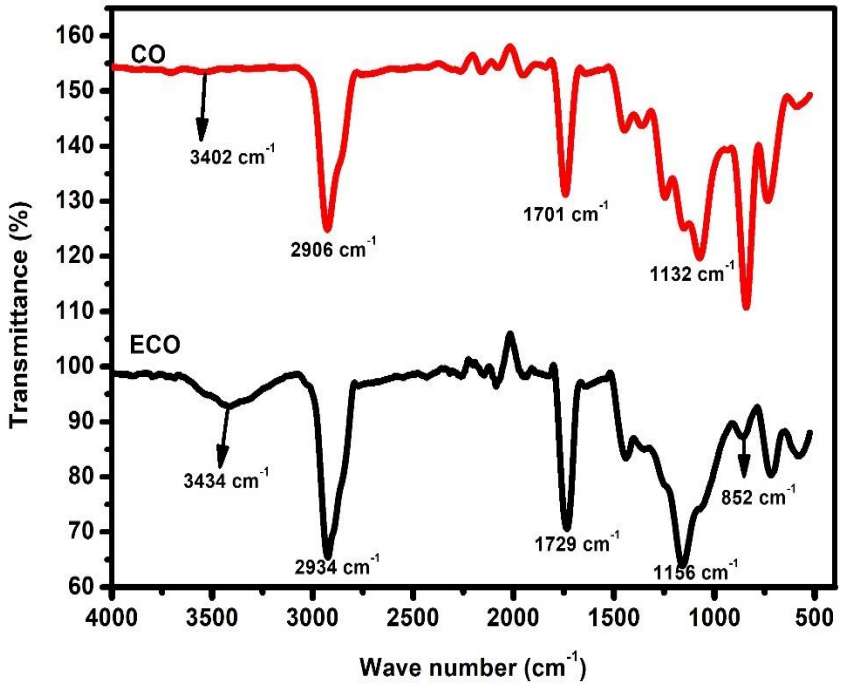

Fig. 4.1.a: FTIR spectra of CO and ECO

From Fig. 4.1.a; it is observed that the CO and ECO have –OH bond noted at 3402 and 3434 cm^{-1} respectively. The spectra of –CH stretching was observed at 2906 and 2934 cm^{-1} for CO and ECO respectively. Conformation of epoxidation was observed from the –COO bond noted at 852 cm^{-1} in the ECO spectra. –C=O stretching was observed at spectra 1701 and 1729 cm^{-1} respectively for CO and ECO [168].

4.1.2 Hydroxyl value

Hydroxyl value of ECO can be calculated by using the graph displayed in Fig. 4.1.b

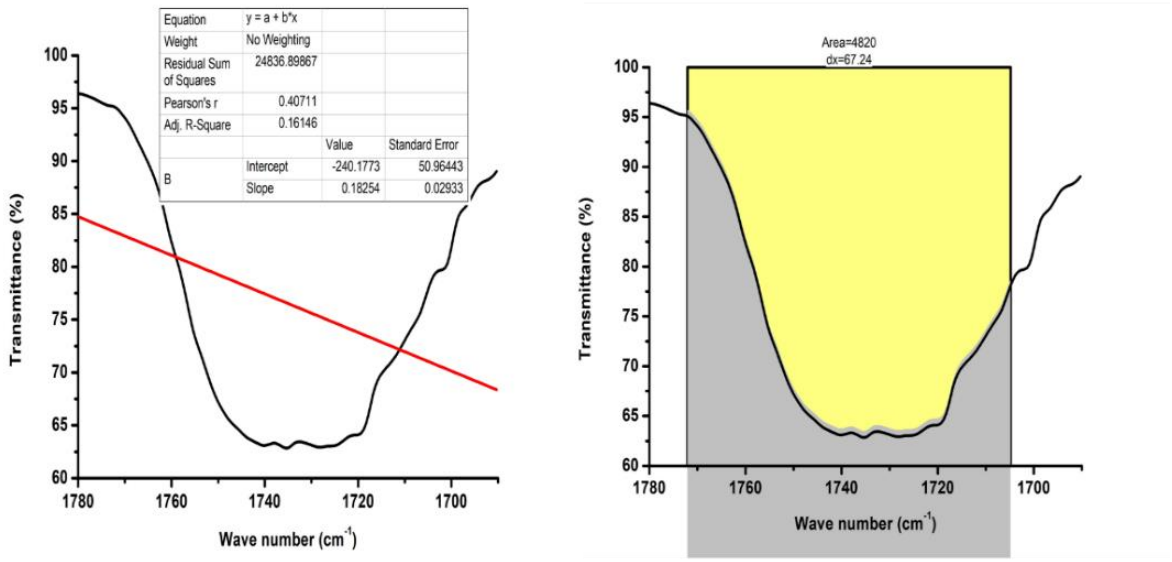

Fig. 4.1.b: Integral, Intercept, and Slope value of ECO-TSI FTIR spectra

Hydroxyl value was calculated from the carbamide ring studied on the FTIR spectra observed in between 1690-1780 cm^{-1} as shown in Fig. 4.1.b. CO procured has a given hydroxyl value of 170 mg/KOH. After epoxidation process, it was observed to be 208 mg/KOH. During Epoxidation process, the unsaturated carbon-carbon double bonds forms the epoxide bond, resulting in increase in functionality as well as hydroxyl value of ECO[165].

4.1.3 Acid value, Amine value, Non-volatile content, and Equivalent weight

Table 4.1: Acid value, Amine value, Non-volatile content, and Equivalent weight of CO and ECO.

Specifications	Acid value (mgKOH/g)	Amine value (mgKOH/g)	Non-volatile content (%)	Equivalent wt. (g/ eqv)
CO	2	12	98.51	330
ECO	1.75	13.09	96.30	270

Table 4.1 reports the acid value, amine value, non-volatile content, and equivalent weight of CO and ECO were studied. ECO has more polar structure than CO, due to the formation of epoxide ring, which leads to decrease in acid value and non-volatile content. On the contrary, the polar structure of ECO increased its amine value in comparison to CO. Equivalent weight is inversely proportional to hydroxyl value. Hence, with increase in hydroxyl value, the equivalent weight of ECO, was observed to be decreased[169].

4.1.4 Viscosity

Viscosity graph is depicted in Fig. 4.1.c

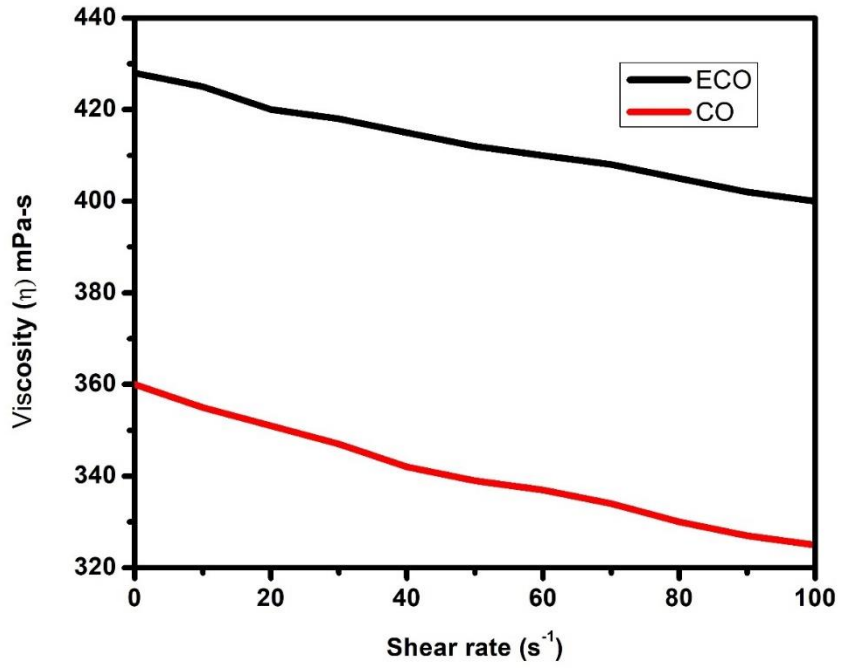

Fig. 4.1.c: Viscosity graph of CO and ECO

Viscosity of CO and ECO were studied from the viscosity graph depicted in Fig. 4.1.c. The viscosity of ECO was observed to increase from 360 mPa-s to 428 mPa-s in comparison to CO. The epoxidation process results in higher entanglement of polymer chain, which leads to significant increase in viscosity[169].

4.1.5 Flash Point

Flash point of CO was observed 240 °C, whereas after epoxidation process, the flash point was increased significantly to 249±5 °C. The increase in flash point occurred due to the presence of antioxidants in ECO.

4.2 Properties of APTES-NS

4.2.1 FTIR

FTIR spectra of APTES-NS is displayed in Fig. 4.2.a

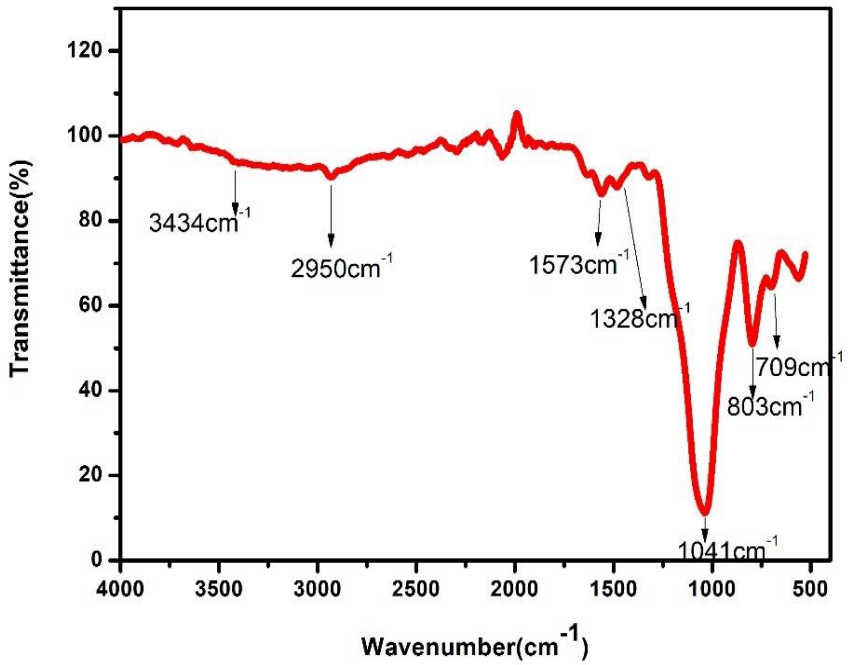

Fig. 4.2.a: FTIR spectra of APTES-NS

FTIR of APTES functionalized NS from Fig. 4.2.a displays a Si-O-Si asymmetric bond noted at 1041cm^{-1} whereas Si-O-Si symmetric bond was noted at 803 cm^{-1}. The spectra of Si-C bond was observed at 709 cm^{-1}. The presence of APTES was confirmed from the peaks at characteristic vibration noted at 1573 cm^{-1} and 1328 cm^{-1} corresponding to the amino propyl group. The C-H bond at 2950 cm^{-1} is due to alkyl chain in APTES. At 1328 cm^{-1} it shows –NH stretching peak while the peak corresponding to 1573 cm^{-1}is due to the N-O stretching [161, 162].

4.2.2 XRD

XRD spectra of NS and APTES-NS is displayed in Fig. 4.2.b

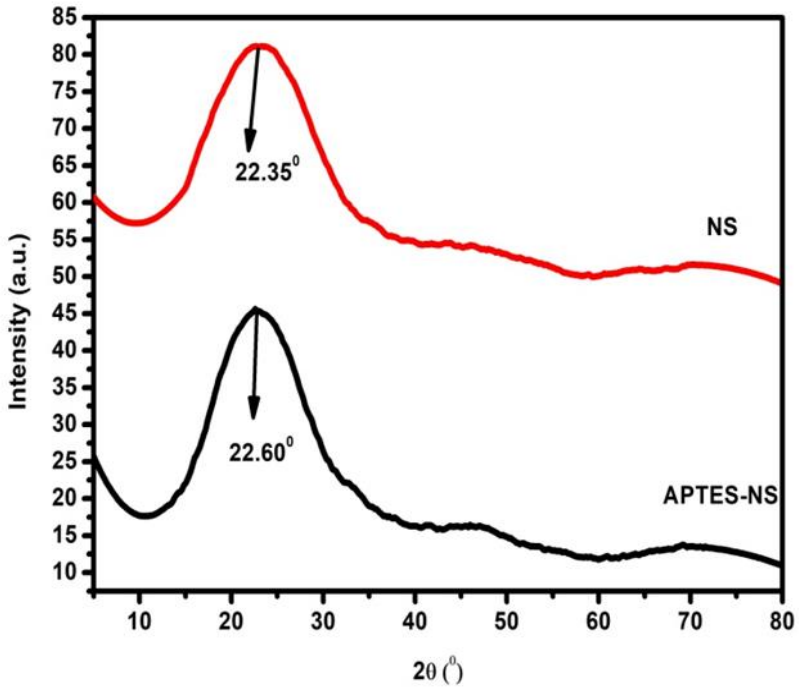

Fig. 4.2.b: XRD of (a) NS (b) APTES functionalized NS

The XRD analysis of NS and APTES functionalized NS is displayed in Fig. 4.2.b. Comparing NS and APTES functionalized NS, the 2-θ value was observed at 22.35 ° for neat NS, while for APTES functionalized NS shifted marginally to 22.6 ° indicating increase in the interplanar distance. Also the presence of broad peaks revealed amorphous nature of APTES functionalized NS particles in comparison to neat NS [172]. From the above study it was found that there was no impurity peak in the spectrum and it was highly amorphous in nature.

4.3 Properties of Base coat derived from CO

4.3.1 Optimization by Cross-cut Tape test

Adhesion strength of paint formulations are described in Table 4.3.a

Table 4.3.a: Adhesion strength of paint formulations

Sample Name	Adhesion (%)
BC	84±3
PU_1	42±4
PU_2	49±3
PU_3	65±5
PU_4	59±4
PU_3NS_1	88±3
PU_3NS_2	83±3
PU_3NS_3	78±1
$PU_3NS_1TP_1$	89±2
$PU_3NS_1TP_2$	92±3
$PU_3NS_1TP_3$	85±4

Cross-cut tape test was performed to evaluate the effect of molar ratio of NCO:OH and the incorporation of NS and TP on the adhesive strength of the paints. The results were shown in Table 4.3.a. BC displays an adhesive strength of 84±3%. The PU paints prepared at a molar ratio of 1:1 and 1.1:1 exhibited an adhesive strength of 42±4 and

49±3%respectively in case of PU_1 and PU_2. Increasing the molar ratio of NCO:OH to 1.2:1, resulted in increased cross-linking density and H-bonding between –OH group ECO and –NCO of isocyanate thereby contributing in the enhancement in adhesive strength to 65±5% in PU_3. However with additional increase of NCO to 1.3, enhanced the rigidity of the system which in turn resulted in decreased adhesion of the paint with the substrate to 59±4% in PU_4. The PU paint with NCO:OH ratio 1:1 and 1.1:1 had very longer curing time compared to other prepared samples and their adhesion strength was also lower as compared to the other PU samples. On the contrary at NCO:OH ratio of 1.2:1 (PU_3), the curing time decreased and the adhesion strength of the paint increased significantly. Thus the PU paint at NCO:OH molar ratio 1.2:1 was optimized and taken for reinforcement with NS. It is evident that incorporation of NS within neat PU paint at variable concentration of 0.5-1.5 wt%, resulted in enhancement of the adhesive strength. The paint at 0.5 wt.% of NS (PU_3NS_1) exhibited complete dispersion of nanoparticles with a significant increase in adhesion strength to the tune of 88±3% as compared with neat PU. However increasing the concentration of NS to 1 wt.% (PU_3NS_2) resulted in agglomeration of NS in the paint which decreased the strength. Addition of NS to 1.5 wt.% (PU_3NS_3) showed higher agglomeration of NS in the paint which further detoriated the adhesive strength. Further, incorporating TP within the PU_3NS_1 paint showed marginal improvement in the adhesive strength. The paint formulation prepared at 0.5 wt.% NS and 0.2 wt.% of TP at NCO:OH ratio 1.2:1 exhibited optimum adhesive strength of 93±2%, which was comparable with BC [173].

4.3.2 FTIR:

FTIR spectra of paint formulations are displayed in Fig. 4.3.a

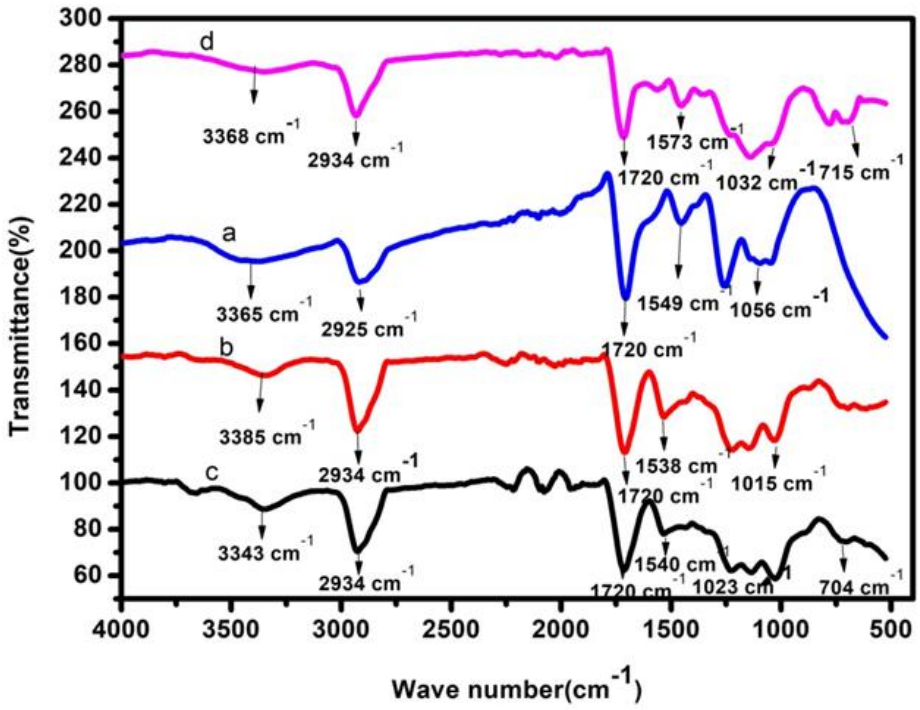

Fig. 4.3.a: FTIR spectra of (a) BC (b) PU_3 (c) PU_3NS_1 (d) $PU_3NS_1TP_2$

As observed from Fig. 4.3.a, the FTIR spectra of the BC shows –NH stretching at 3365 cm^{-1}, while in case of PU_3, PU_3NS_1 and $PU_3NS_1TP_2$, the –NH stretching was noted at the 3343, 3385 and 3368 cm^{-1} respectively. BC shows –CH stretching bond at 2925 cm^{-1}while the same was observed at 2934 cm^{-1}in the developed paint formulations. The peak corresponding 1720 cm^{-1} revealed -C=O stretching in all the samples. The –CH bond was observed at 1549 cm^{-1} in BC 1538 cm^{-1} in PU_3 paint, 1540 cm^{-1} in PU_3NS_1 and 1573 cm^{-1} in $PU_3NS_1TP_2$ respectively. Similarly –NCO stretch was found at 1253 cm^{-1} for BC while in case of the prepared paints, the peak corresponding to 1228cm^{-1} revealed the –NCO stretching. Thus, it is confirmed that commercial BC constitutes of PU. The C-O-O bond stretching was found at 1056 cm^{-1} for BC which was observed at 1015, 1023 and 1032 cm^{-1} in PU_3, PU_3NS_1 and $PU_3NS_1P_2$ respectively. The prepared samples also show another C-O-O bond corresponding to 875, 892 and 950 cm^{-1} in PU_3, PU_3NS_1 and $PU_3NS_1TP_2$ respectively. Complete

disappearance of -NCO peak at around 2250 cm^{-1} for commercial paint, PU_3NS_1 and $PU_3NS_1TP_2$ proved complete polymerization reaction as compared to neat PU. Furthermore, as evident from the spectra of PU_3NS_1 and $PU_3NS_1TP_2$, the Si-O-Si stretching peak corresponding to the presence of APTES functionalized NS was observed at 704 cm^{-1} and 715 cm^{-1} respectively [12]. From the study it was found that the bond formed in neat PU and PUNS have relevant chemical bonding. With the incorporation of TP particles there was no applicable change in chemical bonds as observed from the FTIR spectra.

4.3.3 ^{1}H-NMR Test

^{1}H-NMR spectra of $PU_3NS_1TP_2$ is reported in Fig. 4.3.b

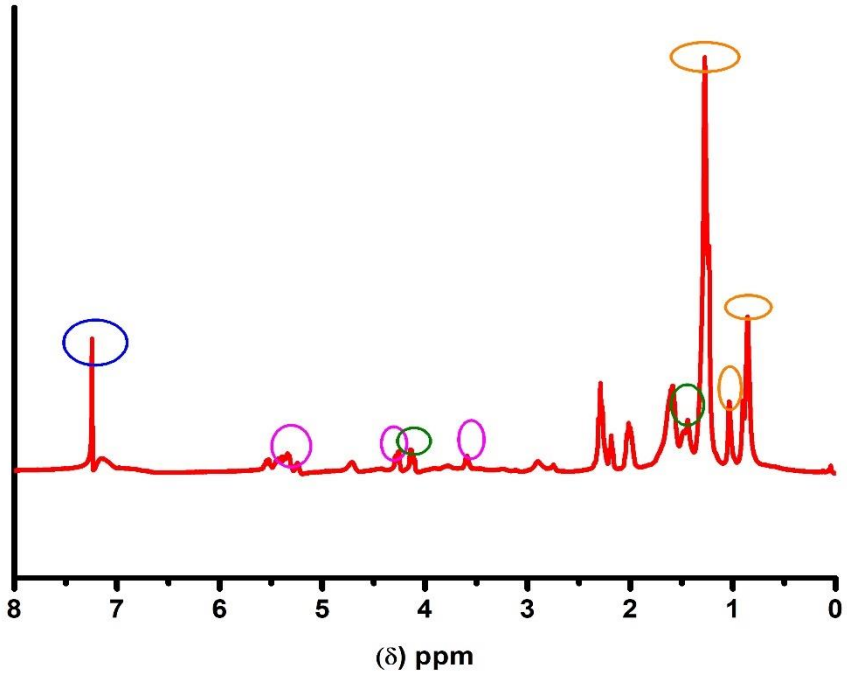

Fig. 4.3.b: ^{1}HNMR spectra of $PU_3NS_1TP_3$

Fig. 4.3.b depicted the ^{1}HNMR spectra of the optimized paint sample. The peak observed in between 7-8 ppm showed the presence of $CDCl_3$. The peaks observed at 5.3, 4.15, and 3.6 corresponds to $-CH_2$, $-CH_2$ allyl and $-CH_2$- vinyl group respectively. The peak observed at 4.1 ppm indicated the $-CH_2$ group attached to secondary carbon.

The peak at 1.81 corresponds to the presence of methyl proton group. This study additionally confirmed the PU formation[174].

4.3.4 DMA and Cross-linking density

DMA micrograph of paint samples is displayed in Fig. 4.3.c (i) and (ii)

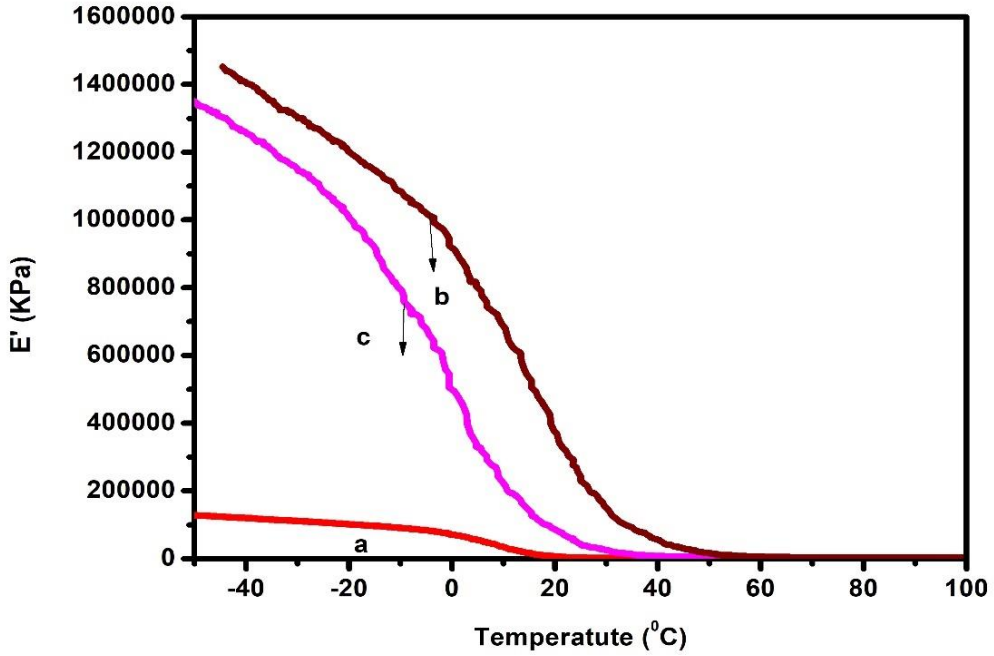

Fig. 4.3.c: (i) DMA curve of Storage modulus vs. Temperature (a) PU_3 (b) PU_3NS_1 (c) $PU_3NS_1TP_2$

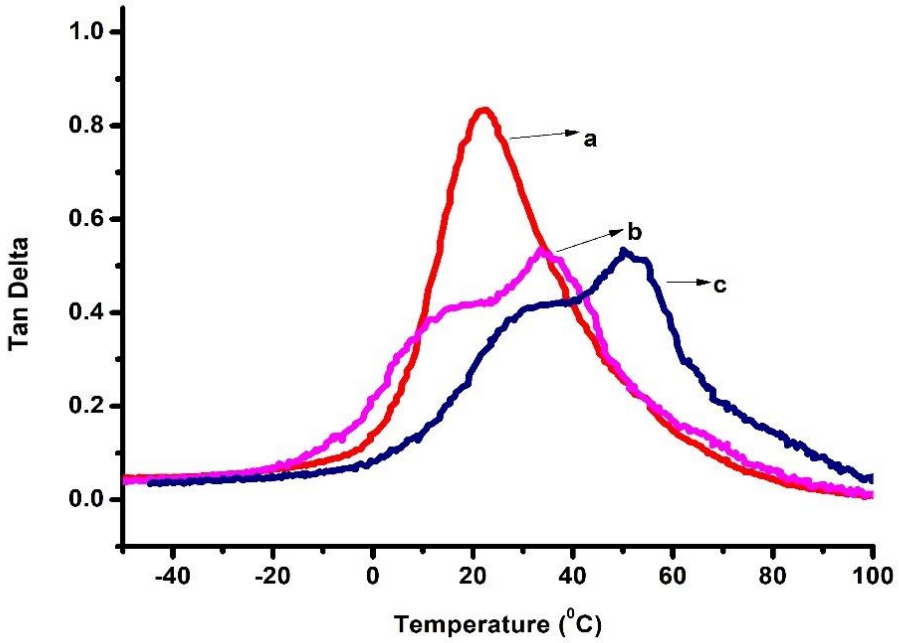

Fig. 4.3.c: (ii) DMA curve of tan delta vs. Temperature (a) PU_3 (b) PU_3NS_1 (c) $PU_3NS_1TP_2$

The plot of damping curve (tan delta) as a function of temperature of the paint samples is depicted in Fig. 4.3.c. It is observed that the all three synthesized polyurethane samples, i.e., PU_3, PU_3NS_1, and $PU_3NS_1TP_2$, exhibit two damping corresponding to the soft segment and hard segment due to phase separation. The low-temperature damping peak corresponds to the glass transition temperature of the soft segment (T_{gs}), whereas the higher temperature damping peak corresponds to the glass transition temperature of the hard segment (T_{gh}). Usually, the T_{gs} and the T_{gh} for polyurethane ranges from –50 to 120 °C wherein the negative temperature corresponds to the soft segment and the positive temperature corresponds to the hard segment [164]. However, in the present study, the T_{gs} for PU_3, PU_3NS_1, and $PU_3NS_1TP_2$ is observed at –24.5, –12.9, and 2.65 °C, respectively, whereas the T_{gh} is observed at 1.94, 6.85, and 11.23 °C, respectively. This might be due to the high compatibilization of hard and soft segments in the synthesized PUs. In addition, the higher T_{gs} and T_{gh} observed for $PU_3NS_1TP_2$ indicates increased restriction of segmental mobility of the polyurethane chain due to higher cross-linking density caused by insertion of both NS and titanium-based pigment particles. The E' falls

drastically near -30 to 20 °C in case of PU_3NS_1 and $PU_3NS_1TP_2$ paints which is due to T_g region of soft segments. Additionally, it was noted that, a minor transition region corresponding to hard segment was noted at +15 to +20 °C in case of PU_3NS_1 and $PU_3NS_1TP_2$. Further as observed from the graph E' followed the following order PU < $PU_3NS_1TP_2$ < PU_3NS_1. This behaviour confirmed the fact that incorporation of NS increased modulus of PU due to segmental immobilization of matrix chains at the interface. Additionally, addition of TP into the PU_3NS_1 matrix possibly leads to agglomeration between NS and TP, which decreased the E'. This further supports the results discussed in confirming higher cross-linking density formed in $PU_3NS_1TP_2$. Cross-linking density of PU_3 was calculated to be 0.16 mol/m^3, which increased significantly to 2.08 and 2.40 mol/m^3 for PU_3NS_1 and $PU_3NS_1TP_2$ respectively. The increased cross-linking density value is due to the presence of NS particles which forms a closed network structure with the PU matrix increasing the interfacial force of the polymer matrix.

4.3.5 TGA

TGA/DTG thermogram of paint samples are displayed in Fig. 4.3.d and Table 4.3.b

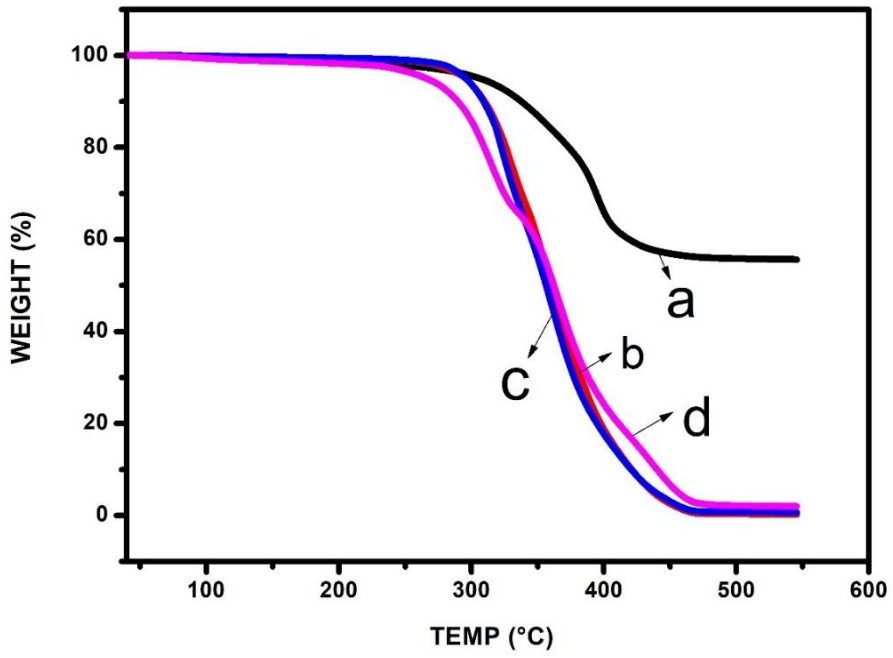

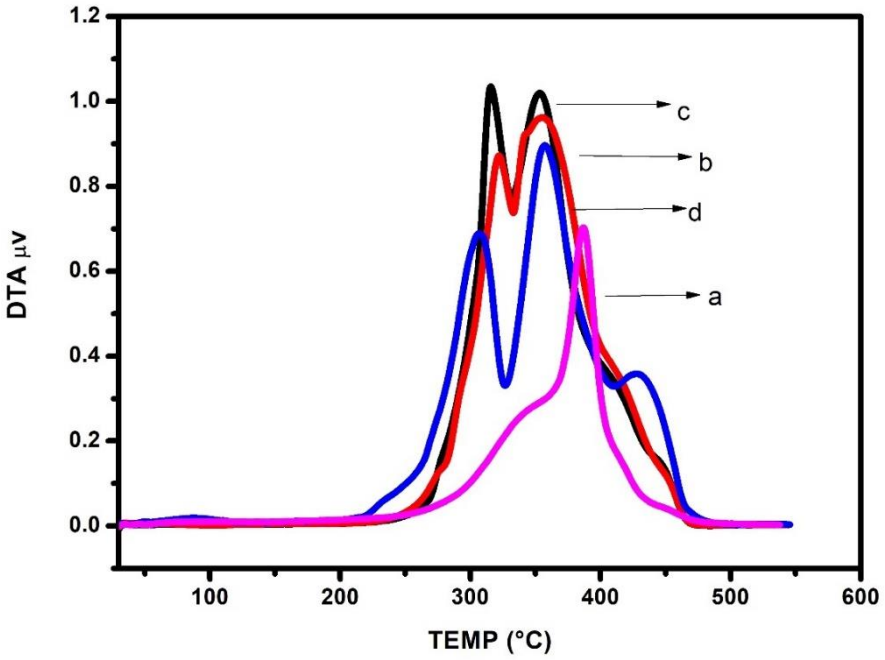

Fig. 4.3.d: TGA/DTG Thermogram of (a) BC (b) PU_3 (c) PU_3NS_1 (d) $PU_3NS_1TP_2$

Table 4.3.b: TGA/DTG data of Paint formulations

Paint formulations	T_i (°C)	$T_{50\%}$ (°C)	T_f (°C)	Char residue (%)
BC	303	427	545	55.4
PU_3	272	393	465	0.29
PU_3NS_1	283	425	545	0.63
$PU_3NS_1TP_2$	268	443	597	1.26

TGA thermograms of BC, PU_3, PU_3NS_1 and $PU_3NS_1TP_2$ are enumerated in Fig. 4.3.d and the thermal parameters are displayed in Table 4.3.b. From the TGA thermograms it is observed that, the T_i for BC is 303 °C, while it is 272 °C, 283 °C and 268 °C for PU_3, PU_3NS_1 and $PU_3NS_1P_2$ respectively. With reinforcement of NS, T_i of PU_3 increased

due to strong interfacial force between PU and NS [175]. In case of BC, there are several additives and plasticizers present resulting in a higher char residue %, which leads to higher thermal stability of BC in comparison to synthesized paint formulations. From the DTG graph, it was studied that for BC there is only single decomposition of paint at 394 °C, which indicates the decomposition of urethane linkage. However, in case of PU_3 and PU_3NS_1 two phase changes were observed. The first one is decomposition of urethane linkage and urea groups in the hard segment while the second one at 355 °C shows decomposition of soft segment from CO. However, when TP was added into the paint formulation, four phase changes are observed. First one at 305 °C shows decomposition of urethane linkage, second and third one at 355 °C and 427 °C shows decomposition of soft segment of CO, while the fourth segment at 584 °C shows decomposition of isocyanates into carbamide and carbon dioxide. The char yield of PU_3 is 0.29%, while for BC it is found to be 55.4% due to presence of number of plasticizers and additives. When NS was reinforced into the PU matrix, the char yield increased to 0.63% and with both NS and TP it is increased to 1.26%. This is due to presence of –Si-O-Si- linkage and amino group present in the APTES functionalized NS. The maximum degradation temperature for PU_3 is 495 °C, while at 545 °C, BC shows char yield. For PU_3NS_1 and $PU_3NS_1TP_2$ the final degradation temperature is found to be at 547 °C and 597 °C respectively.

4.3.6 DSC

DSC thermogram of the paint samples are reported in Fig. 4.3.e

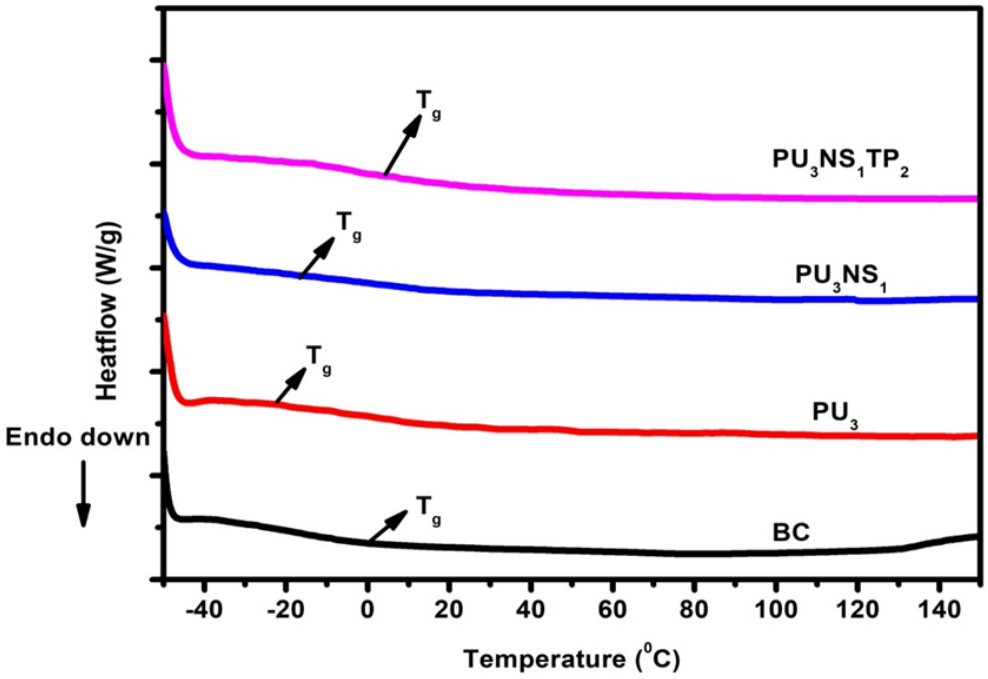

Fig. 4.3.e: DSC thermogram of paint formulations

From the DSC thermogram depicted in Fig. 4.3.e, the glass transition (T_g) temperature of BC, PU_3, PU_3NS_1, and $PU_3NS_1TP_2$ was found to be 1.25. -23.5, -16.94 and -3.55 ^oC respectively. This shift in degradation temperature and T_g shows strong interaction between PU and NS. Hence, it may be apparent from the findings that incorporation of NS and pigment contributed in enhancing the thermal stability of PU [176].

4.3.7 Mechanical properties of BC, PU, and its paint formulations

4.3.7.1 Lap-shear Test

The tensile stress and Young's modulus of BC and PU-based paint formulations is represented in Table 4.3.c and Fig. 4.3.f.

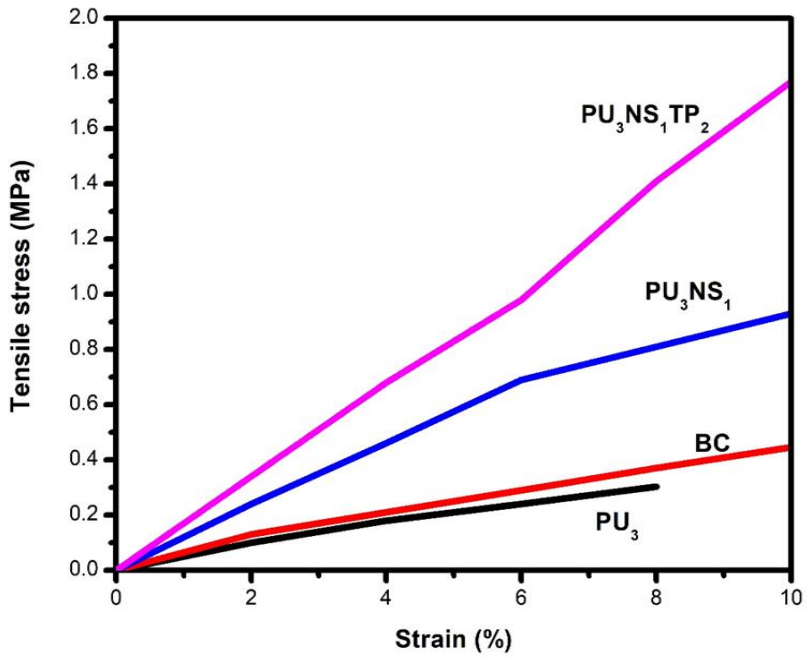

Fig. 4.3.f: Stress-strain curve of (a) BC (b) PU_3 (c) PU_3NS_1 (d) $PU_3NS_1TP_2$

Table 4.3.c: Tensile stress and Young's Modulus data of Paint formulations

Paint samples	Tensile stress (MPa)	Young's Modulus (MPa)	Abrasion Resistance (%)	Pencil Hardness
BC	0.45±0.002	408.35±5	0.052	2H
PU_3	0.30±0.003	251.33±3	0.040	2H
PU_3NS_1	0.93±0.005	782.31±6	0.024	3H
$PU_3NS_1TP_2$	1.77±0.002	1199.66±4	0.016	3H

It was observed that the shear strength of BC was 0.45 MPa, while PU_3 exhibited shear strength of 0.30 MPa. However, when NS particles were added to the PU matrix the shear strength increased to 0.93 MPa, which may be due to presence of Si-O-Si linkage in the NS, which increased the cross-linking density of the paint. However, when TP was reinforced in to the paint, the shear strength of the paint increased significantly to 1.77 MPa. This might be due to the titanium present in the pigment makes a strong interfacial bond with the paint matrix. The Young's modulus of neat PU was observed to be 251.33 MPa, which is 408.35 MPa in case of BC. When NS particles were added to the paint matrix the modulus increased to 782.31 MPa, because of the similar facts of strong interaction between the PU matrix and NS. Conversely, for $PU_3NS_1TP_2$ the modulus increased significantly to 1199.66 MPa, which might be due to similar facts of the presence of TP. Thus, the synergism between NS and TP within the PU matrix improved the mechanical properties of the paint over its virgin and commercial counter parts to the extent of 198.01% and 193.87% respectively [177].

4.3.7.2 Pencil Hardness Test

The pencil hardness test was carried out to evaluate the performance of paints and depicted in Table 4.3.c. The test results indicated that BC did not show any scratch when 2H grade pencil was used. Similarly in case of PU_3 paint the pencil hardness was 2H. While in both PU_3NS_1 and $PU_3NS_1TP_2$ the pencil hardness additionally

increased to 3H. Thus, it confirms the fact that with incorporation of NS, the hardness of the paint surface increased. This behaviour reconfirms increased cross-linking density due to the formation of H-bond between the Si-OH group of NS and NH group of PU [178].

4.3.7.3 Abrasion Resistance Test

The abrasion test results of paints reported in Table 4.3.c revealed that, the weight loss in the taber abrader for BC was 0.052%, which was 0.040%, 0.024% and 0.016% for PU_3, PU_3NS_1 and $PU_3NS_1TP_2$ respectively. This behaviour indicated higher cross-linking density in the synthesized bio-based paints as compared with commercial samples. This is primarily due to presence of cycloaliphatic polyol in the CO having functionality of 2-2.4 with a flexible chain that enables to synthesize a cross-linked structure devoid of steric hindrance. Moreover, the paint with NS and NS with TP exhibited higher abrasion resistance. This indicated strong interfacial adhesion between NS and PU. Also it may be concluded that the NS forms -Si-O-Si- linkage on the PU substrate and the presence of TP that improved the cross-linking density substantially thereby increasing the abrasion resistance [179].

4.3.8 WCA

Base coat is one among the under coats of automobile paint. As it is always protected by the clear coat and never comes in direct contact with water, so hydrophobicity is not a necessary parameter of this coat. The contact angle studies of the samples from Fig. 4.3.g revealed that, WCA is 86.48 $^{\circ}$ for BC and 77.61 $^{\circ}$ for PU_3 paint. However, in case of PU_3NS_1, the WCA increased to 83.46 $^{\circ}$, which additionally increased to 88.89 $^{\circ}$ for $PU_3NS_1TP_2$.

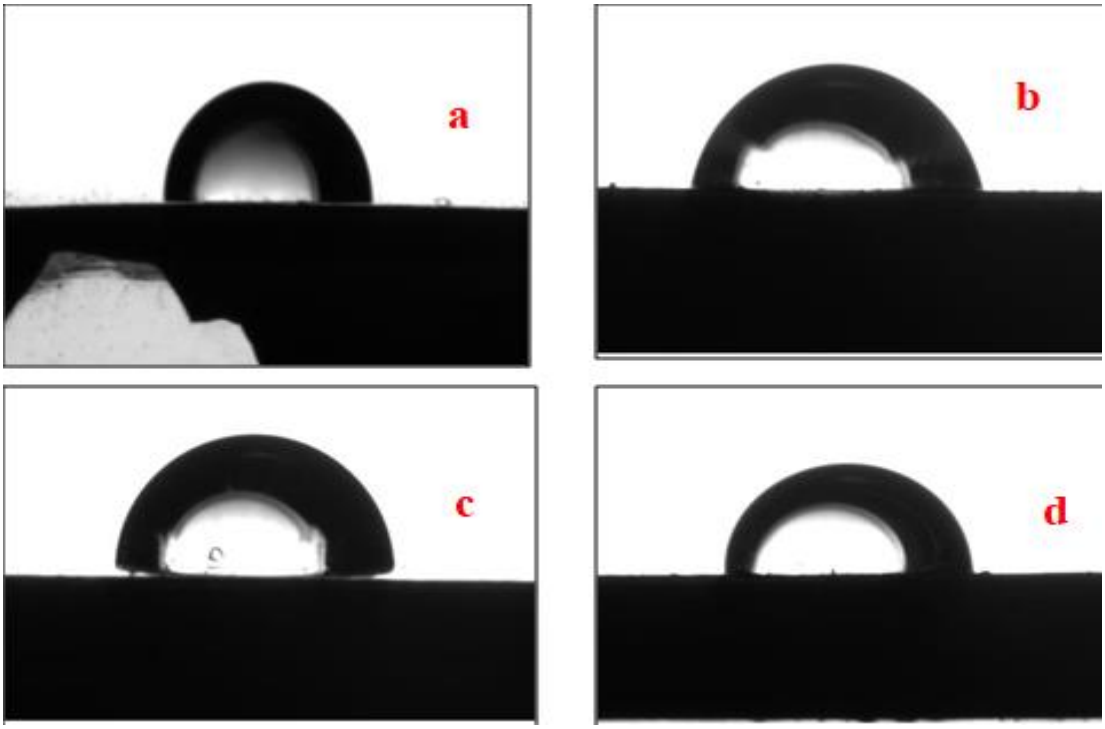

Fig. 4.3.g: Contact angle image of (a) BC (b) PU_3 (c) PU_3NS_1 (d) $PU_3NS_1P_2$

The WCA value for PU_3NS_1 and $PU_3NS_1TP_2$ increased in comparison to neat PU, because the NS particles in the PU matrix results in increase of cross-linking density which forms a closed network structure, thereby increasing the hydrophobicity of the surface. Contact angle is a measure of the surface tension and surface energy of the solid on which liquid is placed. The factors that have effect on contact angle are drop size, surface roughness and heterogeneity of polymer matrix [180]. With increase in heterogeneity and surface roughness the water contact angle increases. From the SEM images depicted in later section it was studied that with addition of NS and NS with TP, the heterogeneity of the polymer matrix increased gradually which leads to increase in WCA for PU_3NS_1 and $PU_3NS_1TP_2$ [178].

4.3.9 SEM

SEM micrograph of paint samples is displayed in Fig. 4.3.h

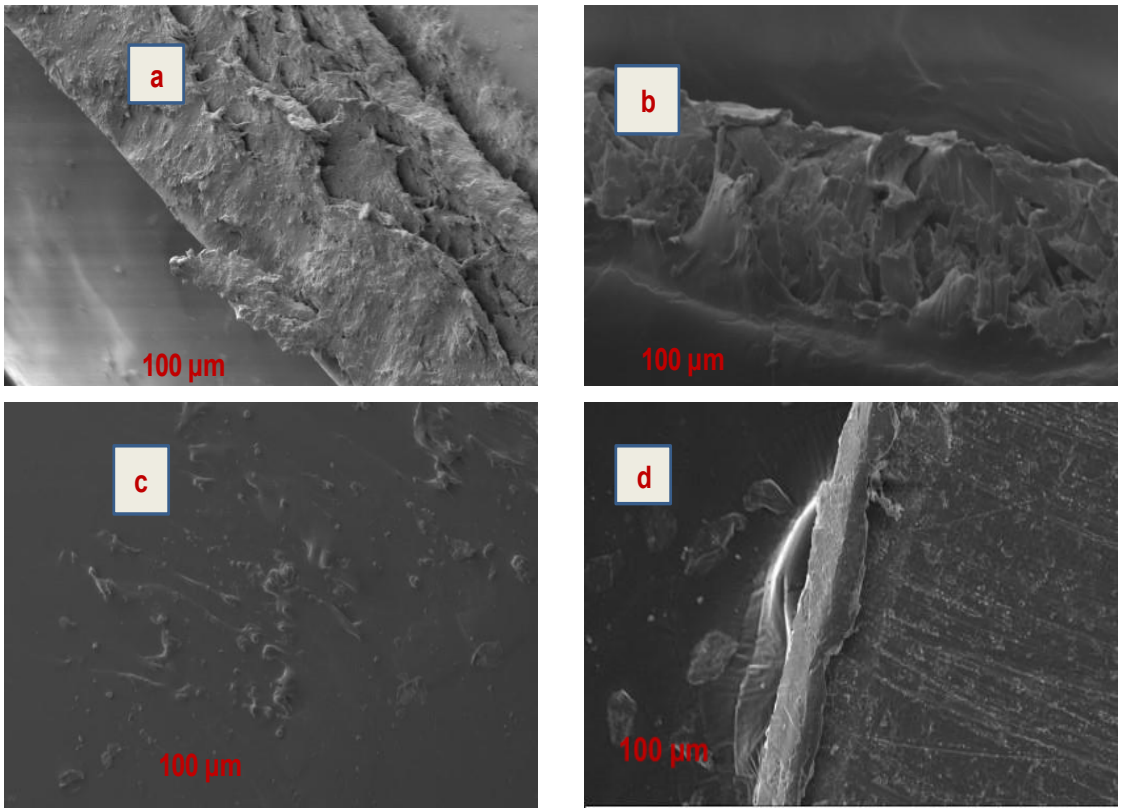

Fig. 4.3.h: Cross-sectional SEM micrographs of (a) BC (b)PU_3 (c) PU_3NS_1 (d) $PU_3NS_1TP_2$

SEM micrographs of the cross-section of commercial paint, PU_3, PU_3NS_1 and $PU_3NS_1TP_2$ is enumerated in Fig. 4.3.h. It is evident that neat PU paint has very less agglomeration present and the homogeneity of the film was good clearly showing the hard segment and soft segment as indicated in Fig. 4.3.h (b). In case of BC the SEM micrograph showed a number of additives present in the paint film. With incorporation of NS the film showed heterogeneity as indicated in Fig. 4.3.h (c). The black surface was for the polyurethane, while the white particles clearly dispersed in PU matrix indicated the NS. The micrograph also showed that there was no traceable agglomeration in the PU_3NS_1 film. However, in case of the $PU_3NS_1TP_2$ paint, the

heterogeneity of the material was observed to be higher. This was due to presence of pigment particles. The dispersion of pigment particles could become more homogeneous by adding suitable binder material to the paint [181].

4.3.10 Resistance Test

Table 4.3.d: Oil, Acid, and Alkali resistance of paint formulations

Paint formulation	Acid	Alkali	Petrol	Diesel	Engine oil
BC	Spotting	No change	No change	Softening	Softening
PU_3	Visible cracking	Spotting	Softening	Softening and cracking	Softening and peeling
PU_3NS_1	Spotting	No change	No change	Change in gloss	Peeling
$PU_3NS_1TP_3$	Negligible spotting	No change	No change	Change in gloss	Change in gloss

4.3.10.1 Acid and Alkali Resistance Test

From the acid test result reported in Table 4.3.d, it was found that, BC exhibited spotting on the area that came in direct contact of acid, whereas for PU_3 paint visible amount of cracking was observed on the area, encountered the acid. Whereas in case of PU_3NS_1 the change in property observed was a spot of little impact while, $PU_3NS_1TP_2$ showed negligible spots on the surface. Alkali resistance test reported in Table 4.3.d of the painted substrates showed these following results. For BC there was a non-resistant impact of the base on the coated surface, but in case of PU_3 very little spot was observed in the area interacted directly with the base. With PU_3NS_1 and $PU_3NS_1TP_2$there was no evident change in the paint surface.

4.3.10.2 Petrol, Diesel, and Engine oil Resistance Test

The petrol, diesel, and engine oil resistance test were also represented in Table 4.3.d. After immersion in petrol for 8 hrs., BC exhibited no peeling, blister and crack or softening with only minor changes in gloss. For PU_3 very small amount of softening, with only minor changes in gloss was observed. However, in case of PU_3NS_1 and $PU_3NS_1TP_2$ exhibited optimum performance with no observable change. Similarly, for diesel resistance of BC there was no peeling or blistering, while a mild softening and change in gloss was observed. Where as in case of PU_3 significant amount of softening and peeling from the panel corner with change in gloss was observed. Conversely $PU_3NS_1$and $PU_3NS_1TP_2$ paints have no peeling, softening and crack in the paint surface. However, in both the aforesaid paints very less change in gloss was observed. After the immersion of the panels in engine oil for 8 hours at 100°C, BC exhibited softening and peeling with change in gloss.PU_3 showed major amount of peeling and gloss was decreased significantly. But in case of PU_3NS_1there was less amount of softening with all other properties intact and negligible change in gloss. Conversely, in case of $PU_3NS_1TP_2$ only spotting was observed, but no other changes in paint surface could be traced.

Conclusions

Eco-friendly base coat of automobile paint was synthesized using ECO and IPDI. With incorporation of NS along with TP particle the paint formulation exhibited very good thermal, mechanical, physico-chemical and coating properties and can be comparable with the properties of commercial base coat. FTIR analysis confirms the structural properties of the polyols, NS, and paint samples. Mechanical properties like cross-cut adhesion %, pencil hardness, tensile stress, and abrasion resistance % were significantly increased with the addition of NS and pigment particles. Furthermore, with incorporation of NS along with TP, thermal properties like TGA final residue %, and T_{gs} increased from 0.29% and -24.5ºC to 1.26% and 1.94ºC. XRD and SEM study reveals the morphological properties. From the above study it is summarized that the paint formulation with 0.5 wt.% NS and 0.2 wt.% TP shows optimum performance and can be utilized for application in automotive paint industry fulfilling many parameters.

CHAPTER 5

Chapter 5

Development of bio-based Clearcoat from Castor oil and chemically modified Nano-silica

Introduction

The top coat of a paint which is known as the clear coat is devoid of any pigment and protects the base coat from degradation[1]. The clear coat provides a protective coating against environmental effects, corrosion, and UV light[182]. Conventional two-component polyurethane systems (2C-PU) have unique cross-linking chemistry and are bestowed with excellent outdoor durability, outstanding chemical resistance, and good mechanical properties[176,177]. Currently, PU-based coating materials are primarily prepared from petroleum-based feedstocks which affect the production process due to the supply chain environmental effects and cost of crude oil prices[185]. Vegetable oils such as castor oil, linseed oil, soybean oil, rapeseed, olive oil, cottonseed oil, etc. are being used to synthesize bio-based polyols, which can be effectively used to make polymers in chemical industries[186]. CO as described in the previous chapter, is the most abundantly used vegetable oil for the synthesis of PU. It possesses inherent structural properties such as a carbon-carbon double bond and free hydroxyl groups[187], which can be suitably used to synthesize bio-derived resins employing varied modification techniques like epoxidation, acrylation, transesterification etc.. As reported by S. Sahoo et al. and G.S. Sudha et al.[30,204], however, complete conversion of unsaturated carbon bonds in the CO is not achievable during the epoxidation process. Hence, epoxidation followed by acrylation not only results in complete conversion but also increases the oligomerization in the resulting polyol, which leads to higher viscosity and limits its applicability in the coating industry [190]. Modification by epoxidation followed by transesterification converts triglycerides to monoglycerides without affecting the epoxy groups which results in the formation of epoxy methyl esters of the same epoxy value. These esters possess lower viscosities and are considered secondary components. Therefore, epoxidation followed by combination of transesterification and acrylation results in the desired polyol, applicable in the coating industry[191].

Surface modification of NS with triallyl isocyanurate (TI) leads to a single-step modification process resulting in the homogeneity of NS in the polymer matrix. In comparison to other isocyanates like Toluene diisocyanate, TI does not need any pre-treatment process with a better grafting modification[159].

In the previous chapter CO was epoxodized and reacted with IPDI to obtain PU. Additionally, CO based PU was reinforced with APTES modified NS and TP to synthesize a basecoat with desired coating performance.

Based on the above study, in the current chapter a transparent PU/NS hybrid coating was synthesized. CO was epoxidized followed by transesterification and acrylation. IPDI has been used as a curing agent and DBTDL as a catalyst, with xylene as the solvent medium. NS was modified with TI and incorporated into the paint matrix to improve the interface balance with PU. Similar to the previous chapter, an in-depth study on the physico-mechanical, thermal, morphological, optical, oil and chemical resistance properties have been studied.

Results and Discussions

Properties of Polyol

5.1.1 FTIR

The FTIR spectra of ECO, TECO, and ATECO is displayed in Fig. 5.1.a

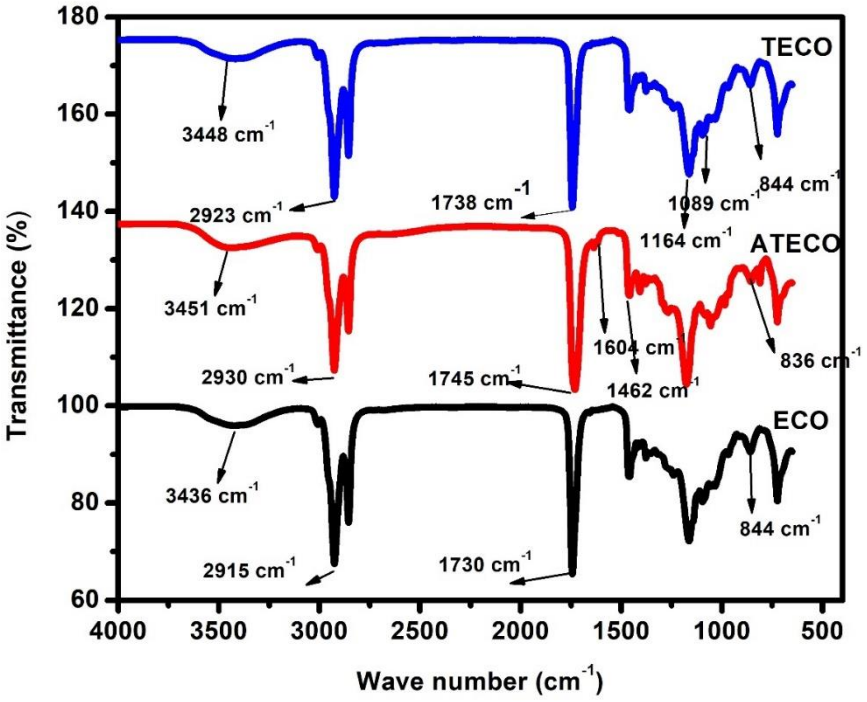

Fig. 5.1.a: FTIR spectra of ECO, TECO, and ATECO

As discussed in chapter 4, the FTIR spectra of ECO in Fig. 5.1.a showed a peak corresponding to the –OH group at 3436 cm^{-1} which after transesterification to TECO, shifted to 3448 cm^{-1} and subsequently, after acrylation to form ATECO displayed the peak at 3451 cm^{-1}. Similarly, the epoxy ring was observed at 844 cm^{-1} in ECO spectra[190]. In TECO the epoxy ring remains unaffected and was also observed in the same range. After transesterification the C=O band was observed to be shifted from 1730 to 1738 cm^{-1} corresponding to the ester linkage. Two additional consecutive bands were observed at1089 and 1164 cm^{-1} confirming the presence of methyl ester in the TECO spectra[192]. In case of ATECO spectra, the peaks corresponding to 836 $cm^{-1}$are related to the oxirane ring and showed a very small peak confirming the

acrylation process. A new doublet was observed at 1604 $cm^{-1}$and 1456 cm^{-1} confirming the presence of double bonds steaming from the acrylated group[193].

5.1.2 ^{1}HNMR

The ^{1}HNMR spectra corresponding to ECO, TECO and ATECO is enumerated in Fig. 5.2. (a), (b), and (c) respectively

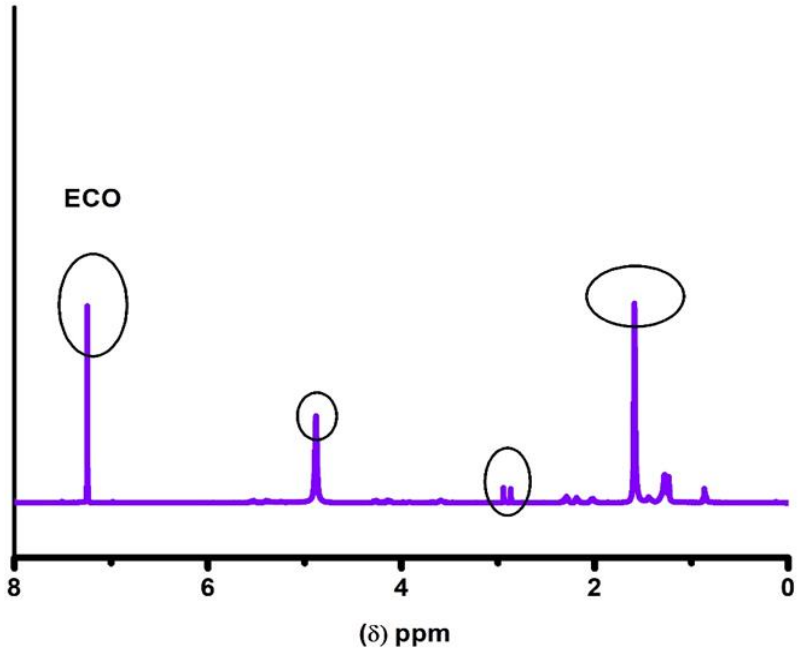

(a)

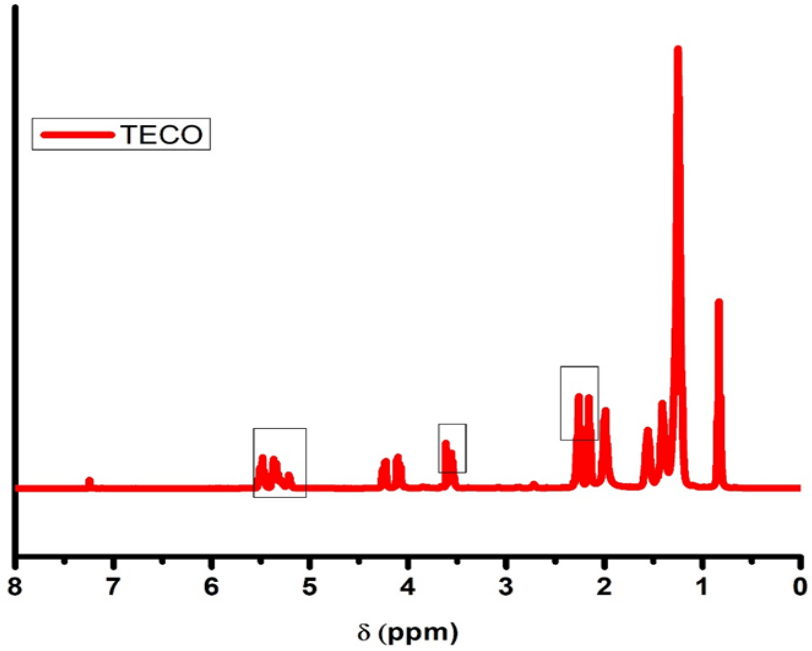

(b)

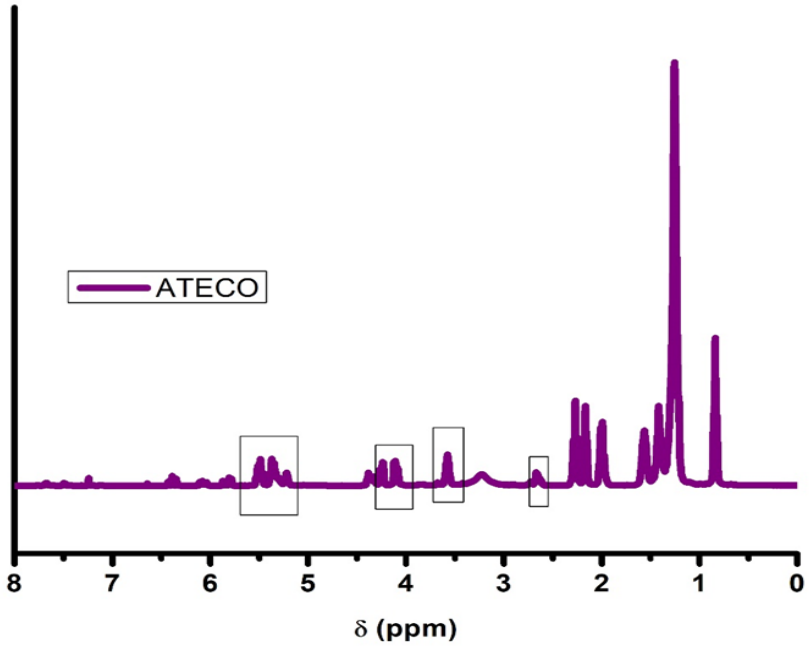

(c)

Fig. 5.1.b: ^{1}HNMR Spectra of (a) ECO, (b) TECO and (c) ATECO

In the NMR spectrum of ECO, the peaks between 2.81-2.95 revealed the characteristics of –CH protons of epoxide group, which showed its chemical structure.

The peak at 4.86 attributed the carbon containing hydroxyl group and the peak at 7.2 attributed to $CDCl_3$[190]. In case of TECO, a peak was observed at 3.56 ppm corresponding to the methyl ester group and signals between 4.1-4.2 ppm reveals the CH and CH_2 hydrogens of glycerides which are dispersed confirming the formation of monoglyceride esters. The epoxide group shifted to 2.27 and 4.1 ppm due to presence of $-CH_2-O-C-O$ and -C=O of ester. The peak observed at 5.6 indicated the presence of triallyl proton i.e., $CH_2-CH-CH_2$[194]. After acrylation to ATECO three consecutive peaks were observed in between 5.1-5.50 ppm corresponding to the three acrylate groups. A negligible epoxide peak was observed at 2.61 ppm showing a very negligible amount of epoxide present due to steric hinderance. The peaks observed at 3.55 ppm attributed to methine proton in α position of -OH group. Another methyl proton α to acrylate group was observed at 4.10-4.38 ppm[195]. The peaks between 7-8 ppm correspond to $CDCl_3$ in all the polyol samples. The ^{1}HNMR spectra confirmed the epoxidation, transesterification, and acrylation of CO.

5.1.3 Hydroxyl Value

The hydroxyl value was calculated from considering the carbamide bond observed on the FTIR spectra formed between 1690-1780 cm^{-1}. This particular bond between these wave numbers was studied and the intercepts, integral and slope of the graph were derived w.r.t. ECO, TECO, and ATECO

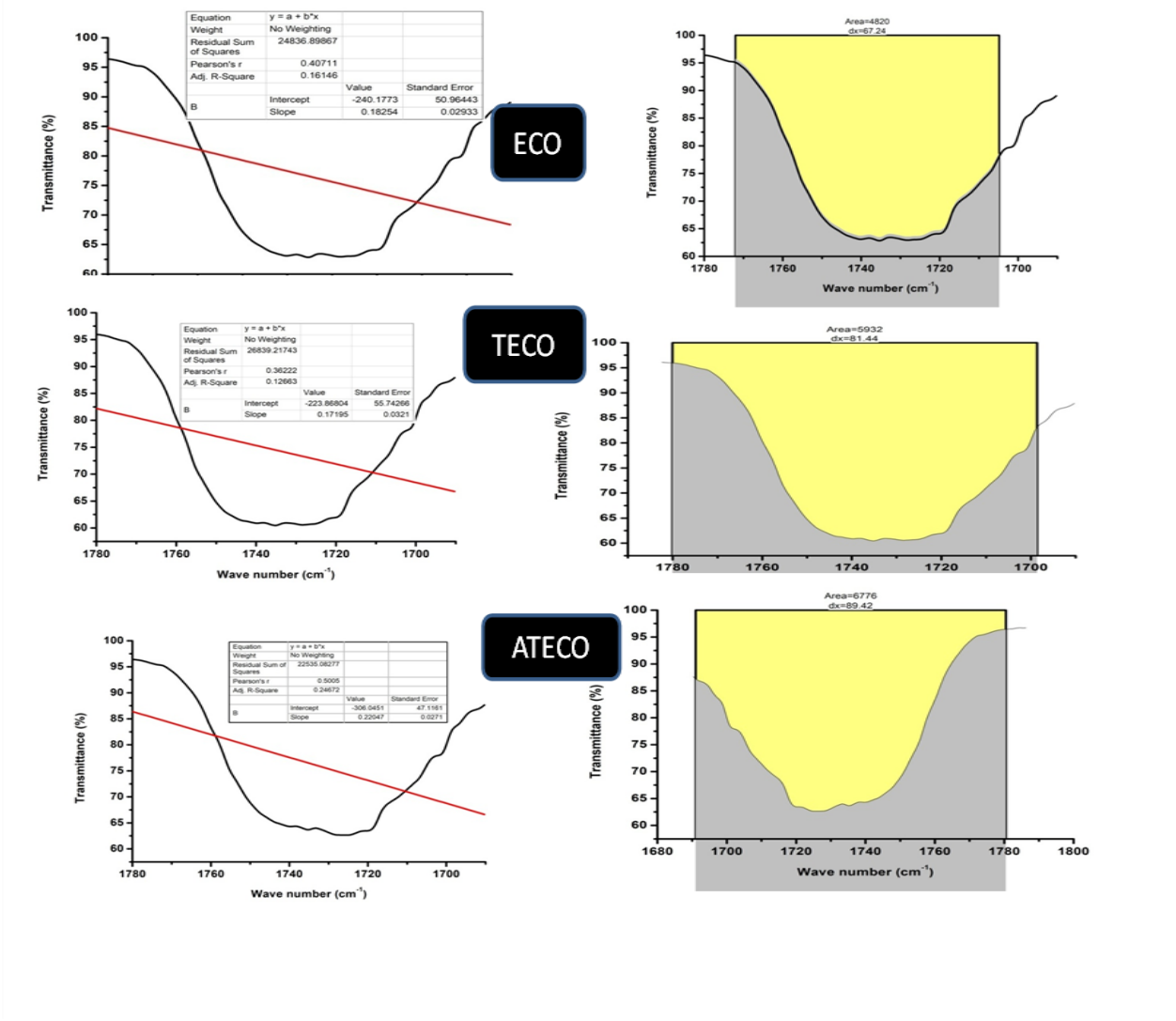

Fig. 5.1.c: Intercept, integral and slope calculation graph derived from (a) ECO blank and ECO solution (b) TECO blank and TECO solution (c) ATECO blank and ATECO solution.

From the above Fig. 5.1.c and the formula described above the hydroxyl value was found to be 208 mg/KOH for ECO. After tranesterification process no change in epoxy value was observed, only additional monoglycerides and ester bond was studied in the spectra. The hydroxyl value thus calculated remains almost same only a slight change in value was studied and was found to be 203 mg/KOH. In case of ATECO the hydroxyl value was observed to be 233 mg/KOH. After acrylation of TECO, a negligible epoxy bond was found in addition with more double bonds and acrylic bonds. These double bonds increase the hydroxyl value of the polyol to significant level.

5.1.4 Acid value, Equivalent weight, Non-volatile Content , and Amine value

Table 5.1.a: Acid value, Non-volatile content and Equivalent weight of ECO, TECO and ATECO.

Sample name	Acid value (mgKOH/g)	Non-volatile content (%)	Equivalent weight (mg)	Amine value (mgKOH/g)
ECO	1.75	96.3	270	13.09
TECO	1.28	96	276	14.21
ATECO	1.16	95	240	19.91

From the Table 5.1.a, it was observed that; ECO has an acid value of 1.75 which decreased after transesterification (TECO) to 1.28. The density and viscosity of ECO is higher than the TECO, which results in more polar structure of ECO. This contributed to lower acid value of TECO than ECO[168]. In case of ATECO, the acid value further decreases to 1.16 due to addition of acrylic acids which forms acrylate bond in the back-bone structure of the polyol thereby making it more polar[196].

The amine value of ECO, TECO, and ATECO is also provided in Table 5.1.a. From the volumetric titration process, the amine value of ECO was found to be 13.09 mgKOH/g, which increased to 14.21 and 19.91 mgKOH/g for TECO and ATECO respectively. With addition of acrylic group, the hydroxyl value of ATECO increased resulting in decreased acid value and equivalent weight. The decreased equivalent weight, lead to more consumption of curing agent in case of ATECO. Which in turn resulted in increased amine value.

5.1.5 TGA

TGA thermogram of ECO, TECO, and ATECO is displayed in Fig. 5.1.c and Table 5.1.b.

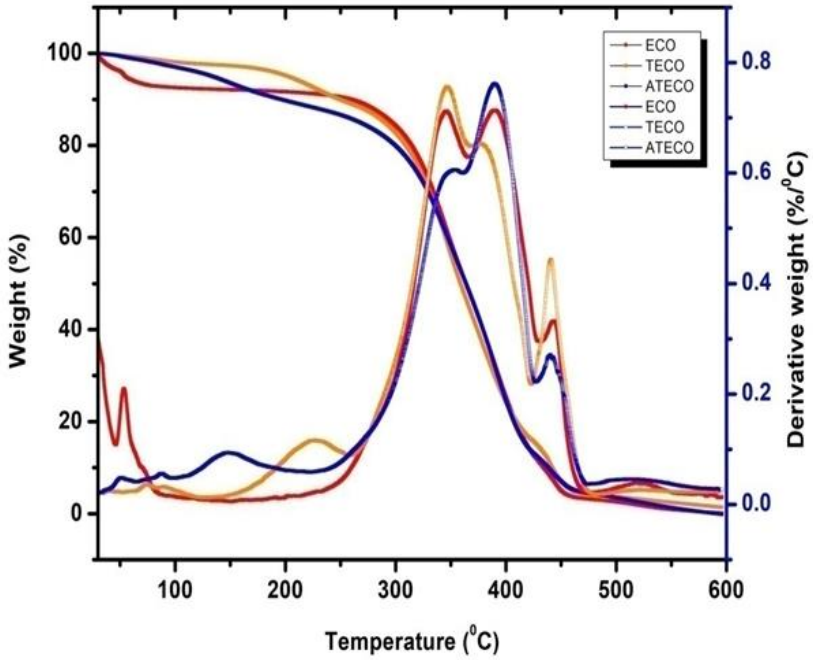

Fig. 5.1.c: TGA/DTG Thermogram of polyols

Table 5.1.b: Thermal data of Polyols

Sample name	T_i (ºC)	$T_{50\%}$ (ºC)	T_f (ºC)	Char residue %
ECO	192	359	558	0.12
TECO	191	360	560	0
ATECO	198	367	568	0

The TGA/DTG thermogram of the derived polyols ECO, TECO and ATECO are enumerated in Fig. 5.1.c and the thermal parameters are displayed in Table 5.1.b. From the thermogram it was found that the T_i was 192 °C, 191 °C and 198 °C for ECO, TECO and ATECO respectively. The initial degradation temperature for ATECO increased due to increase in –OH value, because the –OH values influences the onset vitalization temperature of a polymer. ECO and TECO have almost equivalent hydroxyl value, which results in negligible change in T_i. The decomposition of polyols was studied from the DTG thermogram. In ECO the first decomposition temperature was observed at 53 °C which indicates the decomposition of volatile materials. At temperatures 347 and 389 °C the lower molecular weight hydrocarbons were decomposed and at 443 °C higher molecular weight hydrocarbons were decomposed. However, in case of TECO the initial decomposition temperature where volatile materials decomposed was observed at 223 °C due to presence of ester bonds. In case of ATECO the initial decomposition of volatile materials was observed at 145 °C due to presence of lower thermally stable acrylic bonds. Degradation of lower molecular weight hydrocarbons was observed at 345 and 382 °C in TECO and in case of ATECO, it was observed at 395 °C. Higher molecular weight hydrocarbons decomposition was observed at 441 °C and 452 °C for TECO and ATECO respectively. From the above analysis it was observed that the thermal stability of ATECO is relatively higher than ECO and TECO which is due to increase in hydroxyl value of the polyol[197].

5.1.6 DSC

The DSC thermograms of polyols ECO, TECO, and ATECO are displayed in Fig. 5.1.d

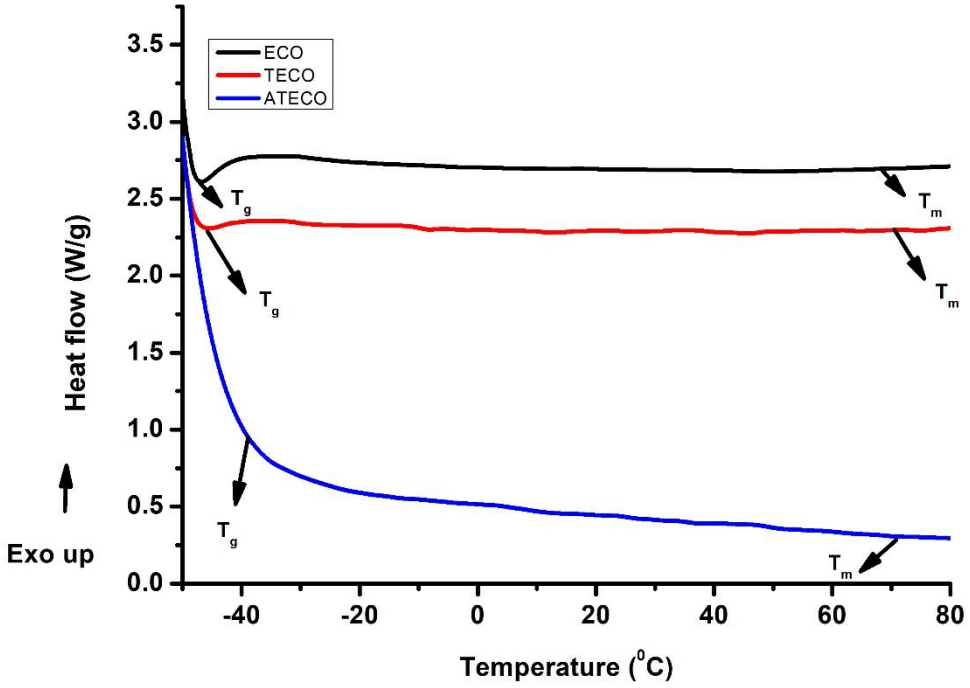

Fig. 5.1.d: DSC thermogram of Polyols

Table 5.1.c: DSC analysis of Polyols

Sample Name	T_g (°C)	T_m (°C)	X (%)
ECO	-46.68	70.30	3.71
TECO	-45.73	70.81	3.64
ATECO	-37.43	74.73	5.12

By analysing the DSC thermogram in Fig. 5.1.d and Table 5.1.c, the glass transition temperature (T_g) of ECO was observed to be at -46.68 °C and the melting temperature (T_m) was observed at 70.30 °C. In case of TECO, the T_g and T_m were observed at -

45.73 °C and 70.81 °C respectively. This minor change in the glass transition and melting temperature value was observed in TECO due to presence of ester bonds and conversion of triglycerides to monoglycerides. After acrylation of TECO the functionality of the polyol increased significantly, which leads to increase in thermal stability. As a result T_g and T_m for ATECO was observed to be at -37.4 °C and 74.73 °C[198]. ATECO was observed to have higher crystallinity % in comparison to TECO and ECO, which indicated that due to presence of higher functional groups and better cross-linking density in paint formulations, resulted in increased crystallinity. A single-phase transition peak was observed during curing of polyols. ATECO was observed to have higher exothermic peak and enthalpy in comparison to TECO and ECO

5.1.6 Viscosity

The viscosity graph of ECO, TECO, and ATECO is displayed in Fig. 5.1.e

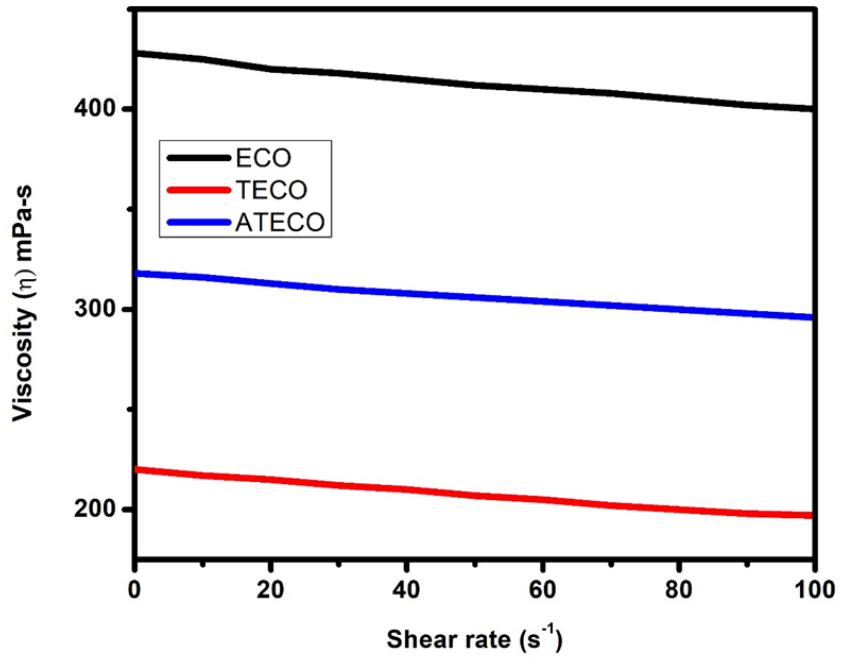

Fig. 5.1.e: Viscosity graph of ECO, TECO, ATECO

Viscosity was measured as a function of shear rate and reported in Fig. 5.1.e. In case of ECO, the viscosity of the polyol was found to be 428 mPa-s and this value is a little bit higher for polyols. After transesterification the viscosity of TECO was observed to

be 220 mPa-s. The decrease in viscosity occurs due to shorter monoglyceride chains and less entanglement. In case of ATECO, higher entanglement was observed which results in higher viscosity of 318 mPa-s as compared with TECO. The viscosity range was found to be appropriate for polyols applicable in coating industry[188].

5.1.8 Flash point Test

The flash point of ECO, TECO, and ATECO is displayed in Fig. 5.1.f

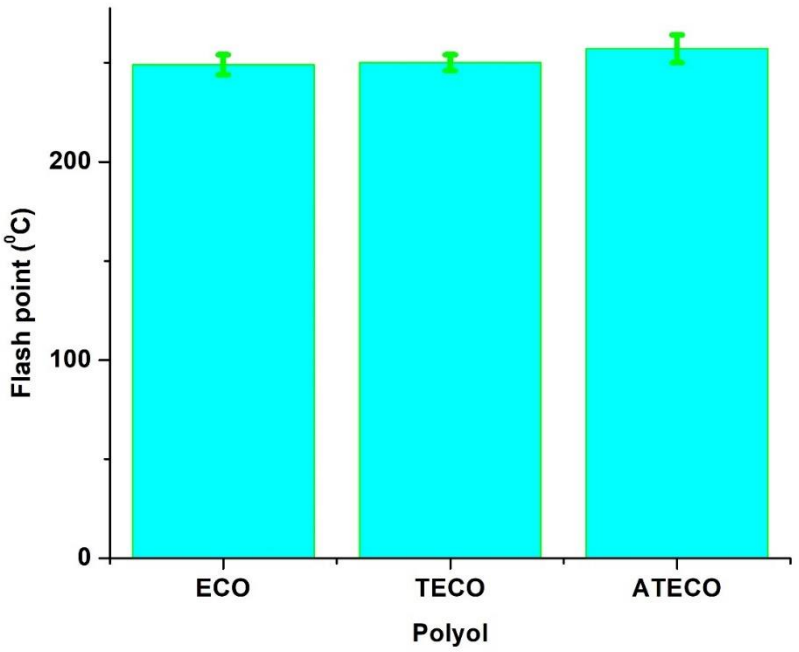

Fig. 5.1.f:

Flash point of ECO, TECO and ATECO

From Fig. 5.1.f, it was observed that, the flash point of castor oil normally ranges from 230-240 °C. The AR grade castor oil used for this work has a given flash point 240 °C. It was observed that, after epoxidation process, the flash point of ECO was observed to be 249±5 °C. The increase in flash point in the modified castor oil is due to the presence of antioxidants. In case of TECO negligible functionality change was observed, which results in no appreciable change in the flash point i.e., 250±4 °C. As discussed in the earlier sections, the hydroxyl value of ATECO was found to increase to a significant level, which in turn increased the functionality of the polyol that contributes to an increase in flash point value i.e., 257±7 °C. With higher flash point

value, the thermal stability of the polyol increased significantly, which can be confirmed from the TGA findings[199].

5.2 Properties of TI-NS and APTES-NS

5.2.1 FTIR

The FTIR spectra of NS, TI-NS, and APTES-NS is displayed in Fig. 5.2.a

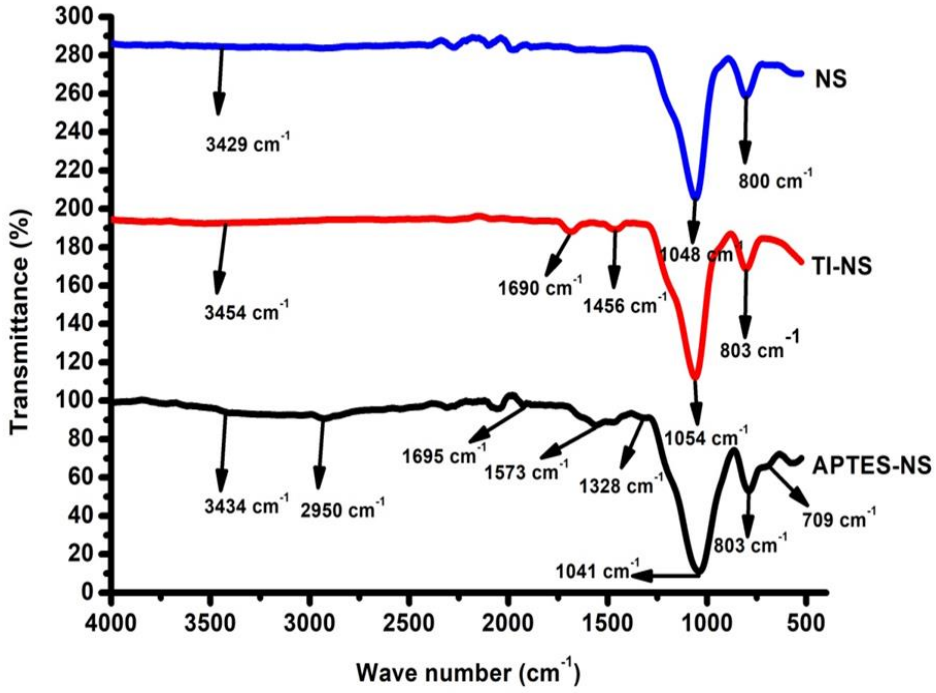

Fig. 5.2.a: FTIR spectra of NS, TI-NS, and APTES-NS

From the FTIR spectra, it is evident that, neat NS, APTES functionalized NS and TI functionalized NS displayed a Si-O-Si asymmetric bond noted at 1048 cm^{-1}, 1041 cm^{-1} and 1054 cm^{-1} respectively, whereas Si-O-Si symmetric bond was noted at 800 cm^{-1} for NS and 803 cm^{-1} in both the spectra of TI-NS and APTES-NS. The spectra of Si-C bond were observed at 709 cm^{-1} in APTES-NS. The presence of APTES was confirmed from the peaks at characteristic vibration peak at 1573 cm^{-1} and 1328 cm^{-1} corresponding to the aminopropyl group. The C-H bond at 2950 cm^{-1} is due to alkyl chain in APTES. At 1328 cm^{-1} it shows –NH stretching peak while the peak corresponding to 1573 cm^{-1} is due to the N-O stretching. At 169 5cm^{-1} NH_2 bending

was observed in APTES-NS. Similar results have been reported by S. Feifelet al.[9]. An absorption peak was observed at 1690 cm^{-1} in TI-NS, which indicates fewer hydroxyl groups while the peak at 1456 cm^{-1} reveals the presence of C=N absorption. Similar results have been reported by X. F. Ye et. al.[159].

5.2.1 XRD

XRD graph of NS, TI-NS, and APTES-NS is displayed in Fig. 5.2.b

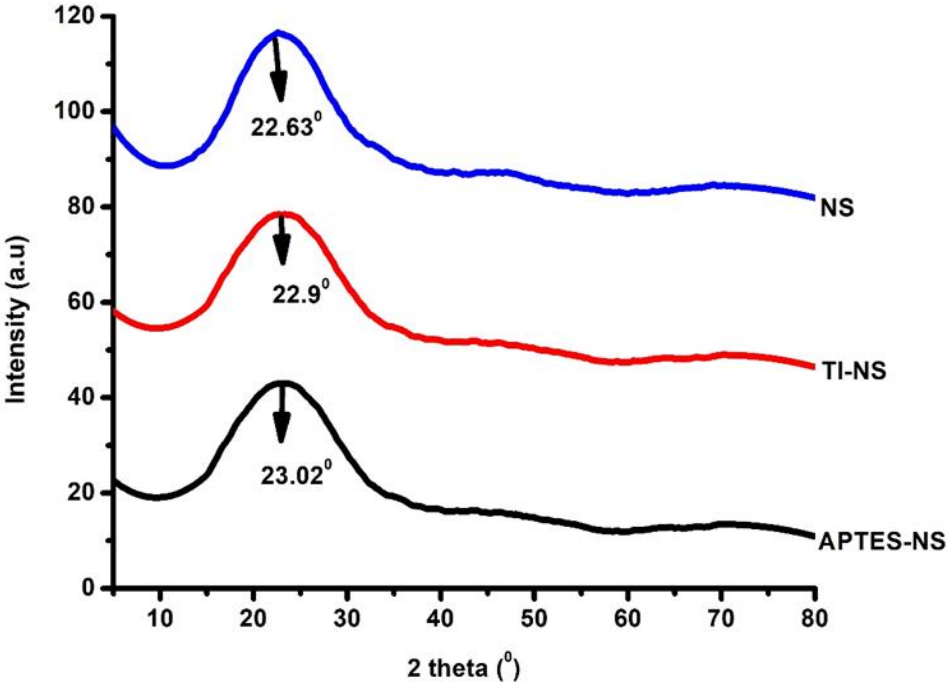

Fig 5.2.b: XRD graph of NS, TI-NS, and APTES-NS

The XRD analysis of modified NS displayed in Fig. 5.2.b. Comparing NS, NS-APTES and NS-TI, the 2-theta value was observed at 22.63 °, 23.02 º, and 22.9 ° indicating similar interplanar distance. From the above study it was found that there was no impurity peak in the spectrum and it was highly amorphous in nature.

5.2.3 Grafting %

Grafting percentage of APTES-NS was found to be 13.8% while for TI-NS it was observed to be 14.1%. The similar grafting percentage reveals that both the modification process is effective for NS.

5.2.4 Water and Ethanol Solubility

(a) (b)

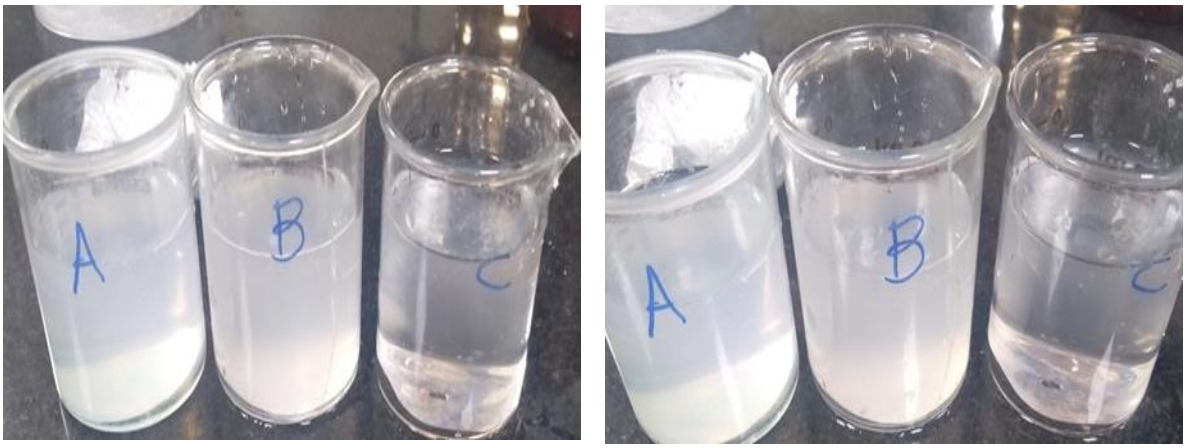

Fig 5.2.c: (a) Water precipitation of A. TI-NS, B. APTES-NS, C. NS (b) Ethanol precipitation of A. TI-NS, B. APTES-NS, C. NS

The NS particles precipitate in water and ethanol, which shows that it is very hydrophilic, and the amount of residual -OH groups on its surface is relatively large. In contrast, for modified NS there is no significant precipitation in water, which reveals the hydrophobicity of modified NS and the amount of residual -OH groups on the surface are small indicating a good modification effect. Fig. 5.2.c showed the water and ethanol precipitation of silica samples.

5.2.5 TEM

TEM micrograph of NS and TI-NS are depicted in Fig. 5.2.d

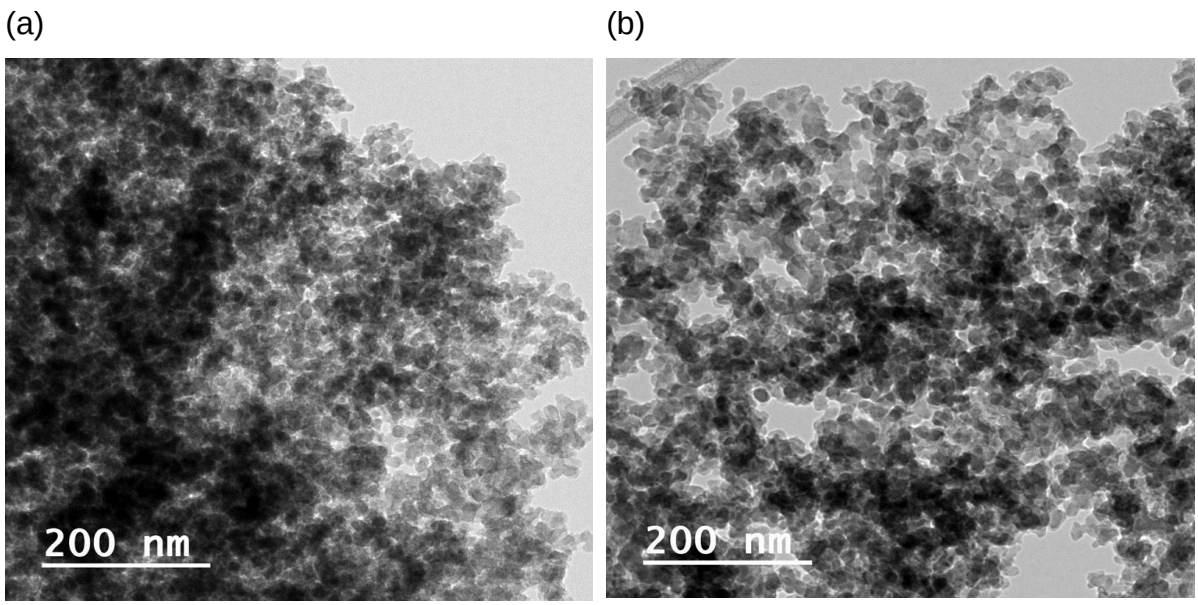

Fig. 5.2.d: TEM image of (a) NS and (b) TI-NS

TEM analysis of NS and TI-NS were studied from Fig. 5.2.d. The TEM image showed that, the NS particles have an irregular spherical shape with aggregations, which is due to covalent bonds present in between the hydroxyl groups present in it. W. He reported similar results in his study[201]. On the contrary, TI-modified NS particles were found to have no large agglomerations, which additionally confirmed that surface modification of NS particles reduced the agglomeration and increased the filler dispersion within the polymer matrix, thereby contributing enhancement in surface and mechanical properties. T. Rahim et al. reported that, surface modified NS reinforced with BisGMA diurethane dimethacylate and triethylene glycol dimethacylate exhibited improved dispersion characteristics within various polymers[202].

5.3 Properties of Clear coat

5.3.1 Optimization by Cross-cut Tape Test

Adhesion strength % of paint formulations is displayed in Table 5.3.a

Table 5.3.a: Adhesion strength of paint formulations

Sl. No.	Paint Formulation	Adhesion (%)
1	CP	96±2
2	PU_i	69±4
	PU_{ii}	74±2
	PU_{iii}	66±4
3	$PU_{ii}NS_1$	85±3
	$PU_{ii}NS_2$	79±5
	$PU_{ii}NS_3$	72±6
4	PU_1	78±3
	PU_2	82±2
	PU_3	76±4
5	PU_2NS_1	93±3
	PU_2NS_2	89±4
	PU_2NS_3	83±3

Cross-cut tape test was performed to evaluate the effect of the molar ratio of NCO: OH, and the incorporation of NS on the adhesive strength of the paints. As observed in Table 5.3.a, commercial paint displays an adhesive strength of 96±2%. The PU paint prepared at a molar ratio of 1:0.9 using TECO and ATECO as polyol exhibited an adhesive strength of 69±4% and 78±3% respectively. Increasing the molar ratio of NCO: OH to 1:1, resulted in increased cross-linking density thereby contributing in the enhancement in adhesive strength to 74±2% and 82±2% for PU_{ii} and PU_2 respectively. However, an additional increase of OH: NCO to 1: 1.1, the rigidity of the system increased, which in turn resulted in a decrease in adhesion strength of the paint with the substrate. Thus, the PU paint at NCO: OH, molar ratio of 1:1 (PU_2) was optimized and taken for reinforcement with NS. It is evident from the Table 5.3.a, that incorporation of NS within neat PU paint at variable concentration of 0.5-1.5 wt.%, resulted in enhancement of the adhesive strength. The paint at 0.5 wt.% of NS exhibited complete dispersion of nanoparticles, which restricted the molecular motion of PU chain, resulting in increased cross-linking density. This behavior contributed to a significant increase in adhesion strength to 85±3% and 93±3% in case of TECO and ATECO respectively. However, increasing the concentration of NS to 1 wt.% and 1.5 wt.%, the interfacial interaction between the PU and nanoparticles decreased resulting in agglomeration of NS in the paint, which leads to a decrease in the adhesive strength of the paint sample. The paint formulation with OH: NCO ratio 1:1 incorporated with 0.5 wt.% NS using ATECO as polyol (PU_2NS_1) exhibited optimum adhesive strength of 93±2%, which was comparable with the commercial clear coat. Similar results were reported by S. Das et al.[192].

5.3.2 FTIR

The FTIR spectra of CP, PU_2, and PU_2NS_1 are displayed in Fig. 5.3.a

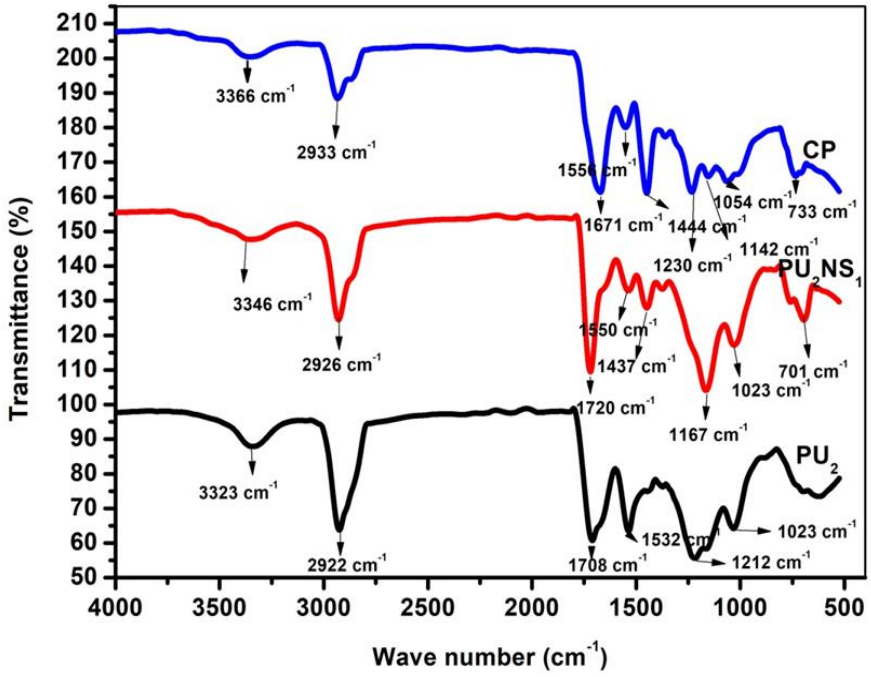

Fig. 5.3.a: FTIR Spectra of (a) CP (b) PU_2 (c) PU_2NS_1

As observed from the Fig. 5.3.a, the FTIR spectra of the CP showed –NH stretching at 3366 cm^{-1}, while in the case of PU_2 and PU_2NS_1 the –NH stretching was noted at 3323 and 3346 cm^{-1} respectively. CP shows a –CH stretching band at 2933 cm^{-1} while the same band was observed at 2922 and 2926 cm^{-1} in PU_2 and PU_2NS_1 respectively. The peak corresponding to 1671, 1708, and 1720 cm^{-1} revealed -C=O stretching in CP, PU_2, and PU_2NS_1 respectively. The –CH band was observed at 1556 cm^{-1} in CP, at 1532 cm^{-1} in PU_2 paint, and at 1550 cm^{-1} in PU_2NS_1 paint. Thus, it is confirmed that the CP is PU-based. The C-O-O band stretching was found at 1054 cm^{-1} for CP which was observed at 1023 cm^{-1} in both the prepared paint formulations. Furthermore, it was observed from the spectra of PU_2NS_1, that the Si-O-Si stretching peak corresponding to the presence of TI functionalized NS was observed at 701 cm^{-1}. Similar results have been reported by J. Martinage et al.[203].

5.3.3 ^{1}HNMR

^{1}HNMR spectra of CP, PU_2, and PU_2NS_1 are displayed in Fig. 5.3.b

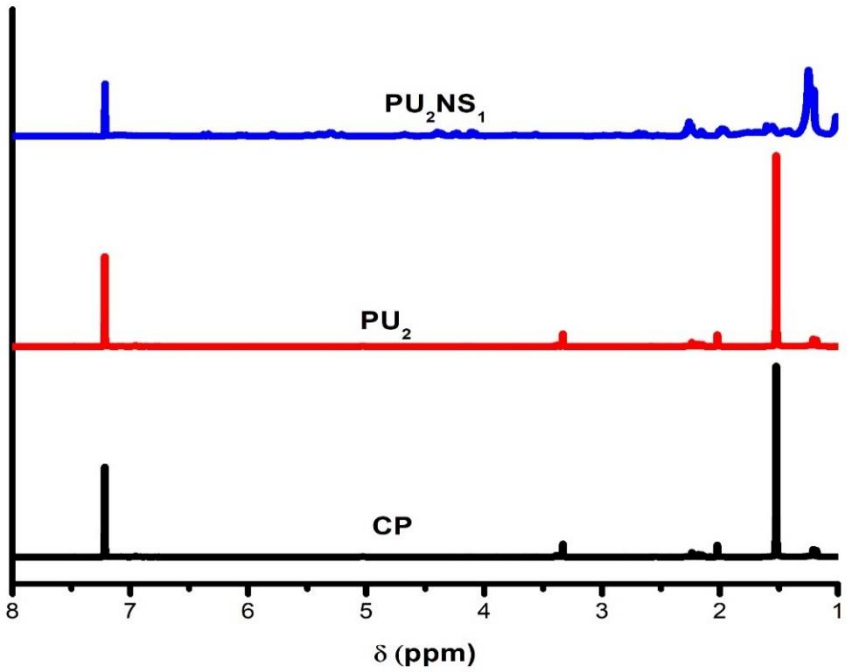

Fig. 5.3.b: ^{1}HNMR spectra of CP, PU_2, and PU_2NS_1

The ^{1}HNMR spectra of CP, PU_2, and PU_2NS_1 are depicted in Fig. 5.3.b. The peaks at 5.15, 4.3, and 3.2 ppm for CP, 5.2, 4.21, and 3.4 ppm for PU_2, and 5.4, 4.41, and 3.5 ppm for PU_2NS_1 corresponds to –CH, CH_2 allyl, and –CH_2– vinyl, respectively. The peaks at 3 and 4 ppm correspond to –CH_2 adjacent to secondary C and CH_2–O–C=O– respectively. The peak at 7.6 ppm for CP, 8 ppm for PU_2, and 7.7 ppm for PU_2NS_1 reveal the presence of $CDCl_3$. The peaks corresponding to 1.9, 1.7, and 1.8 ppm indicate the methyl proton group for CP, PU_2, and PU_2NS_1 respectively. Similarly, peaks at 4.1 and 1.4 ppm for CP, 4.09 and 1.38 ppm for PU_2, and 4.11 and 1.4 ppm for PU_2NS_1 are attributed to the butylene groups linking to the carbonate group[204].

5.3.4 DMA and Cross-linking Density

DMA thermogram and thermal properties of the paint formulations are displayed in Fig. 5.3.c and Table 5.3.b

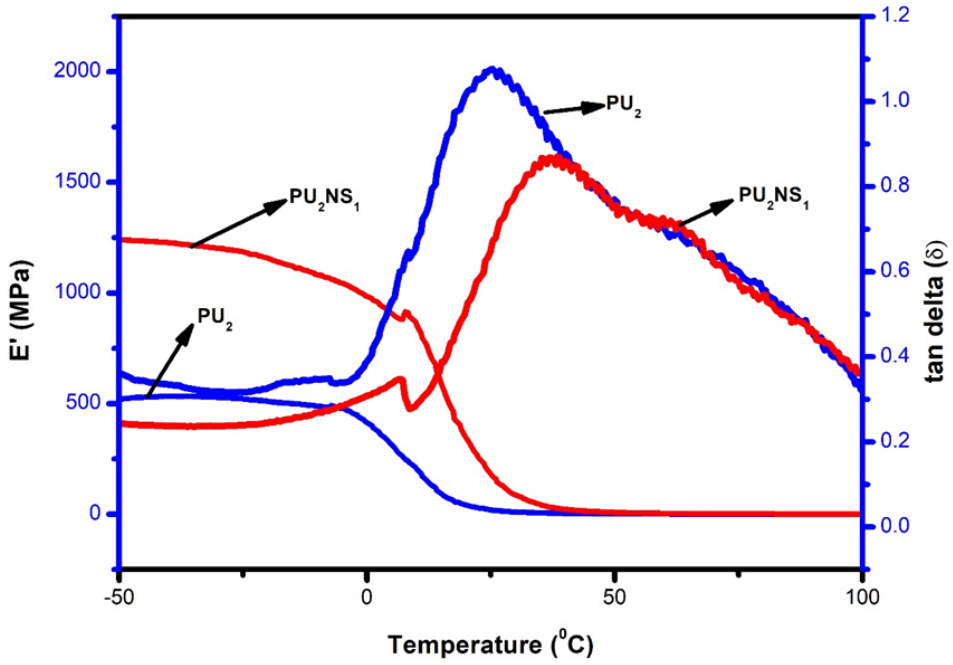

Fig. 5.3.c: Variation of storage modulus (E') and tan δ with the temperature of (a) PU_2 (b) PU_2NS_1

Table 5.3.b: TGA, DMA, and DSC data of hybrid films

Paint sample	TGA Char yield % at 600 ºC	DMA			DSC T_g (ºC)
		T_{gs} (ºC)	E' at 25 ºC	ϑ_c (mol/m^3)	
CP	5.22				1.85
PU_2	0.35	-12.16	0.15	0.90	-17.54
PU_2NS_1	1.22	1.65	0.30	1.78	-2.19

Fig. 5.3.c and Table 5.3.b, depicted the DMA analysis of PU_2 and PU_2NS_1. The ϑ_c was observed to increase from 0.90 to 1.78 mol/m^3 with the incorporation of NS, which is primarily attributed to a strong interfacial bonding between PU matrix and the amorphous NS particles, that transfers the stress from matrix polymer to NS particles at the interface. Further, it may be noted that, NS particles restricts the mobility of PU chains resulting in higher cross-linking density and higher E' value in the paint matrix. It may be noted that, the presence of NS particles lead to an increase in the E' value at 25 ºC from 0.15 to 0.30 MPa. The higher cross-linking density blocks the motion of the molecular chain resulting in a reduction of free volume, which leads to higher T_{gs} and E', values. The tan δ graph revealed the presence of two damping peaks i.e., the low-temperature damping peak corresponds to the T_{gs} of the soft segment and the higher temperature damping peak corresponds to the T_{gh} of the hard segment. From the graph, it was observed that the T_{gs} for PU_2 and PU_2NS_1 were –12.16 and 1.65 °C respectively, whereas the T_{gh} was observed to be 25.29 and 34.19 °C respectively. This behaviour revealed increased T_{gs} and T_{gh} of PU_2 in presence of NS particles, which confirmed increased segmental immobilization of the composite matrix at the interface. These findings were similar to the reports of G. G. Silvia et al.[205].

5.3.5 TGA

The TGA thermogram and thermal properties of the optimized paint formulations are displayed in Fig. 5.3.d and Table 5.3.b respectively.

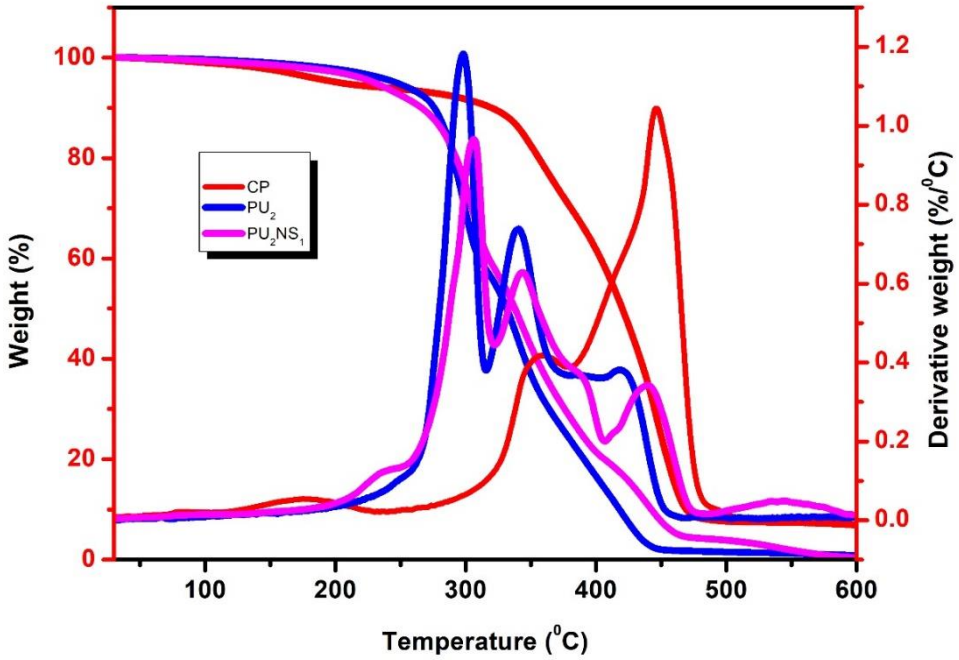

Fig. 5.3.d: DTG/TG thermograms of (a) CP (b) PU_2 (c) PU_2NS_1

The TGA/DTG thermograms of CP, PU_2, and PU_2NS_1 are enumerated in Fig. 5.3.d and the thermal parameters are reported in Table 5.3.b. From the TGA thermograms, it was observed that the T_i for CP was 332 °C, while it is 276 °C and 287 °C for PU_2 and PU_2NS_1 respectively. PU exhibited relatively lower thermal stability due to presence of urethane bond. Incorporation of rigid NS particles as fillers, restricted the chain mobility of PU, resulting in an increased cross-linking density which forms a closed network structure, as reported in the earlier sections. This closed network structure attributed to higher thermal stability of PU in PU/NS matrix. In the case of CP, the decomposition peaks were observed at 333 °C, which indicated the decomposition of urethane linkage, and at 457 ºC which revealed the decomposition of the soft segment. However, in the case of PU_2 and PU_2NS_1, two and three-phase changes were observed respectively. The first peak is attributed to the decomposition

of the hard segment at 301 °C and 315 °C respectively while the second peak revealed at 347 °C and 358 ºC showed the decomposition of the soft segment. However, in case of PU_2NS_1 an extra decomposition peak was observed at 545 °C, which showed the decomposition of isocyanates into carbamide and carbon dioxide. The char yield of PU_2 is 0.35%, while for CP it was found to be 5.22% due to the presence of several additives. When NS was reinforced into the PU matrix, the char yield increased to 1.22% due to the presence of –Si-O-Si- linkage and isocyanate linkage in the functionalized NS particles. The maximum degradation temperature for PU_2 was 498 °C, while it was 556 °C for CP. In case of PU_2NS_1 the final degradation temperature was found to be at 553 °C. This shift in degradation temperature shows a strong interaction between PU and NS. Similar results were reported by K. Ismoilov et al.[206].

5.3.6 DSC

The DSC thermogram and thermal properties of paint samples are showed in Fig. 5.3.e and Table 5.3.b

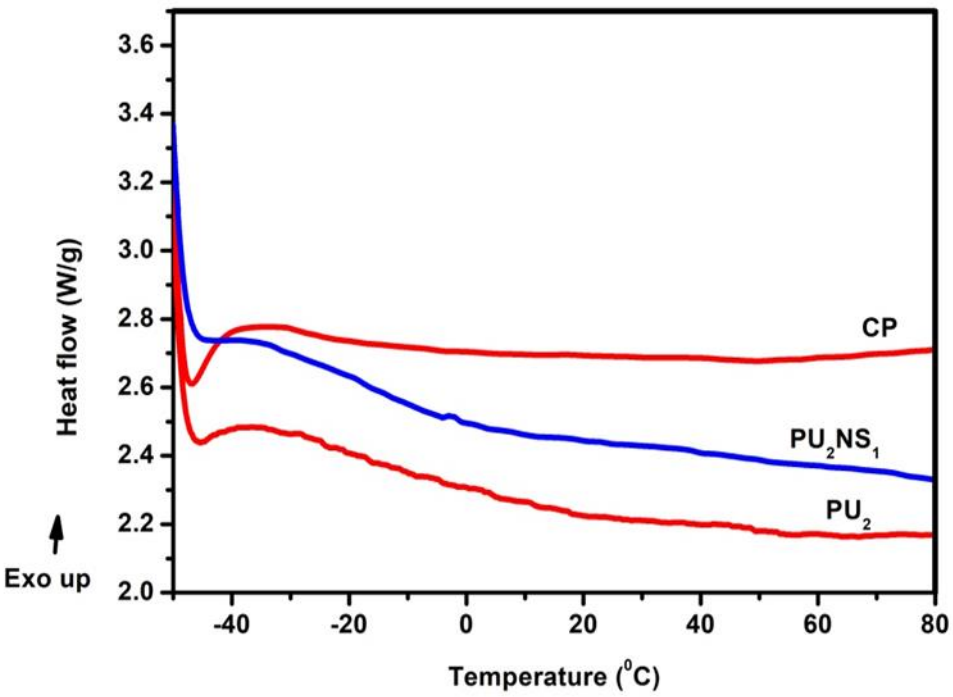

Fig. 5.3.e: DSC thermogram of various Paint formulations

The DSC thermograms of the paint formulations have been reported in Fig. 5.3.e and Table 5.3.b. T_g of PU was observed to increase from -17.54 to -2.19 ºC with the incorporation of NS particles. This behaviour is due to similar fact that, the NS particles present in the PU matrix contributed to strong interfacial interaction with the hard segment of PU matrix, that results in increase in cross-linking density, associated with the formation of closed silica network structure created in the composite matrix. In the case of CP, the T_g is higher in comparison to synthesized paint samples i.e., 1.85 ºC. Somdee. P et al. have also reported similar findings[207].

5.3.7 Lap-shear Test

The lap-shear strength and mechanical properties of CP, PU_2, and PU_2NS_1 are enumerated in Fig. 5.3.f and Table 5.3.c

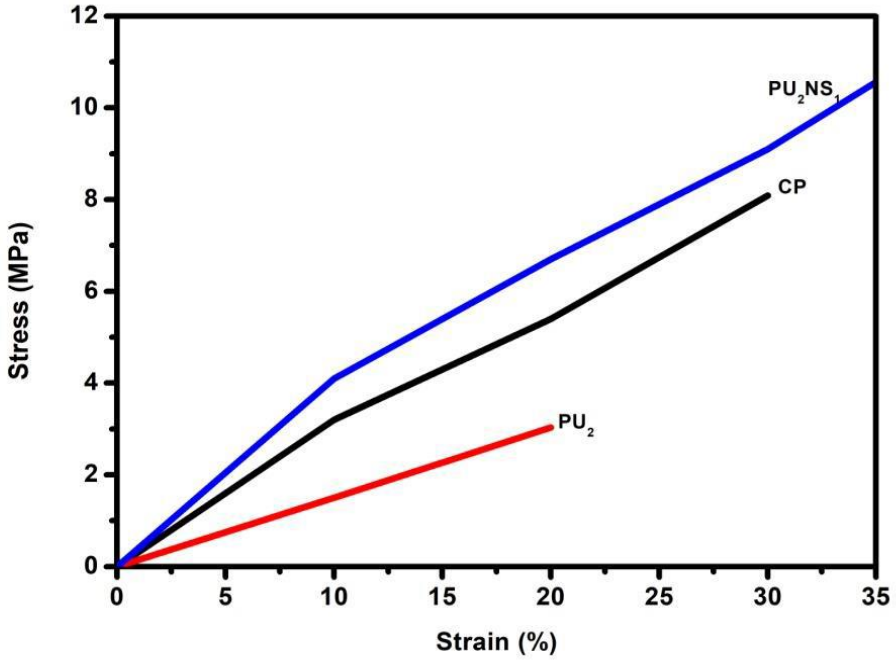

Fig. 5.3.f: Stress-Strain graph of paint samples

Table 5.3.c: Mechanical properties of paint samples

Paint sample	Shear strength (MPa)	Young's modulus (MPa)	Pencil Hardness	Abrasion wt. loss (%)
CP	8.09	1939	3H	0.14
PU_2	3.03	1333	2H	0.46
PU_2NS_1	10.50	2312	3H	0.12

From the Table 5.3.c and Fig. 5.3.f, it was found that the shear strength of CP was 8.09 MPa, while in the case of PU_2, the shear strength was found to be 3.03 MPa. However, incorporation of NS particles to the PU matrix, resulted in increase in shear strength to 10.50 MPa. The mechanical properties of PU/NS composite are greatly influenced by the compatibility and dispersion of NS particles in the PU matrix. When optimized wt.% of NS particles are incorporated into the PU matrix, they hinder the chain mobility of hard segment of PU, resulting in increased cross-linking density. From the above study, PU matrix incorporated with 0.5 wt.% NS particle exhibited optimum shear strength value. The Young's modulus of PU_2 was 1333 MPa, which was 1939 MPa in the case of CP. However, in case of NS particle incorporated PU matrix, the modulus increased to 2312 MPa, because of similar facts of the strong interaction between the PU matrix and amorphous NS particles. The incorporation of NS particles within the PU matrix improved the mechanical properties of the paint over its neat and commercial formulations to the extent of 42% and 16% respectively. Similar findings have been reported by P.A. Khoon et al.[208].

5.3.8 Nanoindentation Test

The force -displacement graph of the paint formulations is displayed in Fig. 5.3.g

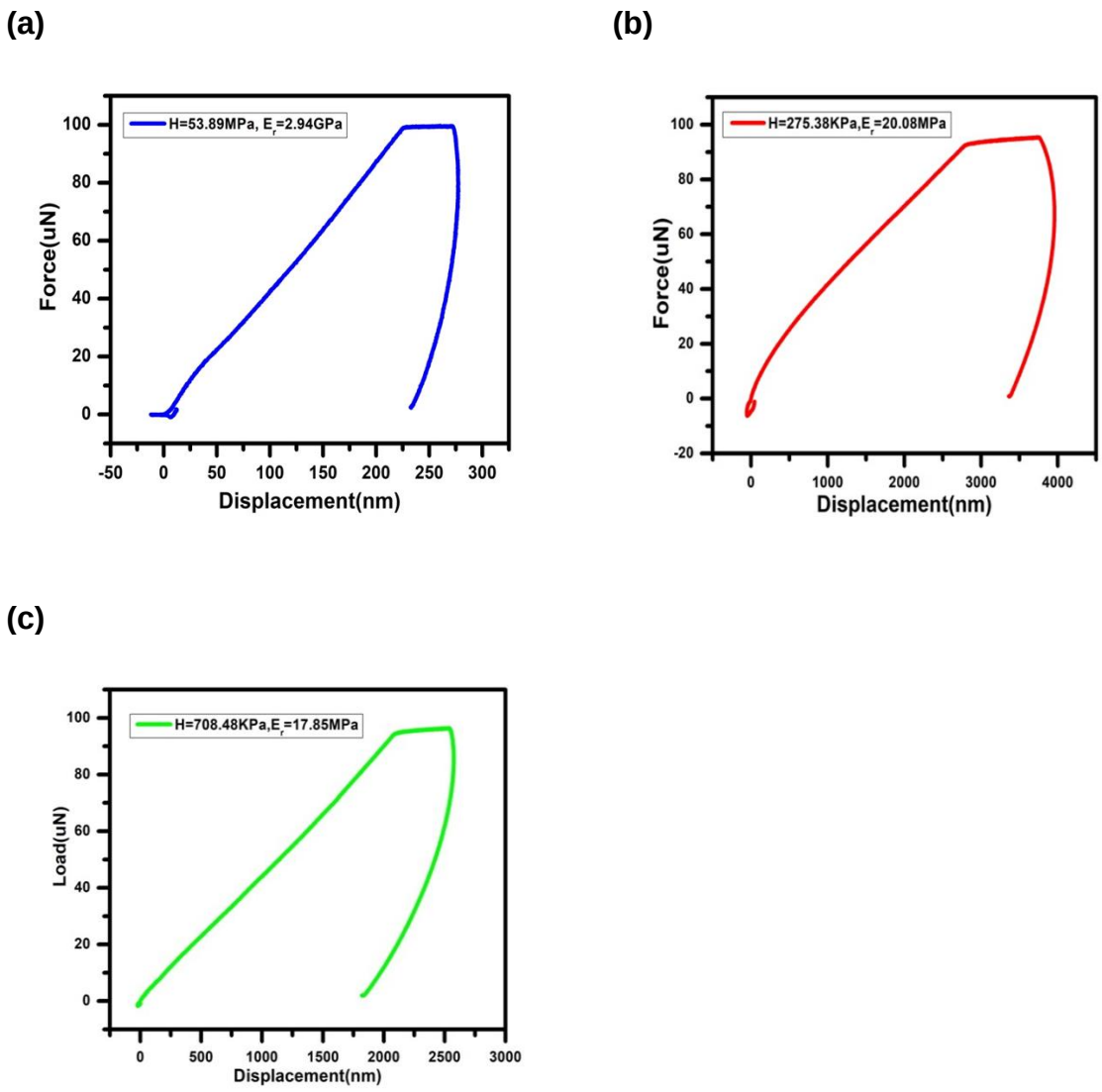

Fig.5.3. g: Force vs. displacement curve of (a) CP (b) PU_2 (c) PU_2NS_1

A nano-indenter with a specific force creates an indentation depth on the coating surface. The penetration depth is studied as a function of time consisting of a single loading and unloading cycle curve. A. Karimazadeh et al. reported that NS fillers enhance the cohesive forces within the matrix, which prevents the penetration of the indenter increasing hardness (H) and elastic modulus (E) values[209]. Fig. 5.3.g showed the typical indentation loading-unloading curves for CP, PU_2, and PU_2NS_1.

The graph was plotted between hardness, elastic modulus vs. indentation depth. In case of PU_2, the maximum indentation depth at the maximum load of 10 mN was observed to be 3300 nm, while in the case of PU_2NS_1 and CP the maximum depth observed was about 2000 nm and 250 nm respectively. After the insertion of NS particles, the hardness of the coating was observed to be increased by 66%. Elastic recovery was 35% in the case of PU_2, while NS particle addition increased the elastic recovery to 25%. Incorporation of NS particles increased the hardness due to the strong interaction between hard segment of PU and amorphous NS particles, which provided improved reinforcement by forming Si-O-Si linkage at the interface, which in turn leads to higher cross-linking density as discussed in the earlier sections. This study concludes that, with the addition of NS particles, the coating developed is bestowed with higher hardness and lower elastic recovery properties, thereby leading to achieve higher scratch resistance properties. N. Jamal et al. have also reported similar behaviour in case of UHMWPE reinforced hybrid composite of carbon fiber and NS[210].

5.3.9 Abrasion Resistance Test

The abrasion test results of paint formulations are enumerated in Table 5.3.c. The weight loss in the Taber abrader for commercial paint was 0.14%, which was 0.46% and 0.12% in case of PU_2 and PU_2NS_1 respectively. The abrasion resistance of paint matrix showed an increase with incorporation of NS particles. This indicated strong interfacial bonding between NS and PU. Also, as explained in the earlier sections it may be concluded that the NS forms -Si-O-Si- linkage on the PU matrix, which enhanced the cross-linking density and thereby enhanced the abrasion resistance. The results obtained from the current study can be corelated from the findings of O. A. Valdes et al.[211].

5.3.10 Pencil Hardness Test

The pencil hardness of CP was observed to be 3H. In case of PU_2 it was found to be 2H, which subsequently increased to 3H with the incorporation of NS particles within the PU-matrix. This result is additionally confirmed increased bond strength of NS reinforced PU matrix which lead to freezing of mobility of PU chains, thus resulting in increased cross-linking density. N. Hussain et al. stated similar results[212].

5.3.11 WCA

The WCA of CP, PU_2, PU_2NS_1 are enumerated in Fig. 5.3.h

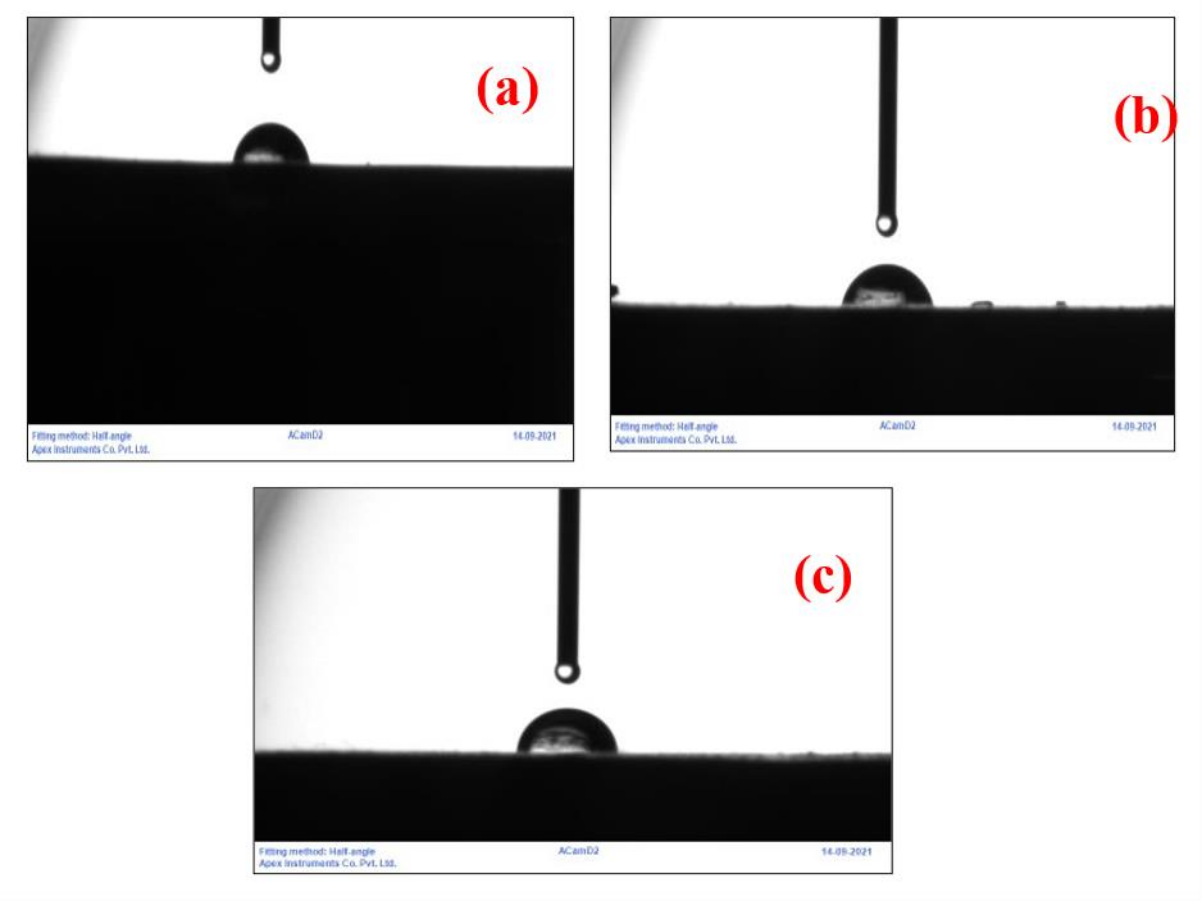

Fig. 5.3.h: WCA of (a) CP (b) PU_2 (c) PU_2NS_1

As observed, increase in heterogeneity and surface roughness increased the WCA. The WCA studies of paint samples revealed that, WCA of CP and PU_2 was 93.52 º, and 81.71 ° respectively. Whereas, in case of PU_2NS_1, the WCA increased to 92.26 °. The WCA value for PU_2NS_1 increased due to the increase in heterogeneity in presence of NS particles in the PU matrix which forms a closed network structure, thereby increasing the hydrophobicity of the surface. S. Das et al. have reported similar findings in case of PU coatings synthesized from TECO[192].

5.3.12 SEM

SEM image of CP, PU_2, and PU_2NS_1 is displayed in Fig. 5.3.i

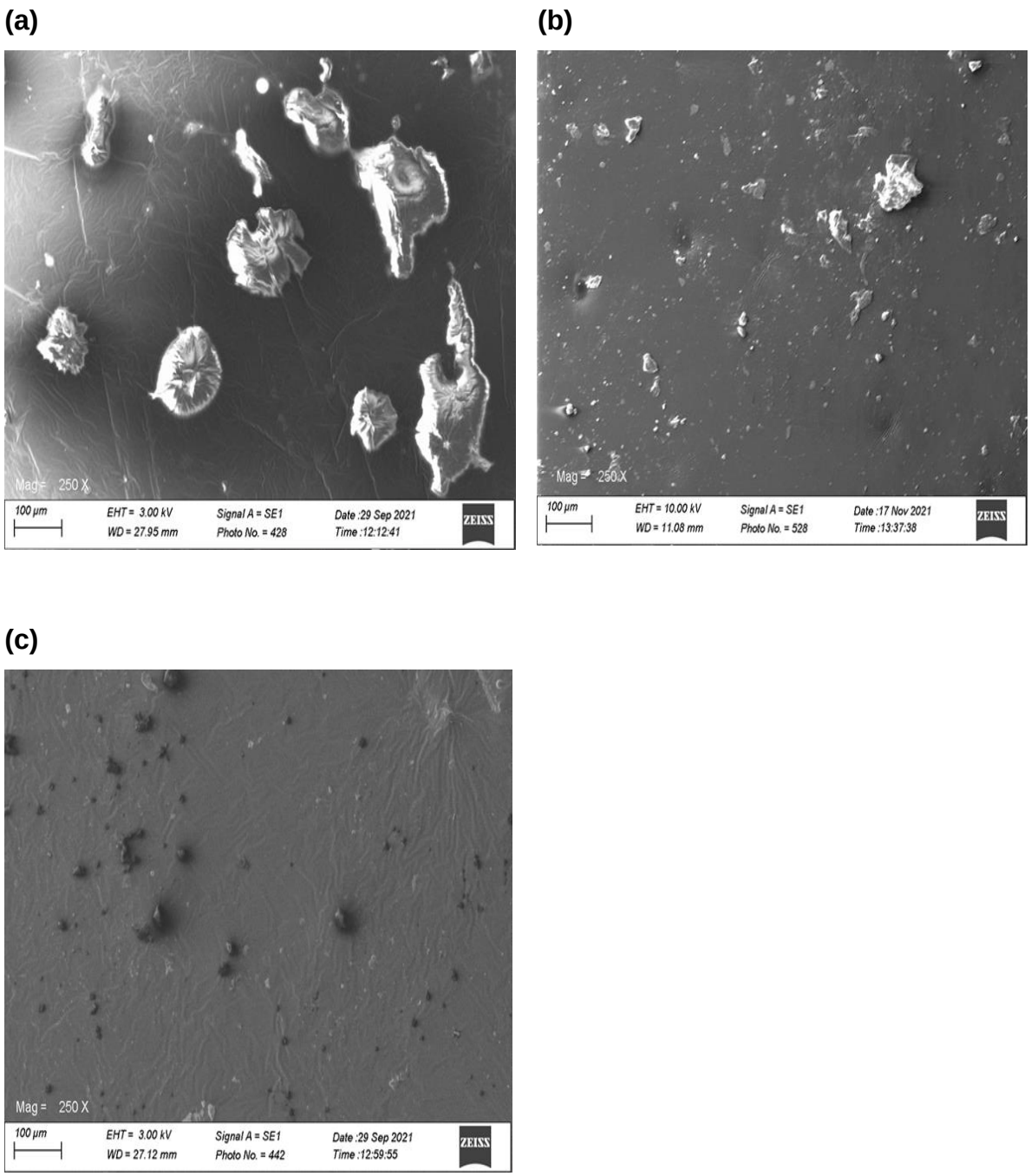

Fig.5.3.i: SEM image of (a) CP (b) PU_2 (c) PU_2NS_1

SEM micrographs of the cross-section of CP, PU_2, and PU_2NS_1 are enumerated in Fig. 5.3.i. It is evident from Fig. 5.3.i (b), that PU_2 paint formulation revealed the

presence of hard segment and soft segment. However, minor traces of agglomeration were observed on the paint surface, with overall picture of a homogenized coating. In the case of CP, the SEM micrograph in Fig. 5.3.i (a) showed several agglomerations which revealed the presence of many additives present in the paint film. Conversely, as observed in Fig. 5.3.i (c), with the incorporation of NS particles within the PU matrix, the paint surface showed a little amount of heterogeneity. The black surface observed from the image indicated the PU, while the white dots and lumps indicated the NS particles. The micrograph also showed that there was no traceable agglomeration in the PU_2NS_1 film. Similar results were also confirmed by L. Chen et al., wherein the authors observed homogenized PU coating employing precipitated silica with silanol moeity[213].

5.3.13 TEM

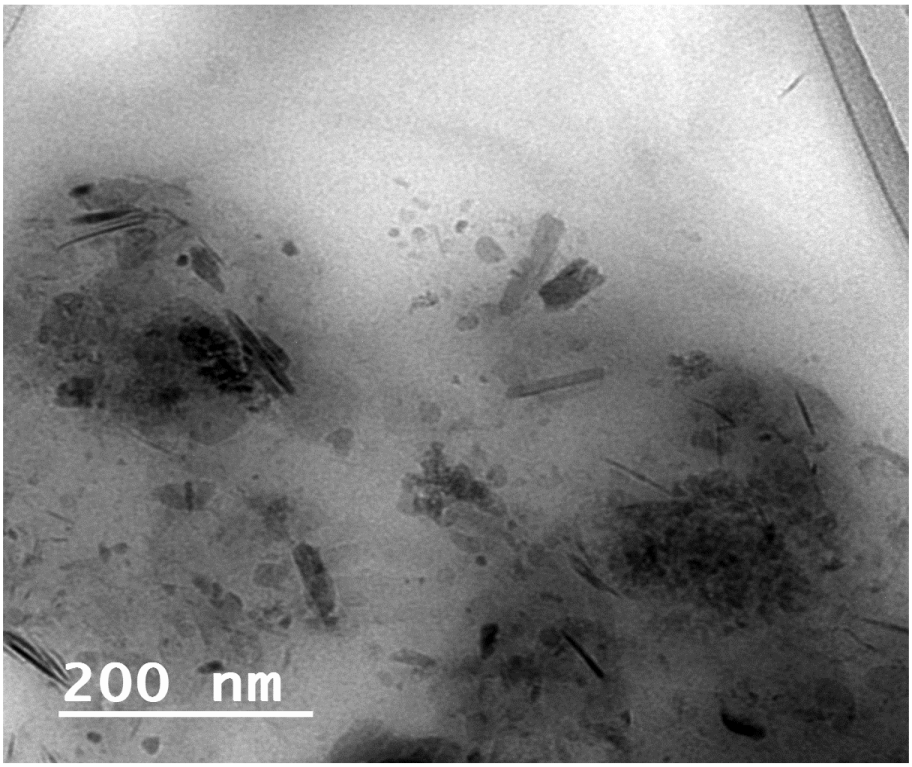

Fig. 5.3.j: TEM micrograph of PU_2NS_1

TEM micrograph of PU_2NS_1 was displayed in Fig. 5.3.j. From the TEM micrograph it was observed that, all NS particles cannot be dispersed completely into the acrylic/PU matrix. Bright spots with dark spots were observed from the micrograph, wherein the

bright spot indicates pores present in the PU matrix, whereas the dark spots indicate the NS particles embedded within the pores. The larger dark spot shows presence of agglomeration in the PU matrix. M. Seeni reported similar results in her study[214].

5.3.14 Gloss and Weather Resistance Test

The variation of gloss after weathering, its retention, transmittance and haze of CP, PU_2, and PU_2NS_1 are represented in Table 5.3.d.

Table 5.3.d: Gloss before and after 400 hrs. weathering, Gloss retention %, transmittance, and haze

Paint formulation	Gloss at 0 hr. weathering	Gloss after 400 hrs. weathering	Gloss retention (%)	Transmittance (%)	Haze (%)
CP	34.12	28.54	83.64	-	-
PU_2	23.76	15.89	66.87	92.51	22.41
PU_2NS_1	32.48	25.51	78.50	99.32	15.63

Table 5.3.d, revealed that, the gloss value of CP is very high and after 400 hrs. exposure in weatherometer, the gloss retention % was found to be around 83%. In case of PU_2, the gloss retention % was observed to be around 66.87%. However, in case of PU_2NS_1, the gloss retention % increased significantly to 78.50%, due to the presence of NS particles. Uniformly dispersed NS particles enhanced the light scattering efficiency, when exposed to light, which lead to higher gloss of the paint matrix. Similar results were observed with L. Zhang et al. in case of water-borne PU-coatings[215].

5.3.15 UV-visible spectra

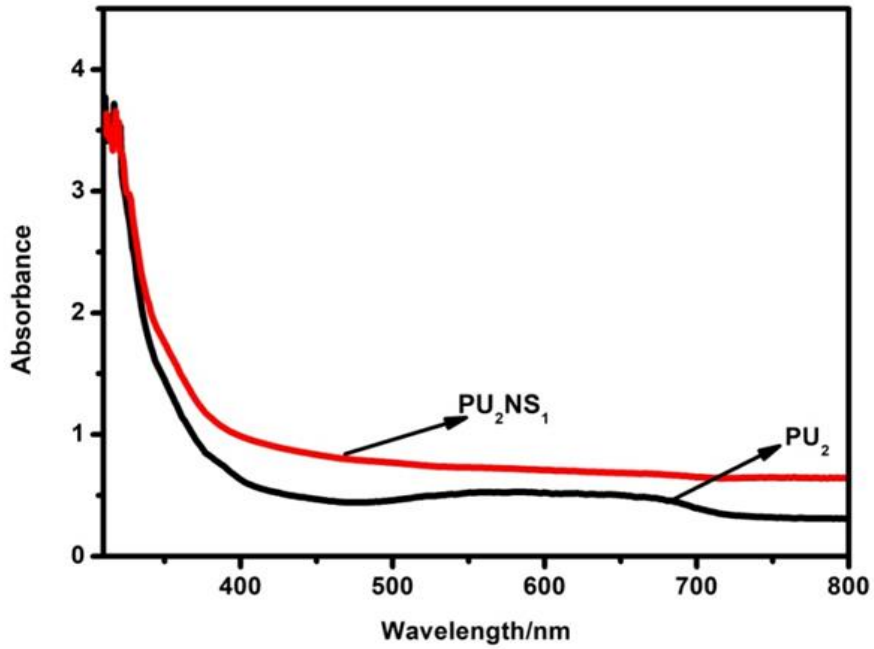

Fig. 5.3.k: Absorbance spectra of PU_2 and PU_2NS_1

The ultraviolet-visible (UV-VIS) spectra of PU_2 and PU_2NS_1 are depicted in Fig. 5.3.k. The absorbance spectra indicated that the absorbance increases after immersion of NS particles, and the increment was more obvious at shorter light wavelength. Because of absorbance and reflection, the transmittance of light also reduced. The reduction of transmittance in the range of 290–400 nm wavelength indicated that both the paint formulations have the UV-shielding property. The PU_2NS_1 coating formulation was observed to have lower transmittance, which made it more opaque in comparison to PU_2. The lower transparency of PU_2NS_1 is caused by the aggregates of NS particles in the paint matrix, which can also be correlated from TEM micrography. Similar results were studied by H.R. Pant et al.[216].

5.3.16 Haze and Transmittance

Haze describes the light scattering of a specimen. Highly transparent materials show lower haze %. From Table 5.3.d it was evident that with the incorporation of NS particles, haze % decreased from 22.41% to 15.63% resulting in an increase in transmittance from 92.51% to 99.32% of the paint matrix. NS has a high refractive index of 1.51, which prevents the scattering of light, resulting in a decrease of haze in contrast to the enhancement of transmittance in the paint film. Similar results have been reported by D. K. Chattopadhyay et al. [50].

5.3.17 Petrol, Diesel, and Engine oil Resistance Test

The effect of petrol, diesel, and engine oil immersion are depicted in Fig. 5.3.m

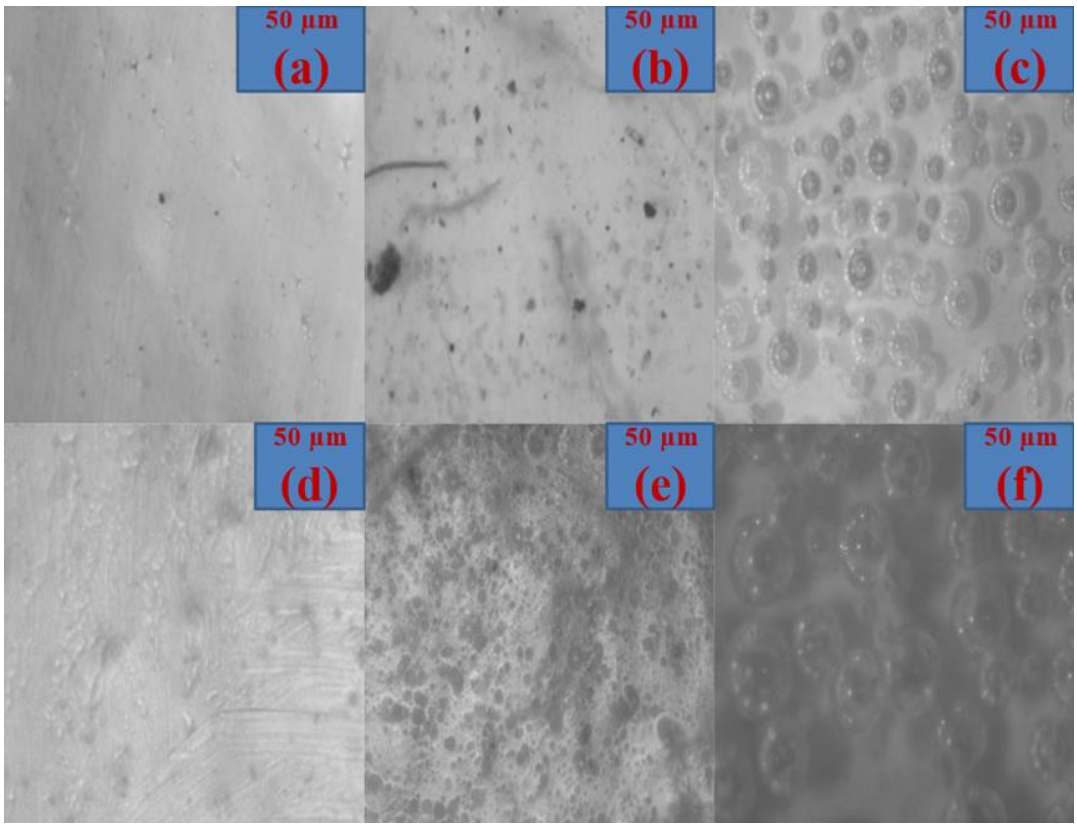

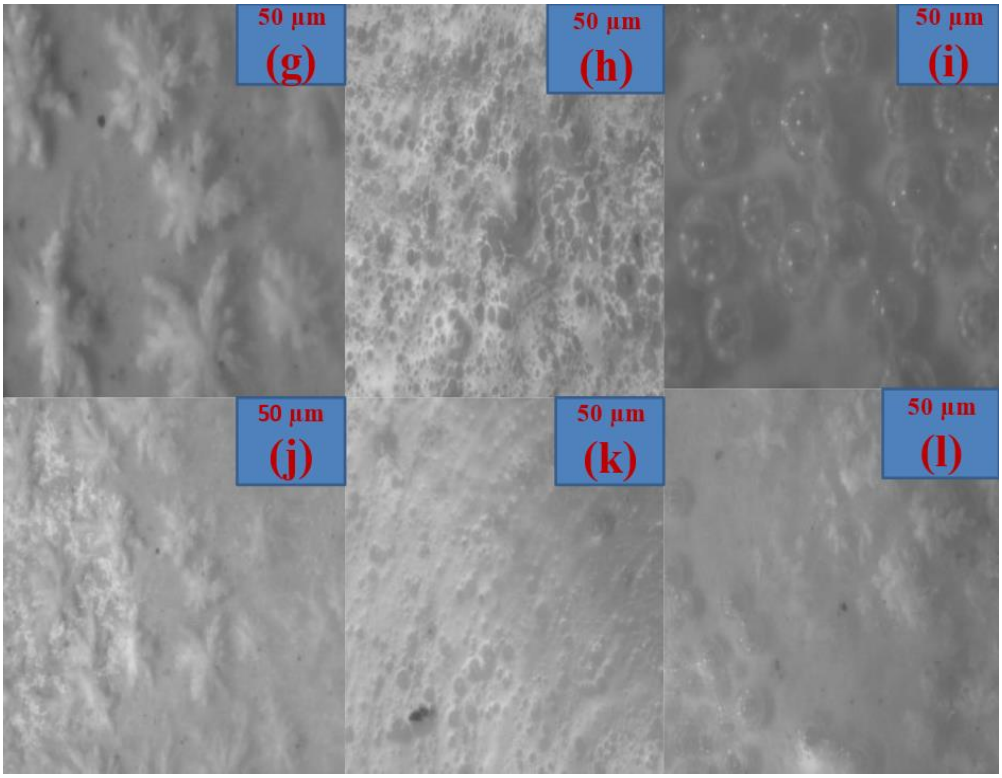

Fig. 5.3.l: Optical microscopy image of paint formulations before immersion in petrol, diesel, and engine oil (a) CP (b) PU_2 c) PU_2NS_1 Petrol immersed paint samples (d) CP (e) PU_2 (f) PU_2NS_1. Diesel immersed paint samples (g) CP (h) PU_2 (i) PU_2NS_1. Engine oil immersed paint samples (j) CP (k) PU_2 (l) PU_2NS_1

From the optical microscopy images reported in the Fig. 5.3.l, it was observed that after immersion in petrol the coated samples did not show any appreciable change as compared with the pre-immersion images of paint samples, which revealed that the paint formulations are resistive to petrol. However, in the case of diesel immersed paint formulations, the structure was observed to change marginally in the case of CP, whereas in case of PU_2 a major change in structure was observed. But with the insertion of NS particles, the diesel resistivity of the paint formulation improved, wherein only a marginal change in gloss was observed. When the paint formulations were immersed in engine oil, all the paint formulations exhibited softening effect, with PU_2, the softening was prominent wherein peeling of the paint was observed. When a paint is immersed in oil, it shows osmotic blistering due to entrapment of accumulated dirts and temperature difference on the paint surface, which leads to paint peeling, softening and blistering. With the incorporation of NS particles, the interfacial bond between the PU

matrix and NS particles increased due to the presence of Si-O-Si linkage. This led to higher cross-linking density, that attributed to increase in oil resistance property of PU/NS composite paint formulation.

5.3.18 Acid and Alkali Resistance Test

The effect of acid and alkali on the paint samples is enumerated in Table 5.3.e.

Table 5.3.e: Acid and Alkali effects on paint formulations

Paint formulations	Acid	Alkali
CP	Change in appearance	No change
PU_2	Change in gloss	No change
PU_2NS_1	Change in appearance	No change

The paint formulations were observed to be resistant to alkali, as no physical change was observed after the immersion of the paint samples in alkali. But in the case of acid immersion, the CP and PU_2NS_1 paints showed very less change in physical appearance, but in the case of PU_2, some variations like change in gloss was observed. This behaviour confirmed that, PU-matrix formed a closed network structure due to formation of Si-O-Si linkage in PU_2NS_1, which lead to less percolation of acid and alkali. L. Chen et al. have also reported similar findings[213].

5.3.19 Solvent Resistance Test

The solvent resistance properties of the paint samples are displayed in Fig. 5.3.m and Table 5.3.f.

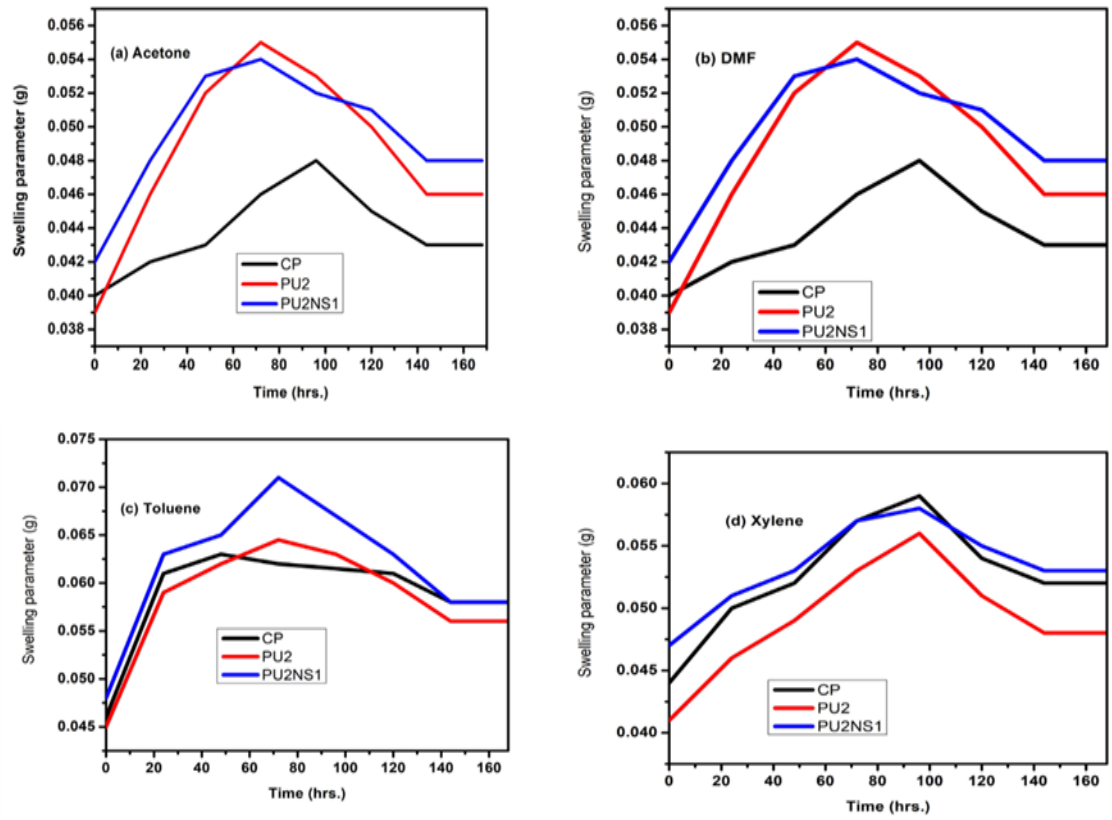

Fig. 5.3.m: Variation in swelling parameter as a function of time of various paint formulations in different solvents, (a) Acetone (b) DMF (c) Toluene (d) Xylene

Table 5.3.f: Change in wt. % after 7 days of immersion in solvents.

	Acetone	DMF	Toluene	Xylene
CP (wt. change %)	14.50	5.71	2.10	2.60
PU_2 (wt. change %)	13	7.81	4.57	6.25
PU_2NS_1 (wt. change %)	6.66	3.26	3.57	2.40

The solvent resistance study depicted in Table 5.3.e and Fig. 5.3.m, showed that the solvent resistance of PU_2 was less than that of CP. However, in the case of PU_2NS_1 film, the solvent resistance was found to be higher due to the similar facts as elaborated in the earlier section of increase in cross-linking density that occurred by the incorporation of NS particles within the PU matrix, which contributed in strong interfacial bond between PU matrix and NS particles. PU_2NS_1 paint showed solvent resistance properties as that of CP. Similar results have been reported by B. Xue et al..[217].

Conclusions

Bio-based automobile PU-based clear coat was synthesized using ATECO and IPDI via in-situ polymerization method. FTIR and ^{1}HNMR studies reveal the formation of urethane linkage confirming the chemical structure of polyurethane. PU-coating reinforced with 0.5 wt.% TI modified NS particles, exhibited improved performance characteristic w.r.t thermal, mechanical, and chemical properties. XRD, SEM, and TEM revealed improved dispersion of TI-modified NS within PU matrix. Thermal properties like char residue % and T_{gs} were increased from 0.35% and -12.16 ºC to 1.22 % and 1.65 ºC with the addition of NS respectively. Incorporation of NS also increased the mechanical properties like cross-cut adhesion %, Young's modulus, pencil hardness, abrasion loss %, and nanoindentation depth from 82±2%, 1333 MPa, 2H, 0.40%, and 3300 nm to 93±3%, 2312 MPa, 3H, 0.12% and 2000 nm respectively. Similarly, WCA, cross-linking density, solvent resistance, oil resistance, and optical properties increased significantly, with the addition of NS particles in the PU matrix. Hence, eco-friendly acrylic PU-based paint formulation, derived from castor oil incorporated with optimized dosage of modified NS can suitably substitute the commercial clear coats.

CHAPTER 6

Chapter 6

Effect of incorporation of TI modified Nanosilica (NS) on the properties of blend nanocomposite for Automobile sealer application

Introduction

Epoxy (EP) resins are one of the most significant adhesive materials with three-dimensional network structure. Despite of having excellent thermal, mechanical and chemical resistance properties, these resins have certain drawback of brittleness, which leads to ease in crack propagation[218]. These problems can be largely avoided by adding a toughening material to the epoxy resin. PU is a versatile polymeric material with higher mechanical, thermal and tensile properties[219] and it is considered as a very good toughening polymer for thermosetting polymeric materials. It has hard segments and soft segments, which are incompatible and leads to phase separation[218]. In recent studies, development of a blend of two polymers to create an interpenetrating network (IPN) have attracted significant research interest[220]. EP has lower toughening and impact properties, whereas PU has higher toughening and impact properties. Hence, a blend of EP and PU, results in an IPN having their maximum characteristic properties[221].

Adhesives and sealers are one of most significant part of automobile paint industry applicable in various parts of automobile body like, windshields, brake shoes, thread lockers etc.[222]. These are binding materials used by automotive original equipment manufacturers (OEMs) to bind different substrates of automobile body parts without using welding and mechanical bolts[222]. Typically, an epoxy/PU composite is considered as one of the mostly used sealer material, which provides higher adhesion effects[223].

With nanoscale fillers becoming more extensive in industries, the characteristic properties of epoxy-PU blend can be improved by incorporation of various nano particles. Surface modified NS particles are the most preferred additive incorporated

in the epoxy-PU blend. Modified NS particles have a large number of hydroxyl groups, which attributed to extensive interaction between the blend matrix and the NS particles, resulting in toughening properties as well as mechanical properties[224].

The current study reported the synthesis of Epoxy-PU blend applicable as automobile sealer using EPOFINE blended with ATECO as matrix, FINE HARD as curing agent and TI-NS as additive. The structural, mechanical and thermal properties of the sealer samples have been studied and reported in current chapter.

Results and Discussion

6.1 Optimization of blend ratio of Epoxy: PU

The blend optimization has been evaluated employing impact test at variable ratios. The impact strength of both notched and unnotched epoxy-PU blends were shown in Table 6.a.

Table 6.a: Impact strength of Epoxy: PU at variable wt. ratio and effect of incorporation of NS

Sealer composition	Epoxy: PU	NS (wt.%)	Impact strength un-notched (J/m)	Impact strength notched (J/m)
EP_1	100: 0	0	55.7±5	13.8±2
EP_2	80: 20	0	91.3±4	21.6±4
EP_3	60: 40	0	73.6±3	16.6±5
EP_2NS	80: 20	0.5	100.2±2	24.7±3

From the Table 6.a, it was observed that, EP_1 has lower impact strength due to presence of large number of epoxy rings. After addition of 20% ATECO into neat epoxy matrix, the EP_2 blend was exhibited an increase in impact strength from 55.7±5 J/m to 93±4 J/m in case of un-notched samples and 13.8±2 J/m to 21.6±4 J/m in case of

notched samples. This behaviour is possible because ATECO has a polymer network of C-C double bond, that led to inhibition of crack propagation, thereby resulting increase in impact strength. However, when the ATECO ratio was increased from 20% to 40%, a decrease in impact strength was observed for both notched and un-notched samples. This result attributed that, excess amount of ATECO in the blend led to agglomeration, resulting in decrease in impact strength. Hence, blend composition with epoxy: PU ratio 80:20 was optimized for sealer applications. From the previous study TI-NS incorporated at 0.5 wt.% showed optimum characteristic properties. Thus, TI-NS of 0.5 wt.% was retained in the optimized blend and was incorporated into the composition. It was observed that, the impact strength was increased from 93±4 J/m to 100.2±2 J/m in case of un-notched sample and from 21.6±6 J/m to 24.7±3 J/m. This phenomenon was possibly because NS created a close network structure in the polymer matrix, which increased its cross-linking density thus, increased the impact strength of the nanocomposite.

6.2 FT-IR:

FTIR spectra of blends of Epoxy: PU at variable composition are displayed in Fig. 6.a

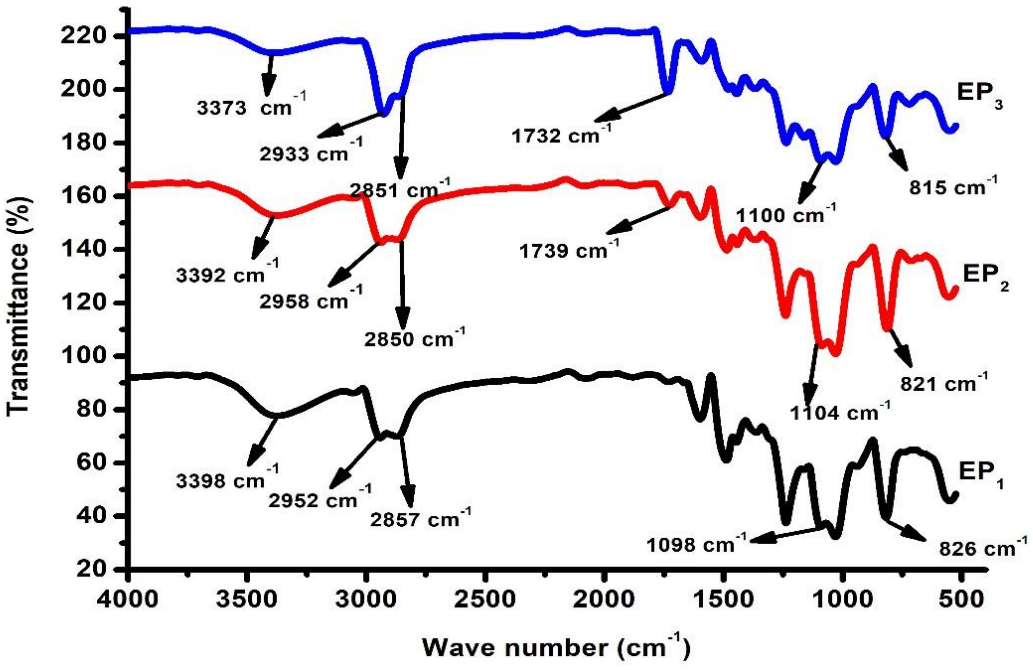

Fig. 6.a: FTIR spectra of (a) EP_1 (b) EP_2 (c) EP_3

From Fig. 6.a, the FTIR spectra of the epoxy-PU blends revealed that, the peaks corresponding to 3398, 3392, and 3373 cm^{-1} represents -OH group for EP_1, EP_2, and EP_3 respectively. -CH_2 symmetric and asymmetric stretching for EP_1 was observed at 2857 and 2952 cm^{-1} respectively. Similarly, for EP_2, -CH_2 symmetric and asymmetric stretching was noted at 2850 and 2958 cm^{-1}. In case of EP_3, the same was observed at 2851 and 2933 cm^{-1}. Peak corresponding to -C=O band was observed at 1739 and 1732 cm^{-1} for EP_2 and EP_3. -COO symmetric bond was observed at 1098, 1104, and 1100 cm^{-1} for EP_1, EP_2, and EP_3 respectively. Similarly, the symmetric epoxide ring was observed at 826, 821, and 815 cm^{-1} in case of EP_1, EP_2, and EP_3. Presence of the above-mentioned chemical bonds confirmed the formation of Epoxy-PU blend.

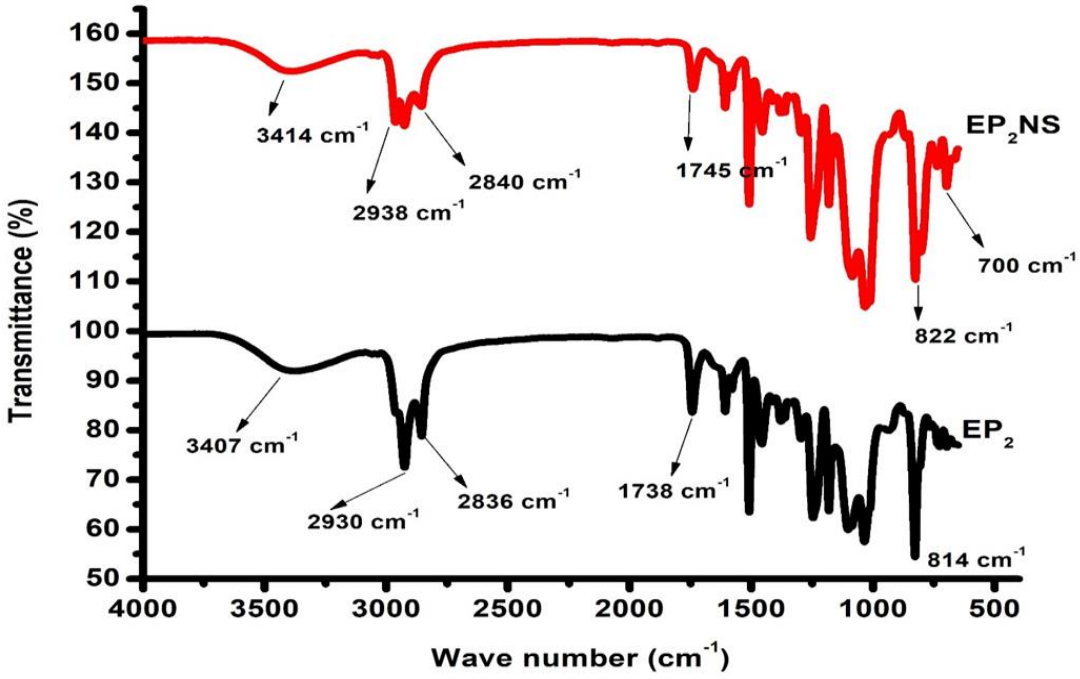

Fig. 6.b: FTIR spectra of (a) EP_2 (b) EP_2NS

FTIR spectra of EP_2 and EP_2NS are represented in Fig. 6.b. The peaks corresponding to -OH group was noted at 3407 and 3414 cm^{-1} for EP_2 and EP_2NS respectively. -CH_2 symmetric and asymmetric band was observed at 2840 and 2938 cm^{-1} for EP_2NS which was noted at 2836 and 2930 cm^{-1} in case of EP_2. -C=O band was observed at 1738 and 1745 cm^{-1} in case of EP_2 and EP_2NS. EP_2 showed symmetric and asymmetric -COO bond at 1058 and 814 cm^{-1}. Similarly, in case of EP_2NS, peaks

corresponding to the symmetric and asymmetric -COO bond was observed at 1088 and 822 cm^{-1} respectively. Additionally, EP_2NS showed another band at 700 cm^{-1}, representing the Si-C bond due incorporation of NS.

6.3 Fracture Toughness and Tensile Strength

Fracture toughness and Tensile strength of the epoxy, epoxy: PU blend and its nanocomposite are displayed in Fig. 6.c and Table 6.b.

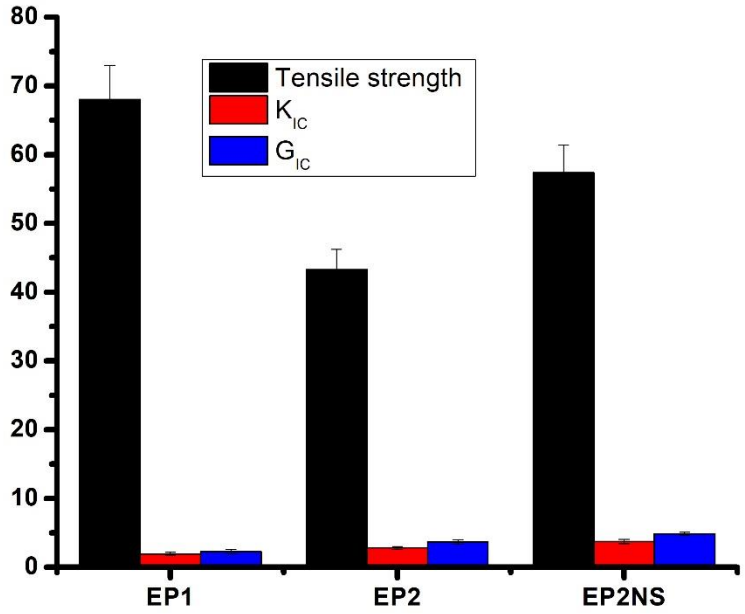

Fig. 6.c: Tensile stress, Critical stress intensity and Critical Strain energy value of EP_1, EP_2 and EP_2NS

Table 6.b: Tensile and Fracture toughness analysis of EP_2 and EP_2NS

Sample name	Tensile strength (MPa)	Elongation at break (%)	Young's Modulus (MPa)	K_{IC} (MPa.$m^{1/2}$)	G_{IC} (KJ/m^2)
EP_1	68.02±5	0.98±0.2	4131.12±6	1.96±0.2	2.27±0.3
EP_2	43.25±3	1.85±0.2	2987.47±8	2.82±0.2	3.69±0.3
EP_2NS	57.38±4	2.21±0.5	3654.83±7	3.74±0.3	4.88±0.2

Fig. 6.c and Table 6.b enumerates the tensile strength, elongation at break, critical stress intensity factor and critical strain energy rate of EP_1, EP_2, and EP_2NS. The tensile strength of EP_1 was 68.02±5 MPa with elongation at break of 0.98±0.2%, which indicated its brittleness characteristics. With addition of 20% ATECO, the tensile strength decreased to 43.25±3 MPa while the elongation at break increased to 1.85±0.2%. A similar decrease in modulus value to the tune of 36% was noted with the incorporation of ATECO within the EP_1 matrix. This behaviour indicated that incorporation of ATECO within the neat epoxy decreased the cross-linking density. neat epoxy, it decreased the cross-linking density, which resulted in a flexible product with more toughness. On the contrary the tensile strength of EP_2 was observed to increase by 32% with incorporation of NS. The elongation at break was also increased by 19% with addition of NS particles into the blend. NS particles when added to the blend, the interfacial interaction between the matrix and the filler increased, resulting in formation of a closed network structure, which increased the cross-linking density of EP_2NS, thereby leading to increase in tensile strength, elongation at break, and modulus in comparison with EP_2 blend.

K_{IC} value indicates the critical amount of stress needed to raise a small amount of crack, which leads to material failure. Similarly, G_{IC} value determines the measure of the critical energy required to extend a crack over a unit area. The K_{IC} and G_{IC} value of neat epoxy i.e., EP_1 was observed to be 1.96±0.2 MPa.$m^{1/2}$ and 2.27±0.3 KJ/m^2 respectively. Similarly, with addition of ATECO, K_{IC} and G_{IC} increased to 2.82±0.2 MPa

$m^{1/2}$ and 3.69±0.3 KJ/m^2 respectively. Addition of ATECO into the epoxy matrix resulted in its change in chemical structure, which led to increase in flexibility of the blend, thus increased the K_{IC} and G_{IC} value of the blend. After incorporation of NS particles into EP_2, the K_{IC} and G_{IC} value were studied to increase by 32% and 33% respectively for EP_2NS. This can be explained due to the fact that, NS particles create a closed network structure in the sealer matrix, resulting in higher cross-linking density, which led to increase in stress intensity factor and strain energy rate.

6.4 DMA and Cross-linking density

The DMA thermogram and thermal properties of the sealer samples are depicted in Fig. 6.d and Table 6.c

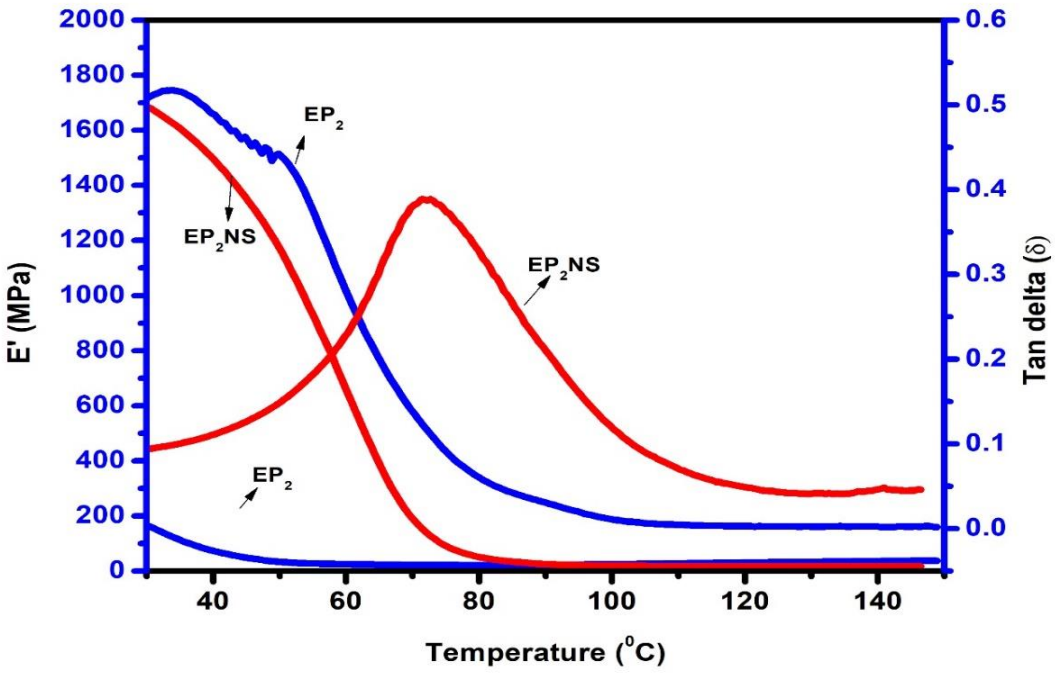

Fig. 6.d: DMA thermogram of sealer samples

Table 6.c: TGA, DMA, and DSC data of sealer samples

Paint sample	TGA Char yield % at 800 °C	DMA			DSC T_g (°C)
		T_{gs} (°C)	E' at T_g±30 °C	ϑ_c (mol/m^3)	
EP_2	3.66	37.16	22.37	0.98	32.28
EP_2NS	4.54	50.81	46.17	3.42	46.37

Fig. 6.d and Table 6.c, depicted the DMA analysis of EP_2 and EP_2NS w.r.t. variation of E' and tan δ as a function of temperature. The ϑ_c was observed to increase from 0.98 to 3.42 mol/m^3 with the incorporation of NS. Incorporation of NS particles attributed to a strong interfacial bonding between the blend matrix and the amorphous NS particles, which transfers the stress from EP_2 to NS particles at the interface. These NS particles restricts the mobility of the polymer chains resulting in higher cross-linking density and higher E' value in the sealer matrix. The higher cross-linking density blocks the motion of the molecular chain resulting in a reduction of free volume, which leads to higher T_g and E', values. The tan δ curve revealed the presence of damping peaks, which revealed the T_g value of the sealer samples. From the graph, it was observed that the T_g for EP_2 and EP_2NS were 37.16 and 50.81 °C respectively. This behaviour revealed increased T_g of EP_2 in presence of NS particles, which confirmed increased segmental immobilization of the composite matrix at the interface.

6.5 TGA

TGA/DTG thermogram of sealer samples is displayed in Fig. 6.e and Table 6.c

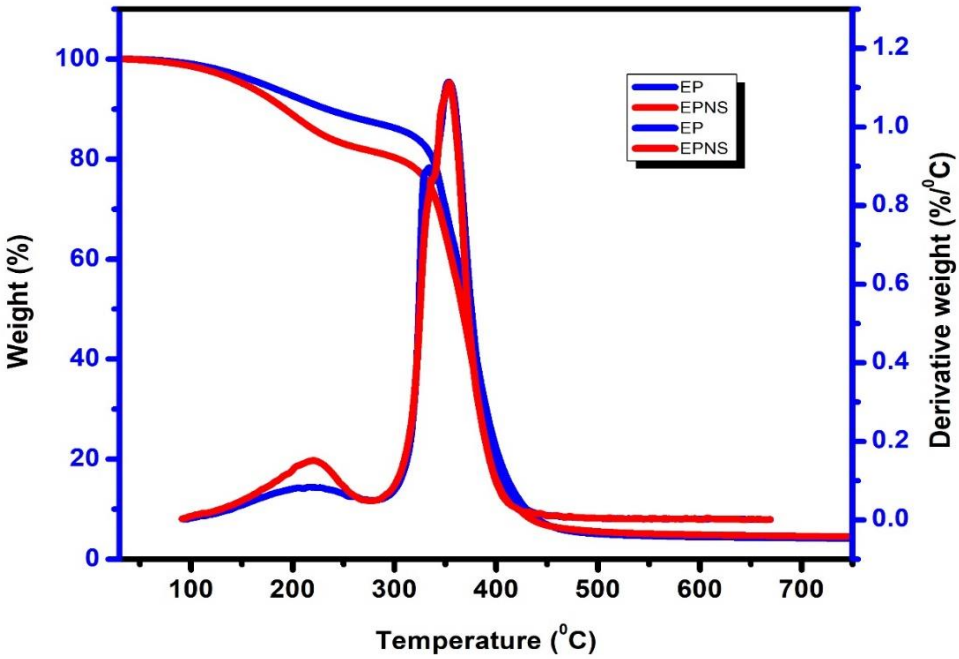

Fig. 6.e: TGA/DTG Thermogram of EP_2 and EP_2NS

The TGA/DTG thermograms of EP_2, and EP_2NS are enumerated in Fig. 6.e and the thermal parameters are reported in Table 6.c. From the TGA thermograms, it was observed that the T_i for EP_2 was 288 °C, while it was 296 °C for EP_2NS. Incorporation of rigid NS particles as fillers, increased the thermal stability of epoxy-PU/NS matrix due to higher cross-linking density. In the case of EP_2, the decomposition peaks were observed at 376 °C, which indicated the decomposition of high molecular weight compounds along with phenolic compounds. However, in the case of EP_2NS, peak at 389 °C indicated the decomposition of high molecular weight compounds along with phenolic compounds. The char yield of EP_2 is 3.66%, while for EP_2NS it was found to be 4.54% due to the presence of –Si-O-Si- linkage and isocyanate linkage in the functionalized NS particles. The maximum degradation temperature for EP_2 was 647 °C, while at 696 °C, EP_2NS showed char yield. This shift in degradation temperature shows a strong interaction between the blend and NS[225].

6.6 DSC

DSC thermogram of blend compositions is reported in Fig. 6.f and Table 6.c

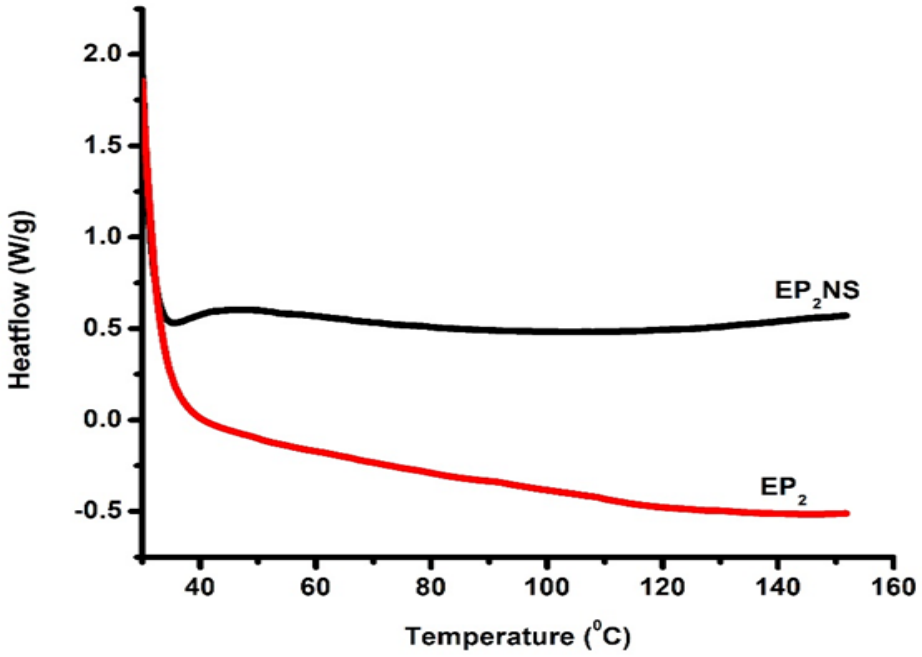

Fig. 6.f: DSC Thermogram of EP_2 and EP_2NS

The DSC thermograms of the EP_2 and EP_2NS have been represented in Fig. 6.f and Table 6.c. The glass transition temperature (T_g) was observed to increase from 32.28 to 46.37 ºC with the incorporation of NS particles within the sealer samples. The increase in T_g value is also due to similar facts of an increased cross-linking density which is due to the formation of closed silica network structure created with the addition of NS particles.

6.7 Water absorption test

Water absorption graph of the blend samples is depicted in Fig. 6.g

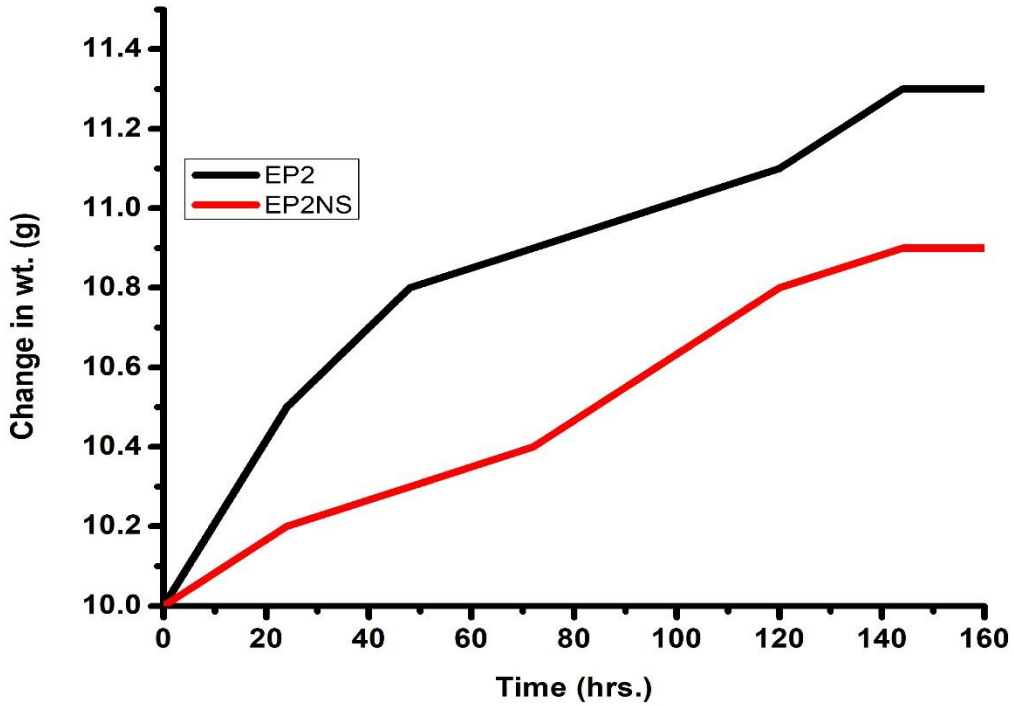

Fig. 6.g: Water absorption graph of sealer samples as function of time

Fig. 6.g enumerated the water absorption behaviour of EP_2 and EP_2NS. The water absorption % was observed to decrease by 5% with the incorporation of NS particles into the EP_2 matrix. The amorphous NS particles when added to the polymer matrix, increased the interfacial interaction between the matrix and the filler, resulting in a formation of a closed network structure. This closed network structure decreased the water absorption capacity of the EP_2NS[226].

6.8 SEM

SEM micrograph of EP_2 and EP_2NS is displayed in Fig. 6.h

(a) (b)

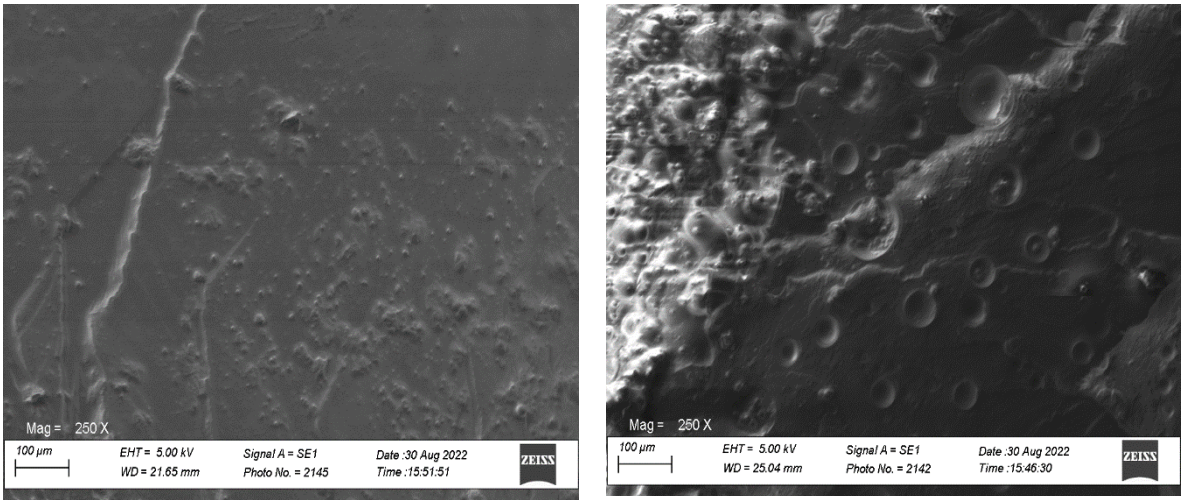

Fig. 6.h: SEM micrograph of (a) EP_2 (b) EP_2NS

The SEM image of the optimized sealer samples were depicted in Fig.6.h. From Fig. 6.h (a), the SEM image of EP_2 was observed, which showed an uneven and rough surface due to increase in ductility of the blend composition. This ductility was achieved by blending epoxy with ATECO. ATECO has special chemical composition which restricted the chain mobility of neat epoxy matrix, thus resulting in development of ductile property. With incorporation of NS particles, the surface roughness of the sealer matrix further increased due to increase of cross-linking density and resulted in higher ductility. It was shown in Fig. 6.h (b)[227].

6.9 WCA

WCA image of the blend samples are displayed in Fig. 6.i

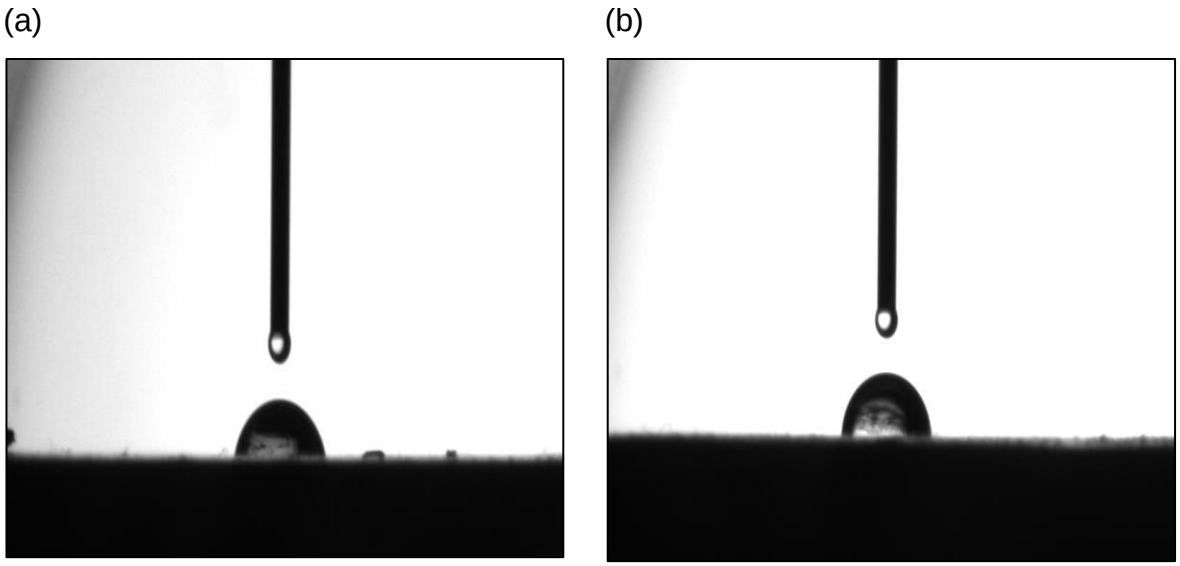

Fig. 6. i: WCA of (a) EP_2 (b) EP_2NS

The contact angle studies of EP_2 and EP_2NS revealed that, WCA of EP_2 was 85.63 °. Whereas, in case of EP_2NS, the WCA increased to 91.45 ° due to the increase in heterogeneity by incorporating NS particles in the polymer blend, which is due to the closed network structure, thereby increasing the hydrophobicity of the surface.

Conclusion

Bio-based cost-effective automobile sealer was synthesized by using EPOFINE 1556, ATECO, and FINEHARD 3486, incorporated with nano-silica. Automobile sealer synthesized with 80% EPOFINE 1556 and 20% ATECO incorporated with 0.5 wt.% NS (EP_2NS) was optimized using impact test. With the incorporation of NS into the neat sealer matrix constituting of Epoxy: PU of 80: 20 ratio, thermal properties like char residue, and glass transition temperature were increased from 3.10%, and 50.6 °C to 4.55%, 73.76 °C, and respectively. From the physical properties, it was observed that water contact angle and cross-linking density increased from 85.63 ° and 0.98

mol/m^3 to 91.45 ° and 3.75 mol/m^3 respectively with the incorporation of NS within the blend. The mechanical studies revealed that with the incorporation of NS, tensile strength, impact strength, and critical stress intensity factor increased to 14.35%, 32.67%, and 32.62% respectively as compared to the neat blend. Thus, epoxy: PU blend at an optimized ratio reinforced with modified nanoparticles can be utilized as sealer.

CHAPTER 7

Conclusion and Future study

Conclusion

The current study attributed synthesis of bio-based automobile basecoat, clearcoat, and sealer using CO as the polyol. Surface modified NS particles were used as the filler material to enhance the physico-mechanical, thermal, optical, and chemical resistance properties.

Eco-friendly basecoat of automobile paint was synthesized using ECO and IPDI using in-situ polymerization process. Incorporation of APTES modified NS along with TP, increased the characteristic properties of the paint formulations. Paint formulation with 0.5 wt.% APTES-NS along with 0.2 wt.% TP depicted optimized properties like thermal, mechanical, and chemical resistance. As per mechanical properties aspect the cross-cut adhesion %, abrasion resistance %, Young's modulus, and pencil hardness were studied to increase by 28%, 0.024%, 131.5 %, and H, after incorporation of the filler materials. FTIR and ^{1}HNMR test confirmed the structural properties of the paint formulations. Thermal and chemical resistance properties were also studied to improve significantly with incorporation of filler materials.

Bio-based automobile clearcoat was synthesized using ATECO and IPDI via in-situ polymerization process. 0.5 wt.% of TI modified NS particles were reinforced into the paint matrix to improve the performance characteristic of the paint formulation. FTIR and ^{1}HNMR studies confirmed the chemical structure of the paint matrix. SEM, and TEM study revealed the morphological properties of the paint formulation. Thermal properties like char residue % and T_{gs} were increased from 0.35% and -12.16 ºC to 1.22 % and 1.65 ºC with the addition of NS respectively. Mechanical properties like cross-cut adhesion %, Young's modulus, abrasion resistance %, pencil hardness were studied to increase by 11%, 979 MPa, 0.28%, and H respectively with incorporation of NS. Furthermore, cross-linking density, chemical resistance, and optical properties increased significantly, with the addition of NS particles into the paint formulations. Hence, bio-based acrylic PU-based paint formulation, incorporated with optimized amount of modified NS can be applicable as the alternative of the commercial clear coats.

Bio-based Epoxy-PU blend was synthesized by using ultrasonication mixing process to be applicable as automobile sealer. Optimized TI modified NS particles were incorporated into the blend to improve the physical, thermal, and mechanical properties of the sealer. FTIR study confirmed the chemical structure of the sealer. SEM study showed the proper dispersion of TI-NS in the blend matrix. Physical properties like WCA, and water absorption % were observed to increase by addition of NS particles in the blend. Mechanical and thermal properties of the nanocomposite was observed to increase significantly with reinforcement of NS particles into the epoxy-PU blend. This implies that, the nanocomposite synthesized can be used as a substitute of commercial automobile sealer.

Future Study

In the future aspects of this current work, further investigation will be carried out for the paint samples exposed to weatherometer for 400 hrs. to study the physical, mechanical, thermal, optical, and chemical resistance properties. This investigation will be very helpful to implement the synthesized bio-based automobile paint samples in commercial level.

Furthermore, the bio-based automobile sealer properties can be compared with the commercially available automobile sealer to study its mechanical, thermal, and physical properties and its implication as an alternative to the commercial automobile sealer.

Further studies will also be carried out to synthesize a hyperbranched polyol derived from CO via in-situ polymerization process. The hyperbranched polyol is predicted to have a hydroxyl value in the range of 400 mg/KOH. The significant increase in hydroxyl value will also increase the performance characteristics of the PU-based paint formulations.

- Study of change in physical, chemical, optical, and mechanical properties after exposure to weatherometer for 400 hrs.
- Comparison of properties in between commercially available automobile sealer and the synthesized bio-based automobile sealer.
- Further study on synthesis of hyper-branched polyol, derived from CO by in-situ polymerization method.

Appendix 1

Prototypes

Basecoat

Clearcoat

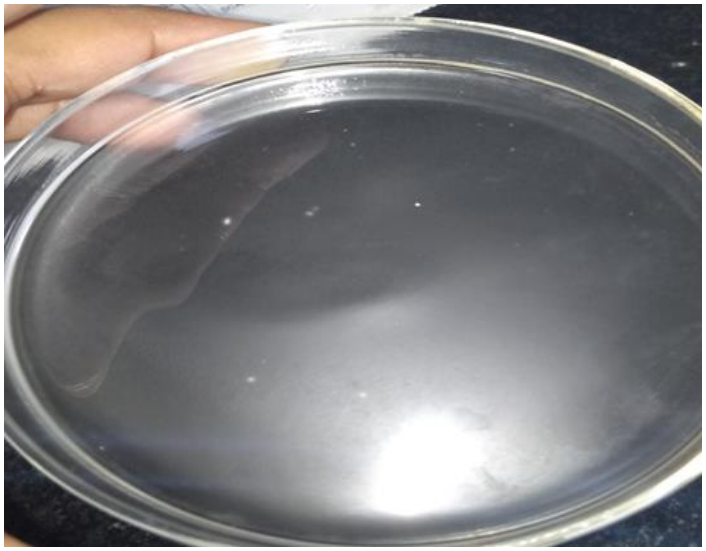

Sealer

References

[1] N. K. Akafuah, S. Poozesh, A. Salaimeh, G. Patrick, K. Lawler, and K. Saito, "Evolution of the automotive body coating process-A review," *Coatings*, vol. 6, no. 2, 2016, doi: 10.3390/coatings6020024.

[2] H. Standeven, "The development of decorative gloss paints in britain and the united states C. 1910-1960," *J. Am. Inst. Conserv.*, vol. 45, no. 1, pp. 51–65, 2006, doi: 10.1179/019713606806082210.

[3] H. Kwaambwa, "a Review of Current and Future Challenges in Paints and Coatings Chemistry," *Prog. Multidiscip. Res. J.*, vol. 3, no. 1, pp. 1–28, 2013.

[4] S. Planning and P. Northwest, "Suppliers and Environmental Innovation : The Automotive Paint Process," vol. 20, no. 20, pp. 166–186, 2000.

[5] T. Sagar, R. Pathanna, R. Bijoy, and D. Herle, "Indian Journal of Advances in Chemical Science Study of High-performance Coating System for Automotive Application," pp. 33–37, 2017, doi: 10.22607/IJACS.2017.S02008.

[6] O. Taghizadeh, P. Sirvi, S. Narasimha, J. A. L. Calvo, and R. Mathar, "Ref. [4]," *IEEE Systems Journal*, vol. 13, no. 3. pp. 2582–2593, 2019.

[7] I. A. D. Lopes, P. J. V. C. Monteiro, J. J. B. Mendes, J. M. R. Gonçalves, and F. J. F. Caldeira, "The effect of different finishing and polishing techniques on surface roughness and gloss of two nanocomposites," *Saudi Dent. J.*, vol. 30, no. 3, pp. 197–207, 2018, doi: 10.1016/j.sdentj.2018.04.003.

[8] Y. G. June, K. I. Jung, M. Choi, T. H. Lee, S. M. Noh, and H. W. Jung, "Effect of urethane crosslinking by blocked isocyanates with Pyrazole-based blocking agents on rheological and mechanical performance of clearcoats," *Coatings*, vol. 10, no. 10, pp. 1–11, 2020, doi: 10.3390/coatings10100961.

[9] N. Co-investigator *et al.*, "Effect of Nano-Zinc Oxide Particles on the Performance Behavior of Waterborne Polyurethane Composite Coatings," *Weather. Test. Guideb.*, vol. 53, p. 13934, 2013.

[10] C. Seubert, K. Nietering, M. Nichols, R. Wykoff, and S. Bollin, “An overview of the scratch resistance of automotive coatings: Exterior clearcoats and polycarbonate hardcoats,” *Coatings*, vol. 2, no. 4, pp. 221–234, 2012, doi: 10.3390/coatings2040221.

[11] M. A. Alaa, K. Yusoh, and S. F. Hasany, “Pure polyurethane and castor oil based polyurethane: Synthesis and characterization,” *J. Mech. Eng. Sci.*, vol. 8, no. June, pp. 1507–1515, 2015, doi: 10.15282/jmes.8.2015.25.0147.

[12] S. Das, P. Pandey, S. Mohanty, and S. Nayak, “Progress in Organic Coatings Effect of nanosilica on the physicochemical , morphological and curing characteristics of transesterified castor oil based polyurethane coatings,” *Prog. Org. Coatings*, vol. 97, pp. 233–243, 2016, doi: 10.1016/j.porgcoat.2016.04.012.

[13] G. Acik, M. Kamaci, C. Altinkok, H. R. F. Karabulut, and M. A. Tasdelen, “Synthesis and properties of soybean oil-based biodegradable polyurethane films,” *Prog. Org. Coatings*, vol. 123, no. June, pp. 261–266, 2018, doi: 10.1016/j.porgcoat.2018.07.020.

[14] R. Liu *et al.*, “Castor oil-based polyurethane networks containing diselenide bonds: Self-healing, shape memory, and high flexibility,” *Prog. Org. Coatings*, vol. 163, no. November 2021, p. 106615, 2022, doi: 10.1016/j.porgcoat.2021.106615.

[15] R. Shen, M. Long, C. Lei, L. Dong, G. Yu, and J. Tang, “Anticorrosive waterborne polyurethane coatings derived from castor oil and renewable diols,” *Chem. Eng. J.*, vol. 433, no. P1, p. 134470, 2022, doi: 10.1016/j.cej.2021.134470.

[16] J. Zhang *et al.*, “Castor-oil-based UV-curable hybrid coatings with self-healing, recyclability, removability, and hydrophobicity,” *Prog. Org. Coatings*, vol. 165, no. November 2021, p. 106742, 2022, doi: 10.1016/j.porgcoat.2022.106742.

[17] P. Alagi, Y. J. Choi, and S. C. Hong, “Preparation of vegetable oil-based polyols with controlled hydroxyl functionalities for thermoplastic polyurethane,” *Eur. Polym. J.*, vol. 78, pp. 46–60, 2016, doi: 10.1016/j.eurpolymj.2016.03.003.

[18] D. Moreno, M. Velasco, and D. Malagón-Romero, “Production of polyurethanes from used vegetable oil-based polyols,” *Chem. Eng. Trans.*, vol. 79, no. July 2019, pp. 337–342, 2020, doi: 10.3303/CET2079057.

[19] L. Maisonneuve, G. Chollet, E. Grau, and H. Cramail, “Vegetable oils: A source of polyols for polyurethane materials,” *OCL - Oilseeds fats, Crop. Lipids*, vol. 23, no. 5, 2016, doi: 10.1051/ocl/2016031.

[20] A. Badan and T. Majka, “The influence of vegetable-oil based polyols on physico-mechanical and thermal properties of polyurethane foams.,” p. 4763, 2017, doi: 10.3390/ecsoc-21-04763.

[21] H. Pulikkalparambil, S. Siengchin, and J. Parameswaranpillai, “Corrosion protective self-healing epoxy resin coatings based on inhibitor and polymeric healing agents encapsulated in organic and inorganic micro and nanocontainers,” *Nano-Structures and Nano-Objects*, vol. 16, pp. 381–395, 2018, doi: 10.1016/j.nanoso.2018.09.010.

[22] J. S. George *et al.*, “Advances and future outlook in epoxy/graphene composites for anticorrosive applications,” *Prog. Org. Coatings*, vol. 162, no. August 2021, p. 106571, 2022, doi: 10.1016/j.porgcoat.2021.106571.

[23] S. Ibrahim, A. Ahmad, and N. S. Mohamed, “Synthesis and characterization of castor oil-based polyurethane for potential application as host in polymer electrolytes,” *Bull. Mater. Sci.*, vol. 38, no. 5, pp. 1155–1161, 2015, doi: 10.1007/s12034-015-0995-8.

[24] A. Das and P. Mahanwar, “A brief discussion on advances in polyurethane applications,” *Adv. Ind. Eng. Polym. Res.*, vol. 3, no. 3, pp. 93–101, 2020, doi: 10.1016/j.aiepr.2020.07.002.

[25] G. Acik, “Preparation of antimicrobial and biodegradable hybrid soybean oil and poly (L-lactide) based polymer with quaternized ammonium salt,” *Polym. Degrad. Stab.*, vol. 181, p. 109317, 2020, doi: 10.1016/j.polymdegradstab.2020.109317.

[26] G. Acik, H. R. F. Karabulut, C. Altinkok, and A. O. Karatavuk, “Synthesis and characterization of biodegradable polyurethanes made from cholic acid and L-lysine diisocyanate ethyl ester,” *Polym. Degrad. Stab.*, vol. 165, pp. 43–48, 2019, doi: 10.1016/j.polymdegradstab.2019.04.015.

[27] Y. C. Ching and N. Syamimie, “Effect of nanosilica filled polyurethane composite coating on polypropylene substrate,” *J. Nanomater.*, vol. 2013, 2013, doi:

10.1155/2013/567908.

[28] A. Giampieri, J. Ling-Chin, Z. Ma, A. Smallbone, and A. P. Roskilly, “A review of the current automotive manufacturing practice from an energy perspective,” *Appl. Energy*, vol. 261, no. March, 2020, doi: 10.1016/j.apenergy.2019.114074.

[29] “Challenges faced by Indian Telecom Industry.” 2010, [Online]. Available: http://www.indiatelecomonline.com/challenges-faced-by-indian-telecom-industry/.

[30] “Raw Material Issues In Indian Paint Industry _ Coatings World.” .

[31] T. Newbould, “Industrial coatings,” *Engineer*, vol. 293, no. 7661. p. 44, 2004, doi: 10.1016/s0026-0576(02)80337-3.

[32] T. Code, “For the purposes of the,” no. January, pp. 1–12, 2012.

[33] Z. W. Wicks, F. N. Jones, S. P. Pappas, and D. A. Wicks, “Special Purpose Coatings,” *Org. Coatings*, vol. i, pp. 658–678, 2006, doi: 10.1002/9780470079072.ch33.

[34] A. Michelis and G. Gougoulidis, “Current and Future Trends in Marine Antifouling Coatings and the Study of Energy Efficiency Benefits for a Naval Fleet,” *Environ. Energy Ships EEinS 2015*, no. May 2015, 2015, [Online]. Available: https://www.researchgate.net/publication/331207510.

[35] F. Sbardella, L. Pronti, M. L. Santarelli, J. M. A. Gonzàlez, and M. P. Bracciale, “Waterborne acrylate-based hybrid coatings with enhanced resistance properties on stone surfaces,” *Coatings*, vol. 8, no. 8, pp. 1–14, 2018, doi: 10.3390/coatings8080283.

[36] P. Judeinstein and C. Sanchez, “Jmc1996,” *J. Mater. Chem.*, vol. 6, no. 4, pp. 511–525, 1996.

[37] “ebook-the-state-of-scientific-marketing.” .

[38] “Water soluble oil paints - three key advantages.” .

[39] “JPS56857A - Water-dispersible coating composition - Google Patents.” .

[40] “Emulsion Paint_ All you need to Know.” .

[41] G. P. Thomas, “Waterborne Coatings Methods Benefits and Applications.” 2013.

[42] US Coatings, “Water-based coating vs. solvent-based coating.” 2021, [Online]. Available: https://www.uscoatings.com/blog/water-based-coating-vs-solvent-based-coating/.

[43] P. Pandey and U. V Kiran, “SOLVENT BASED PAINT AND ITS IMPACT ON ENVIRONMENT AND HUMAN BEINGS ENVIRONMENT AND SOCIETY Ergonomical evaluation of kitchen tools View project Development of smart cane for visually impaired View project SOLVENT BASED PAINT AND ITS IMPACT ON ENVIRONMENT ,” no. October, 2020, [Online]. Available: https://www.researchgate.net/publication/344677732.

[44] R. Jain, M. Wasnik, A. Sharma, M. Kr Bhadu, T. K. Rout, and A. S. Khanna, “Development of Epoxy Based Surface Tolerant Coating Improvised with Zn Dust and MIO on Steel Surfaces,” *J. Coatings*, vol. 2014, pp. 1–15, 2014, doi: 10.1155/2014/574028.

[45] H. J. Naghash, S. Mallakpour, and N. Kayhan, “Synthesis and characterization of silicone modified acrylic resin and its uses in the emulsion paints,” *Iran. Polym. J. (English Ed.*, vol. 14, no. 3, pp. 211–222, 2005.

[46] Omnexus, “Epoxy Resin: Types, Uses, Properties & Chemical Structure.” 2019, [Online]. Available: https://omnexus.specialchem.com/selection-guide/epoxy-resins-a-to-z-technical-review-of-thermosetting-polymer#properties.

[47] Y. Kamiyama, F. Application, P. Data, P. Examiner, and J. M. Reddick, “United States Patent (19),” no. 19, 1998.

[48] “Acrylic vs Porcelain teeth.” .

[49] C. Jiao *et al.*, “Advances in Waterborne Acrylic Resins: Synthesis Principle, Modification Strategies, and Their Applications,” *ACS Omega*, vol. 6, no. 4, pp. 2443–2449, 2021, doi: 10.1021/acsomega.0c05593.

[50] D. K. Chattopadhyay and K. V. S. N. Raju, “Structural engineering of polyurethane coatings for high performance applications,” *Prog. Polym. Sci.*, vol. 32, no. 3, pp. 352–

418, 2007, doi: 10.1016/j.progpolymsci.2006.05.003.

[51] Mike Agosta, “Polyurethane Technology - Coatings World.” [Online]. Available: https://www.coatingsworld.com/issues/2002-06/view_features/polyurethane-technology/7878.

[52] E. A. Ismail, A. M. Motawie, and E. M. Sadek, “Synthesis and characterization of polyurethane coatings based on soybean oil–polyester polyols,” *Egypt. J. Pet.*, vol. 20, no. 2, pp. 1–8, 2011, doi: 10.1016/j.ejpe.2011.06.009.

[53] M. Alam, D. Akram, E. Sharmin, F. Zafar, and S. Ahmad, “Vegetable oil based eco-friendly coating materials: A review article,” *Arab. J. Chem.*, vol. 7, no. 4, pp. 469–479, 2014, doi: 10.1016/j.arabjc.2013.12.023.

[54] “Polyurethane Paint & Coatings_ Uses, Chemistry, Process & Formulation.” .

[55] “1K Coating VS 2K Coatings - Information On The Different Paint Types.” .

[56] W. A. Frye, “Environmentally Conscious Finishes : Powder Coatings on IBM Products,” pp. 33–37.

[57] S. Papasavva, S. Kia, J. Claya, and R. Gunther, “Characterization of automotive paints : an environmental impact analysis ଝ,” vol. 43, pp. 193–206, 2001.

[58] R. J. Gray and G. Incorporated, “Paint and Coatings : a Mature Transition Industry,” *Science (80-.).*, vol. 22, no. 96, pp. 203–245, 1997.

[59] S. Kara, “Electricity Metering and Monitoring in Manufacturing Systems,” 2011, doi: 10.1007/978-3-642-19692-8.

[60] “ref 27.pdf.” .

[61] C. N. E. and A. C. O. R. D.J. Fernandes, “Ref. 28.pdf,” *Materials*, vol. 8. pp. 6558–6569, 2015.

[62] N. Ab Rahim, Z. Hamedon, F. M. Turan, and I. Iskandar, “Reducing Bits in Electrodeposition Process of Commercial Vehicle - A Case Study,” *IOP Conf. Ser. Mater. Sci. Eng.*, vol. 114, no. 1, 2016, doi: 10.1088/1757-899X/114/1/012051.

[63] S. Mishra and I. A. Rizvi, “Study of Different Painting Process Improvement in Automotive Industry,” *Int. J. Recent Technol. Mech. Electr. Eng.*, vol. 5, no. 6, pp. 8–11, 2018, [Online]. Available: https://www.academia.edu/36997501/Study_of_Different_Painting_Process_Improvement_in_Automotive_Industry.

[64] “PRETREATMENT - PPG - Paints, Coatings and Materials.” [Online]. Available: http://corporate.ppg.com/China/PPG-China-Automotive-OEM-Coatings/Products-and-Service/Pretreatment.aspx.

[65] Http://www.aahks.org/care-for-hips-and-knees/do-i-need-a-joint-replacement/total-knee-replacement/., “Ref 31.Pdf.” .

[66] M. S.M, V. Mayur A, M. Pratiksha N, and P. Sneha V, “Review on Automotive Body Coating Process,” *Int. J. Eng. Manag. Res.*, vol. 9, no. 2, pp. 103–106, 2019, doi: 10.31033/ijemr.9.2.11.

[67] “Ref_33.pdf.” .

[68] “REF (58).pdf.” .

[69] “Ref_59.pdf.” .

[70] M. C. Comstock, “Past, present, and future of high performance inorganic pigments,” *Soc. Plast. Eng. - Reg. Tech. Conf. SPE Color Appear. Div. CAD RETEC 2006 - Back to Basics*, no. January 2006, pp. 27–33, 2006.

[71] J. Russell, B. W. Singer, J. J. Perry, and A. Bacon, “The identification of synthetic organic pigments in modern paints and modern paintings using pyrolysis-gas chromatography-mass spectrometry,” *Anal. Bioanal. Chem.*, vol. 400, no. 5, pp. 1473–1491, 2011, doi: 10.1007/s00216-011-4822-9.

[72] J. Parker, “How Binders Work in Industrial Coatings.” 2018, [Online]. Available: https://www.performance-painting.com/blog/how-binders-work-in-industrial-coatings#:~:text=Binders are an essential part,ingredients of the coating together.&text=Binders can also be acknowledged,as the vehicle or catalyst.

[73] “Binders + Resins for Paint - Ingredients Guide _ Coating.” .

[74] T. Bosveld, “Paint Ingredients: What’s In Paint?,” *Dunn Edwards*. 2013, [Online]. Available: https://www.dunnedwards.com/colors/specs/posts/what-is-paint-made-of.

[75] R. Ruckle, “Understanding The Function Of Additives - Coatings World.” [Online]. Available: https://www.coatingsworld.com/issues/2015-12-01/view_features/understanding-the-function-of-additives/.

[76] “Additives For Paints And Inks,” *Pigment & Resin Technology*, vol. 23, no. 4. pp. 12–13, 1994, doi: 10.1108/eb043115.

[77] M. D. Cookson and P. M. R. Stirk, *済無No Title No Title No Title*. 2019.

[78] “The Car Detailing Guide by GoMechanic _ How to Properly Detail a Car.” .

[79] R. H. Cayton and T. Sawitowski, “The impact of nano-materials on coating technologies,” *2005 NSTI Nanotechnol. Conf. Trade Show - NSTI Nanotech 2005 Tech. Proc.*, vol. 2, pp. 83–85, 2005.

[80] H. Li, X. Zhou, X. Li, W. Chen, and Y. Zuo, “Research and Optimization Design of Mixing Characteristics of High-speed Centrifugal Mixer Based on DEM,” *J. Phys. Conf. Ser.*, vol. 2095, no. 1, pp. 2–8, 2021, doi: 10.1088/1742-6596/2095/1/012071.

[81] P. Zapata, R. Quijada, J. Retuer, and E. Moncada, “Preparation of nanocomposites by in situ polimerization,” *J. Chil. Chem. Soc.*, vol. 53, no. 1, 2008, doi: 10.4067/S0717-97072008000100006.

[82] X. Wang, “Preparation , synthesis and application of Sol-gel method University Tutor : Pr . Olivia GIANI Internship Tutor : Mme . WANG Zhen,” no. October, 2020.

[83] U. Eduok, O. Faye, and J. Szpunar, “Recent developments and applications of protective silicone coatings: A review of PDMS functional materials,” *Prog. Org. Coatings*, vol. 111, no. May, pp. 124–163, 2017, doi: 10.1016/j.porgcoat.2017.05.012.

[84] N. Atthi *et al.*, “Superhydrophobic and superoleophobic properties enhancement on PDMS micro-structure using simple flame treatment method,” *Microelectron. Eng.*, vol.

230, p. 111362, 2020, doi: 10.1016/j.mee.2020.111362.

[85] X. Xue *et al.*, "Superhydrophobic self-cleaning solar reflective orange-gray paint coating," *Sol. Energy Mater. Sol. Cells*, vol. 174, no. June 2017, pp. 292–299, 2018, doi: 10.1016/j.solmat.2017.09.014.

[86] K. Hosseinzadeh, D. D. Ganji, and F. Ommi, "Effect of SiO2 super-hydrophobic coating and self-rewetting fluid on two phase closed thermosyphon heat transfer characteristics: An experimental and numerical study," *J. Mol. Liq.*, vol. 315, p. 113748, 2020, doi: 10.1016/j.molliq.2020.113748.

[87] G. Commentary, "De fi nitions for Hydrophilicity, Hydrophobicity, and Superhydrophobicity: Getting the Basics Right," pp. 686–688, 2014.

[88] "A PDMS modified polyurethane_Ag composite coating with super-hydrophobicity and low infrared emissivity - NASA_ADS." .

[89] Z. Dong, H. Zhu, Y. Hang, G. Liu, and W. Jin, "Polydimethylsiloxane (PDMS) Composite Membrane Fabricated on the Inner Surface of a Ceramic Hollow Fiber: From Single-Channel to Multi-Channel," *Engineering*, vol. 6, no. 1, pp. 89–99, 2020, doi: 10.1016/j.eng.2019.10.012.

[90] C. V. Srinivasa, A. S. Ani, and B. M. Jyothi Prasad, "Protective Coatings for Bio-Composites - A Review," *IOP Conf. Ser. Mater. Sci. Eng.*, vol. 925, no. 1, 2020, doi: 10.1088/1757-899X/925/1/012048.

[91] F. Sales *et al.*, "Composite material of PDMS with interchangeable transmittance: Study of optical, mechanical properties and wettability," *J. Compos. Sci.*, vol. 5, no. 4, 2021, doi: 10.3390/jcs5040110.

[92] M. Francis Luther King, G. Robert Singh, R. Sanjeev Kumar, and V. Srinivasan, "Hardness and surface scratch resistance of Basalt/Bagasse fibre reinforced poly lactic acid polymer composites," *Int. J. Eng. Trends Technol.*, vol. 68, no. 6, pp. 13–21, 2020, doi: 10.14445/22315381/IJETT-V68I6P203S.

[93] F. Fallah, M. Khorasani, and M. Ebrahimi, "Improving the mechanical properties of waterborne nitrocellulose coating using nano-silica particles," *Prog. Org. Coatings*, vol.

109, no. April, pp. 110–116, 2017, doi: 10.1016/j.porgcoat.2017.04.016.

[94] M. Fernández-álvarez, F. Velasco, A. Bautista, F. C. M. Lobo, E. M. Fernandes, and R. L. Reis, "Manufacturing and characterization of coatings from polyamide powders functionalized with nanosilica," *Polymers (Basel).*, vol. 12, no. 10, pp. 1–20, 2020, doi: 10.3390/polym12102298.

[95] M. A. El-Fattah, A. M. El Saeed, and R. A. El-Ghazawy, "Chemical interaction of different sized fumed silica with epoxy via ultrasonication for improved coating," *Prog. Org. Coatings*, vol. 129, no. November 2018, pp. 1–9, 2019, doi: 10.1016/j.porgcoat.2018.12.023.

[96] M. Malaki, Y. Hashemzadeh, and A. Fadaei Tehrani, "Abrasion resistance of acrylic polyurethane coatings reinforced by nano-silica," *Prog. Org. Coatings*, vol. 125, no. November 2017, pp. 507–515, 2018, doi: 10.1016/j.porgcoat.2018.07.034.

[97] A. Dashtizadeh, M. Abdouss, M. Tabarzadi, and A. Rahimi, "Preparation of a silica Nano-composite emulsion resin and study of properties and behaviors," *Materwiss. Werksttech.*, vol. 40, no. 9, pp. 684–689, 2009, doi: 10.1002/mawe.200900506.

[98] M. Nikolic, A. R. Sanadi, D. Löf, and S. T. Barsberg, "Influence of colloidal nano-silica on alkyd autoxidation," *J. Mater. Sci.*, vol. 52, no. 12, pp. 7158–7165, 2017, doi: 10.1007/s10853-017-0951-7.

[99] I. A. Rahman and V. Padavettan, "Synthesis of Silica Nanoparticles by Sol-Gel : Size-Dependent Properties , Surface Modification , and Applications in Silica-Polymer Nanocomposites — A Review," vol. 2012, 2012, doi: 10.1155/2012/132424.

[100] M. Alghdeir, K. Mayya, and M. Dib, "Nanosilica Composite for Greenhouse Application," *Compos. Nanocomposite Mater. - From Knowl. to Ind. Appl.*, no. July, 2020, doi: 10.5772/intechopen.92181.

[101] X. Shi, T. A. Nguyen, Z. Suo, Y. Liu, and R. Avci, "Effect of nanoparticles on the anticorrosion and mechanical properties of epoxy coating," *Surf. Coatings Technol.*, vol. 204, no. 3, pp. 237–245, 2009, doi: 10.1016/j.surfcoat.2009.06.048.

[102] S. Das, P. Pandey, S. Mohanty, and S. K. Nayak, "Insight on Castor Oil Based

Polyurethane and Nanocomposites: Recent Trends and Development," *Polym. - Plast. Technol. Eng.*, vol. 56, no. 14, pp. 1556–1585, 2017, doi: 10.1080/03602559.2017.1280685.

[103] Y. Li, L. Zhang, and C. Li, "Highly transparent and scratch resistant polysiloxane coatings containing silica nanoparticles," *J. Colloid Interface Sci.*, vol. 559, pp. 273–281, 2020, doi: 10.1016/j.jcis.2019.09.031.

[104] Y. Wang, L. Zhang, Y. Hu, and C. Li, "Comparative Study on Optical Properties and Scratch Resistance of Nanocomposite Coatings Incorporated with Flame Spray Pyrolyzed Silica Modified via in-situ Route and ex-situ Route," *J. Mater. Sci. Technol.*, vol. 32, no. 3, pp. 251–258, 2016, doi: 10.1016/j.jmst.2015.11.008.

[105] C. Fuentes, M. Ruiz-Rico, A. Fuentes, M. J. Ruiz, and J. M. Barat, "Degradation of silica particles functionalised with essential oil components under simulated physiological conditions," *J. Hazard. Mater.*, vol. 399, no. April, p. 123120, 2020, doi: 10.1016/j.jhazmat.2020.123120.

[106] K. Monjezi, M. Mohammadi, and A. R. Khaz'ali, *Stabilizing CO2 foams using APTES surface-modified nanosilica: Foamability, foaminess, foam stability, and transport in oil-wet fractured porous media*, vol. 311. Elsevier B.V, 2020.

[107] K. Yu, L. Yang, J. Wang, Z. Zhu, and T. J. Wang, "Modification of nanosilica particles with hydrophobic modifier bis[3-(triethoxysilyl)propyl]tetrasulfide by using micro-injection in aqueous solutions," *Colloids Surfaces A Physicochem. Eng. Asp.*, vol. 599, no. February, p. 124852, 2020, doi: 10.1016/j.colsurfa.2020.124852.

[108] B. Qiao, Y. Liang, T. J. Wang, and Y. Jiang, "Surface modification to produce hydrophobic nano-silica particles using sodium dodecyl sulfate as a modifier," *Appl. Surf. Sci.*, vol. 364, pp. 103–109, 2016, doi: 10.1016/j.apsusc.2015.12.116.

[109] N. Suzuki, M. Ito, and F. Yatsuyanagi, "Effects of rubber/filler interactions on deformation behavior of silica filled SBR systems," *Polymer (Guildf).*, vol. 46, no. 1, pp. 193–201, 2005, doi: 10.1016/j.polymer.2004.10.066.

[110] P. Nguyen-Tri, T. A. Nguyen, P. Carriere, and C. Ngo Xuan, "Nanocomposite Coatings:

Preparation, Characterization, Properties, and Applications," *Int. J. Corros.*, vol. 2018, no. ii, 2018, doi: 10.1155/2018/4749501.

[111] E. Richard, S. T. Aruna, and B. J. Basu, "Superhydrophobic surfaces fabricated by surface modification of alumina particles," *Appl. Surf. Sci.*, vol. 258, no. 24, pp. 10199–10204, 2012, doi: 10.1016/j.apsusc.2012.07.009.

[112] L. Chen, F. Chenli, Z. Luo, and Y. Xin, "Study of Nano-Alumina Impact on the Performance of a CaCO3-Epoxy Composite Coating," *Nanomater. Nanotechnol.*, vol. 6, pp. 1–7, 2016, doi: 10.5772/63786.

[113] S. K. Dhoke, N. Rajgopalan, and A. S. Khanna, "Effect of Nanoalumina on the Electrochemical and Mechanical Properties of Waterborne Polyurethane Composite Coatings," *J. Nanoparticles*, vol. 2013, pp. 1–11, 2013, doi: 10.1155/2013/527432.

[114] O. M. Yousri, M. H. Abdellatif, and G. Bassioni, "Effect of Al 2O 3 Nanoparticles on the Mechanical and Physical Properties of Epoxy Composite," *Arab. J. Sci. Eng.*, vol. 43, no. 3, pp. 1511–1517, 2018, doi: 10.1007/s13369-017-2955-7.

[115] M. I. Hussain, "Fluorinated Polyurethane," 2019.

[116] W. Al-Shatty, A. M. Lord, S. Alexander, and A. R. Barron, "Tunable Surface Properties of Aluminum Oxide Nanoparticles from Highly Hydrophobic to Highly Hydrophilic," *ACS Omega*, vol. 2, no. 6, pp. 2507–2514, 2017, doi: 10.1021/acsomega.7b00279.

[117] F. Ahmad, E. S. B. Zulkurnain, S. Ullah, A. G. Al-Sehemi, and M. R. Raza, "Improved fire resistance of boron nitride/epoxy intumescent coating upon minor addition of nano-alumina," *Mater. Chem. Phys.*, vol. 256, p. 123634, 2020, doi: 10.1016/j.matchemphys.2020.123634.

[118] S. Said, S. Mikhail, and M. Riad, "Recent processes for the production of alumina nano-particles," *Mater. Sci. Energy Technol.*, vol. 3, pp. 344–363, 2020, doi: 10.1016/j.mset.2020.02.001.

[119] S. Alexander *et al.*, "Low-surface energy surfactants with branched hydrocarbon architectures," *Langmuir*, vol. 30, no. 12, pp. 3413–3421, 2014, doi: 10.1021/la500332s.

[120] S. Swain, R. A. Sharma, S. Bhattacharya, and L. Chaudhary, “Effects of nano-silica/nano-alumina on mechanical and physical properties of polyurethane composites and coatings,” *Trans. Electr. Electron. Mater.*, vol. 14, no. 1, pp. 1–8, 2013, doi: 10.4313/TEEM.2013.14.1.1.

[121] H. Sivrikaya and A. Can, “Effect of weathering on wood treated with tall oil combined with some additives,” *Maderas Cienc. y Tecnol.*, vol. 18, no. 4, pp. 723–732, 2016, doi: 10.4067/S0718-221X2016005000063.

[122] W. Su, J. Zou, and L. Sun, “Effects of nano-alumina on mechanical properties and wear resistance of WC-8Co cemented carbide by spark plasma sintering,” *Int. J. Refract. Met. Hard Mater.*, vol. 92, no. June, p. 105337, 2020, doi: 10.1016/j.ijrmhm.2020.105337.

[123] L. F. Sturdy, M. S. Wright, A. Yee, F. Casadio, K. T. Faber, and K. R. Shull, “Effects of zinc oxide filler on the curing and mechanical response of alkyd coatings,” *Polymer (Guildf).*, vol. 191, p. 122222, 2020, doi: 10.1016/j.polymer.2020.122222.

[124] N. Wint *et al.*, “The kinetics and mechanism of filiform corrosion occurring on zinc-aluminium-magnesium coated steel,” *Corros. Sci.*, vol. 158, no. June, p. 108073, 2019, doi: 10.1016/j.corsci.2019.06.028.

[125] S. L. de Armentia, M. Pantoja, J. Abenojar, and M. A. Martinez, “Development of silane-based coatings with zirconia nanoparticles combining wetting, tribological, and aesthetical properties,” *Coatings*, vol. 8, no. 10, 2018, doi: 10.3390/COATINGS8100368.

[126] R. Z. Zand, V. Flexer, M. De Keersmaecker, K. Verbeken, and A. Adriaens, “Effects of activated ceria and zirconia nanoparticles on the protective behaviour of silane coatings in chloride solutions,” *Int. J. Electrochem. Sci.*, vol. 10, no. 1, pp. 997–1014, 2015.

[127] A. M. Atta, M. A. Ahmed, A. M. El-Saeed, O. M. Abo-Elenien, and M. A. El-Sockary, “Hybrid zro2/cr2o3 epoxy nanocomposites as organic coatings for steel,” *Coatings*, vol. 10, no. 10, pp. 1–12, 2020, doi: 10.3390/coatings10100997.

[128] A. J. Salman, A. A. Al-Obaidi, D. H. Al-Mamoori, L. M. Shaker, and A. A. Al-Amiery, “Thermal, mechanical and morphological properties of polyurethane-zirconia loading,”

Int. J. Low-Carbon Technol., vol. 16, no. 2, pp. 454–462, 2021, doi: 10.1093/ijlct/ctaa078.

[129] U. Eduok, J. Szpunar, and E. Ebenso, "Synthesis and characterization of anticorrosion zirconia/acrylic nanocomposite resin coatings for steel," *Prog. Org. Coatings*, vol. 137, no. September, p. 105337, 2019, doi: 10.1016/j.porgcoat.2019.105337.

[130] H. thekra I, "Biomechanical evaluation of Nano-Zirconia Coatings on Ti-6Al-7Nb." 2018.

[131] N. Senthilkumar, E. Nandhakumar, P. Priya, D. Soni, M. Vimalan, and I. Vetha Potheher, "Synthesis of ZnO nanoparticles using leaf extract of: Tectona grandis (L.) and their anti-bacterial, anti-arthritic, anti-oxidant and in vitro cytotoxicity activities," *New J. Chem.*, vol. 41, no. 18, pp. 10347–10356, 2017, doi: 10.1039/c7nj02664a.

[132] R. Suriano, R. Ciapponi, G. Griffini, M. Levi, and S. Turri, "Fluorinated zirconia-based sol-gel hybrid coatings on polycarbonate with high durability and improved scratch resistance," *Surf. Coatings Technol.*, vol. 311, pp. 80–89, 2017, doi: 10.1016/j.surfcoat.2016.12.095.

[133] P. fei He *et al.*, "Interface characterization and scratch resistance of plasma sprayed TiO2-CNTs nanocomposite coating," *J. Alloys Compd.*, vol. 819, no. xxxx, p. 153009, 2020, doi: 10.1016/j.jallcom.2019.153009.

[134] F. Tikhani *et al.*, "Polyurethane/silane-functionalized ZrO2 nanocomposite powder coatings: Thermal degradation kinetics," *Coatings*, vol. 10, no. 4, pp. 1–17, 2020, doi: 10.3390/coatings10040413.

[135] B. T. Sevda, D. C. Ayfer, and O. Turgay, "The synergistic effect of intumescent coating containing titanium dioxide and antimony trioxide onto spruce and alder wood species," *J. Build. Eng.*, vol. 31, no. April, p. 101407, 2020, doi: 10.1016/j.jobe.2020.101407.

[136] N. S. Allen *et al.*, "Interrelationship of spectroscopic properties with the thermal and photochemical behaviour of titanium dioxide pigments in metallocene polyethylene and alkyd based paint films: Micron versus nanoparticles," *Polym. Degrad. Stab.*, vol. 76, no. 2, pp. 305–319, 2002, doi: 10.1016/S0141-3910(02)00027-7.

[137] S. Saha, D. Kocaefe, C. Krause, and T. Larouche, “Effect of titania and zinc oxide particles on acrylic polyurethane coating performance,” *Prog. Org. Coatings*, vol. 70, no. 4, pp. 170–177, 2011, doi: 10.1016/j.porgcoat.2010.09.021.

[138] L. Ying, Y. Wu, C. Nie, C. Wu, and G. Wang, “Improvement of the tribological properties and corrosion resistance of epoxy–ptfe composite coating by nanoparticle modification,” *Coatings*, vol. 11, no. 1, pp. 1–12, 2021, doi: 10.3390/coatings11010010.

[139] T. V. Nguyen *et al.*, “Effect of rutile titania dioxide nanoparticles on the mechanical property, thermal stability, weathering resistance and antibacterial property of styrene acrylic polyurethane coating,” *Adv. Nat. Sci. Nanosci. Nanotechnol.*, vol. 7, no. 4, 2016, doi: 10.1088/2043-6262/7/4/045015.

[140] B. Du, F. Chen, R. Luo, S. Zhou, and Z. Wu, “Composite Resin,” vol. 2019, 2019.

[141] A. Grozdanov, G. Gentile, M. Avella, T. Dobreva, and R. Kotsilkova, “Nanocomposite coatings based on alkyd resin with TiO2 and SiO2 nanoparticles,” *Mater. Sci. Eng. Int. J.*, vol. 3, no. 6, pp. 210–215, 2019, doi: 10.15406/mseij.2019.03.00116.

[142] T. Luttrell, S. Halpegamage, J. Tao, A. Kramer, E. Sutter, and M. Batzill, “Why is anatase a better photocatalyst than rutile? - Model studies on epitaxial TiO2 films,” *Sci. Rep.*, vol. 4, pp. 1–8, 2015, doi: 10.1038/srep04043.

[143] L. Uon, G. N. Santos, and A. Chua, “Synthesis and characterization of titanium dioxide nanomaterials via horizontal vapor phase growth (hvpg) technique,” *ASEAN Eng. J.*, vol. 10, no. 1, pp. 93–100, 2020, doi: 10.11113/aej.v10.16699.

[144] M. C. F. Karlsson *et al.*, “Characterisation of silicon, zirconium and aluminium coated titanium dioxide pigments recovered from paint waste,” *Dye. Pigment.*, vol. 162, pp. 145–152, 2019, doi: 10.1016/j.dyepig.2018.06.028.

[145] A. J. Haider, Z. N. Jameel, and I. H. M. Al-Hussaini, “Review on: Titanium dioxide applications,” *Energy Procedia*, vol. 157, pp. 17–29, 2019, doi: 10.1016/j.egypro.2018.11.159.

[146] E. M. Samsudin, S. N. Goh, T. Y. Wu, T. T. Ling, S. B. A. Hamid, and J. C. Juan, “Evaluation on the photocatalytic degradation activity of reactive Blue 4 using pure

anatase nano-TiO2," *Sains Malaysiana*, vol. 44, no. 7, pp. 1011–1019, 2015, doi: 10.17576/jsm-2015-4407-13.

[147] B. Ohtani, Y. Ogawa, and S. I. Nishimoto, "Photocatalytic activity of amorphous-anatase mixture of titanium(IV) oxide particles suspended in aqueous solutions," *J. Phys. Chem. B*, vol. 101, no. 19, pp. 3746–3752, 1997, doi: 10.1021/jp962702+.

[148] J. A. Byrne, P. A. Fernandez-Ibañez, P. S. M. Dunlop, D. M. A. Alrousan, and J. W. J. Hamilton, "Photocatalytic enhancement for solar disinfection of water: A review," *Int. J. Photoenergy*, vol. 2011, 2011, doi: 10.1155/2011/798051.

[149] P. K. Jaseela, M. Kuruvilla, L. Williams, C. Jacob, K. O. Shamsheera, and A. Joseph, "Excellent protection of mild steel in sodium chloride solution for a substantial period of time using a hybrid nanocoating of poly vinyl alcohol and Titania," *Arab. J. Chem.*, vol. 13, no. 8, pp. 6921–6930, 2020, doi: 10.1016/j.arabjc.2020.07.005.

[150] Umwelt Bundes Amt, "Use of Nanomaterials," *Bundesamt Umwelt Ger.*, pp. 1–12, 2013.

[151] "Spray Technologies & Types of Paint Spraying Systems." .

[152] F. S. A. L. S. Company, "What is Conventional Air Spray Atomization Spray Technology?" [Online]. Available: https://www.finishsystems.com/blogs/news/what-is-conventional-air-spray-atomization-spray-technology.

[153] "Paint Booth Temperature Settings – A Practical Guide – GFS Booth Blog." [Online]. Available: https://gfsboothblog.com/2012/04/20/paint-booth-temperature-settings-a-practical-guide/.

[154] Graco, "The basics of airless spraying," *Graco*, vol. 7, no. c, pp. 1–5, 2010, [Online]. Available: http://www.graco.com/content/dam/graco/ced/literature/misc/321132/321132EN-F.pdf.

[155] Graco industries, "Airless Spray Techniques Concept and Theory," no. 300, 1995.

[156] A. Spray, "<CT_Airless_Spray_Tech_300071.pdf>."

[157] J. Rupp, E. Guffey, and G. Jacobsen, “Electrostatic spray processes,” *Met. Finish.*, vol. 108, no. 11–12, pp. 150–163, 2010, doi: 10.1016/S0026-0576(10)80225-9.

[158] A. Sardari, A. A. Sabbagh Alvani, and S. R. Ghaffarian, “shatakshi.verma23@gmail.comCastor oil-derived water-based polyurethane coatings: Structure manipulation for property enhancement,” *Prog. Org. Coatings*, vol. 133, no. April, pp. 198–205, 2019, doi: 10.1016/j.porgcoat.2019.04.030.

[159] X. F. Ye *et al.*, “Isocyanate-modified Nano-SiO2 and Corresponding Process Optimization,” *IOP Conf. Ser. Mater. Sci. Eng.*, vol. 229, no. 1, 2017, doi: 10.1088/1757-899X/229/1/012023.

[160] W. S. Abdel-Wakil, E. A. Kamoun, A. Fahmy, W. Hassan, F. Abdelhai, and T. M. Salama, “Assessment of vinyl acetate polyurethane-based graft terpolymers for emulsion coatings: Synthesis and characterization,” *J. Macromol. Sci. Part A Pure Appl. Chem.*, vol. 57, no. 4, pp. 229–243, 2020, doi: 10.1080/10601325.2019.1691448.

[161] M. Alam, N. M. Alandis, F. Zafar, A. Ghosal, and M. Ahmed, “Linseed oil derived terpolymer/silica nanocomposite materials for anticorrosive coatings,” *Polym. Eng. Sci.*, vol. 61, no. 9, pp. 2243–2256, 2021, doi: 10.1002/pen.25752.

[162] Z. Dai *et al.*, “Preparation of degradable vegetable oil-based waterborne polyurethane with tunable mechanical and thermal properties,” *Eur. Polym. J.*, vol. 139, no. September, p. 109994, 2020, doi: 10.1016/j.eurpolymj.2020.109994.

[163] Z. S. Petrovic, “Polyurethanes from vegetable oils,” *Polym. Rev.*, vol. 48, no. 1, pp. 109–155, 2008, doi: 10.1080/15583720701834224.

[164] S. Sahoo, H. Kalita, S. Mohanty, and S. K. Nayak, “Synthesis of Vegetable Oil-Based Polyurethane: A Study on Curing Kinetics Behavior,” *Int. J. Chem. Kinet.*, vol. 48, no. 10, pp. 622–634, 2016, doi: 10.1002/kin.21020.

[165] N. L. Parada Hernandez *et al.*, “(Epoxidized castor oil – citric acid) copolyester as a candidate polymer for biomedical applications,” *J. Polym. Res.*, vol. 26, no. 6, 2019, doi: 10.1007/s10965-019-1814-5.

[166] M. A. Alam, U. A. Samad, A. Anis, M. Alam, M. Ubaidullah, and S. M. Al-Zahrani,

"Effects of SiO2 and ZnO nanoparticles on epoxy coatings and its performance investigation using thermal and nanoindentation technique," *Polymers (Basel).*, vol. 13, no. 9, 2021, doi: 10.3390/polym13091490.

[167] B. Qiao, T. J. Wang, H. Gao, and Y. Jin, "High density silanization of nano-silica particles using γ-aminopropyltriethoxysilane (APTES)," *Appl. Surf. Sci.*, vol. 351, pp. 646–654, 2015, doi: 10.1016/j.apsusc.2015.05.174.

[168] V. B. Borugadda and V. V. Goud, "Epoxidation of castor oil fatty acid methyl esters (COFAME) as a lubricant base stock using heterogeneous ion-exchange resin (IR-120) as a catalyst," *Energy Procedia*, vol. 54, no. 0361, pp. 75–84, 2014, doi: 10.1016/j.egypro.2014.07.249.

[169] J. Zhang, J. J. Tang, and J. X. Zhang, "Polyols prepared from ring-opening epoxidized soybean oil by a castor oil-based fatty diol," *Int. J. Polym. Sci.*, vol. 2015, 2015, doi: 10.1155/2015/529235.

[170] A. Fahmy, T. A. Mohamed, M. Abu-Saied, H. Helaly, and F. El-Dossoki, "Structure/property relationship of polyvinyl alcohol/dimethoxydimethylsilane composite membrane: Experimental and theoretical studies," *Spectrochim. Acta - Part A Mol. Biomol. Spectrosc.*, vol. 228, p. 117810, 2020, doi: 10.1016/j.saa.2019.117810.

[171] A. Fahmy, T. A. Mohamed, and J. F. Friedrich, "XPS and IR studies of plasma polymers layer deposited from allylamine with addition of ammonia," *Appl. Surf. Sci.*, vol. 458, no. April, pp. 1006–1017, 2018, doi: 10.1016/j.apsusc.2018.07.160.

[172] M. C. Ruiz-Cañas, L. M. Corredor, H. I. Quintero, E. Manrique, and A. R. Romero Bohórquez, "Morphological and structural properties of amino-functionalized fumed nanosilica and its comparison with nanoparticles obtained by modified Stöber method," *Molecules*, vol. 25, no. 12, 2020, doi: 10.3390/molecules25122868.

[173] W. Pathanatecha, "A Study of Various Parameters Affecting Adhesion of Coatings to Metal Substrates," 2019.

[174] C. Defeyt, J. Langenbacher, and R. Rivenc, "Polyurethane coatings used in twentieth century outdoor painted sculptures. Part I: Comparative study of various systems by

means of ATR-FTIR spectroscopy," *Herit. Sci.*, vol. 5, no. 1, pp. 1–11, 2017, doi: 10.1186/s40494-017-0124-7.

[175] H. Bakhshi, H. Yeganeh, A. Yari, and S. K. Nezhad, "Castor oil-based polyurethane coatings containing benzyl triethanol ammonium chloride: Synthesis, characterization, and biological properties," *J. Mater. Sci.*, vol. 49, no. 15, pp. 5365–5377, 2014, doi: 10.1007/s10853-014-8244-x.

[176] H. Mikulčić *et al.*, "Thermogravimetric analysis investigation of polyurethane plastic thermal properties under different atmospheric conditions," *J. Sustain. Dev. Energy, Water Environ. Syst.*, vol. 7, no. 2, pp. 355–367, 2019, doi: 10.13044/j.sdewes.d6.0254.

[177] Z. Jia, G. Yuan, X. Feng, Y. Zou, and J. Yu, "Shear properties of polyurethane ductile adhesive at low temperatures under high strain rate conditions," *Compos. Part B Eng.*, vol. 156, pp. 292–302, 2019, doi: 10.1016/j.compositesb.2018.08.060.

[178] F. Meng, Z. Qiao, Y. Yao, and J. Luo, "Synthesis of polyurethanes with pendant azide groups attached on the soft segments and the surface modification with mPEG by click chemistry for antifouling applications," *RSC Adv.*, vol. 8, no. 35, pp. 19642–19650, 2018, doi: 10.1039/c8ra02912a.

[179] H. Ashrafizadeh, A. McDonald, and P. Mertiny, "Erosive and Abrasive Wear Resistance of Polyurethane Liners," *Asp. Polyurethanes*, no. October, 2017, doi: 10.5772/intechopen.68870.

[180] A. M. Munshi, V. N. Singh, M. Kumar, and J. P. Singh, "Effect of nanoparticle size on sessile droplet contact angle," *J. Appl. Phys.*, vol. 103, no. 8, 2008, doi: 10.1063/1.2912464.

[181] T. V. Nguyen, T. A. Nguyen, and T. H. Nguyen, "The synergistic effects of SiO2 nanoparticles and organic photostabilizers for enhanced weathering resistance of acrylic polyurethane coating," *J. Compos. Sci.*, vol. 4, no. 1, pp. 1–11, 2020, doi: 10.3390/jcs4010023.

[182] E. A. Liszewski, S. W. Lewis, J. A. Siegel, and J. V. Goodpaster, "Characterization of automotive paint clear coats by ultraviolet absorption microspectrophotometry with

subsequent chemometric analysis," *Appl. Spectrosc.*, vol. 64, no. 10, pp. 1122–1125, 2010, doi: 10.1366/000370210792973631.

[183] K. Yusoh, J. Jin, and M. Song, "Subsurface mechanical properties of polyurethane/organoclay nanocomposite thin films studied by nanoindentation," *Prog. Org. Coatings*, vol. 67, no. 2, pp. 220–224, 2010, doi: 10.1016/j.porgcoat.2009.10.003.

[184] S. Cakic *et al.*, "Effects of the acrylic polyol structure and the selectivity of the employed catalyst on the performance of two-component aqueous polyurethane coatings," *Sensors*, vol. 7, no. 3, pp. 308–318, 2007, doi: 10.3390/s7030308.

[185] L. M. Gradinaru *et al.*, "Composite materials based on iron oxide nanoparticles and polyurethane for improving the quality of mri," *Polymers (Basel).*, vol. 13, no. 24, pp. 1–22, 2021, doi: 10.3390/polym13244316.

[186] V. R. Patel, G. G. Dumancas, L. C. K. Viswanath, R. Maples, and B. J. J. Subong, "Castor oil: Properties, uses, and optimization of processing parameters in commercial production," *Lipid Insights*, vol. 9, no. 1. 2016, doi: 10.4137/LPI.S40233.

[187] S. Tayde, P. Thorat, A. Sonawane, and M. T. Scholar, "Synthesis of Polyurethane Coating Using Castor Oil as a Bio-polyol and Its Characterization," vol. 2, no. 4, pp. 254–264, 2017.

[188] S. K. Sahoo, V. Khandelwal, and G. Manik, "Synthesis and characterization of low viscous and highly acrylated epoxidized methyl ester based green adhesives derived from linseed oil," *Int. J. Adhes. Adhes.*, vol. 89, no. January, pp. 174–177, 2019, doi: 10.1016/j.ijadhadh.2019.01.007.

[189] D. O. F. Philosophy and F. O. F. Technology, "SYNTHESIS OF BIOBASED EPOXY RESINS : EFFECT OF MODIFICATION OF CASTOR OIL AND INCORPORATION OF CARBON FIBER ON MECHANICAL , THERMAL , VISCOELASTIC PROPERTIES AND MORPHOLOGICAL BEHAVIOUR OF THE COMPOSITES Submitted by," no. March, 2018.

[190] N. L. Parada Hernandez, A. J. Bonon, J. O. Bahú, M. I. R. Barbosa, M. R. Wolf Maciel, and R. M. Filho, "Epoxy monomers obtained from castor oil using a toxicity-free

catalytic system," *J. Mol. Catal. A Chem.*, vol. 426, no. October, pp. 550–556, 2017, doi: 10.1016/j.molcata.2016.08.005.

[191] J. Manivannan, S. Kalaiselvan, and N. Velmani, "Comparative Study of Polyol with Varying Hydroxyl Values in Polyurethane Coatings | Kalai S - Academia.edu," *Int. J. Res. Eng. Appl. Manag.*, vol. 4, no. 4, pp. 74–77, 2018, doi: 10.18231/2454-9150.2018.0457.

[192] S. Das, P. Pandey, S. Mohanty, and S. K. Nayak, "Influence of NCO/OH and transesterified castor oil on the structure and properties of polyurethane: Synthesis and characterization," *Mater. Express*, vol. 5, no. 5, pp. 377–389, 2015, doi: 10.1166/mex.2015.1254.

[193] N. R. Paluvai, S. Mohanty, and S. K. Nayak, "Synthesis and Characterization of Acrylated Epoxidized Castor Oil Nanocomposites," *Int. J. Polym. Anal. Charact.*, vol. 20, no. 4, pp. 298–306, 2015, doi: 10.1080/1023666X.2015.1016322.

[194] S. K. Narwal, N. K. Saun, P. Dogra, G. Chauhan, and R. Gupta, "Production and characterization of biodiesel using nonedible castor oil by immobilized lipase from bacillus Aerius," *Biomed Res. Int.*, vol. 2015, 2015, doi: 10.1155/2015/281934.

[195] A. M. Salih *et al.*, "Synthesis of radiation curable palm oil-based epoxy acrylate: NMR and FTIR spectroscopic investigations," *Molecules*, vol. 20, no. 8, pp. 14191–14211, 2015, doi: 10.3390/molecules200814191.

[196] R. In, "Research & Reviews In," vol. 4, no. 3, 2013.

[197] M. Hoque, D. Roy, and P. Ghosh, "Castor oil and acrylate based copolymer as green additive for lubricating oil," *J. Sci. Ind. Res. (India).*, vol. 79, no. 6, pp. 537–540, 2020.

[198] N. R. Paluvai, S. Mohanty, and S. K. Nayak, "Cure kinetics of exfoliated bio-based epoxy/clay nanocomposites developed from acrylated epoxidized castor oil and diglycidyl ether bisphenol A networks," *High Perform. Polym.*, vol. 27, no. 8, pp. 918–929, 2015, doi: 10.1177/0954008314566052.

[199] "Lubricants _ Free Full-Text _ Chemically Modifying Vegetable Oils to Prepare Green Lubricants _ HTML." .

[200] S. C. Feifel and F. Lisdat, “Silica nanoparticles for the layer-by-layer assembly of fully electro-active cytochrome c multilayers,” *J. Nanobiotechnology*, vol. 9, no. 1, p. 59, 2011, doi: 10.1186/1477-3155-9-59.

[201] W. He *et al.*, “Surface modification of colloidal silica nanoparticles: Controlling the size and grafting process,” *Bull. Korean Chem. Soc.*, vol. 34, no. 9, pp. 2747–2752, 2013, doi: 10.5012/bkcs.2013.34.9.2747.

[202] T. N. A. T. Rahim, D. Mohamad, A. R. Ismail, and H. M. Akil, “Synthesis of nanosilica fillers for experimental dental nanocomposites and their characterisations,” *J. Phys. Sci.*, vol. 22, no. 1, pp. 93–105, 2011.

[203] J. Zhang, G. Jiang, T. Huang, W. Yu, and Y. Gao, “Synthesis and performance of polyurethane / silicon oxide nano-composite coatings,” pp. 301–307, 2019.

[204] A. Madhi, B. Shirkavand Hadavand, and A. Amoozadeh, “UV-curable urethane acrylate zirconium oxide nanocomposites: Synthesis, study on viscoelastic properties and thermal behavior,” *J. Compos. Mater.*, vol. 52, no. 21, pp. 2973–2982, 2018, doi: 10.1177/0021998318756173.

[205] F. L. Q. Ferreira, M. C. Lopes, A. P. M. Lopes, R. L. Lavall, and G. G. Silva, “Evaluation of the dispersion of carbon nanotubes in an elastomeric polyurethane and fatigue test,” *Polimeros*, vol. 29, no. 1, pp. 1–7, 2019, doi: 10.1590/0104-1428.02718.

[206] K. Ismoilov *et al.*, “Synthesis and Evaluation of Properties of a Novel Cationic Waterborne Polyurethane Finishing Agent,” *J. Chem. Eng. Process Technol.*, vol. 10, no. 3, 2019, doi: 10.35248/2157-7048.19.10.398.

[207] P. Somdee, T. Lassú-Kuknyó, C. Kónya, T. Szabó, and K. Marossy, “Thermal analysis of polyurethane elastomers matrix with different chain extender contents for thermal conductive application,” *J. Therm. Anal. Calorim.*, vol. 138, no. 2, pp. 1003–1010, 2019, doi: 10.1007/s10973-019-08183-y.

[208] A. Khoon Poh, L. Choy Sin, C. Sit Foon, and C. Cheng Hock, “Polyurethane wood adhesive from palm oil-based polyester polyol,” *J. Adhes. Sci. Technol.*, vol. 28, no. 11, pp. 1020–1033, 2014, doi: 10.1080/01694243.2014.883772.

[209] A. Karimzadeh, S. S. R. Koloor, M. R. Ayatollahi, A. R. Bushroa, and M. Y. Yahya, "Assessment of Nano-Indentation Method in Mechanical Characterization of Heterogeneous Nanocomposite Materials Using Experimental and Computational Approaches," *Sci. Rep.*, vol. 9, no. 1, pp. 1–14, 2019, doi: 10.1038/s41598-019-51904-4.

[210] M. Sattari, M. R. Naimi-Jamal, and A. Khavandi, "Interphase evaluation and nano-mechanical responses of UHMWPE/SCF/nano- SiO2 hybrid composites," *Polym. Test.*, vol. 38, no. September, pp. 26–34, 2014, doi: 10.1016/j.polymertesting.2014.06.006.

[211] O. Valdes-Aguilera, "Acrylated performance products for floor coatings with high scratch and abrasion resistance," *Paint and Coatings Industry*, vol. 21, no. 11. pp. 32–36, 2005.

[212] N. I. A. M. Hussain, N. N. Bonnia, S. N. S. Ismail, R. Ramli, and S. N. Surip, "Physical properties of a soy-based polyol as polyurethane coatings," *AIP Conf. Proc.*, vol. 2020, no. February 2020, 2018, doi: 10.1063/1.5062684.

[213] L. Chen, X. Wang, Z. Jia, Y. Luo, and D. Jia, "Use of precipitated silica with silanol groups as an inorganic chain extender in polyurethane," *Mater. Des.*, vol. 87, pp. 324–330, 2015, doi: 10.1016/j.matdes.2015.08.049.

[214] K. M. Seeni Meera, R. Murali Sankar, J. Paul, S. N. Jaisankar, and A. B. Mandal, "The influence of applied silica nanoparticles on a bio-renewable castor oil based polyurethane nanocomposite and its physicochemical properties," *Phys. Chem. Chem. Phys.*, vol. 16, no. 20, pp. 9276–9288, 2014, doi: 10.1039/c4cp00516c.

[215] L. Zhang, "Preparation and Characterization of Low-gloss Waterborne Polyurethane Coatings," *Proc. Int. Conf. Logist. Eng. Manag. Comput. Sci.*, vol. 117, no. Lemcs, pp. 828–831, 2015, doi: 10.2991/lemcs-15.2015.163.

[216] H. Joo Kim, H. Raj Pant, J. Hee Kim, N. Jung Choi, and C. Sang Kim, "Fabrication of multifunctional TiO2-fly ash/polyurethane nanocomposite membrane via electrospinning," *Ceram. Int.*, vol. 40, no. 2, pp. 3023–3029, 2014, doi: 10.1016/j.ceramint.2013.10.005.

[217] B. Xue, Y. Yang, R. Tang, Y. Sun, S. Sun, and X. Cao, “Polyurethane Composite Films Based on Modified Lignin and Reinforced with Silica Nanoparticles : Synthesis and Characterization,” vol. 14, no. 3, pp. 6100–6113, 2019.

[218] T. H. Kim, M. Kim, W. Lee, H. G. Kim, C. S. Lim, and B. Seo, “Synthesis and characterization of a polyurethane phase separated to nano size in an epoxy polymer,” *Coatings*, vol. 9, no. 5, 2019, doi: 10.3390/coatings9050319.

[219] “Polyurethane_Epoxy Interpenetrating Polymer Network _ IntechOpen.” .

[220] P. By, “World ’ s largest Science , Technology & Medicine Open Access book publisher Polyurethane / Epoxy Interpenetrating Polymer Network Polyurethane / Epoxy Interpenetrating Polymer Network.”

[221] G. Lu, C. Shuai, Y. Liu, X. Yang, and X. Hu, “Design and preparation of PU/EP blend resin grafted by hydrophilic molecular segments,” *Coatings*, vol. 11, no. 11, 2021, doi: 10.3390/coatings11111345.

[222] “Automotive Adhesives and Sealants - Bonding for Betterment.” .

[223] P. Cement, “Concrete sealer.” pp. 1–3, 2016.

[224] S. Sprenger, “Nanosilica-toughened epoxy resins,” *Polymers (Basel).*, vol. 12, no. 8, 2020, doi: 10.3390/polym12081777.

[225] A. Bifulco *et al.*, “Thermal and fire behavior of a bio-based epoxy/silica hybrid cured with methyl nadic anhydride,” *Polymers (Basel).*, vol. 12, no. 8, 2020, doi: 10.3390/POLYM12081661.

[226] S. KUMAR, S. MOHANTY, and S. G, “Synthesis and Optimization of Epoxidized Castor Oil in the Presence of a Sulphonated Polystyrene Type Cation Exchange Resin Catalyst,” pp. 70–72, 2015, doi: 10.15224/978-1-63248-075-0-74.

[227] C. Zhang, Y. Chen, H. Li, and H. Liu, “Facile fabrication of polyurethane/epoxy IPNs filled graphene aerogel with improved damping, thermal and mechanical properties,” *RSC Adv.*, vol. 8, no. 48, pp. 27390–27399, 2018, doi: 10.1039/c8ra04718a.